3-11-2011

Optical Metamaterial Design, Fabrication and Test

Jack P. Lombardi

OPTICAL METAMATERIAL DESIGN, FABRICATION, AND TEST

THESIS

Jack P. Lombardi III, Second Lieutenant, USAF

AFIT/GE/ENG/11-25

DEPARTMENT OF THE AIR FORCE
AIR UNIVERSITY

AIR FORCE INSTITUTE OF TECHNOLOGY

Wright-Patterson Air Force Base, Ohio

AFIT/GE/ENG/11-25

OPTICAL METAMATERIAL DESIGN, FABRICATION, AND TEST

THESIS

Presented to the Faculty

Department of Electrical Engineering

Graduate School of Engineering and Management

Air Force Institute of Technology

Air University

Air Education and Training Command

In Partial Fulfillment of the Requirements for the

Degree of Master of Science in Electrical Engineering

Jack P. Lombardi III, BSEE

2d Lt, USAF

March 2011
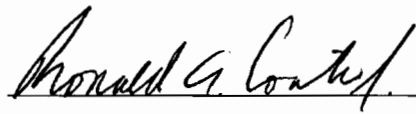
APPROVED FOR PUBLIC RELEASE; DISTRIBUTION UNLIMITED

AFIT/GE/ENG/11-25

OPTICAL METAMATERIAL DESIGN, FABRICATION, AND TEST

Jack P. Lombardi III, BSEE

2d Lt, USAF

Approved:

(signature)	7 Mar 11
Ronald A. Coutu, Jr., Ph.D., P.E. (Chairman)	Date
(signature)	7 Mar 11
Michael A. Marciniak, Ph.D. (Member)	Date
(signature)	7 Mar 11
Michael C. Pochet, Capt, USAF, Ph.D. (Member)	Date

AFIT/GE/ENG/11-25

Abstract

Metamaterials, materials that make use of naturally occurring materials and designed structures to create materials with special properties not found in nature, are a fascinating new area of research, combining the fields of physics, microfabrication, and material science. This work will focus on the development of metamaterials operating in the visible and infrared which will be constructed and tested for basic optical properties. Possible applications for these materials will not be investigated. This work will go into the fabrication and test of layered metal-dielectric structures, called layered metamaterials, as these structures hold potential for applications in advanced optical systems. These structures are designed to have a low index of refraction, with a designed permittivity approaching zero due to the permittivity of the metal, which is negative, and dielectric, which is positive, effectively canceling each other out. The other effort of this investigation is the fabrication and test of a 3D or "fishnet" metamaterial, one that is a sandwich of metal and dielectric, with holes in those layers, creating an interwoven strips of layered material. These interwoven layered strips combine elements with negative permittivity and permeability to create a negative refractive index. In this work, five different combinations of metal and dielectric are fabricated and tested, with one showing behavior indicative of a low permittivity at an infrared wavelength. The investigations into the 3D material did yield a possible for design using a novel material for the dielectric, but fabrication was not completed and only results from simulation were obtained, which suggest a negative index may occur.

Acknowledgments

Table of Contents

List of Figures

List of Tables

List of Acronyms

AFIT	Air Force Institute of Technology
AFRL	Air Force Research Laboratory
BOE	Buffered Oxide Etch
DC	Direct Current
DI	Deionized
ENZ	Epsilon Near Zero
FDTD	Finite Difference Time Domain
FEM	Finite Element Method
FTIR	Fourier Transform Infrared Spectrometer
IR	Infrared
RF	Radio Frequency
RIE	Reactive Ion Etching
RMS	Root Mean Squared
SEM	Scanning Electron Microscope
TIR	Total Internal Reflection
UV	Ultraviolet

OPTICAL METAMATERIAL DESIGN, FABRICATION, AND TEST

I. Introduction

One of the newest and most exciting technologies being developed today is that of metamaterials. As their name implies, meta- being from the Greek for "beyond" [1], these materials have characteristics that are beyond those of "normal" materials; characteristics that are not observed in the materials that make up a metamaterial, and that are not observed anywhere in nature [2]. For electromagnetics, the parameter of interest is the ability to produce unusual effects such as extremely high absorbance, artificial electric permittivity and magnetic permeability, or negative refractive index, characteristics that is not seen in conventional materials [2]. Figure 1 gives a graphical representation of how metamaterials may have a designed index or artificial index based on how the permittivity or permeability of material is changed. Many important applications exist for these materials, such as advanced optical systems with super resolution, able to image below the diffraction limit, to invisibility shells that can guide light around an object and completely hide it [3], [4]. Though these materials hold the promise of realizing these incredible abilities, they are far from perfect, with loss and dispersion limiting the strength of their effects and a narrow bandwidth limiting the wavelengths that these effects can occur [1]. Subsequent sections in this introduction will discuss the operation and fabrication of these metamaterials.
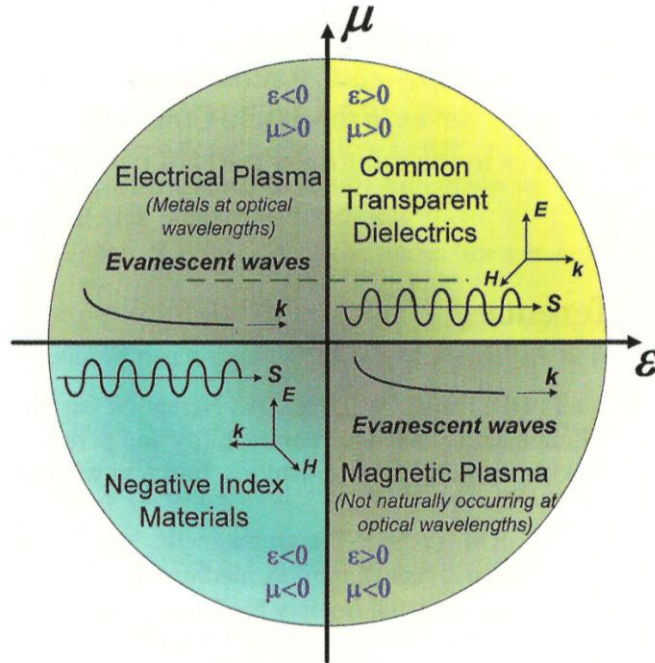
Figure 1   **Graphical representation of regular and metamaterial based on permittivity and permeability.   The structures to be designed and fabricated in this investigation would be on the positive μ axis with zero permittivity, or in the third quadrant with a negative index** [5]**.**

1.1 Material Properties and Operation

As was stated above, metamaterials have properties that are not found in nature or in the constituent materials used to fabricate them, though they derive their unique properties based on the constituent materials and structure, and how it interacts with incident electric and magnetic fields. A key property of metamaterials is that all features are very small, so that they are much smaller, ideally orders of magnitude smaller, than the wavelength of the light they are interacting with [1]. A general rule of thumb for this is that the largest feature in a structure should be no larger than one tenth the wavelength of radiation the material is designed to interact with.   In this way, the individual structures are not resolved by the incident light, and the overall interaction of the structures and the light can be seen in the bulk properties as if it were a homogeneous

medium [1]. This is different from a photonic crystal, where the material is not considered to be homogeneous, derives its effects from the periodic structure of the materials and the structure is about the same size as the wavelength of light [1]. It can be helpful to think of these small structures like atoms that are interacting with light in a normal material, only these are manmade atoms, with designed properties [6]. A wide variety of structures are used to fabricate metamaterials, but for most optical applications, they consist of layered periodic structures. A general example of such a structure can be seen in Figure 2.

(a)

(b)
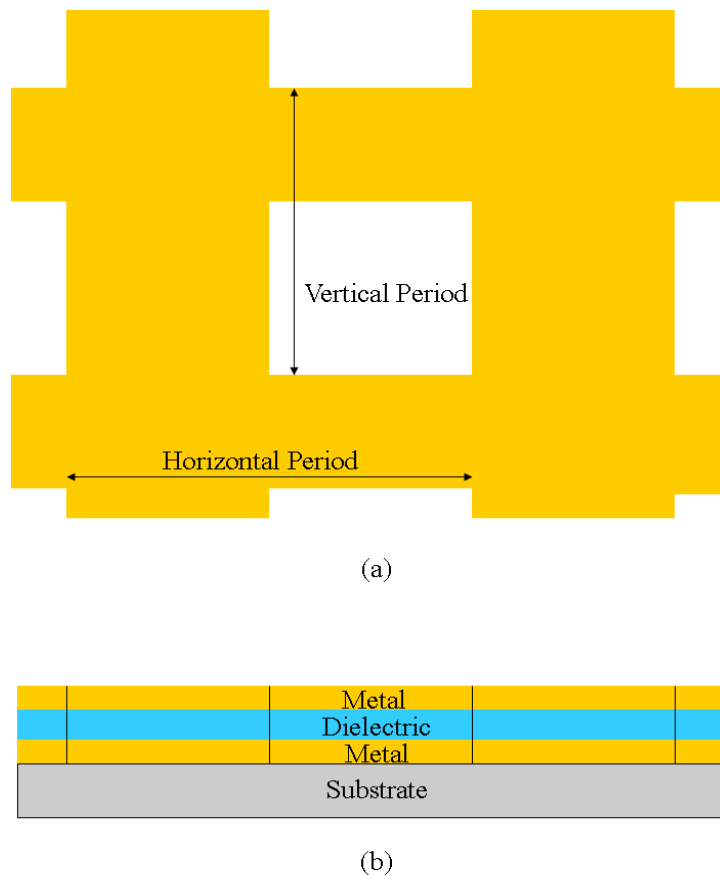
Figure 2 Example of a layered periodic structure with (a), the top view, showing the periodicity of the structure in two directions and (b), the side view, showing the periodicity of the layers.

It is highly desired to create metamaterials that can be designed, tailored create certain effects at a given wavelength. Knowing the wavelength and desired effect, other specifications, such as layer thickness and structure size, needed to create a material to give these effects can be determined. Depending on the desired effects, the structure may be very simple or more complex. To create an artificial permittivity, a simple periodic layered structure of metal and dielectric or a periodic array of metal wires in can be used [5]. The layered structure takes advantage of metals, which naturally have a negative permittivity when the wavelength of the incident light is shorter than the material's plasma wavelength, the wavelength at which the electrons in the metal oscillate, and dielectrics, which have a positive permittivity[3], [5]. By combining these metals and dielectrics in very small structures, the positive and negative permittivity can cancel each other out and result in an effective permittivity approaching zero [5]. This type of metamaterial is commonly known as an epsilon near zero, or ENZ metamaterial.

Creating an artificial permeability requires a different structure, such as layered metal-dielectric nanostrips that are coupled to resonate at a certain frequency [5]. This structure has capacitive and inductive elements in it that can form something like an LC circuit, with a particular resonance frequency [1]. When the incident light is at the resonant frequency of this circuit, the interaction between the light's electric and magnetic fields and the circuit will produce a negative permeability in a relatively narrow band of frequencies [6].

A negative index material can be created by using both of these structures together, creating a 3D metamaterial structure that is generically known as a "fishnet" to interact with the incident radiation, specifically with the electric and magnetic fields of

4

the light creating voltages and inducing currents in the metamaterial structure. Micrographs of fabricated fishnet structures can be seen in Figure 3. This creates the effect of having the real parts of the effective permittivity and permeability being negative, as is the case in a double negative, negative index metamaterial ($\varepsilon' < 0$ and $\mu' < 0$) or, satisfy the requirement that $\varepsilon'\mu'' + \varepsilon''\mu' < 0$ for a single negative index metamaterial, where a negative index may not be accomplished by having only a negative permittivity and low permeability structure, which is easier to accomplish. The single negative condition also implies that a negative index cannot be accomplished without loss from the artificial permeability as well [7]. Limitations of current optical metamaterials include the bandwidth of where their unique properties occur and losses, especially since the greatest loss occurs near resonance, which is also where the negative index metamaterials have their unique properties [1], [5].

(a)   (b)
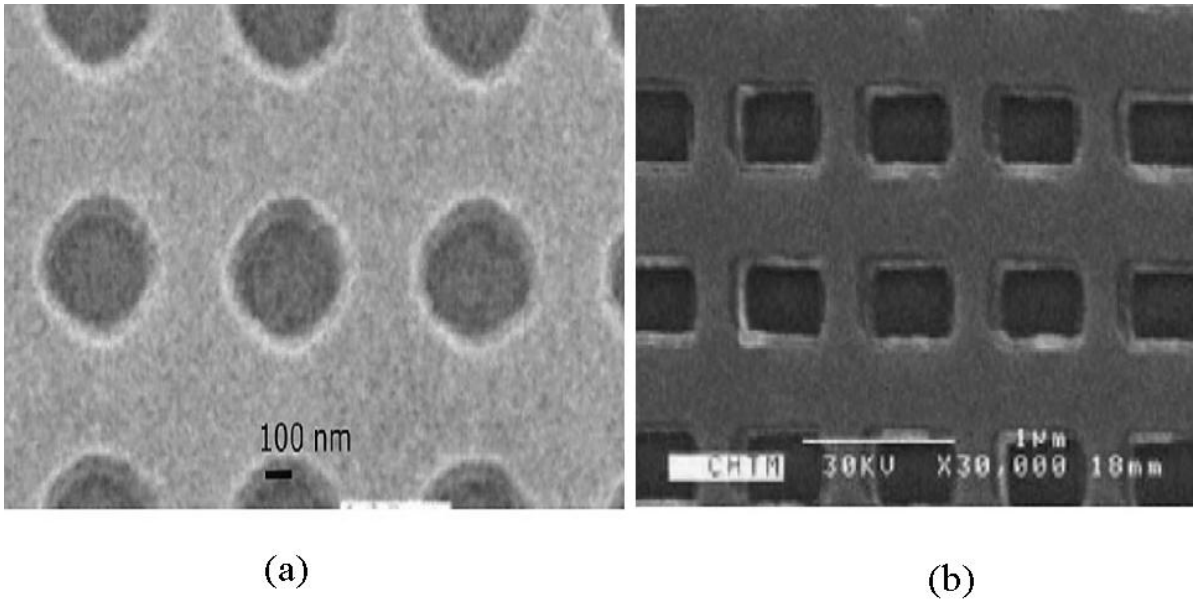
Figure 3 Examples of fishnet metamaterials (a) is a fishnet with holes cut in layered materials, while (b) is a fishnet using strips of layered material [6]**.**

1.2 Motivation

Motivation for this research comes from the fact that this new technology has many far ranging applications, including many that are of interest to the defense community. Research presented in this work will be more basic in nature, and focus on the fabrication and development of metamaterials, not on the applications and use. By developing and characterizing these materials fully, they can then be integrated into new advanced systems.

1.3 Metamaterial Design Proposal

The efforts of this research will focus on a few areas that are interrelated and necessary for the design, fabrication and test of a metamaterial. First, the way metals and dielectrics are deposited to make the layers needed for a metamaterial will be investigated and characterized. Research will then be done into making layered, designed permittivity metamaterials. Data will be gathered on the properties of the materials to be used and calculations done for the thickness of the layers needed. The layered materials will be fabricated and tested. Analytical methods will also be used to characterize these layers their response, and optical properties. Investigations will then be made into creating a 3D metamaterial, determining the thickness of the layers and size of the structure needed. Studies will be made into characterizing the etching of the deposited material, and the lithography needed to create the structures. Simulations will be done to predict the response of the fabricated structure. The fabricated structure will then be tested to determine its optical response and properties.

1.4 Summary

Optical metamaterials are a bold new class of materials that allow light to be controlled in ways that are not seen in nature and were previously not thought possible. The unique properties of these materials include designed permittivity, permeability, and refractive index, giving the ability to control and design a material's optical properties by changing the constituent materials, layers and structures of the metamaterial. Investigations will be made to characterize the processes needed to fabricate these materials, following the guidance of models and analysis that predict effects at certain testable wavelengths. The next section of this document will give background information on the processes needed to fabricate and test the metamaterials in the investigation. Subsequent sections will describe the methodology used for design and analysis, and then the results of the fabrication and testing. Final sections will give conclusions and suggestions for future work.

II. Background

In this section, the background information needed for the fabrication of an optical metamaterial will be discussed, including the characterization of the fabrication processes and materials.

2.1 Material deposition using Plasma Deposition (Sputtering)

Materials used for fabrication were deposited using a Denton Discovery 18 magnetron plasma deposition or sputtering system. This method of deposition was chosen because of its ability to deposit high purity thin films of both metals and dielectrics in a pristine high vacuum environment. This system uses argon or nitrogen plasmas created by a DC or RF bias to create a plasma in front of a target, a 2 inch diameter, one eighth of an inch thick piece of the material, to be deposited. Though the system is capable of using either nitrogen or argon, argon was the only gas used for all the depositions. The highly energetic ions of the plasma remove atoms from a target by hitting it and physically knocking them into the evacuated chamber. Once removed from the target, the atoms then fly through the chamber until they hit something, such as the substrate on which the material is to be deposited. The plasma density and the rate at which ions impinge on the target, and thus the deposition rate, are increased by the presence of magnets placed behind the target. This type of system, with magnets used to increase the plasma density and deposition rate, is known as a magnetron sputtering system [8].

2.1.1 Deposition Characterization

Before structures could be made, investigations were made into how this system and the targets it used deposited materials. The data for this characterization came from silicon test pieces with a step profile. These test pieces were small pieces of silicon wafer that were coated with Rohm & Haas Electronic Materials' 1818 positive photoresist, a polymer that is sensitive to ultraviolet light, on one side, as can be seen in Figure 4(a). 1818, as it is commonly called, is used here simply to provide a layer that is easily removed with a solvent like acetone. A deposition is then made, with the times and voltage for the pre-sputter, the time that the plasma is in front of the target, but the material is blocked by a shutter so the material it is not deposited on the test piece, and deposition noted. This deposition covers the entire test piece with a conformal layer of material, as can be seen in Figure 4(b). The next step was to remove the photoresist using acetone, methanol and DI water, and then dry the sample with nitrogen. Often times, the deposited material on top of the 1818 would have to be scored to allow the solvents to get to the 1818 and remove it.
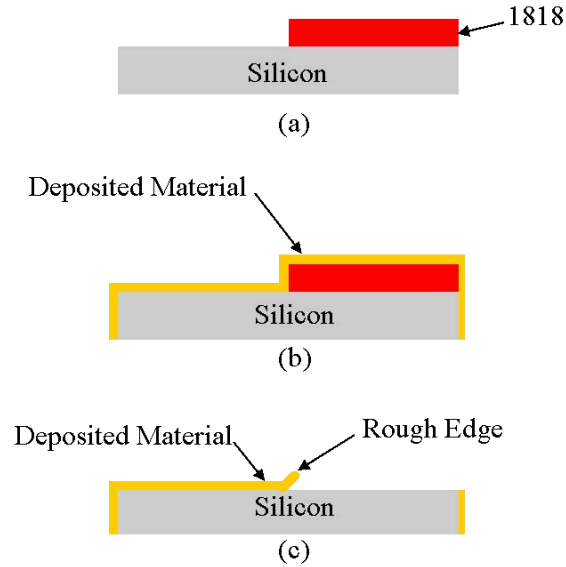
Figure 4 Graphical description of test piece usage. (a) shows the test piece before deposition, with 1818 photoresist on one side. (b) shows the piece after material deposition, which covers the whole sample in a conformal layer of material. (c) shows the piece after the 1818 and deposited material is removed, often leaving a rough edge.

Once the 1818 and the material on top of it were removed, a profile with a side covered with deposited material and a side where there is just bare silicon was created, with an interface area between them. This interface can often be rough, with some of the deposited film not breaking off cleanly when the photoresist is removed, which can be seen in Figure 4(c). Once a step profile was created, the thickness of the deposition could be measured using a stylus profilometer. This tool uses a stylus that follows the surface contours of a sample, and software that allows one to choose a zero point and see the difference in height between that point and the original zero point. In this way, the thickness of the deposited layer could be found by having the profilometer scan from the side of the sample with the deposited layer to the side with bare silicon, and choosing the height of the bare silicon to be zero. To deal with samples that had a rough interface, two things could be done; a tear-off could be attempted, using a piece of scotch tape to tear

off the rough edge pieces, leaving a clean profile of deposited material or a long profilometer scan could used, where the measurement begins on the deposited material far away from the interface, and goes over the rough interface before going to the bare silicon. Each method had advantages, as the tear off provided a clean interface, but could also tear off or damage the material on the side to be measured, while the long scan could be hard to analyze. The difficulty in analyzing the long scan was due to the auto-scaling of the profilometer, which would scale the profile to the highest measurement from the rough area, which could be an order of magnitude taller than the deposited material, making it hard to measure, and drift in the profilometer where the relatively flat areas of deposited material and bare silicon would be displayed as having a curved surface, increasing or decreasing in thickness. Five measurements were made for sample height, with the measurements made across the length of the step profile and then averaged to give an average thickness for the sample. The deposition rate was then calculated by dividing the measured thickness by the time of the deposition. At first, an exhaustive design of experiments analysis was done to characterize the deposition rate of a material, varying the time and applied voltage; however, it was found that a simpler approach using fewer samples could be used. For subsequent depositions and characterizations, three samples were made at a spread of voltages (DC) or power (RF). An example of this would be for the characterization of a dielectric doing three 50nm depositions at 150W, 250W and 350W, and then examining the depositions using the profilometer, light microscope and interferometric microscope, commonly known by the brand name of Zygo, for undesirable characteristics, such as a very rough surface, cracks, or holes in the film. The profilometer was used to provide information on the thickness of the film,

11

using the method detailed above. The light microscope allowed one to see if there were large cracks or holes in the film, which were signs of a poor deposition. The interferometric microscope is a tool that uses the interference of light to determine the height of features on an object down to the nanometer range. This tool had the ability to provide a reading of the roughness of a sample by giving a root mean squared (RMS) height and showing a distribution of height values over a scanned area, and a qualitative comparison of the results from different samples could be done. After the films were examined, the settings of the best sample would be used, or sometimes a split between those of two good samples would be used. The details of the settings used in the deposition of each material and fabrication will be discussed in the results section.

2.1.2 Deposition Monitor Use

In addition to determining the thickness of the deposition based on the deposition time and voltage, the Denton sputtering system is also equipped with an Infincon XTM\2 deposition monitor. This monitor works by using a standing acoustic wave on a crystalline quartz wafer, known simply as the crystal, which undergoes a change in frequency as material is deposited on it. Given certain parameters about the material being deposited and system the monitor is used in, the thickness of the material being deposited on a substrate can be calculated [9]. The needed parameters of the material being deposited are the density and z-ratio, a parameter that corrects for the impedance mismatch between the crystal and the deposited material, so that the change in the frequency of the oscillating crystal is due only to the to the buildup of deposited material on the crystal, both of these parameters are found in deposition monitor manual, and the

12

tooling factor, a parameter that corrects for the deposition monitor being located away from the sample [9]. Since the monitor was also located different distances away from each cathode, different tooling factors for each cathode also had to be calculated for the thickness of material deposited to be accurately monitored. The tooling factors that had to be determined to use this tool were found by measuring the step heights from depositions of Cu, Ni, and Al_2O_3 using the profilometer. The tooling was computed using the method described in the deposition monitor's manual based on the measured step height and the value displayed by the monitor. It was found that the monitor did not have a large enough tooling percentage to allow it to display the thickness in the units it was designed to display, kilo Angstroms, but is able to accurately display the thickness in µm, a difference of an order of magnitude. The tooling factors for each cathode can be seen in Table 1. The tooling factors are the same for any target used in a particular cathode, as this factor is only correcting for the difference in distance between each cathode and the deposition monitor. This is a valuable tool that is especially useful, as the current, and thus deposition rate, fluctuates and doing a deposition based only on time and applied voltage would not compensate for this.

Table 1 Tooling Factors for the Discovery 18 Sputtering System

Cathode	Tooling Factor (%)
Cathode 1 (RF)	40.6
Cathode 2 (DC 1)	20.3
Cathode 3 (DC 3)	66.2

2.2 Lithography

For the fabrication of patterned and etched metamaterial structures, it was decided to use standard lithographic processes to define the patterns to be fabricated. This was done because the structures that were being fabricated were for infrared wavelengths, where the larger wavelengths would allow structures big enough to be defined by standard lithographic processes, which use masks, pieces of glass patterned with chrome, to control where ultraviolet light is transmitted, and define a pattern in a layer of sensitive photoresist. A general illustration of this photolithography process using a positive photoresist can be seen in Figure 5.
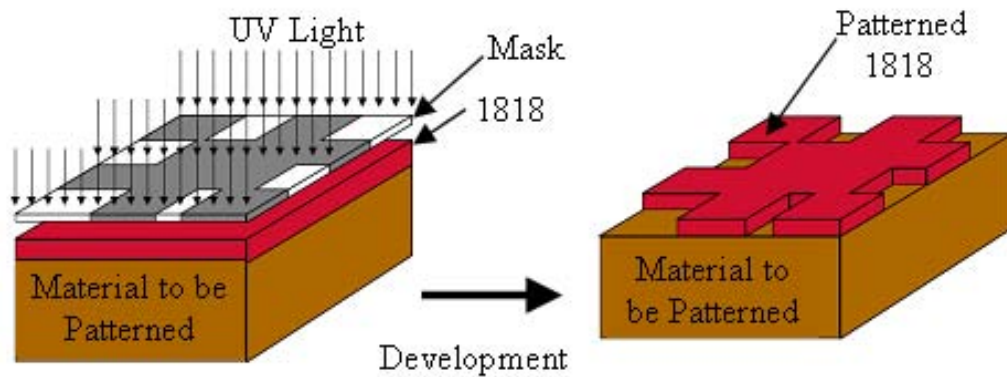
Figure 5 Graphic showing the photolithography process with positive photoresist, showing how the mask determines what areas are exposed and developed away. Notice how the patterned photoresist is the same as the mask [10]**.**

The Heidelberg μPG 101 direct write laser system will be used to create masks needed for fabrication. This piece of equipment is able to take a layout, created in the microfabrication design software L-Edit, and using a laser, write the pattern into photoresist, similar to the way a plotter creates a pattern on paper. The minimum dimension size, and thus smallest feature able to be produced by this system, is 1μm,

with 40nm address spacing, meaning the smallest change in size it can make is 40nm. This means that a feature could be made to be 1μm, or 1.04μm, but cannot be made to be 1.03μm [11]. The size and resolution of this machine will dictate the size of smallest features in a metamaterial design. A mask is produced by this system when a purchased mask blank, a 4-inch square of soda lime glass with a layer of chrome and a positive photoresist, a polymer that can be removed after it has been exposed to ultraviolet light, has the desired pattern written in the photoresist layer using the Heidelberg system. The exposed photoresist is then developed away, leaving openings where the chrome is exposed and can be etched away, creating an opening where light can pass through for photolithography. After the etching of the chrome, the rest of the photoresist is removed, and the mask is ready for use. The masks produced will then be used in the Karl Suss MJB 3 mask aligner to create these patterns in photoresist spin coated onto sputtered layers of metal and dielectric. The photoresist used is Rohm and Haas's 1818 photoresist, a positive photoresist. This is done by loading the mask and sample covered with photoresist into the mask aligner. Once the sample is loaded, it can be positioned so it is in the proper orientation with respect to the mask. After it is properly aligned, ultraviolet light produced by a lamp inside the mask aligner is then shined on the mask, which lets light through the holes in the chrome layer of the mask and blocks all the rest. This means that the photoresist in areas that were blocked by the photoresist will stay, and those that received the light will develop away, creating holes in the photoresist layer. This patterned layer of photoresist will serve as a mask for the etching of the layers and creation of the 3D metamaterial structure.

2.3 Material Removal by Wet Etching

Once the layers of metal and dielectric have been deposited, and a mask lithographically patterned, the layers are then etched to form the fishnet structure. Etching to form this structure will be a multistep process, as metals and dielectrics cannot be etched by the same processes. Wet etchants will be used to etch the metal and the dielectric. Etch studies are conducted to determine the best etch times for the materials used in fabrication. The results of the studies and best etch parameters are detailed in the discussion on the fabrication.

2.4 Testing Using Spectrophotometry

The first piece of equipment used for testing was a Cary 5000 ultraviolet (UV)-visible-infrared (IR) spectrophotometer, with a range of 175nm to 3.3μm. This instrument was used for the structure that was fabricated to operate at visible frequencies, with measurements taken from 200nm-2.5μm, with a resolution of 1nm. This instrument operates by producing light using a broadband lamp and then producing monochromatic light using a diffraction grating [12]. The monochromatic light is then shined on the sample to be measured, and the reflectance or transmittance of the sample measured by comparing the light from the sample with a reference beam [12]. The testing done here used an internal diffuse reflectance accessory, which allows any light that reflects off the sample at any angle to be collected and measured. This is done by the sample being placed in front of a hole in a reflective sphere. The beam of light enters the sphere and impinges on the sample in front of the hole at an angle of approximately 3°, and reflects off the sample into the sphere. The reflected light bounces around the sphere and the

intensity of light at any point in the sphere becomes homogenized and averaged. A sensor mounted in another hole in the sphere is then able to sense the average intensity at that one area, and then integrate for the area of the sphere to give the reflection of the sample [13].

2.5 Testing Using Fourier Transform Infrared Spectroscopy (FTIR)

Measurements of the reflection and transmission in the infrared are made using a Bomem MB 157S FTIR, for a range of $1.3\mu m$-$25\mu m$ (7900-$399cm^{-1}$). This instrument works by using a broadband IR source to create a beam of light that is then reflected or transmitted through a sample. The light coming from the sample is then put into a Michelson interferometer, which has one of the two mirrors fixed and the other moving back and forth very precisely, and changing the optical path length [14]. This change in optical path length creates interference fringe patterns that vary with respect to the position of the mirror and the optical frequencies that are present. This interference pattern, that is a function of the change in optical path length, is known as an interferogram, and has peaks that correspond to the intensities of different frequencies [14]. To find the reflection and transmission, a Fast Fourier Transform is done on the interferogram, taking the collected results that are a function of the mirror position and transforming them to a function of wavelength or frequency [14]. Before any measurements are made, a calibration has to be done by having the instrument make a measurement with no sample loaded, and then using the results of that measurement to compensate for variations due to atmospheric conditions and tool condition. The FTIR measurements for transmission were made at an incident angle 0˚ by holding the sample

and shining infrared radiation from the source port of the instrument onto the fabricated structure and substrate, and collecting the radiation from the back of the substrate and channeling it into the receiver port of the instrument for measurement. Reflection measurements made use of a Specac Selector diffuse reflectance accessory, in which the infrared radiation from the source port was reflected down towards the sample at an angle 33.15° to the horizontal and 56.85° to the vertical, giving an incident angle of 61.3° from normal. The beam is reflected off the sample and then reflected by another mirror to the receiver port of the instrument.

2.6 Testing Using Ellipsometry

Ellipsometry is a widely used technique for the determination of a thin film's thickness or optical properties based on the amplitude and polarization of incident and reflected light. Specifically, what is done is that linearly polarized light, with known parallel and perpendicular electric field values, is shined on a sample at some angle, and a detector, positioned at the same reflected angle, is able to detect the change in the amplitude of the electric field components and the change in phase between these two components, which causes a change in polarization [15]. This data is collected over a range of wavelengths. Using this data and a known thickness for the material being measured, the complex index of refraction can be found by fitting a model to the collected data. A model is assumed, such as a structure of some thickness on a substrate with a certain index of refraction, and the index of the structure found by fitting the collected data to a model of the sample being tested, and varying the index of the unknown structure until the model data matches the collected data [15]. Other

parameters, such as surface roughness can also be added to the model the help it fit the collected results. This procedure of finding the index of the material can also be done over a range of wavelengths. In addition to these specialized measurements, an ellipsometer is also able to make reflection and transmission measurements at various angles of incidence. The measurements used in this investigation were first made using a Horiba UVISEL ellipsometer, which is able to make measurements in from the ultraviolet to the near infrared, and also with a J.A. Wollam V-VASE and IR-VASE ellipsometers, which measured in the visible to near IR and near to mid IR, respectively.

2.7 Simulation with the Finite Difference, Time Domain Method (FDTD)

For the 3D metamaterials, simulation was done using commercially available finite difference, time domain (FDTD) software Lumerical®. This was done since the response of these complex structures, consisting of different layers of materials with complicated structures cannot be easily modeled and solved by analytic means. This software is used to numerically solve for the response of a structure to incident light using Maxwell's Equations, and solving for the electromagnetic fields as a function of time [16]. This means that a simulated pulse of many frequencies of light is used as a source, and that Fourier transforms are then used to decompose the results that are a function of time to create results as a function of wavelength [16]. First, a model of the structure, with the needed optical properties, is built within the software. The software then takes the constructed model and creates a mesh of points where Maxwell's Equations are to be solved. Within this mesh, boundary conditions, sources, the location and type of light wave injected, and monitors, places to collect the data, are designated. The simulation is

19

then run, with the results collected using the monitors. Data from the simulation can then be analyzed and plotted to give the reflection and transmission of the structure.

2.8 Summary

In order to fabricate a metamaterial, some of the fabrication techniques and methods first need to be studied and characterized. This study involves making deposits of material and analyzing the quality of the film, identifying how the layers of material needed for layered metamaterials and 3D metamaterials should be deposited. Background work was also done into the processes needed to remove those deposited materials by etching. In addition to just studying the processes needed for deposition and removal of materials, lithography is also needed to allow proper fabrication. Finally, the equipment and means needed for testing and simulating the fabricated structures was described.

The research methodology described here will follow the same order as was described in previous sections, with the layered metamaterials, stacks of metal and dielectric layers, designed to have an ENZ layered metamaterials are discussed first. Increasing in complexity, 3D metamaterials are then considered. These materials are more complex because they involve an etching step to create strips of layered material. The layered metamaterials will be analytically designed and modeled, while the more complex 3D metamaterial will be designed using an analytical method and modeled using FDTD modeling. The fabricated materials will then be tested using spectrophotometry, FTIR, and ellipsometry to find their electromagnetic properties and see how the experimental results compare the analytical results.

3.1 Layered Metamaterials

The simplest metamaterial to fabricate is the layered metamaterial or metal dielectric stack, as it does not involve lithography or etching to fabricate. An example of this structure can be seen in Figure 6. First, the methods of calculation to determine what layer thicknesses are needed for a structure with certain materials at a certain wavelength will be described. Next, a mathematical framework describing the optical properties of the will be defined, providing a way to analyze and model these structures, and find the reflection and transmission from them. Finally, the different ways in which these structures can be analyzed and viewed as either a layered or homogeneous structure will be described, and how those modeled results will be used with the experimental reflection and transmission to describe the behavior of the structure.
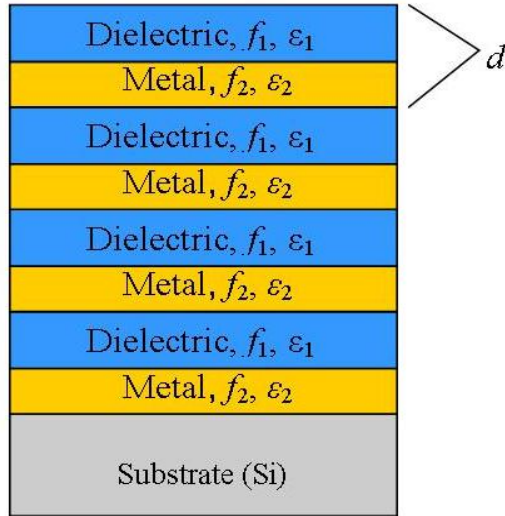
Figure 6 Example of a layered metal dielectric structure.

3.1.1 Layer Thickness Determination

The method for determining the thickness of each layer in the structure is first discussed. Since the structures that are to be fabricated are periodic, with each metal layer having a complementary dielectric layer, one can think of a pair of layers, one metal and one dielectric, being a period with some thickness, *d*, as can be seen in Figure 6. The determination of the thickness of each metal or dielectric layer is based on the permittivity of material and the fraction of space it must take up in a given period, with the overall aim to determine the thicknesses of the materials such that their permittivities cancel out. This derivation begins with the statement defining the effective permittivity of the structure, known as the Maxwell-Garnett approximation,

$$\varepsilon_{eff} = f_1 \varepsilon'_1 + f_2 \varepsilon'_2 \tag{1}$$

where ε_{eff} is the effective permittivity of one period, with electric field of the incident light parallel to the layer and the light propagating into the structure, ε'_1 and ε'_2 are the real parts of the permittivities of each layer, and f_1 and f_2 are the filling fractions, the fraction of the total period thickness taken by each of the materials in a period. If a low, approaching zero, effective permittivity is desired, Equation (1) can be rearranged to form the relation of

$$f_1\varepsilon'_1 = -f_2\varepsilon'_2, \qquad (2)$$

and given that the filling fractions are part of a whole,

$$f_1 + f_2 = 1, \qquad (3)$$

provides everything needed to determine the filling fractions and thickness of each layer of metal or dielectric, given the permittivity of each material [5], [17]. Note how there is a negative on the ε_2 term, owing to the fact that the metals used here have negative permittivity. Using the above equations, one of the filling fractions can be determined as

$$f_2 = \frac{\varepsilon'_1}{\varepsilon'_1 - \varepsilon'_2} \qquad (4)$$

and the other found by using Equation (3), to give

$$f_1 = 1 - f_2. \tag{5}$$

The thicknesses of each layer can then be found by multiplying each filling fraction by the period thickness, d. Using this equation and the material properties for metals and dielectrics, which can be found in Appendix A, and a few chosen values for d, the thickness of each layer in a proposed structure was determined in a spreadsheet for the various materials available. The lengths for d were chosen so that the overall thickness of each layer would ideally be much smaller, and would be more likely to be viewed as a homogeneous structure. The schedules of different period thicknesses and materials can be found in Appendix B. Of the various combinations of materials and thicknesses, only those in which all layers were thicker than 10nm were considered viable for fabrication, as a layer thinner than that was considered to be too thin to be of a consistent film. The metal layer is the first layer deposited, as many metals oxidize when exposed to air, and would be protected by the dielectric layer. Silicon wafers were used as substrates since they are polished and transparent in the infrared, as well as being easy to procure. For most of the structures, a four-period structure was fabricated, as fabricating many periods would allow a more substantial structure, which was hoped to produce more readily observable effects.

3.1.1 Analysis

Once a set of layers is found to be viable for fabrication from the calculations, analysis is done to determine the properties of the stack using methods developed for layered media. This analysis is useful as it provides analytical results for the reflection

and transmission which can be compared to the observed reflection and transmission of the structure. This analysis is based on the treatment of layered media described in [17], and [18]. An example of a multilayer stack of N layers can be seen in Figure 7, where the arrow shows the incident light and incident angle, θ_i, the n's are the indicies of refraction, and d's are the thicknesses of each layer.
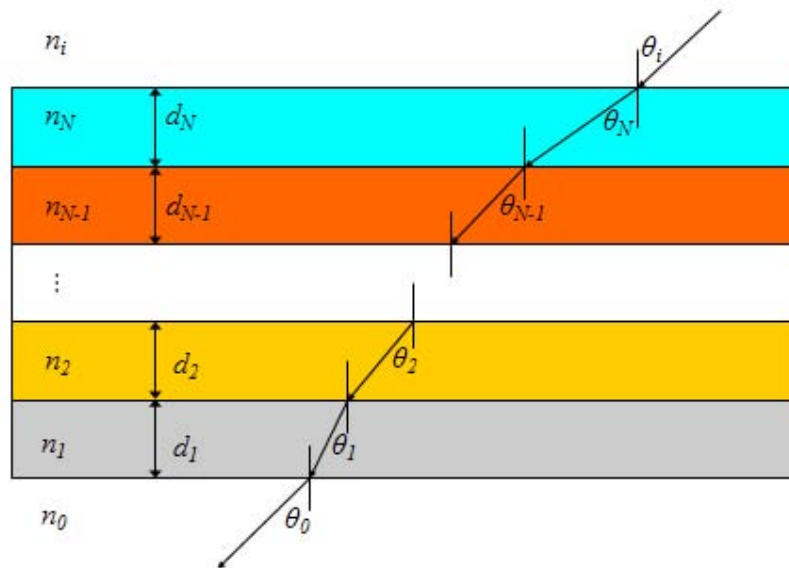
Figure 7 Example of a multilayer stack with N layers, showing the thickness, index of refraction and angle for each layer, as well as the angle of the incident light.

Since this study is dealing with light at other than normal incidence, descriptions and calculations will have to be made for both TE and TM polarized light, and then averaged to give the response of the structure to unpolarized light. Another consequence of this is that the angle at which the light propagates through each layer must be calculated using Snell's Law, and can take the form of

$$\theta_\alpha = \arcsin\left(\frac{n_{\alpha+1}\sin(\theta_{\alpha+1})}{n_\alpha}\right) \tag{6}$$

for some layer α, where θ_α is the angle transmitted into the layer and n_α is the index of refraction in layer α, and $\theta_{\alpha+1}$ is the angle and $n_{\alpha+1}$ is the index of refraction in layer $\alpha+1$, the layer right before layer α. At certain angle and with a certain difference between the indices of refraction between the two layers, total internal reflection (TIR) can occur, which is when all of the beam incident on the interface is reflected due to the higher index of the first material and the incident angle. This phenomenon is indicated when the calculated angle for θ_α becomes 90°, and the light propagates along the interface of the material as an evanescent wave that is not included in this modeling.

The next part of this method involves making 2x2 *M* matrices to describe the propagation of light through an individual layer of the structure, with two different forms for the two different polarizations of light. These forms can be seen for a general layer α, where Equation (7) is for the TE case and Equation (8) the TM case,

$$M_{\alpha,TE} = \begin{pmatrix} \cos(k\,n_\alpha\,d_\alpha\cos\theta_\alpha) & \dfrac{-i}{n\cos\theta_\alpha}\sin(k\,n_\alpha\,d_\alpha\cos\theta_\alpha) \\ -i\,n\cos\theta_\alpha\sin(k\,n_\alpha\,d_\alpha\cos\theta_\alpha) & \cos(k\,n_\alpha\,d_\alpha\cos\theta_\alpha) \end{pmatrix} \tag{7}$$

and

$$M_{\alpha,TM} = \begin{pmatrix} \cos(k\,n_\alpha\,d_\alpha\,\cos\theta_\alpha) & \dfrac{-i}{n\cos\theta_\alpha}\sin(k\,n_\alpha\,d_\alpha\,\cos\theta_\alpha) \\ -i\,n\cos\theta_\alpha\,\sin(k\,n_\alpha\,d_\alpha\,\cos\theta_\alpha) & \cos(k\,n_\alpha\,d_\alpha\,\cos\theta_\alpha) \end{pmatrix} \qquad (8)$$

where θ_α is the angle, n_α the index of refraction and d_α the thickness in layer α. The term k, the wavenumber, is defined by

$$k = \frac{2\pi}{\lambda}. \qquad (9)$$

Using these matrices to describe a layer, a stack of layers is built up by multiplying the M matrices for each individual layer to form an M matrix for the stack as follows,

$$M = M_1\,M_2\,M_3\,...M_N = \begin{pmatrix} m_{1,1} & m_{1,2} \\ m_{2,1} & m_{2,2} \end{pmatrix} \qquad (10)$$

with separate M matrices for the TE and TM cases, and both following the same form given in Equation (10). Once an M matrix has been formed, the complex reflectance and transmittance can be calculated, using

$$r_{TE} = \frac{(m_{1,1} + n_0 \cos\theta_0\, m_{1,2})\,n_i \cos\theta_i - (m_{2,1} + n_0 \cos\theta_0\, m_{2,2})}{(m_{1,1} + n_0 \cos\theta_0\, m_{1,2})\,n_i \cos\theta_i + (m_{2,1} + n_0 \cos\theta_0\, m_{2,2})}, \qquad (11)$$

and

$$t_{TE} = \frac{2 n_i \cos \theta_i}{(m_{1,1} + n_0 \cos \theta_0\, m_{1,2})\, n_i \cos \theta_i + (m_{2,1} + n_0 \cos \theta_0\, m_{2,2})}, \quad (12)$$

for the TE case, and

$$r_{TM} = \frac{\left(m_{1,1} + \dfrac{\cos \theta_0\, m_{1,2}}{n_0} \right) \dfrac{\cos \theta_i}{n_i} - \left(m_{2,1} + \dfrac{\cos \theta_0\, m_{2,2}}{n_0} \right)}{\left(m_{1,1} + \dfrac{\cos \theta_0\, m_{1,2}}{n_0} \right) \dfrac{\cos \theta_i}{n_i} + \left(m_{2,1} + \dfrac{\cos \theta_0\, m_{2,2}}{n_0} \right)} \quad (13)$$

and

$$t_{TM} = \frac{2 \cos \theta_i}{\left(m_{1,1} + \dfrac{\cos \theta_0\, m_{1,2}}{n_0} \right) \cos \theta_i + \left(m_{2,1} + \dfrac{\cos \theta_0\, m_{2,2}}{n_0} \right) n_i}, \quad (14)$$

for the TM case, where n_0 is the index of the substrate below the stack, n_i is the index of the material above the stack, and θ_i and θ_0 the angles of the light entering and exiting the stack, respectively. The reflection and transmission can then be found for each case. The equation for reflection is the same for both cases,

$$R_{TE,TM} = \left| r_{TE,TM} \right|^2, \quad (15)$$

28

and the transmission is either

$$T_{TE} = \frac{n_0 \cos \theta_0}{n_i \cos \theta_i} \left| t_{TE} \right|^2 , \tag{16}$$

or

$$T_{TM} = \frac{n_i \cos \theta_0}{n_0 \cos \theta_i} \left| t_{TM} \right|^2 , \tag{17}$$

depending on the polarization. To get the reflection and transmission for unpolarized light, the average of the reflection and transmission of the two polarizations is taken. This averaged value is what will be used to determine the reflection and transmission from the structure as it correctly compares to the unpolarized measurements made by the spectrophotometer and FTIR. This type of modeling is simple, and has shortcomings and places where it breaks. One of these places is the case of total internal reflection, where the angle of the transmitted light goes to 90˚. At this point the model breaks down and the results are not valid, as the light then travels as a decaying evanescent wave along the boundary between the two materials, which this method of modeling does not take into account. As a result of this, large angles of incidence cannot be accurately modeled in certain situations, and can give unrealizable and incorrect results that need to be discarded, such as transmission and reflection values greater than 100%.

Using this mathematical treatment, the fabricated structures could be analyzed in two different ways. The first way is to view the structure as simply a layered structure, on a substrate of silicon, and compute the reflection and transmission from that. The mathematical framework described above is used to model each layer in the structure and the substrate, and the reflection and transmission calculated. Another method is to treat the fabricated structure as one homogeneous slab, on a substrate of silicon, with an index that is determined by the complex effective permittivity of one period of the structure using the effective media approximation given in Equation (1) and the complex permittivity of the metal and dielectric, so the index of the homogeneous layer can be modeled as

$$n_{eff} = \sqrt{\varepsilon_{eff\ complex}} = \sqrt{f_1(\varepsilon_1{'}+i\varepsilon_1{''}) + f_2(\varepsilon_2{'}+i\varepsilon_2{''})}. \tag{18}$$

The refractive index derived from the complex effective permittivity, is then applied to the whole thickness of the structure. The reflectance and transmittance of the structure on the substrate is then calculated, using only the two layers of structure and substrate. These two different methods of modeling can be seen in Figure 8.
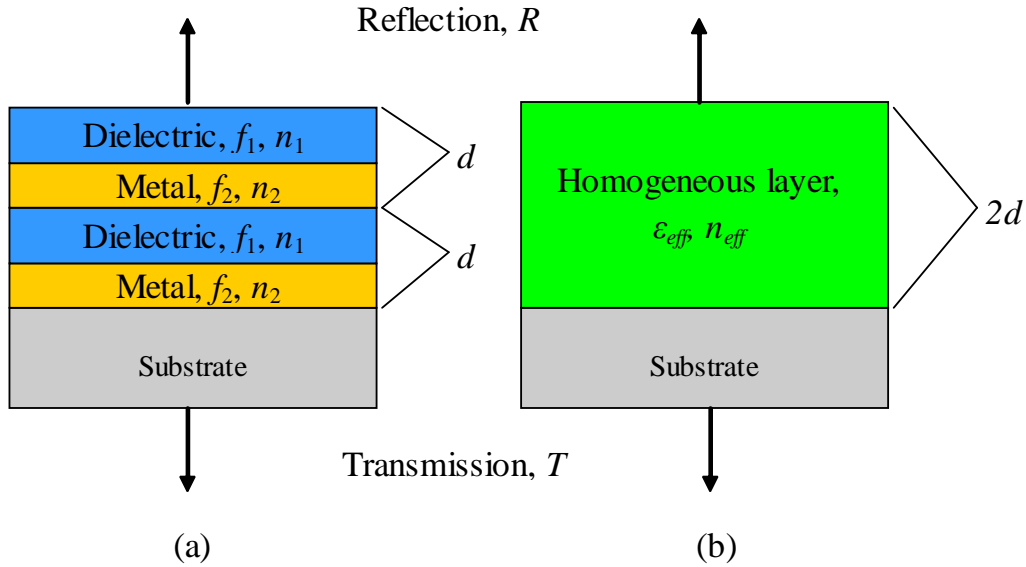
Figure 8 Comparison of structures analyzed as layers (a) and a homogeneous media (b).

3.1.2 Testing and Results

After the layers were deposited, they are tested using a few different measurement methods. This was done to get as much information about the fabricated structures as possible, and be able to determine whether they were behaving like layered media or homogeneous media. The main technique used was finding the reflection and transmission of a sample using a Bomem 157S FTIR for measurements in the IR, and a Cary 5000 spectrophotometer for visible to near IR measurements. These measurements were done to see the reflection and transmission of the structure, with special attention paid to wavelengths where the transmission peaks and the reflection dips; these are indicators of the permittivity approaching zero. This is due to the fact that as the permittivity of the structure changes, the index of the structure changes as well, and when the index of the layers becomes equal to the square root of the index of the substrate, and

acts like an antireflection coating, and is indicative of the structure acting like a homogeneous structure, and having a permittivity and index that are decreasing [17].

Samples were also measured using ellipsometry, where the material properties, and not just the reflection and transmission, could be measured. A few different types of ellipsometry measurements were made, such as taking the whole thickness of the deposited structure, *i.e.* the thickness of all the layers combined, and having the optical parameters of the whole structure fit to the collected data, directly finding the effective index of refraction and permittivity of the structure.

Data from the analysis of the structures as both layered and homogeneous media is then compared to the experimental measurements. The differences among them will be important, with the model closest to the experimental data being the one that more closely describes the behavior of the structure. Differences among these results will be discussed and explanations for these differences will be sought. Comparisons will also be made with the results of the ellipsometry measurements by taking the index of refraction calculated by the measurement, and finding the refection and transmittance and comparing it to the measured reflection and transmission.

3.2 3D Metamaterials

The other main thrust of this investigation is the fabrication of the more complex fishnet structure, which can show a negative index of refraction. The methodology here starts with analytically describing the magnetic resonators and using that description and the capabilities of the direct write laser system to determine the layer thicknesses and dimensions of the structure to be created. Once this design has been made the structure is

fabricated, tested, and simulated, with the results of the simulation compared to those of the testing.

3.2.1 Fishnet design

The design of the fishnets used in this study follow the method put forward in [5], in which two components, one that is resonant and provides the negative permeability, is combined with non resonant parts that provide negative permittivity. The fishnet combines these two components by having thick magnetic strips, designed to resonate and provide the negative permeability, combined with thin electric strips, designed to provide negative permittivity, at a right angle to the magnetic strips. Together, these two elements provide the components for a negative index to be formed. An illustration of the fishnet structure can be seen in Figure 9.
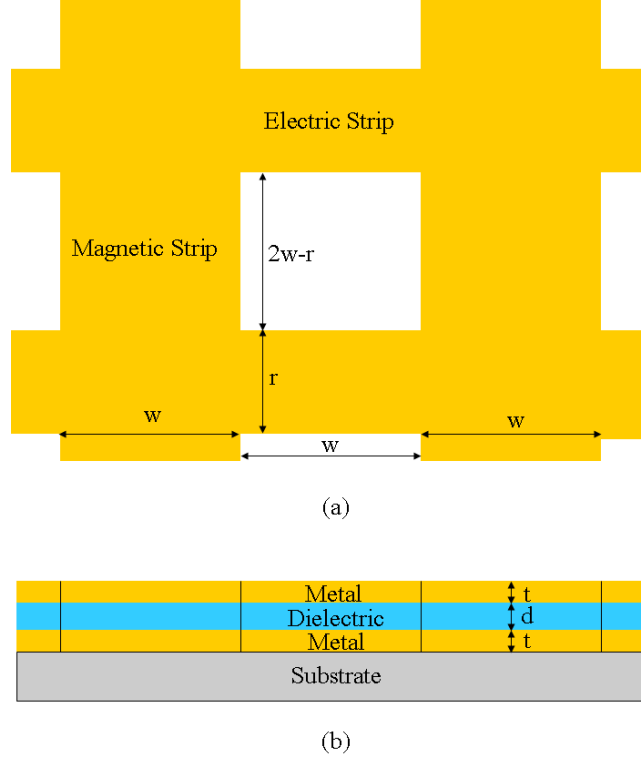
Figure 9 Illustration of the fishnet metamaterial. (a) shows a top view and the electric and magnetic strips, along with the widths of each and the period of the structure. (b) shows a side view with the layers of the structure and their thicknesses.

The design of the magnetic strips followed the analytical description given in [5]. Equation (19) describes where the magnetic resonant wavelength would be based on structural and material parameters, with a period of two times the width, *w*, of the resonator.

$$\varepsilon'(\lambda_m) = 1 - \frac{n_d^2}{t\kappa}\left[1 + \coth\left(\frac{d\kappa}{2}\right)\right] \tag{19}$$

where λ_m is the wavelength at which the strips are resonant, $\varepsilon'(\lambda_m)$ is the real part of the metal permittivity at the resonant frequency, n_d is the index of the dielectric spacer, *d* is

the thickness of the dielectric spacer, t is the thickness of the metal, and κ is defined as

$$\kappa = \sqrt{\left(\frac{\pi}{w}\right)^2 - \left(\frac{2\pi n_d}{\lambda_m}\right)^2},\qquad(20)$$

where w is the width of the resonator. Notice from Equation (20) that there is a point that defines the largest value of w,

$$w = \frac{\lambda_m}{2n_d}.\qquad(21)$$

κ becomes imaginary where w is larger than this.

Using these equations, a MATLAB program is written to help determine the width of the resonator. Since it is a challenging mathematical problem to solve the above equations exactly, and the range of values for the sizes and thicknesses are restricted to certain ranges and are not continuous, the MATLAB code was written to compute values for the right-hand side of Equation (19), with t, w, and d being incremented. The values of t and d are incremented from 10 to 500nm by 1nm increments, the range and estimated precision of the sputtering system and deposition monitor, and w from 1μm to the maximum width defined in Equation (21), incremented by 40nm, using the range and precision of the Heidelberg laser writer. The values for λ_m, n_d, and $\varepsilon'(\lambda_m)$ are all fixed, based on the wavelength at which the resonance is desired to occur. The value of each combination is calculated following the right side of Equation (19), and then subtracted from the value of $\varepsilon'(\lambda_m)$. The difference is then stored in a matrix and the program then

selects and displays the combinations that have the smallest difference, which are the structures that most closely fit the model in Equation (19).

Once the width of the magnetic strips was determined, the electric strips and the size of the spacing could be determined. The negative permittivity comes from the material used in the resonator, and is not dependent on the structure. With that fact, it is then desirable to make the width of these strips, r, as small as possible to reduce the loss of the structure, due to the losses associated with metals [5]. The same period of $2w$ is used, so that the structure is symmetric, with the space between the strips simply $2w$-r.

3.2.2 Analysis

Unlike the simple layered structures, the reflection and transmission of the fishnet structure cannot be modeled and analyzed using the analytical methods, like was done with the layered metamaterials, and instead must be simulated. The Lumerical® electromagnetic FDTD program is used to simulate this structure to find the reflection and transmission from it. The simulation will be run twice, one for each polarization of light, and the results averaged, so they can be compared to the unpolarized experimental measurements.

3.2.3 Testing

After the sample is fabricated, it will be tested to find the reflection and transmission of the structure using the FTIR. After these measurements are made, they would then be compared to the simulated results, and any discrepancies between the two results investigated. In addition to just looking at the reflection and transmission, the

absorption will also be of interest. This is because the resonance that allows

metamaterials to create a negative permeability also creates loss, and a peak in absorption

would be indicative of this.

3.3 Summary

   This chapter outlined how this investigation will be conducted. The method for

how the structure of a layered metamaterial is designed to have a low permittivity and

how these structures can be analyzed as either layered or homogeneous was described.

Details were also given on the testing of the fabricated structure, and how this structure

would be compared to the analysis to determine if a low permittivity was reached. The

design of 3D metamaterials was also discussed, with the equations that describe the

magnetic resonance that causes a negative permeability, and the process to solve for the

best dimensions for the design. The simulation and testing of this structure were also

discussed.

IV. Results

This section will detail the development, fabrication, simulation and testing of fabricated structures. This section will be broken into two sections, one on the layered materials and the other on the 3D materials. Within each section, each fabrication will be described individually and include all the results that were collected.

4.1 Layered Metamaterials

Most of the investigations made were in layered metamatierials. These fabrications used a variety of materials and were designed for three different wavelengths 0.544μm (544nm), 4.45μm and 5μm. After the fabrication of the first layer set, a change in the overall aim of the layered metamaterials occurred. Instead of designing these materials for visible light, they would instead be designed for the IR, where they could be better utilized in other research and take advantage of the ease at which IR is able to pass through the silicon wafers used as substrates. Initially, all layers were deposited on one side polished wafers, but this was found to scatter the radiation and result in low transmission. Layers that were already made were then polished to improve their transmission, and subsequent structures were fabricated on double sided polished wafers.

4.1.1 Silver-Alumina

Layer deign.

The first structure fabricated was a multilayer stack of silver (Ag) and alumina or aluminum oxide (Al_2O_3). Using material properties found on the PhotonicsDB tool in [19], which interpolated the published results of [20] for Ag and [21] for Al_2O_3, the ratio

of f_1 to f_2 was found to be 4.0023 for 544nm. Using this and Equation (4), the different layer thicknesses were found for period thickness of d=75, 100, 150, and 200nm. These different layer combinations were then simulated using the PhotonicsSHA-2D tool, which computed the reflection and transmission of the structure using spatial harmonic analysis. A four-period structure (four layers of each material) and no substrate was simulated and to find the reflection and transmission [19]. This tool was used for this structure only, as it has a limited set of material data that can be used, which did include these materials at visible wavelengths, but did not include data for the IR wavelengths that were used in the other structures. The d=150nm period material, with thicknesses of 30 and 120nm, for Ag and Al_2O_3, respectively, was then selected for fabrication, as it had increased transmission and absorption and reduced reflection near the 544nm wavelength, as can be seen in Figure 10.
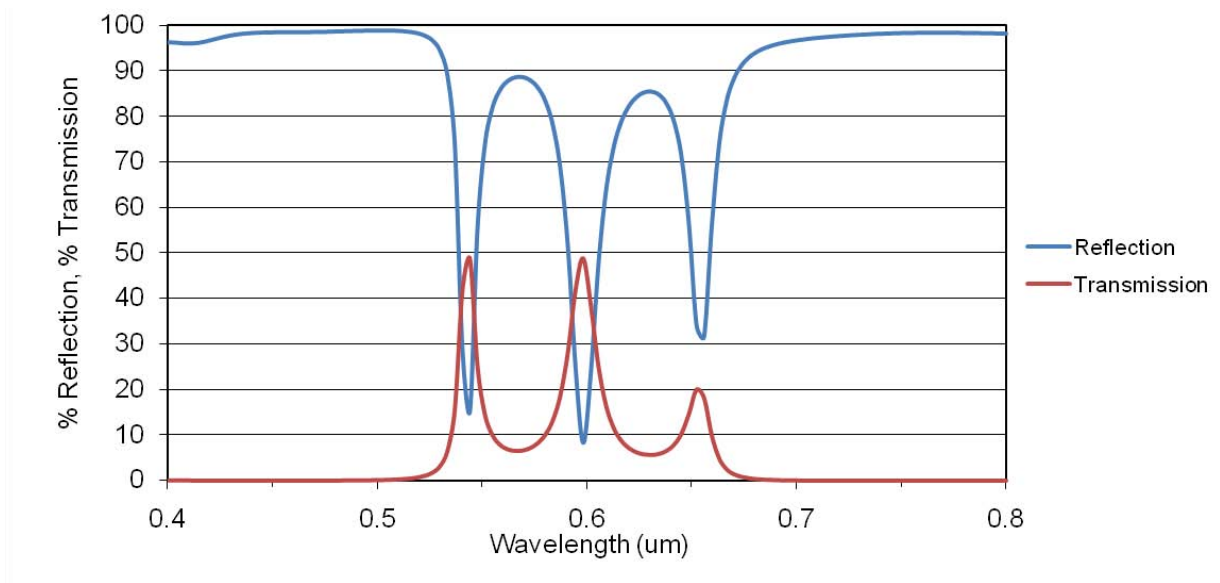
Figure 10 Simulated reflection and transmission of the Ag-Al$_2$O$_3$ structure using the PhotonicsSHA-2D tool, showing the peak in transmission and dip in reflection at 544nm, the first one of the three features on the graph.

The effective permittivity and index were then determined by viewing the structure as homogeneous and taking the weighted sum of the real part of permittivity of each material as was done in Equation (1), and for the complex index taking a weighted sum of the complex permittivity and then taking the square root of it, as was done in Equation (18). The effective permittivity and index as a function of wavelength can be seen in Figure 11 and Figure 12, respectively.
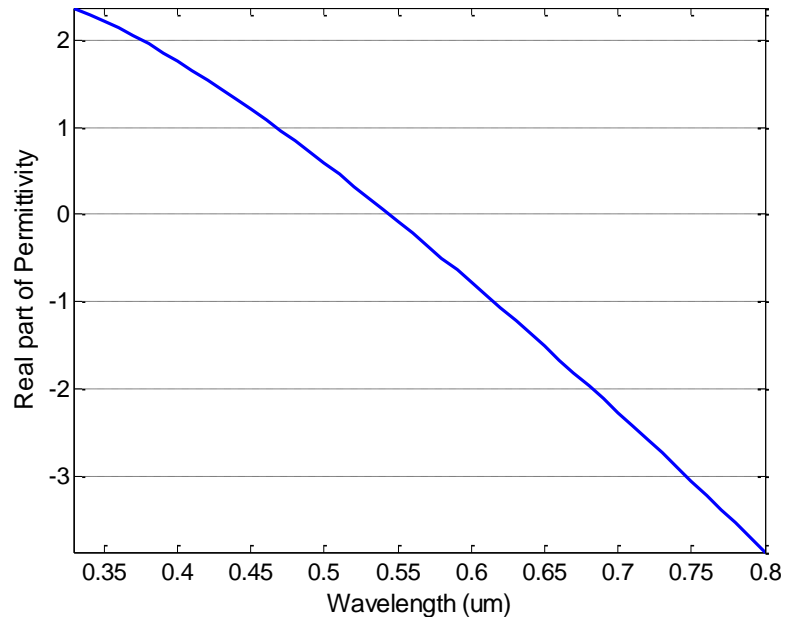
Figure 11 Effective permittivity of Ag- Al$_2$O$_3$ structure. The permittivity can be seen to go to zero at 544nm.
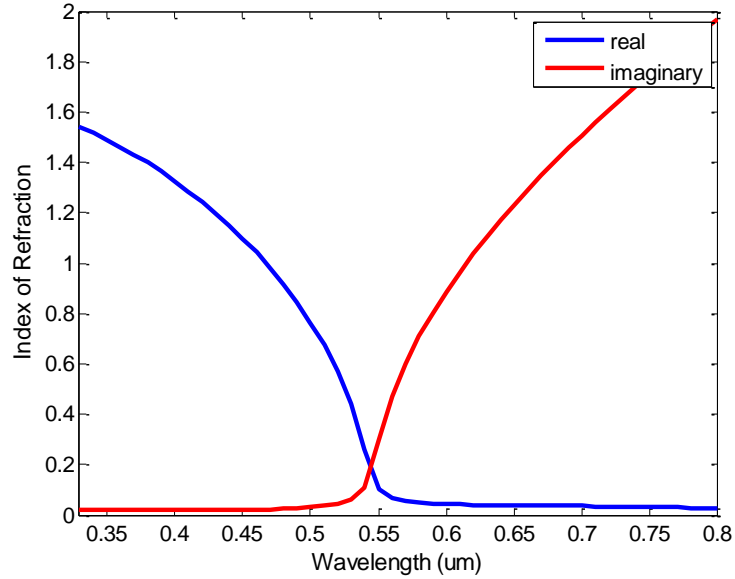
Figure 12 Effective index from the complex effective permittivity of Ag-Al₂O₃ structure.

Layer fabrication.

An overview of the process used to deposit materials can be seen in Appendix C, and the key parameters for the deposition being displayed in Table 2. Silicon was used as the substrate in this fabrication.

Table 2 Sputtering parameters for Ag- Al₂O₃ structure

	Pre-sputter Voltage/Power	Pre-sputter Time	Deposition Voltage/Power	Approximate Deposition Time	Deposition Thickness
Ag	500V	1 minute	340V	6.5 minutes	30nm
Al₂O₃	200W	1 minute	200W	30 minutes	120nm

After fabrication, a piece of a sample was cleaved off and put vertically into the Hitachi S4700 scanning electron microscope (SEM) to examine the profile of the layers. A micrograph of the layers can be seen in Figure 13. This figure shows that the

fabricated structure matches very closely with the designed structure, and the desired layer thicknesses.
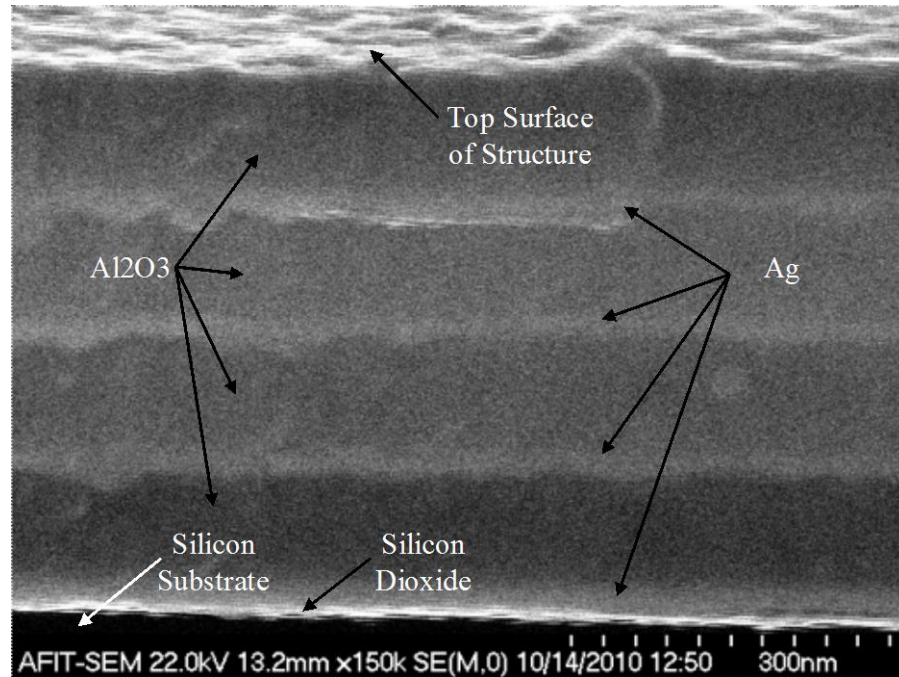
Figure 13 SEM micrograph of the fabricated layers, showing the complete stack as well as the silicon substrate. The reason why the last layer of the stack is thought to be very bright is due to the thin layer of silicon dioxide present on the silicon wafer.

Testing and Analysis.

The first analysis done was to model the fabricated structure as layered media, and compute the behavior of the structure using the mathematical methods described previously. This modeling was done only for the reflection, as the silicon wafer used as substrate would not allow any transmission, and at an incident angle of 3°, the angle at which the spectrophotometer was able to take reflection data. A 2nm thick layer of silicon dioxide was also added to the model to account for its presence on the substrate,

which is seen as the bright layer in Figure 13. The results of these calculations can be seen in Figure 14 and Figure 15.
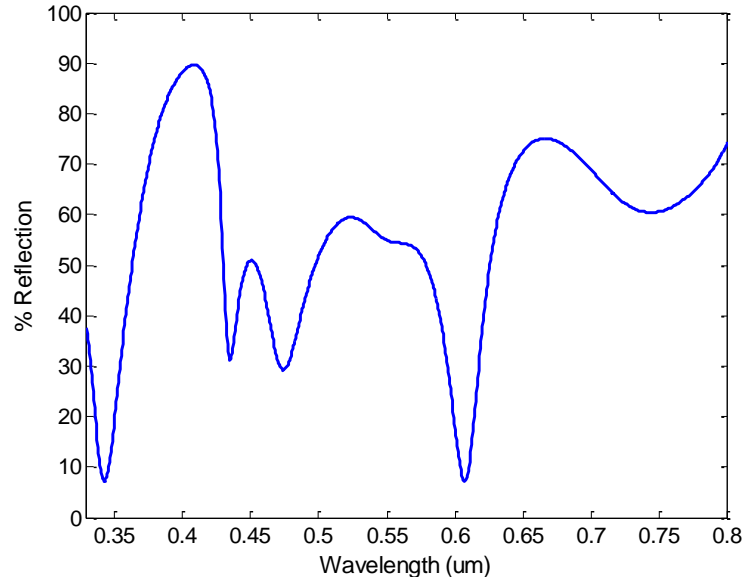
Figure 14 Plot of reflection from the Ag- Al$_2$O$_3$ structure modeled as layered material at a 3° angle of incidence. Note that there total internal reflection is seen at 0.419-0.644μm, and 0.754-0.8μm, where the angle between two interfaces goes to 90°, and the reflection values are not accurate.
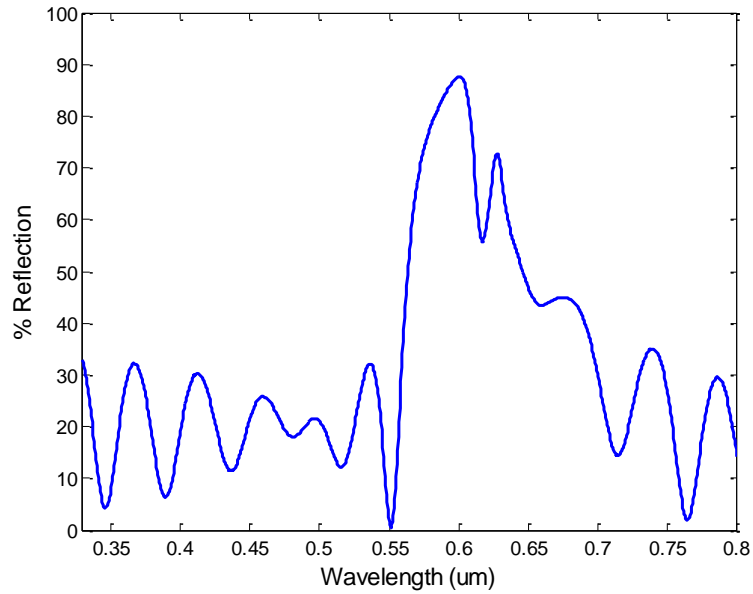
Figure 15 Plot of reflection from the Ag-Al$_2$O$_3$ structure modeled as homogeneous at a 3° angle of incidence. Note that there total internal reflection is seen at 0.608-0.8μm, where the angle between two interfaces goes to 90°, and the reflection values are not accurate.

Considering Figure 14 and Figure 15, this way of modeling the structures does not work very well because of the large contrast between the refractive indices of Ag and Al_2O_3, which leads to total internal reflection at even small angles, such as the 3° incidence here. When the computed angles for the two simulations are examined, it is found that the layered model entered total internal reflection in the areas of 0.419-0.644μm, and 0.754-0.8μm, the homogeneous model entered it for 0.608-0.8μm, as was seen from the angles that were calculated for the boundaries between layers of material going to 90°. TIR and the evanescent nature of the light at the interface is not taken into account in this modeling, and as such, the results here are not accurate for the wavelengths where TIR is reached. Reflectance measurements were also made with a Cary spectrophotometer, the results of which can be seen in Figure 16.
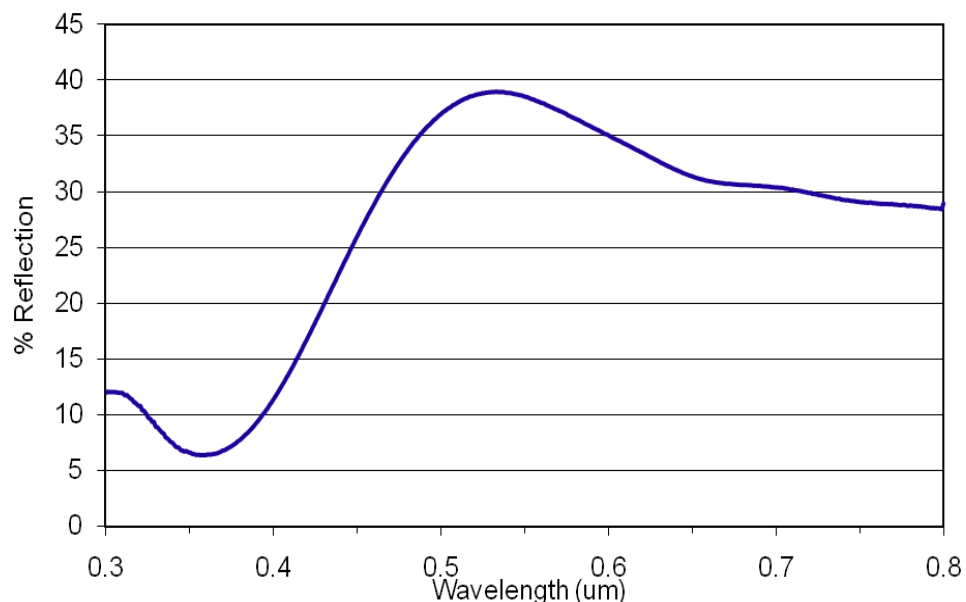
Figure 16 Plot of the reflection data taken by the spectrophotometer for the Ag- Al_2O_3 structure at an incident angle of 3°.

FTIR measurements were also made, though these layers were designed to operate at visible wavelengths, and it was thought that this test still may provide interesting data. It was found that these layers did not allow any transmission, which was due to the reflection of the silver and also the rough backside of the wafer, which would scatter anything that did get transmitted, but did provide reflectance measurements, which can be seen in Figure 17. The data is unremarkable, as it just shows high reflection across the infrared.
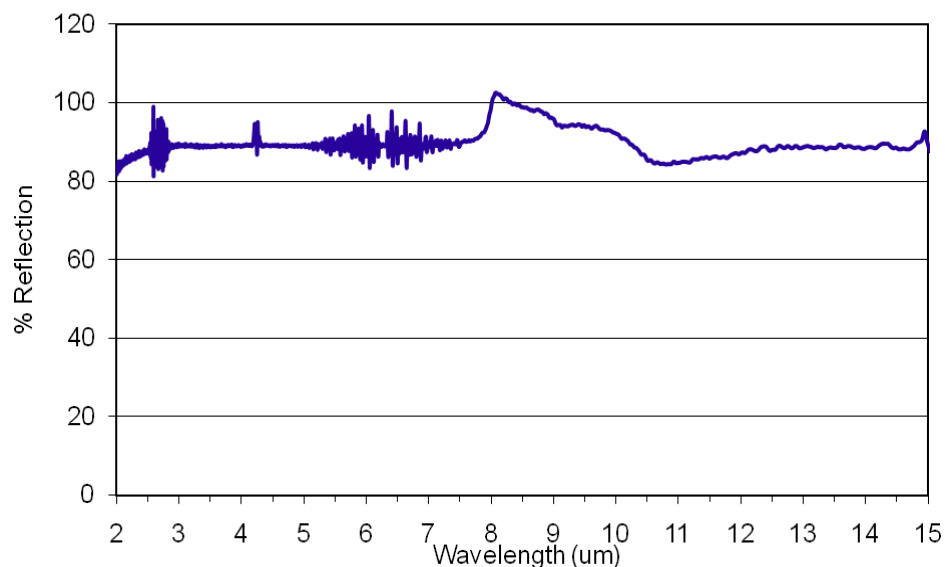
Figure 17 Reflectance measurement of Ag- Al$_2$O$_3$ structure in the infrared at an angle of 61.3°. Notice that there is a peak that goes beyond 100% at 8μm and is not reliable data, likely due to a calibration error.

Ellipsometry measurements were performed on the sample using a Horiba ellipsometer, with a 70° angle of incidence and scanning through a spectral range of 0.6-4.7eV (2.06μm-264nm). The data collected was then analyzed to fit a model the

deposited material as one homogeneous layer, and the optical properties calculated. The

results of this testing can be seen in Figure 18 and Figure 19.
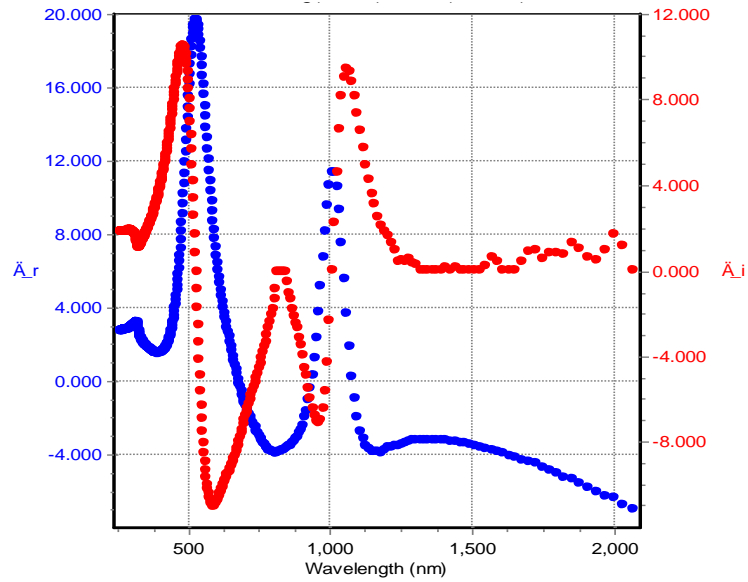
Figure 18 Calculated permittivity of the Ag-Al$_2$O$_3$ structure as homogeneous using ellipsometry. The blue points and left axis are for the real part of the permittivity, and the red points and right axis display the imaginary parts. Note that the plots are a function of wavelength in nm.
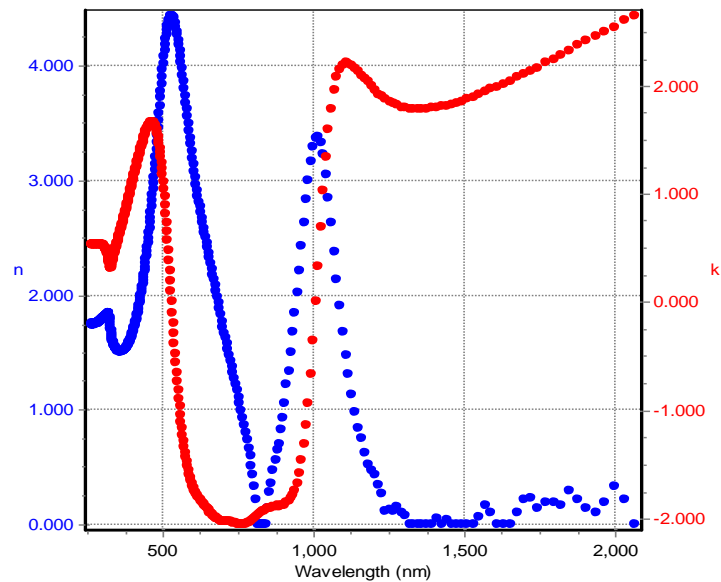
Figure 19 Calculated refractive index of the Ag-Al$_2$O$_3$ structure as homogeneous using ellipsometry. The blue line and left axis are for the real part of the permittivity, and the red points and right axis display the imaginary parts. Note that the plots are a function of wavelength in nm.

Figure 18 shows that the point where the permittivity goes to zero is not near the 544nm mark, but around 700nm. An additional inconsistency with this measurement is the fact that the imaginary terms for both the permittivity and index go negative, which is not possible for a dispersive material, and indicates an error in the parameter extraction, though this error may only be in the extraction of the imaginary part.

When all the data and modeling up to this point is considered, it is hard to draw any conclusions about what is happening in this structure and its response to the incident light. This is due to the fact that the modeling of the structure breaks down due to total internal reflection in the calculations, making a large portion of the modeled results unreliable. Additionally, the simple modeling of the structure as just a homogeneous slab and then solving for the effective index and permittivity using ellipsometry was not accurate either, as the extracted parameters showed negative complex parts, indicating gain, which is certainly not correct.

Considering this experience, a new approach was taken, that would start with the basic materials and build up a structure, testing the individual layers and then fabricating just one period for testing. These new samples would use the same deposition parameters and thicknesses as those used in the four-layer stack, and would be fabricated on substrates of silicon and glass microscope slides. Fabricating samples in this way was advantageous in that it would then provide samples that had a simple structure, only one or two layers, that could be better analyzed with the ellipsometer, and were also on transparent substrates, allowing transmission measurements to be made. These samples would then be analyzed with a J.A. Woollam V-VASE ellipsometer. By using single layers and a one period stack, the ellipsometer should be able to create more accurate

47

measurements and data than in its previous use. This is a powerful tool that is able to find the optical properties and thickness of the deposited layers, as well as the reflection and transmission of a sample.

Analysis and measurements were then done on the one period Ag-Al$_2$O$_3$ structure fabricated on glass. Using the ellipsometer, reflection measurements were made at 20˚, the smallest angle the instrument could go to for reflection, and 0˚ for transmission. Using this new set of samples and measurements, the reflection and transmission of the structure as a layered or homogeneous structure is done, though using the material models from before. The results of the layered model can be seen in Figure 20 and Figure 21, while the homogeneous results are displayed in Figure 22 and Figure 23. The measured reflection and transmission results are also plotted and can be seen in Figure 24 and Figure 25. The reflection values for both models show TIR, and areas where the results cannot be trusted.
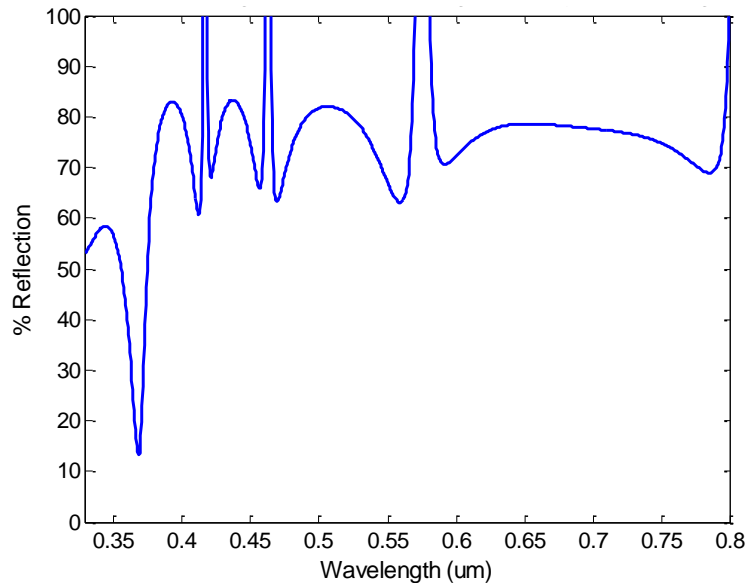
Figure 20 Plot of the reflection from one period of the Ag-Al$_2$O$_3$ structure on glass, modeled as layers at 20˚ incidence. This model goes into total internal reflection at all wavelengths, and the data produced cannot be accurate as can be seen from values greater than 100%.
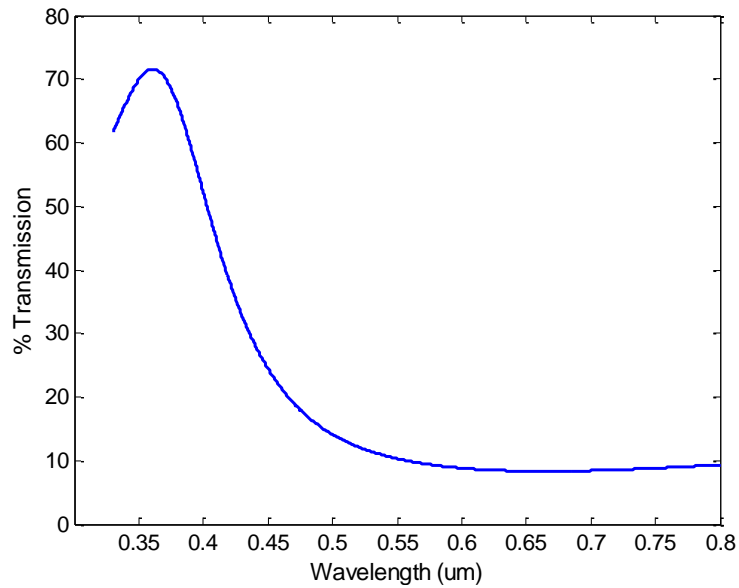
Figure 21 Plot of the transmission from one period of the Ag-Al$_2$O$_3$ structure on glass modeled as layers at 0° incidence.
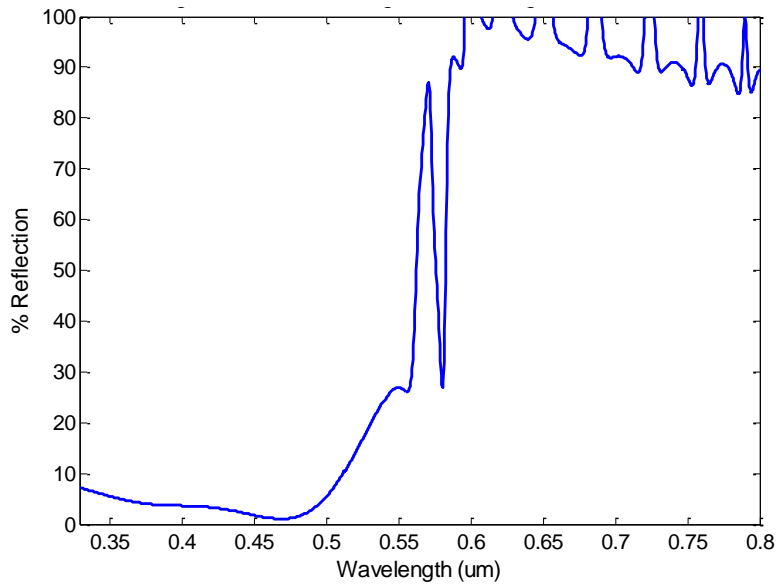
Figure 22 Plot of the reflection from one period of the Ag-Al$_2$O$_3$ structure on glass modeled as homogenous at 20° incidence. This model goes into total internal reflection in the 0.558-0.8μm range, and the data produced cannot be accurate as can be seen from values greater than 100%.
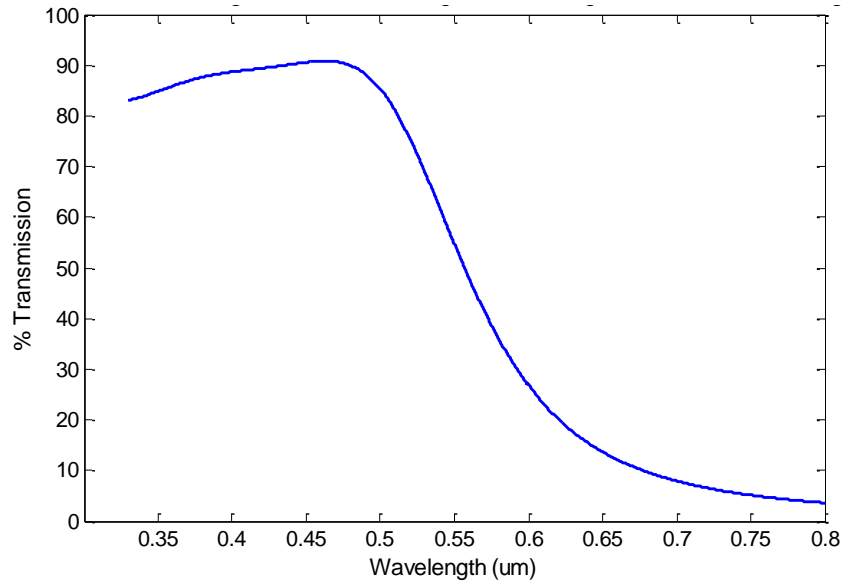
Figure 23 Plot of the transmission from one period of the Ag-Al$_2$O$_3$ structure modeled as homogeneous.
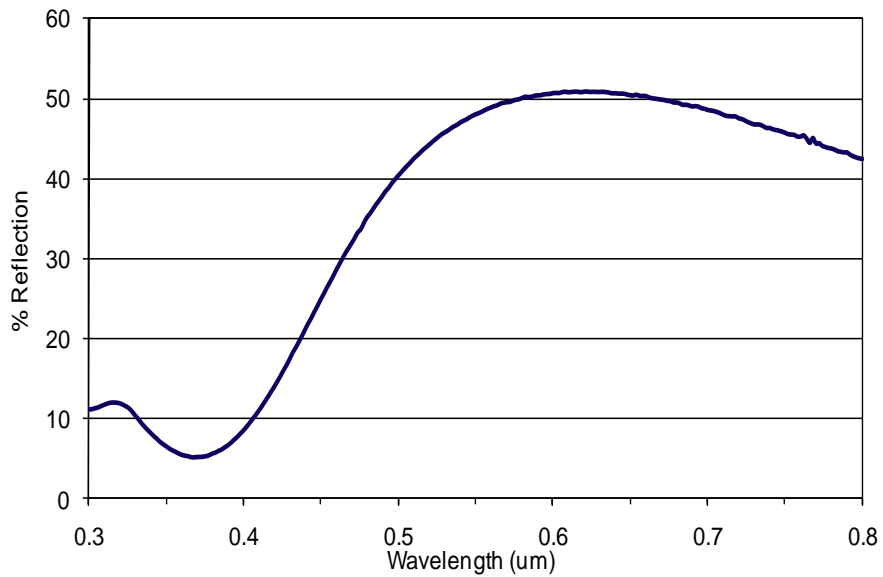
Figure 24 Plot of the reflection data from the single period of the Ag-Al$_2$O$_3$ structure on glass at 20°incidence.
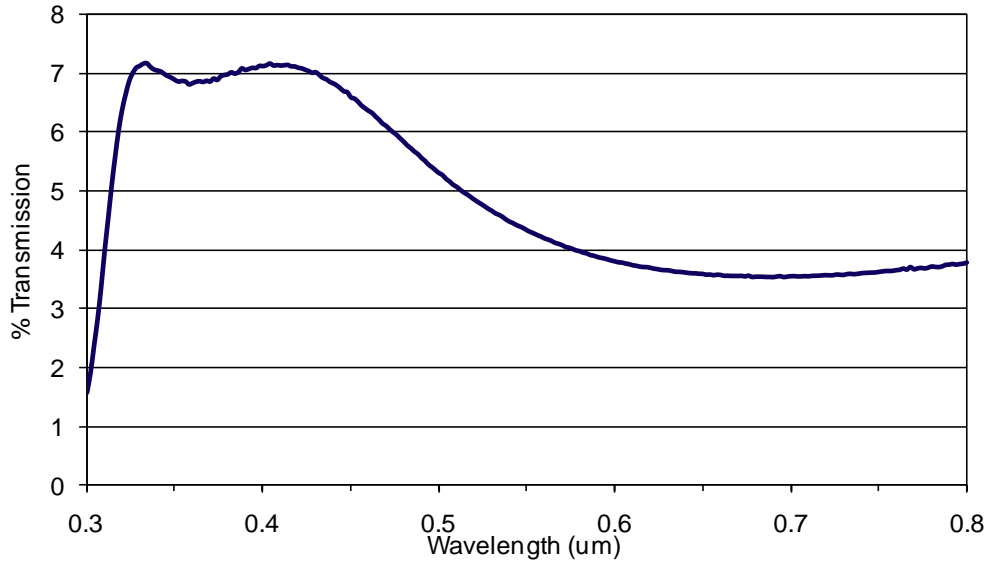
Figure 25 Plot of the collected transmission data from a single period of the Ag-Al$_2$O$_3$ structure on glass at 0° incidence.

A good comparison of the transmission results can be seen in Figure 26. Looking a this plot, it is clear that a closer fit between the model and the measurement can be seen, with all having peaks in the same area, however, the amplitudes of these peaks are quite different from each other.
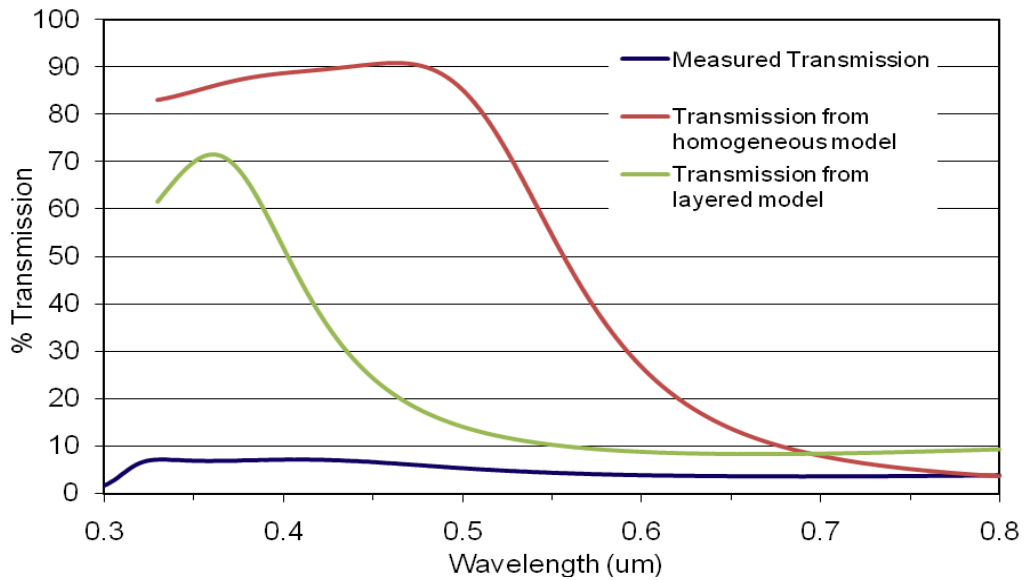
Figure 26 Plot of the modeled and experimental transmission data. Notice how all rise at similar wavelengths and show similar shapes, though the amplitude of the experimental data is much lower than the others, likely due to loss not included in the material models.

To investigate this difference, spectrophotometer measurements were made of the one period sample, as the ability of this instrument to capture diffuse reflection would indicate if light is being scattered by the sample and not collected by the ellipsometer measurements. These measurements were made, and they were found to be almost identical to the ellipsometer measurements, indicating that the material was absorbing the light, and not just scattering it, requiring different optical constants for the materials to be found.

The optical constants for the Ag and Al_2O_3 were then found using ellipsometry data from the Ag, Al_2O_3 and one period structure on glass, as well as the transmission from the Ag on glass. This data was fed into the ellipsometer software package, and then a best fit for the thickness of the deposited materials and optical parameters run. This fitting indicated that the layers of Ag and Al_2O_3 in the one period structure on glass were

38 and 108nm respectively. Plots comparing the indices of the Ag and Al_2O_3 used in the

modeling and those that are measured can be seen in Figure 27 and Figure 28.
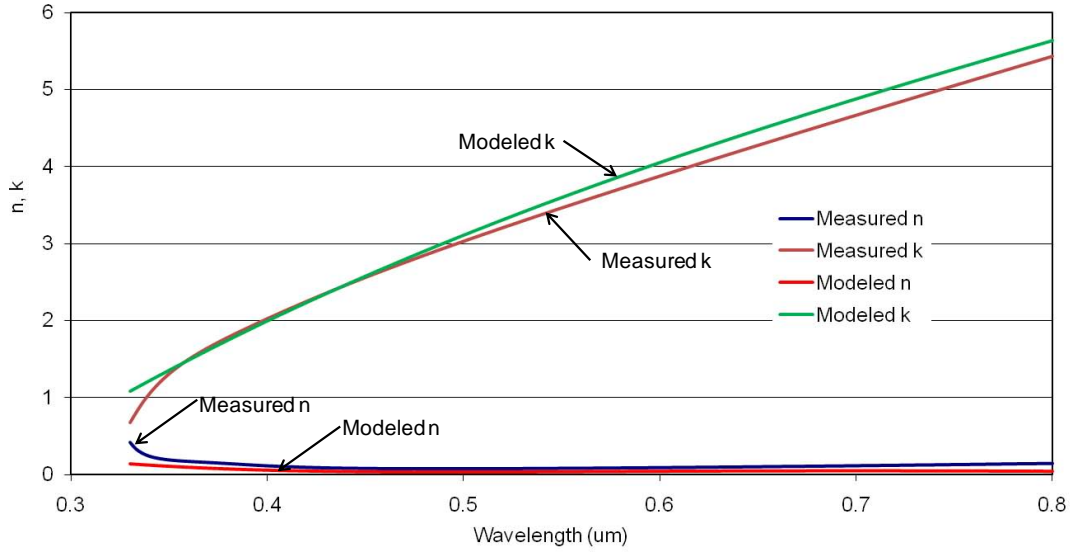
Figure 27 Plot of the modeled and measured index of Ag deposited on glass.
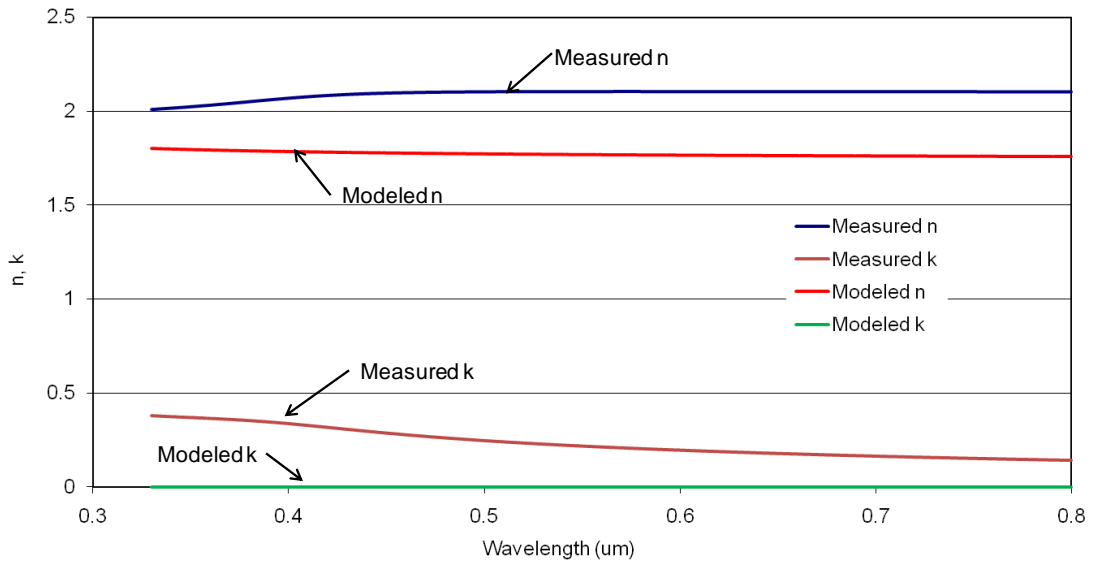
Figure 28 Plot of the modeled and measured index of Al2O3 deposited on glass.

From these figures, it is seen that the index of the silver is pretty close to the modeled value, however, the Al_2O_3 was a bit different, having an index of around 2.1, instead of the modeled 1.7, and was not lossless. Using these results, calculations were then rerun for the one period stack and new indices to find the new ENZ point and effective index. The results of this can be seen in Figure 29 and Figure 30.
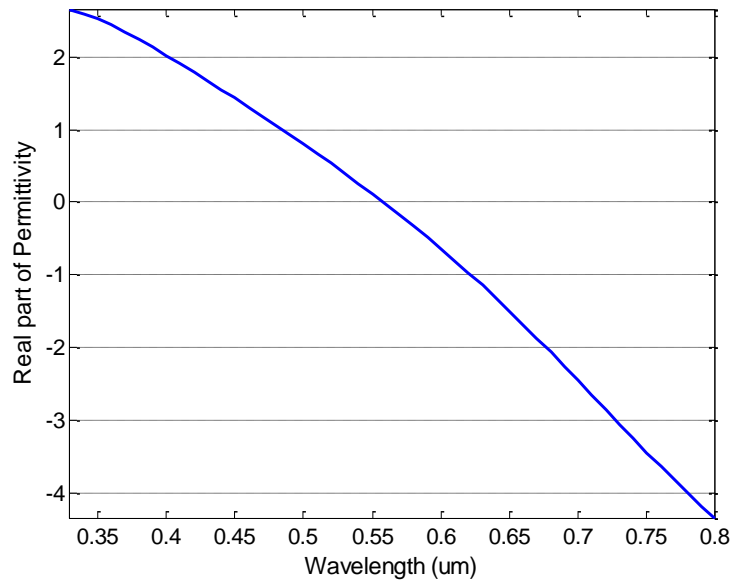
Figure 29 Plot of the effective permittivity of the one period Ag-Al$_2$O$_3$ structure on glass using the permittivity for the materials derived from the measured indices.
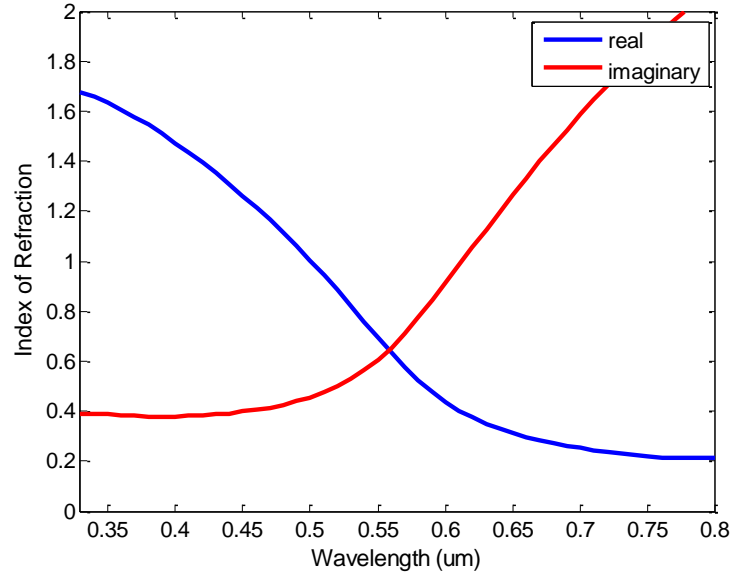
Figure 30 Plot of the effective index of the one period Ag-Al$_2$O$_3$ structure on glass using the measured indices of the materials.

Taking the effective index and layer thicknesses, the models of the single period on glass as layered and homogeneous can then be redone, and the results for transmission, which is used since the values do not become invalid due to TIR, are shown in Figure 31 and Figure 32. A plot is then made of all three results to compare them, and can be seen in Figure 33.
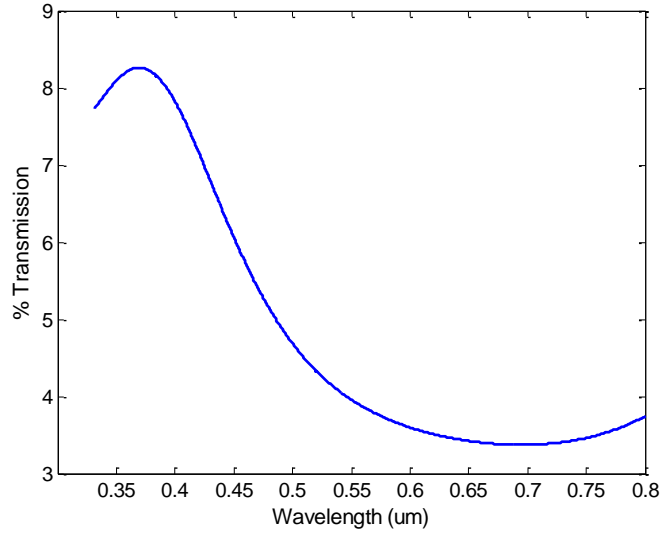
Figure 31 Plot of the transmission of the one period Ag-Al$_2$O$_3$ structure on glass modeled as layers.
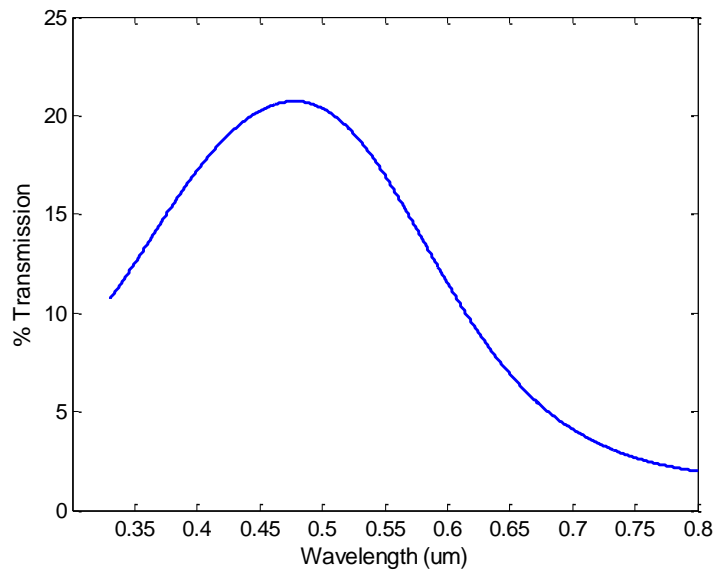
Figure 32 Plot of the transmission of the one period Ag-Al$_2$O$_3$ structure on glass modeled as homogeneous.
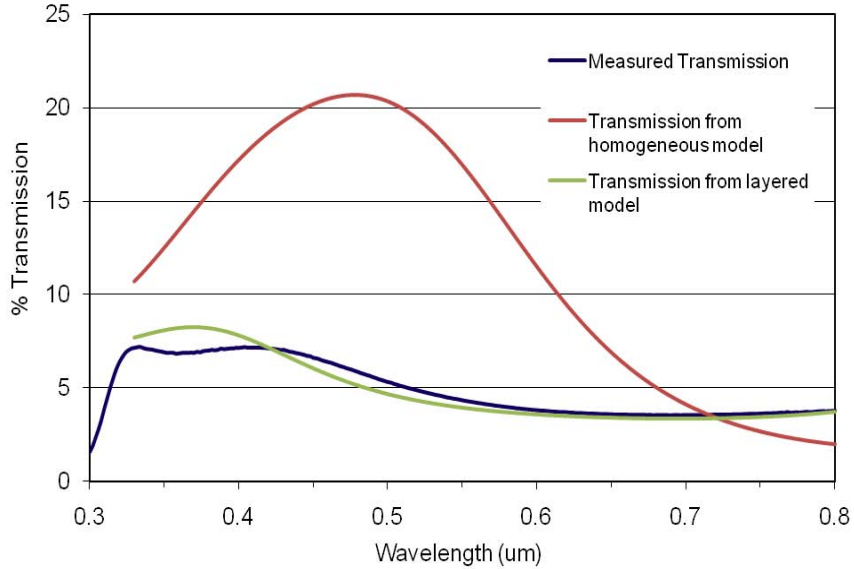
Figure 33 Plot of modeled and measured data for transmission from the one period Ag-Al2O3 structure on glass.

Results.

Comparing these new results, it can be seen that modeled reflection and measured reflection don't line up. Much of this mismatch is due to the problem of the model going into total internal reflection, and either reflection measurements should be done on an instrument that is able to do reflection measurements at a very small angle or another method, such as FDTD, should be used for the modeling.

Looking at the transmission data, it can be seen that there is close agreement between the measured and the layered model when the new material properties are used. This is a strong indication that the fabricated structure is a layered material that is not behaving as a homogeneous, ENZ material.

This result is important as it shows that a definitive answer could be produced only after the properties of the materials were using ellipsometry. This shows the importance of having accurate material data when modeling a fabricated structure.

57

4.1.2 Titanium-Alumina

Layer deign.

The design of the Ti-Al$_2$O$_3$ layers was based on the material properties found in Appendix A, and solving for the layer thicknesses with period thicknesses of *d*=75, 100, 200, 300, 400, and 500nm, the results of which can be seen in Appendix B. After looking at these different options for the wavelength of 4.45µm, it was decided to fabricate the *d*=150nm set, with the thickness of the Ti 10nm and the Al$_2$O$_3$ 140nm. This decision was made on the basis that this period had the metal at the thinnest allowable thickness of 10nm, and be much smaller than the wavelength of incident light. Instead of fabricating a four period structure, only a two period, with four layers, was fabricated, with the idea of trying to test if two periods was enough material to show the effects of the low permittivity design. The effective permittivity and index from the filling fractions of the materials can be seen in Figure 34 and Figure 35.
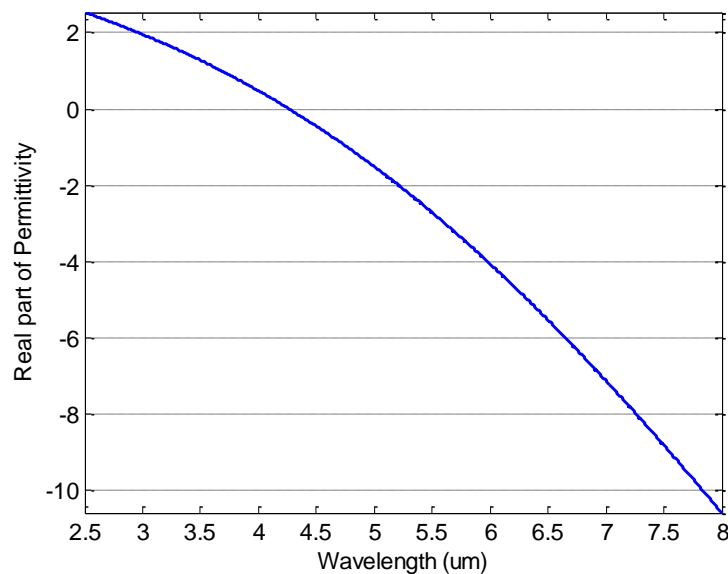
Figure 34 Plot of the effective permittivity for Ti-Al$_2$O$_3$ structure showing zero permittivity 4.45µm.
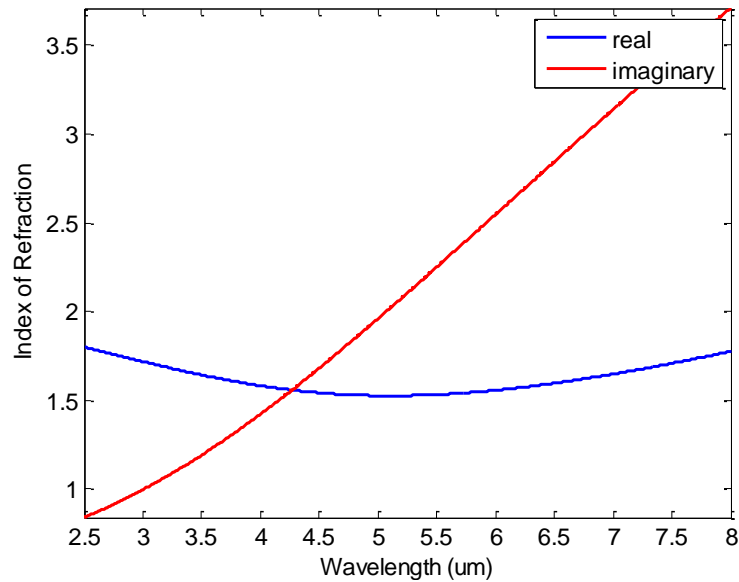
Figure 35 Plots of the effective index for Ti- Al$_2$O$_3$ structure derived from the effective permittivity.

Layer fabrication

The layers were then fabricated using the sputtering system. The general procedure for the fabrication can be found in Appendix C, with the specific parameters used to deposit the layers found in Table 3.

Table 3 Sputtering parameters for Ti- Al$_2$O$_3$ structure

	Pre-sputter Voltage/Power	Pre-sputter Time	Deposition Voltage/Power	Approximate Deposition Time	Deposition Thickness
Ti	500V	1 minute	315V	11 minutes	10nm
Al$_2$O$_3$	200W	1 minute	200W	35 minutes	140nm

The deposition monitor was used to determine the thickness of each layer, and say when the desired thickness had been reached. After fabrication, a piece of a sample was

59

cleaved off and put vertically into the scanning electron microscope to examine the profile of the layers. A micrograph of the layers can be seen in Figure 36. By examining the micrograph, it can be seen that the deposited layer thicknesses are very close to the desired thickness of 10nm and 140nm for Ti and Al_2O_3, respectively.
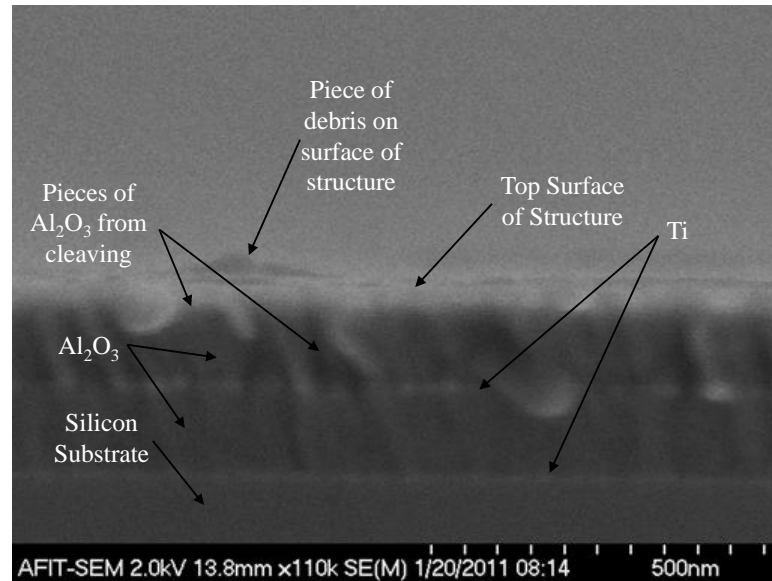
Figure 36 Micrograph of Ti-Al$_2$O$_3$ structure, showing the layers and the substrate. Notice that there is some debris on the layers since the Al$_2$O$_3$ did not cleave cleanly.

Testing and Analysis.

The first step in the analysis of these layers was to compute the reflection and transmission of the structure when it is treated as a layered structure or homogeneous structure. In both the layered and homogeneous analysis, a 2nm thick silicon dioxide layer was added to the model to account for the surface oxide on the wafer. The results of treating the structure as layered material can be seen in Figure 37 and Figure 38. Plots

of the reflectance and transmittance using the effective index are also produced, and can be seen in Figure 39 and Figure 40.
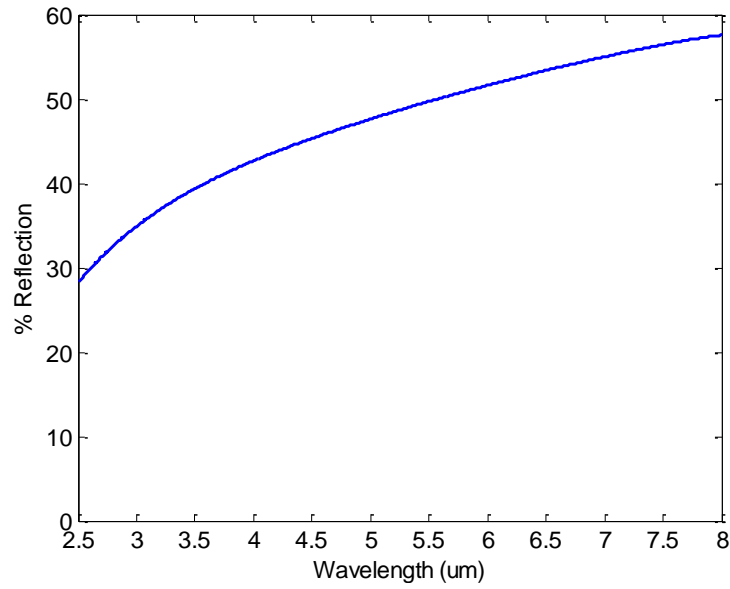
Figure 37 Plot of reflection from Ti-Al$_2$O$_3$ structure modeled as layers at 61.3°.
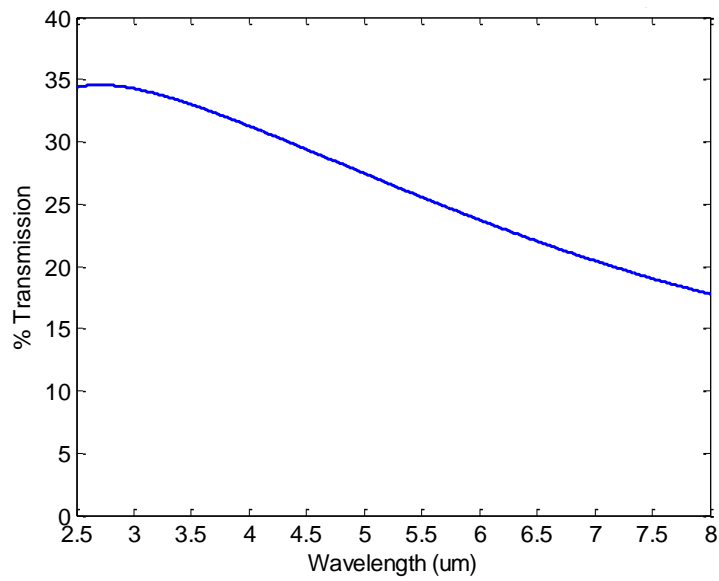
Figure 38 Plot of transmission from Ti-Al$_2$O$_3$ structure modeled as layers at 0°.
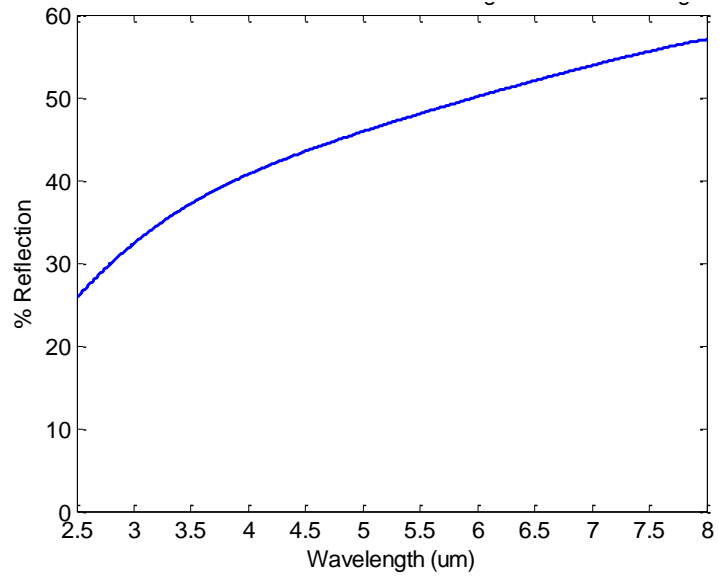
Figure 39 Plot of reflection from Ti-Al$_2$O$_3$ structure modeled as homogeneous at 61.3˚.
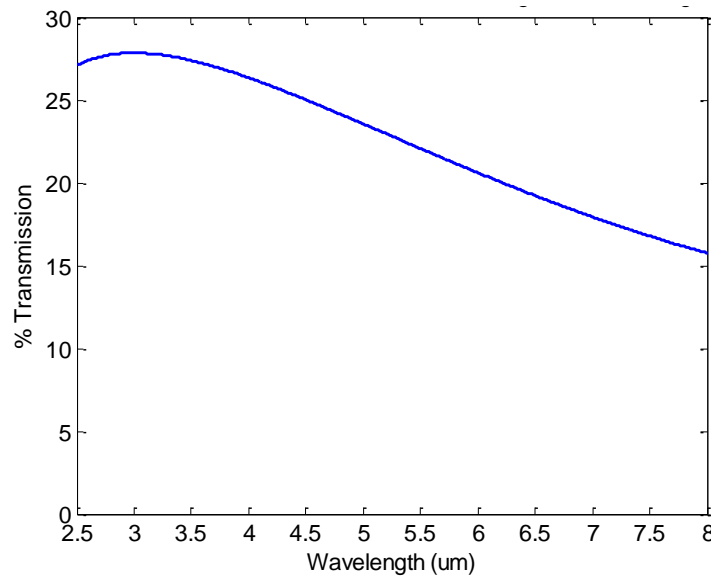
Figure 40 Plot of Transmission from Ti- Al$_2$O$_3$ Structure treated as homogeneous at 0˚.

Looking at these two plots, it can be seen that they are similar in shape but have slightly different values at certain points, as can be seen between the two reflection plots. The reflection from the homogeneous material starts out about 5% lower than the layered

media, but both plots go to about 58%. Similarly, the reflection values have a similar shape, but with different values. The layered transmission model has values 2-7% higher than the homogeneous model, and the peak of the homogeneous case is shifted to 3.03μm from 2.72μm seen in the layered case. This closeness of the results for these two models suggests that the treating this structure as a homogeneous material is not a bad approximation. The reflection and transmission data from the structure is found using the FTIR, and can be seen in Figure 41 and Figure 42.
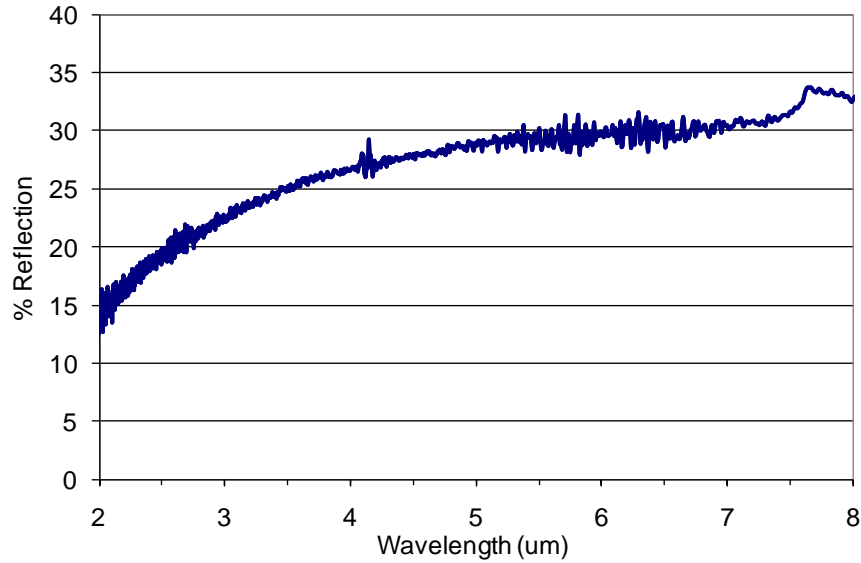
Figure 41 Plot of the FTIR reflection data for the Ti-Al$_2$O$_3$ structure at 61.3˚.
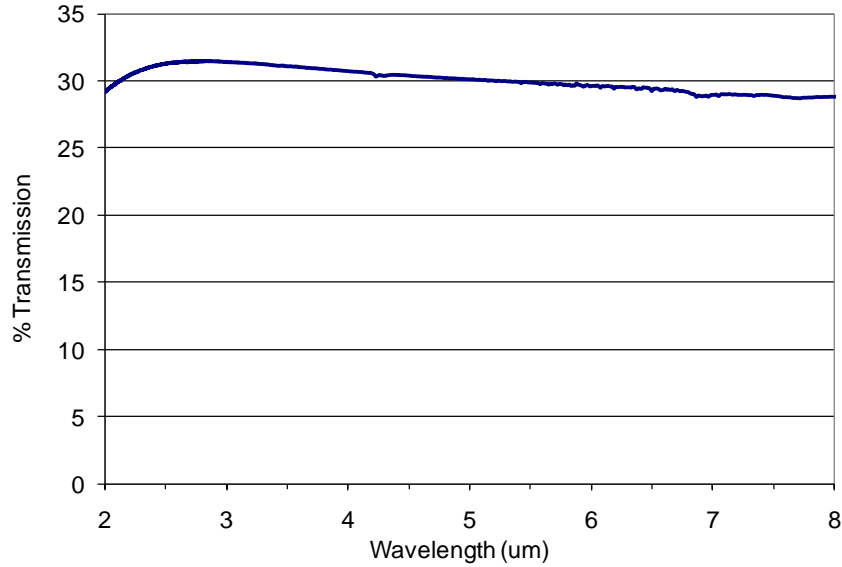
Figure 42 Plot of the FTIR transmission data for the Ti- Al$_2$O$_3$ structure at 0°. The maximum is 31% at 2.76µm.

Results.

As was noted before the results from the two models for this structure were close, indicating that the treatment of the structure as homogeneous was accurate. Comparing these results to the measured data, it is seen that the measured falls somewhere between the two cases. Plots of the two models and the collected data can be seen in Figure 43 and Figure 44. This can be seen by the fact that the maximum transmission point in the collected data is 31% at 2.76µm, between the 34% at 2.72µm and 27.84% at 3.03µm for the layered and homogeneous cases, respectively. Looking at the endpoints of the observed transmission curve, it is noted that the start point is closer to start point of the homogenous curve, but both models do not follow the higher transmission of the collected data at the longer wavelengths. Looking at the reflection curves, it can be seen that all follow the same trend and have a similar shape, but the experimental curve has much lower values.

Looking at the modeling and data, and considering how close the two models are, it appears that the structure is acting like a homogeneous material, based on the closeness of the data, and the fact that there is a peak in both the modeling and data, indicating that the structure has a changing homogeneous index and permittivity. The differences between the models and the measured data are likely due to the differences between the material properties in the model and those of the fabricated structure. Though the structure may be acting as a homogeneous media, it is not possible to say that the material is acting as ENZ material with a zero permittivity at 5.44µm due to the differences between the homogeneous model and the measured data. Like the Ag-Al$_2$O$_3$, the properties of each material will need to be known to get a definitive answer.
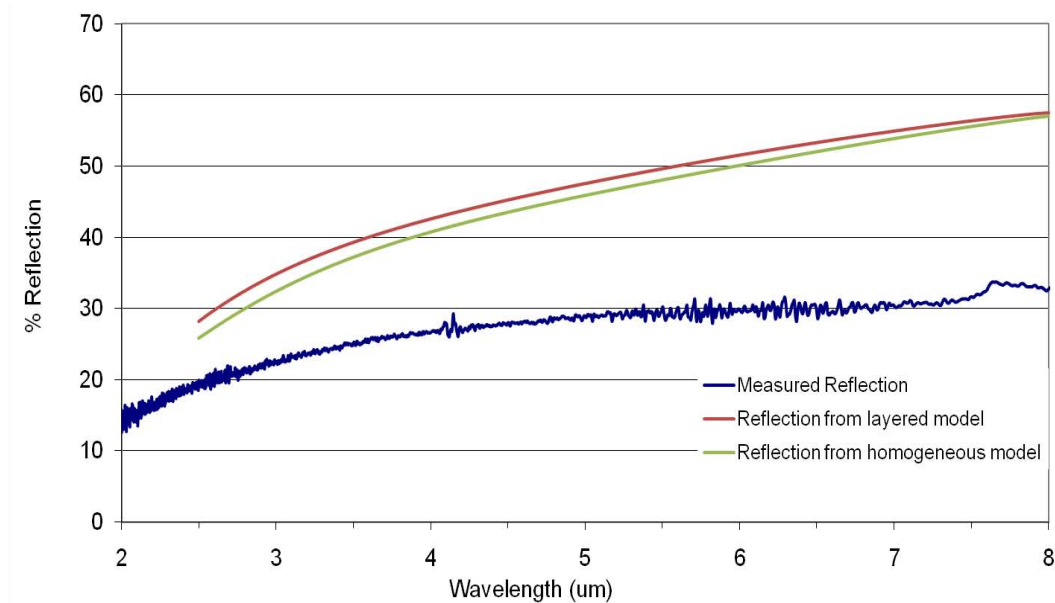
Figure 43 Plot of the measured and modeled reflection from the Ti-Al$_2$O$_3$ structure.
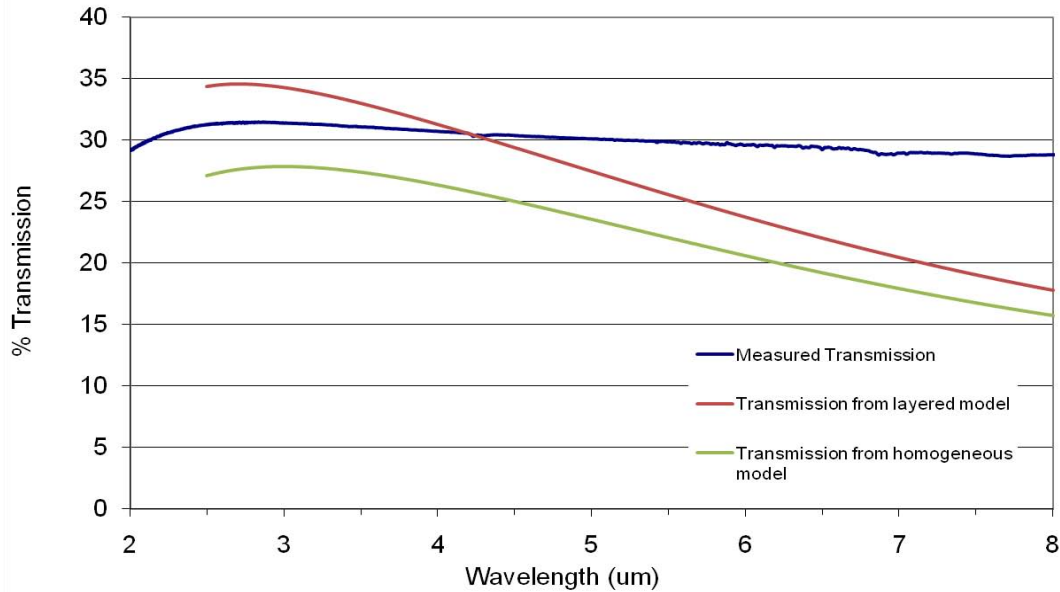
Figure 44 Plot of the measured and modeled reflection from the Ti- Al_2O_3 structure.

4.1.3 Titanium-Magnesium Fluoride

Layer deign.

The design of the Ti-MgF_2 layers was based on the material properties found in Appendix A, and solving for the layer thicknesses with period thicknesses of *d*=75, 100, 200, 300, 400, and 500nm, the results of which can be seen in Appendix B. After looking at these different options for the wavelength of 4.45μm, it was decided to fabricate the *d*=300nm set, with the thickness of the Ti being 12nm and the MgF_2 being 288nm. This decision was made on the basis that this period had the metal thickness of 12nm, which met the requirement for all layers being at or greater than 10nm thick, and be much smaller than the wavelength of the incident light. The effective permittivity and index as a function of wavelength for the structure as a homogeneous media are plotted and can be seen in Figure 38 and Figure 39, respectively.
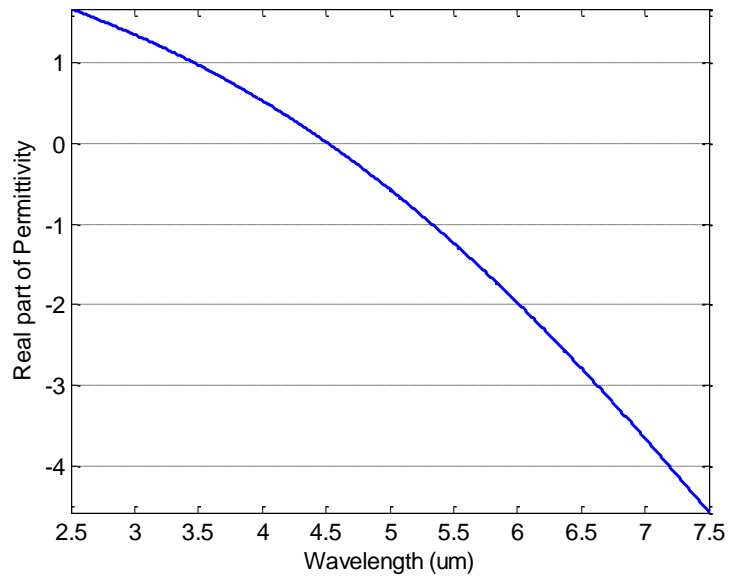
Figure 45 Plot of the effective permittivity of a period of the Ti-MgF$_2$ structure as a function of wavelength.
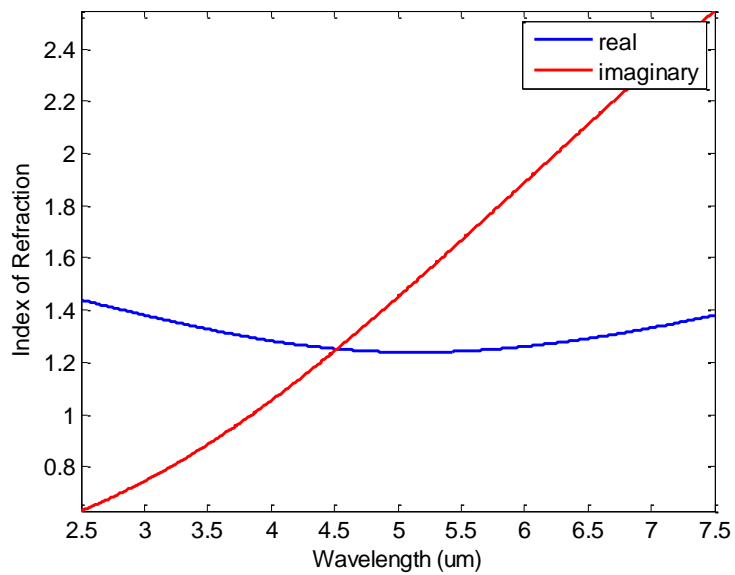
Figure 46 Plot of effective index of the Ti-MgF$_2$ structure from the effective permittivity as a function of wavelength.

Layer fabrication

A four-layer structure was then fabricated. An overview of the process used to deposit materials can be seen in Appendix C, and the key parameters for the deposition being displayed in Table 4. Silicon was used as a substrate in this fabrication.

Table 4 Sputtering parameters for Ti- MgF$_2$ structure

	Pre-sputter Voltage/Power	Pre-sputter Time	Deposition Voltage/Power	Approximate Deposition Time	Deposition Thickness
Ti	400V	30 seconds	340V	5 minutes	12nm
MgF$_2$	200W	1 minute	200W	34 minutes	288nm

After fabrication, a piece of a sample was cleaved off and put vertically into the SEM to examine the profile of the layers. A micrograph of the layers can be seen in Figure 47.
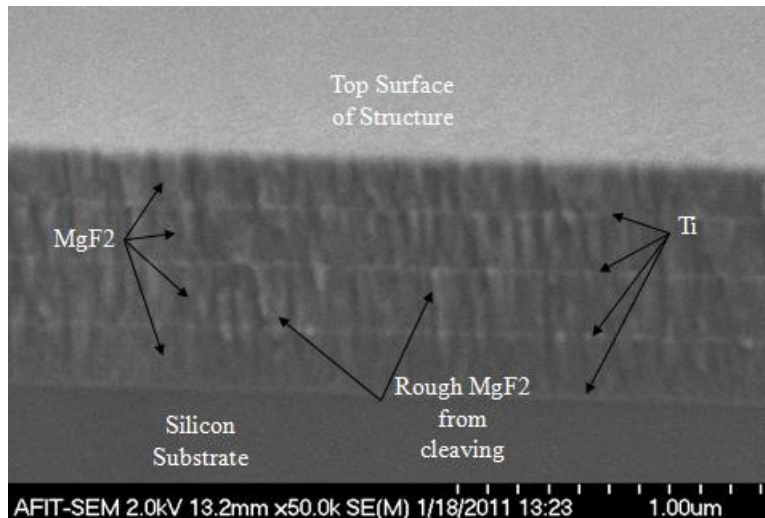
Figure 47 Micrograph of the fabricated MgF$_2$ structure. Note the thickness of the MgF$_2$ layers is approximately 155nm.

This figure shows that the fabricated structure has Ti layers that match the desired thickness but the MgF_2 layers are much thinner than the intended thickness of 288nm, and are about 155nm thick. The exact reasons for why the deposition monitor did not display the proper thickness are not known, but possible reasons for this could be inaccuracies in the z-ratio, or inaccuracy in the crystal. The z-ratio, the factor the monitor uses to maintain its accuracy as the material being deposited builds up on the crystal, was accurate enough for a thin deposition, since this inaccuracy was not seen in earlier, or thinner, depositions, but due to the inaccuracies of the z-ratio, a much thinner deposition resulted. Another possible reason is that there were inaccuracies in the monitor due to some fault or inaccuracy in the system or crystal, possibly due to a buildup of material on the crystal, however, no fault was registered on the monitor, and the crystal health display showed that the crystal was in good condition with plenty of life left.

Testing and Analysis.

The first analysis of this structure that could be done is to model it as a layered of homogeneous structure. This modeling will be done with the observed layer thicknesses of 12nm and 155nm for Ti and MgF_2, respectively. The calculations for the effective permittivity and index can be redone with the new layer thicknesses, and can be seen in Figure 48 and Figure 49, and show a shifted zero permittivity to 3.66μm.

69
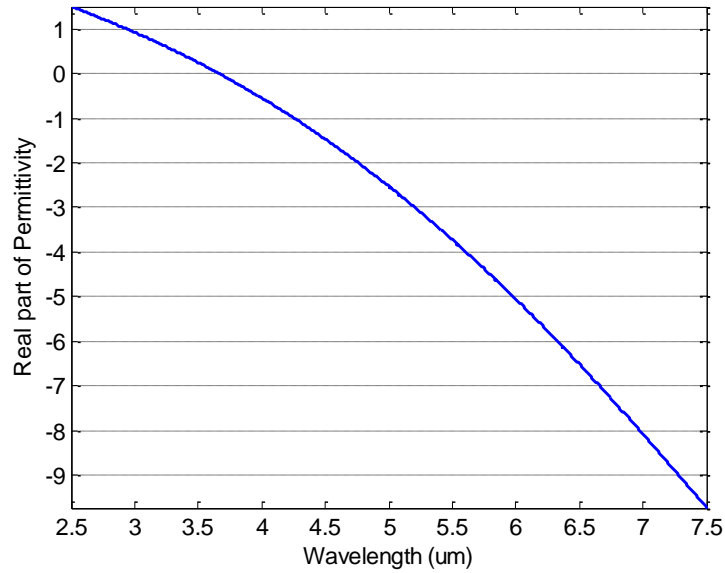
Figure 48 Plot of revised effective permittivity of the Ti-MgF$_2$ structure with thinner MgF$_2$ layers, showing a shift in the zero permittivity point.
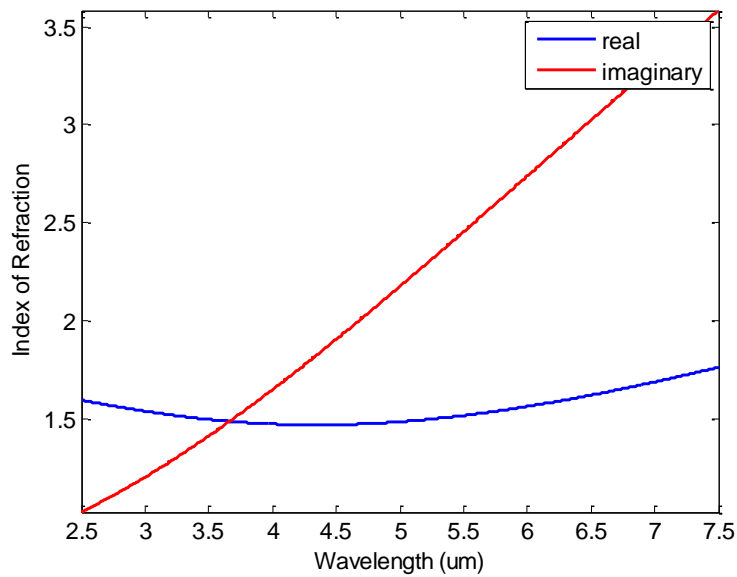
Figure 49 Plot of effective index from the revised effective permittivity of the Ti-MgF$_2$ structure with thinner MgF$_2$ layers.

The results of modeling the structure as layered and homogeneous media can be seen in Figure 50 through Figure 53Figure 46, with the angle of incidence for the reflection being 61.3˚, and 0˚ for transmission. These angles are used because they are

the angles at which the FTIR data was taken. A thin, 2nm layer of silicon dioxide is also added to the model to account for the thin layer that will grow on the substrate. The results of the layered model are seen in Figure 50 and Figure 51. The reflection and transmission from the structure when it is treated as a homogenous structure are plotted in Figure 52 and Figure 53. The data collected using the FTIR is also plotted, and can be seen in Figure 54 and Figure 55.
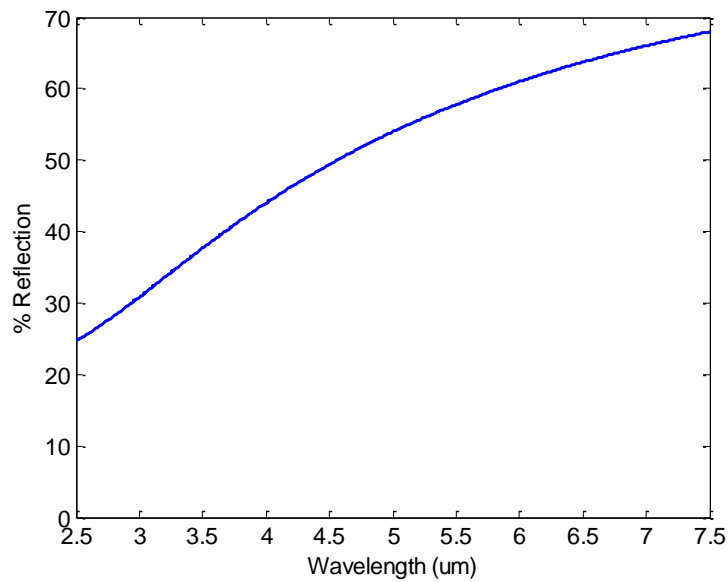
Figure 50 Plot of reflection of Ti-MgF$_2$ structure modeled as layers at 61.3°.
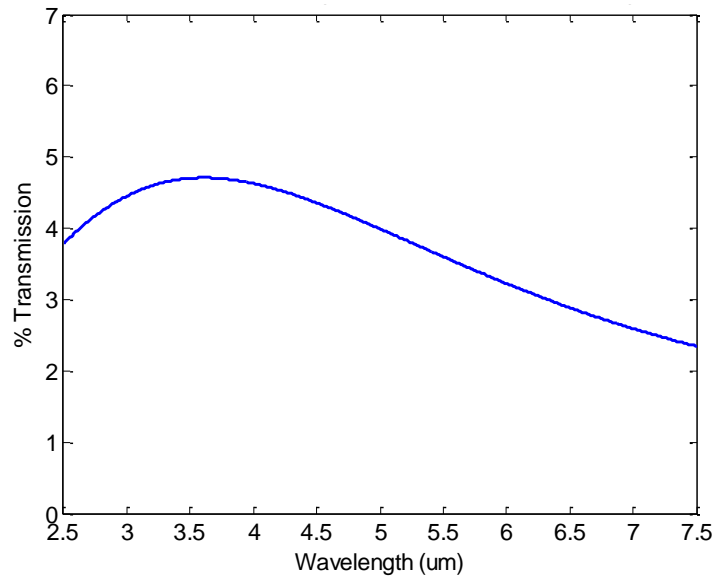
Figure 51 Plot of the transmission from the Ti-MgF$_2$ structure modeled as layers at 0°.
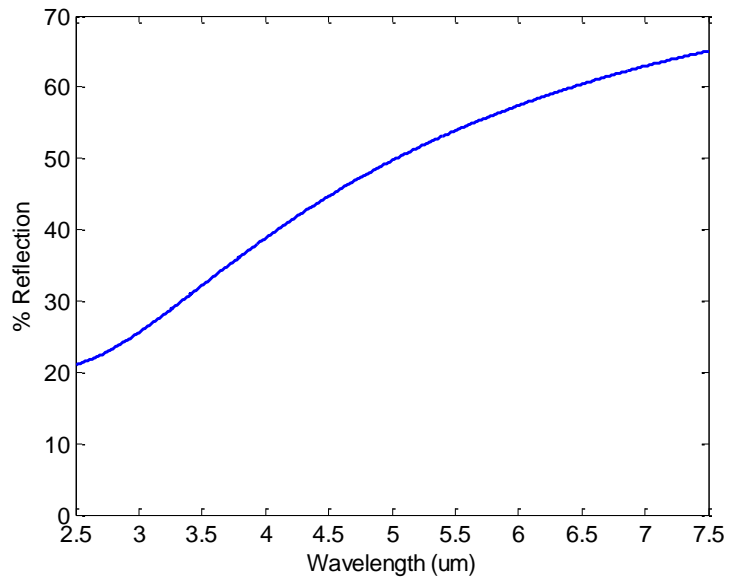
Figure 52 Plot of reflection from Ti-MgF$_2$ structure modeled as homogenous at 61.3°.
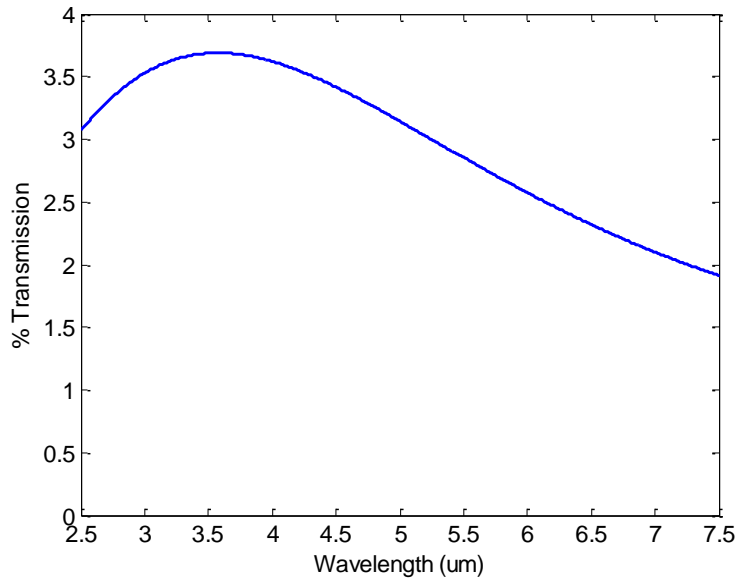
Figure 53 Plot of transmission from Ti-MgF$_2$ structure modeled as homogeneous at 0°.
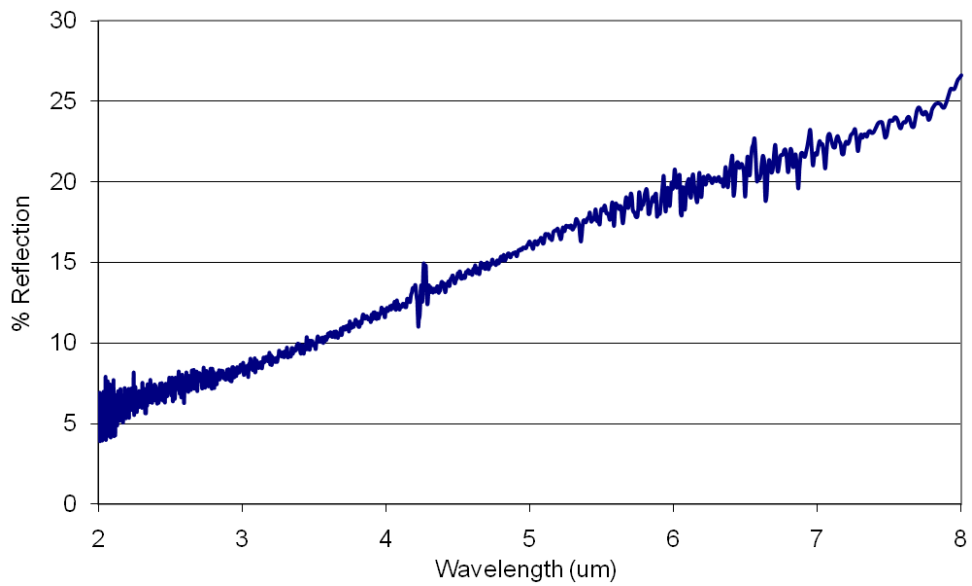
Figure 54 Plot of the reflection data from the Ti-MgF$_2$ structure at 61.3°. The spike near 4.25um seems to be a characteristic of the FTIR and is visible in other data plots.
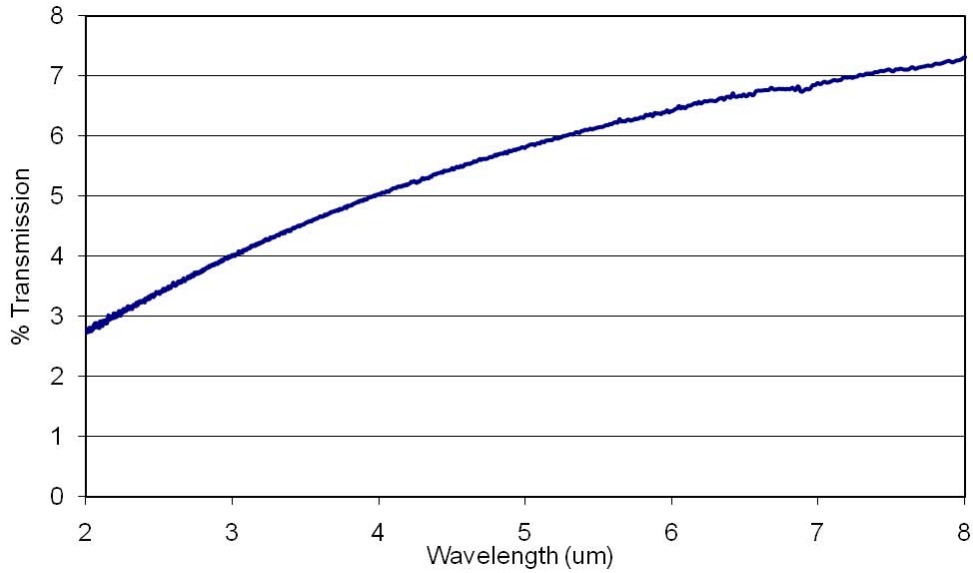
Figure 55 Plot of transmission data from the Ti- MgF$_2$ structure at 0˚.

Results.

Plots of all the modeled and measured reflection and transmission data can be seen in Figure 56 and Figure 57. Comparing these results, the graphs of the modeled reflection and transmission of the structure as layered or homogeneous were very close, indicating that the layers in the structure are thin enough that the structure can be considered homogeneous for these wavelengths of light. Comparing these results to the collected experimental data, it is found that the experimental data does not line up with either model, and though the structure may be homogeneous, it is not acting like the homogeneous ENZ that was desired. Reasons for this lack of agreement are likely differences between the properties of the materials used in the model and those in the fabricated structure. More work would have to be done to find the material properties of the materials used in the structure, especially MgF$_2$, to be able to model it accurately.

74
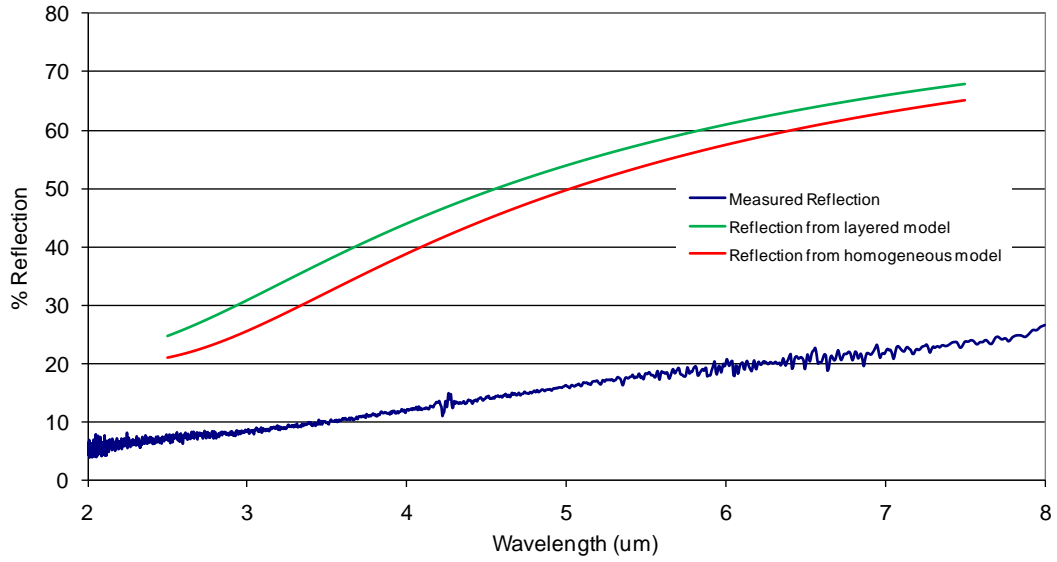
Figure 56 Plot of modeled and collected reflection data from the Ti-MgF₂ structure.
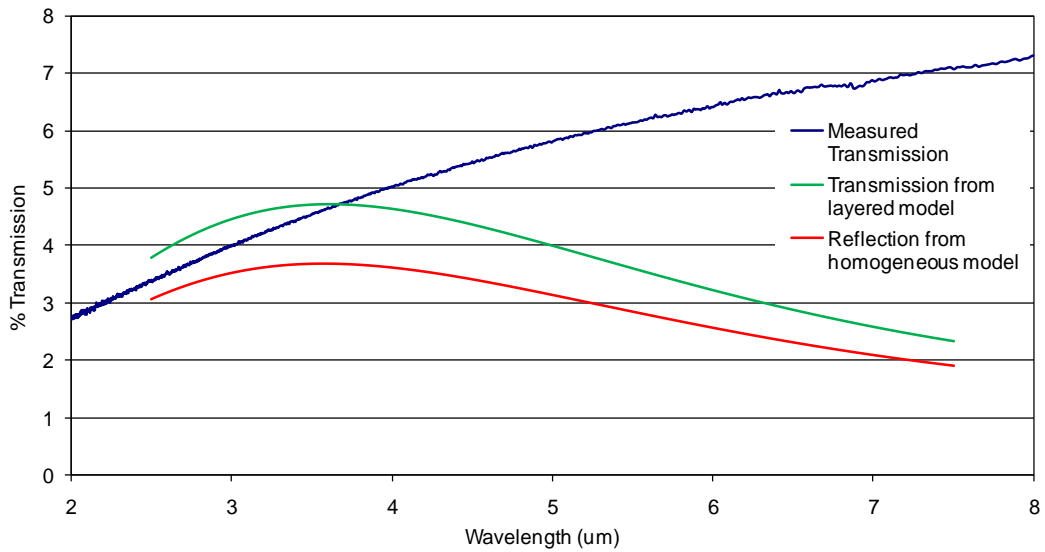
Figure 57 Plot of modeled and collected transmission data from the Ti-MgF₂ structure.

4.1.1 Gold-SU-8

Layer deign.

The design of the Au-SU-8 layers was based on the material properties found in Appendix B, and solving for the layer thicknesses with period thicknesses of d=5000nm, the results of which can be seen in Appendix A. Only the results for 5000nm were considered because that is the thickness which SU-8 spins on. After looking at these different options, the gold-SU-8 combination for the wavelength of 5μm was chosen. This decision was made on the basis that this period had the metal thickness of 10nm, which met the requirement for all layers being equal to or greater than 10nm thick. Though the designed wavelength is comparable to the period of the structure, it was thought that this fabrication would be easy and worth attempting to see what results could be gathered. The effective permittivity and index of refraction as a function of wavelength were also calculated, and can be seen in Figure 58 and Figure 59, respectively.
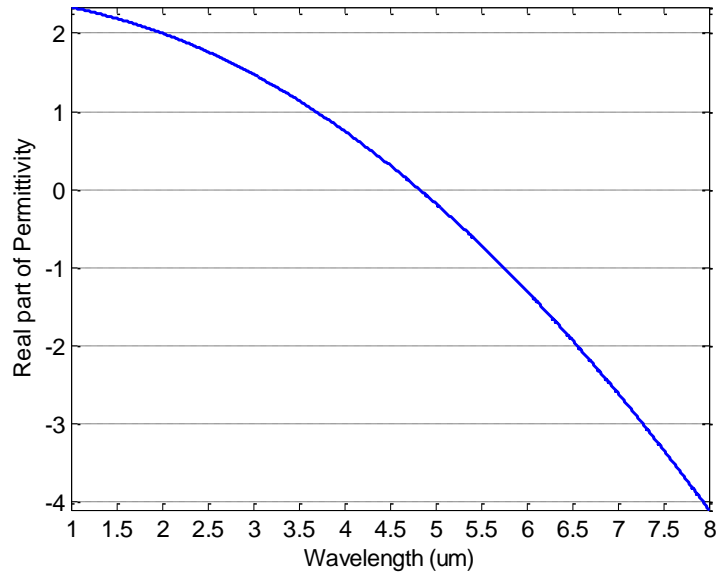
Figure 58 Plot of effective permittivity of a period of Au-SU-8 structure with 5μm thick SU-8 showing the zero permittivity point at 5μm.
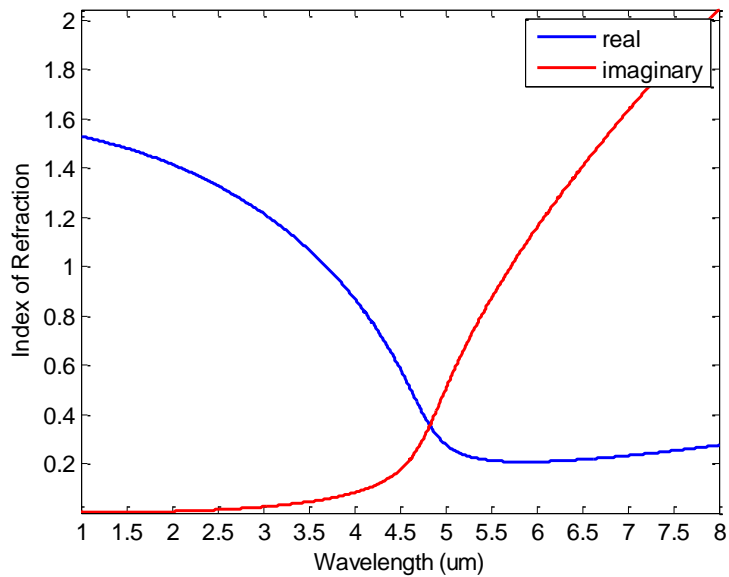
Figure 59 Effective index of Au-SU-8 structure calculated from the effective permittivity of 5μm thick SU-8 layers.

Layer fabrication.

The fabrication of this structure was unique among the all the others fabricated because it used a polymer photoresist that needed to be spun on for a dielectric instead of

77

one that would be sputtered. The Au was deposited using the sputtering system, and the fabrication followed the steps in Appendix C for the deposition up to the point where the dielectric was to be deposited. The parameters for the Au deposition can be seen in Table 5. After the Au is deposited, the sample was then unloaded from the sputtering system and brought to the photoresist spinner to be coated with SU-8.

Table 5 Sputtering parameters for Au-SU-8 structure

	Pre-sputter Voltage/Power	Pre-sputter Time	Deposition Voltage/Power	Approximate Deposition Time	Deposition Thickness
Au	400V	30 seconds	390V	1.5 minutes	10nm

Following the steps listed in the product data sheet, 5000nm (5μm) of SU-8 was then spun onto the sample using the photoresist spinner, set to a spread of 500RPM for 5 seconds, followed by a spin of 3000RPM for 30 seconds. The SU-8 was then prebaked on a hotplate, using a two step bake of 65°C for one minute followed by 95°C for three minutes. The SU-8 was then flood exposed, meaning that no mask was used to control where the light went on the sample, and the whole sample was exposed on the MJB-3 mask aligner for nine seconds, and then post baked on a hotplate at 65°C and then 95°C for one minute each to crosslink and fully develop the photoresist. Since this is a negative photoresist, all the exposed material will harden and stay, hence why the whole sample was exposed. The sample was then loaded back into the sputtering system, where the next layer of Au could be deposited and the whole process repeated. After fabrication, a piece of a sample was cleaved off and put vertically into the SEM to examine the profile of the layers. A micrograph of the layers can be seen in Figure 60.

Examining the micrograph, it can be seen that the SU-8 layers did not spin on to be 5μm as the data sheet had specified, but were instead 4μm thick.
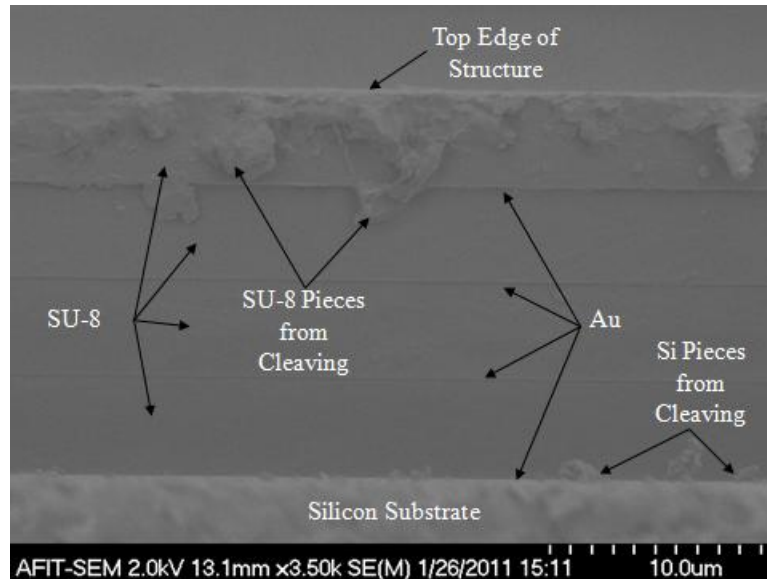
Figure 60 Micrograph of Au-SU-8 structure. The arrows denoting Au are not pointing to the to the physical thickness of the Au, but to the interface between the layers where the Au is deposited. Also, the SU-8 thickness of the SU-8 layers can be seen to be 4μm.

Testing and Analysis

The Au-SU-8 structure can now be modeled to predict the reflection and transmission from the structure. Another unique characteristic of this structure was the ability of it to be removed from the silicon substrate intact. This was discovered accidentally during the polishing of the backside of a sample, the structure delaminated but remained intact. Knowing this, the structure could now be tested without a substrate by carefully pealing it from the substrate. The modeling of this structure will use the layer thickness of the fabricated structure, and the calculations for the effective permittivity and index can be

redone, and show a shift of the point of zero effective permittivity to 4.31μm. The revised results can be seen in Figure 61 and Figure 62.
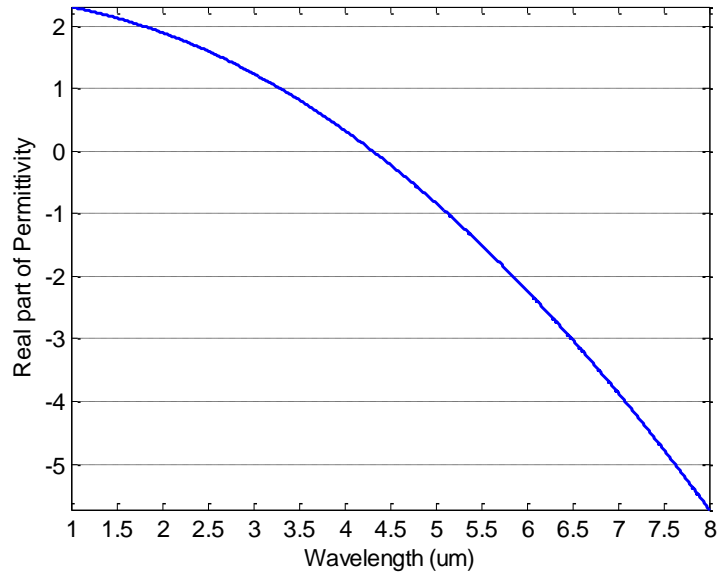
Figure 61 Revised plot of the effective permittivity of the Au-SU-8 structure with 4μm thick SU-8 layers, showing the shifted zero point.
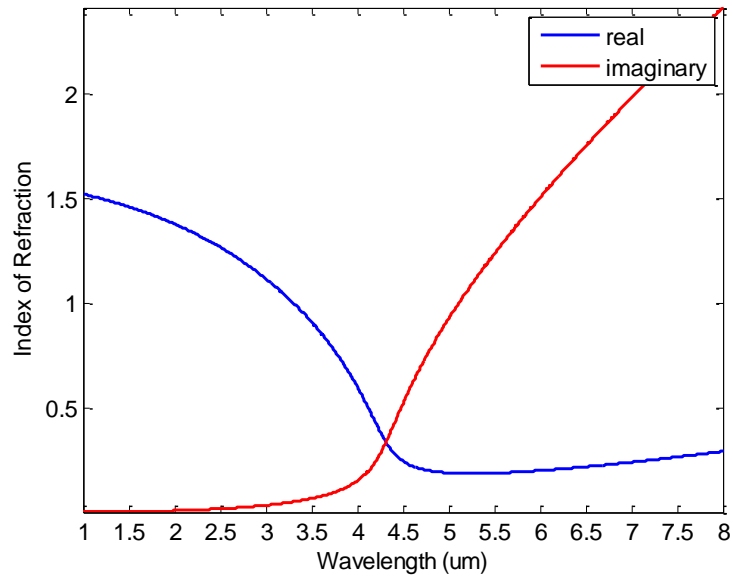
Figure 62 Plot of the revised index of refraction extracted from the revised index of permittivity of the Au-SU-8 structure with 4μm thick SU-8 layers.
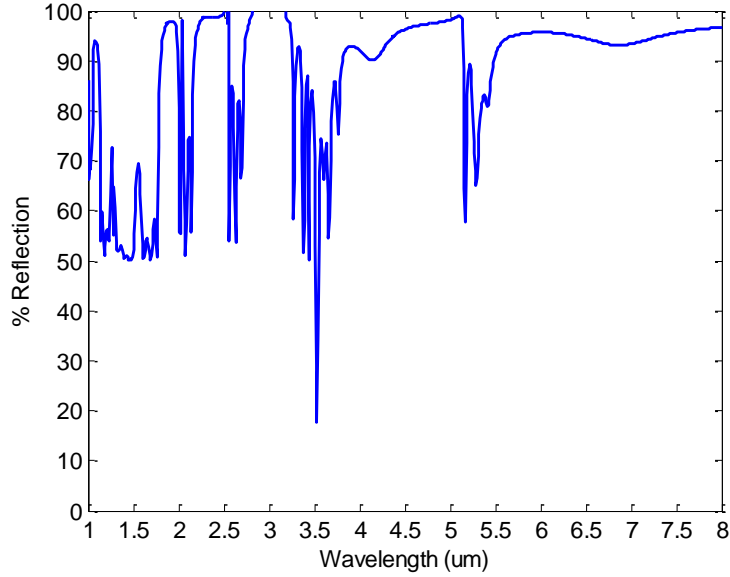
Figure 63 Plot of the reflection from the Au-SU-8 structure treated as a layered material at 61.3°. Note that there are points at 1.25um, 2.5um, and 3um where the reflection goes above 100%. This is due to total internal reflection that occurs from 1µm to 3.55µm.
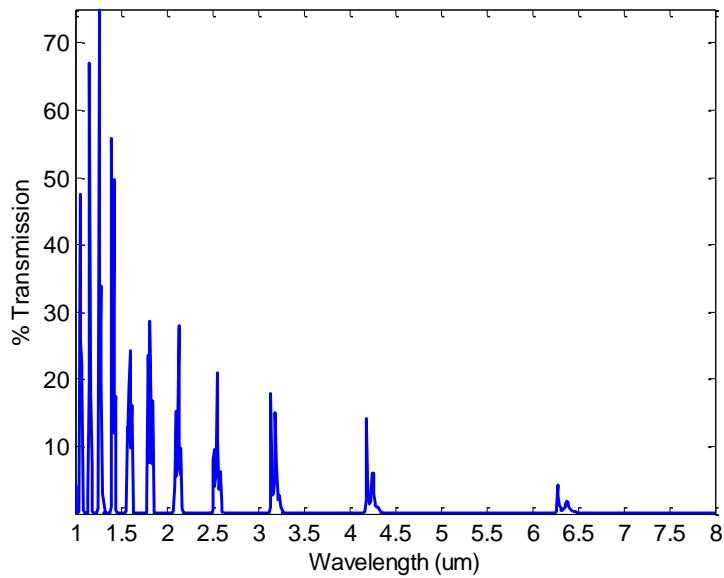
Figure 64 Plot of the reflection from the Au-SU-8 structure treated as a layered material at 0°. Note that this calculation was made at normal incidence and does not have the total internal reflection that is occurring in reflection.

The substrate-less structures could then be modeled as layered material, and the results can be seen in Figure 63 and Figure 64. Looking at these plots, it is seen that there are values that go above 100% for the reflection, which are obviously not accurate or correct. The cause of this result is investigated, and the reason is found to be total internal reflection that occurs in the transition between the higher index SU-8 and the lower index Au, and causes the model to give incorrect data. The wavelengths at which total internal reflection is observed were from 1-3.5µm. The results for the transmission do not show this behavior, as they were made at 0˚ incidence.
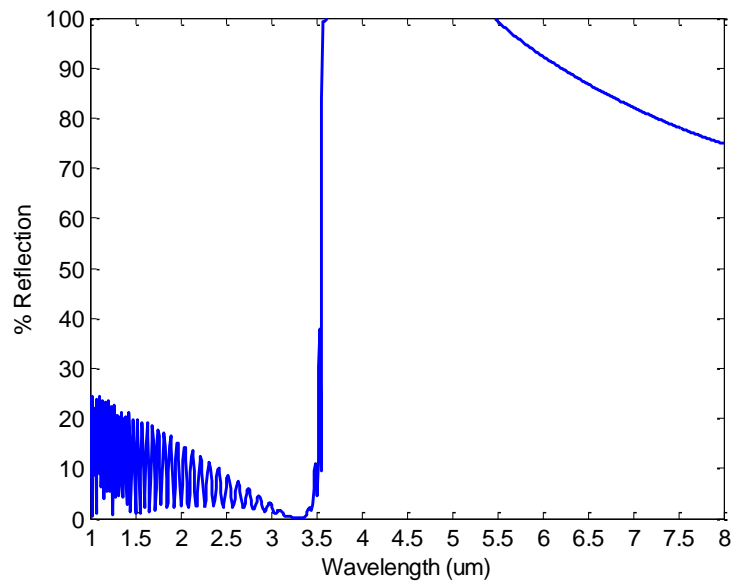
Figure 65 Plot of reflection from the Au-SU-8 structure treated as a homogeneous material at 61.3˚. Reflection values greater than 100% are observed, due to total internal reflection which occurs from 3.56µm to 8µm.
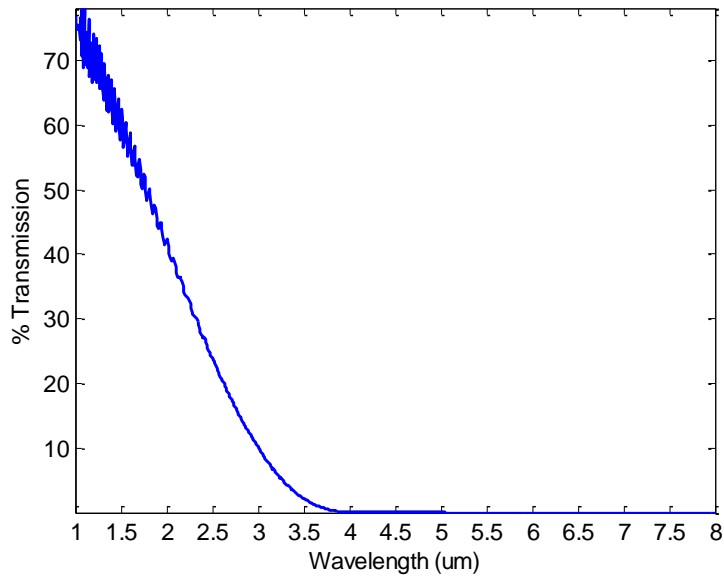
**Figure 66 Plot of the transmission of the Au-SU-8 structure treated as a homogeneous material at 0°.
Note that there is no total internal reflection due to the angle of incidence.**

The behavior of the structure is also calculated treating it as a homogeneous material, and can be seen in Figure 65 and Figure 66. Again, total internal reflection was seen in the reflection of this model. Total internal reflection was observed for the wavelengths of 3.56μm to 8μm, when the angle computed transmission angle from the homogeneous stack became 90°. This wavelength lines up well with the wavelength at which the effective index of the material crosses the value of one, as can be seen in Figure 59. A lot of ringing is seen in the shorter wavelengths of these plots, suggesting reflections occurring within the structure.
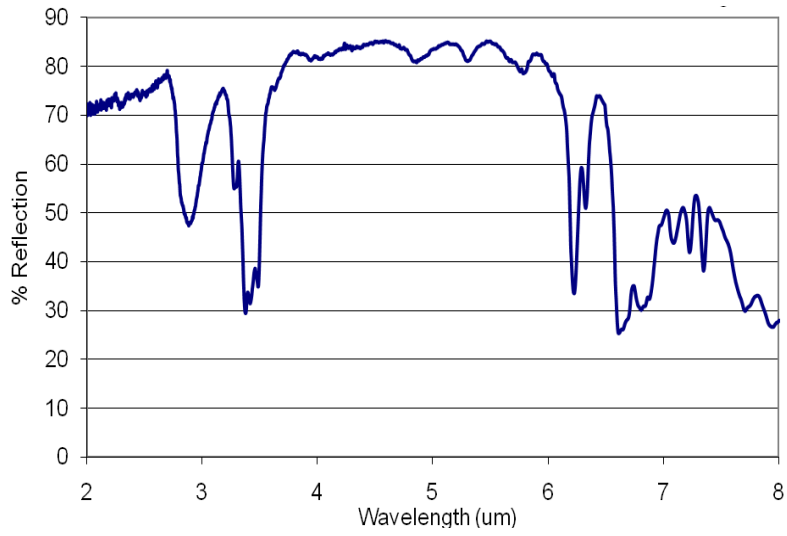
Figure 67 Plot of refection from the Au-SU-8 structure at 61.3˚.
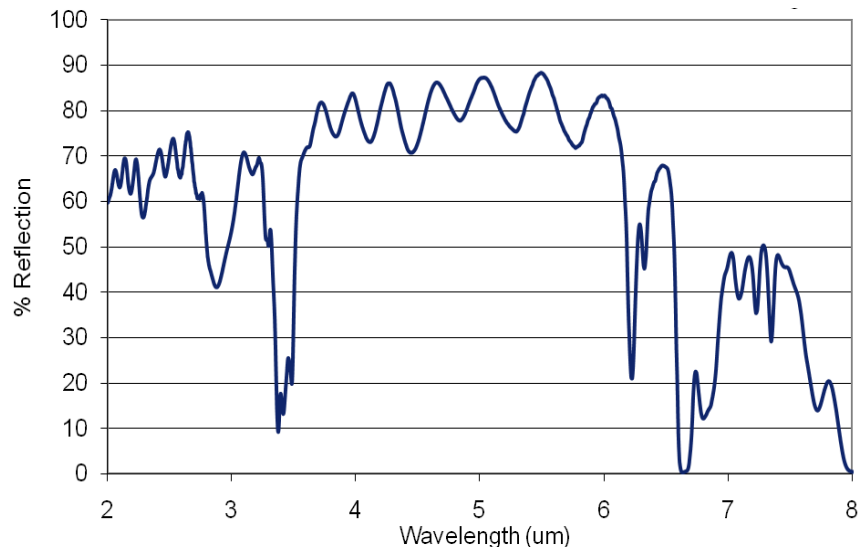
Figure 68 Plot of the transmission from the Au-SU-8 structure at 0˚.

Finally, plots are made of the collected reflection and transmission data, which can be seen in Figure 67 and Figure 68. These results can then be compared to the computed

reflectance treating the structure as a layered media and as a homogeneous media with the index of refraction seen in Figure 59.

Results.

Plots comparing all the reflection and transmission data can be seen in Figure 69 and Figure 70. Looking at these plots, a close fit cannot be seen between the collected data or either model, especially since the models broke down in many areas where the incident angles and indices were such that total internal reflection resulted. It does appear that there is some agreement between the collected data and the layered model, as both show a broad reflection band in the 3.5μm to 5μm range, and the transmission data have similar peaks, suggesting that this material is best treated as a layered structure. This makes sense considering the thickness of the layered being used and the wavelengths of light. Further investigations would need to be done to accurately model this structure to determine what is happening as well as check possible for photonic crystal effects, given that the period of the structure is on the order of the wavelength of the radiation it is to interact with. The properties of the constituent materials should be further investigated, and other modeling means that can account for the total internal reflection that can occur at the angle used by the FTIR, such as FDTD simulation, or a reflection measurement that is at a smaller angle should be used.
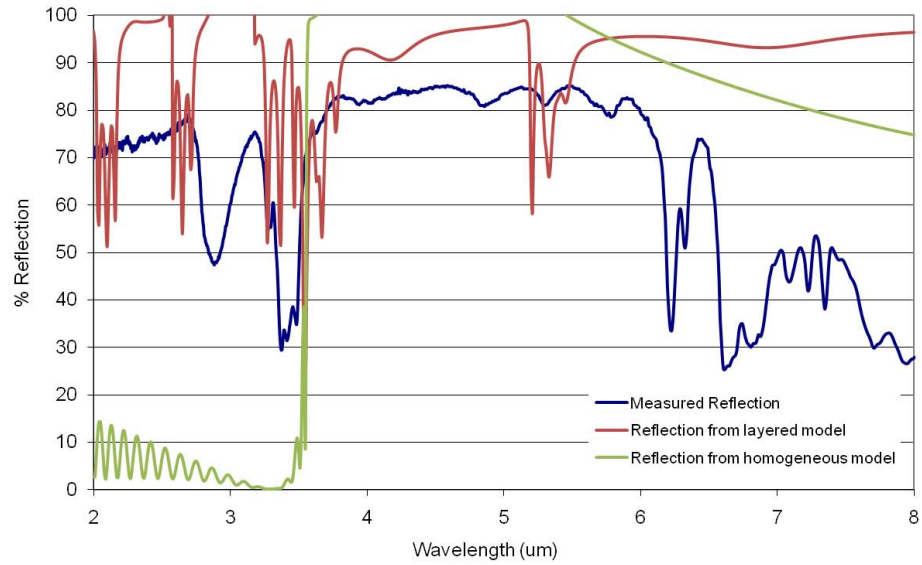
Figure 69 Comparison of modeled and measured reflection from the Au-SU-8 structure. Note that the layered model goes into TIR for 1µm to 3.55µm, and the homogeneous for 3.56µm to 8µm.
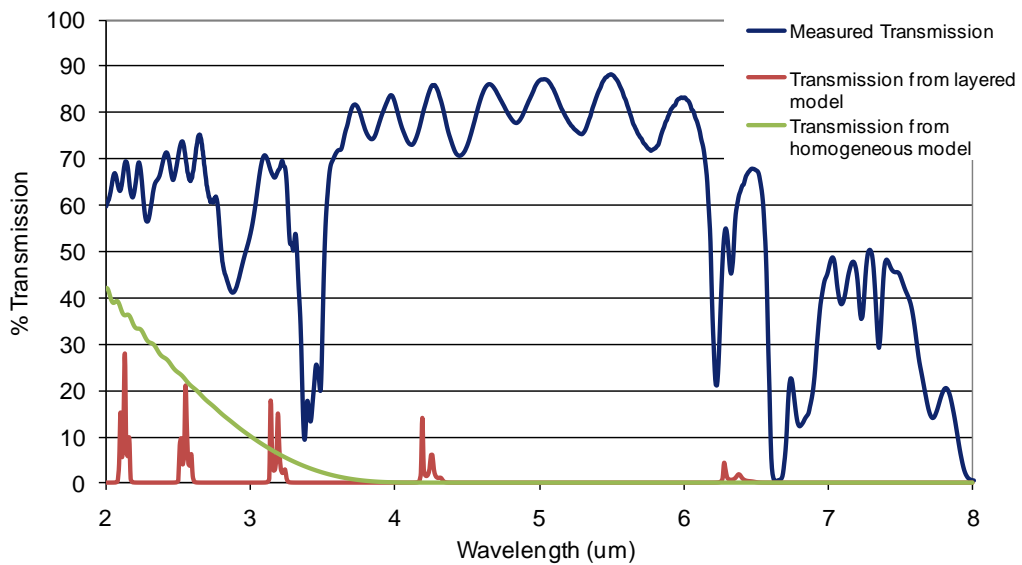
Figure 70 Comparison of modeled and measured reflection from the Au-SU-8 structure.

4.1.1 Nickel-Silicon

Layer deign.

The design of the Ni-Si layers was based on the material properties found in

Appendix A, and solving for the layer thicknesses with period thicknesses of *d*=75, 100,

200, 300, 400, and 500nm, the results of which can be seen in Appendix B. After looking

at the different options for the wavelength of 4.45μm, it was decided to fabricate the

d=200nm set, with the Ni 11nm thick and the Si 189nm. This decision was made on the

basis that this period had the metal thickness of 11nm, which met the requirement for all

layers being at or greater than 10nm thick, and be much smaller than the wavelength of

the incident light. The effective permittivity and index as a function of wavelength for a

homogeneous structure are plotted and can be seen in Figure 71 and Figure 72,

respectively.
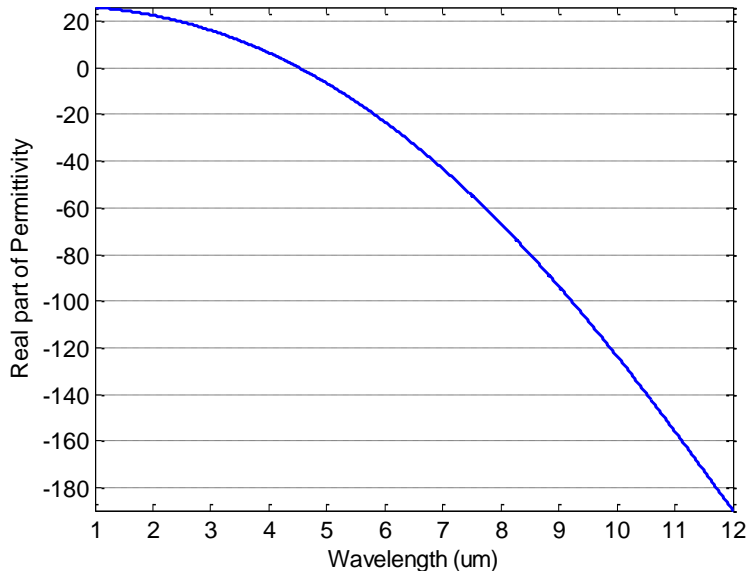
Figure 71 Graph of the real part of the effective permittivity for the Ni-Si structure for 189nm thick Si layers, with the zero crossing near 4.45um.
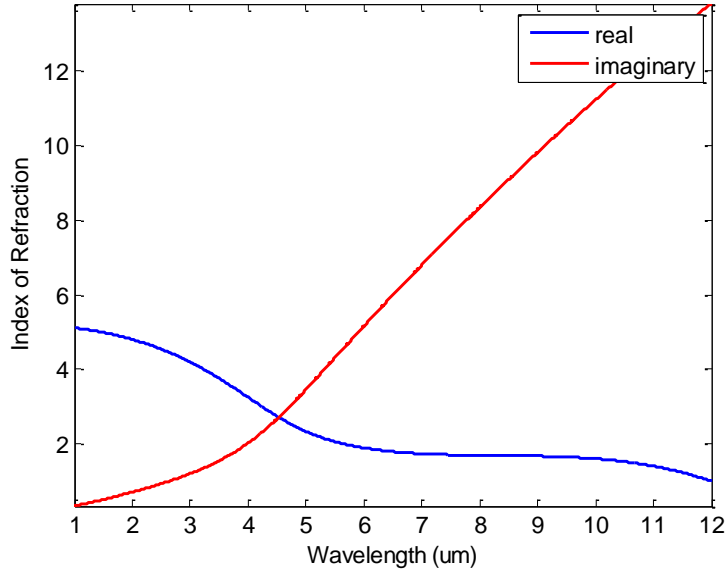
Figure 72 Graph of the effective index of the Ni-Si structure with 189nm thick Si layers, as a function of wavelength based on the effective permittivity.

Layer fabrication.

An overview of the process used to deposit materials can be seen in Appendix C, and the key parameters for the deposition being displayed in Table 6. Silicon was used as a substrate in this fabrication.

Table 6 Sputtering parameters for Ni-Si structure

	Pre-sputter Voltage/Power	Pre-sputter Time	Deposition Voltage/Power	Approximate Deposition Time	Deposition Thickness
Ni	400V	30 seconds	360V	5 minutes	11nm
Si	200W	1 minute	200W	27 minutes	189nm

After fabrication, a piece of a sample was cleaved off and put vertically into the SEM to examine the profile of the layers. A micrograph of the layers can be seen in Figure 73. This figure shows that the fabricated structure has Ni layers that match the desired thickness but the Si layers are much thinner than the intended thickness of

189nm, and are about 89nm thick. Possible reasons for this are the same as those reasons listed for the Ti-MgF$_2$ case of inaccuracies in the z-ratio, or a problem with the deposition monitor or crystal, though the monitor and crystal gave no indication of a malfunction or need of a replacement crystal.
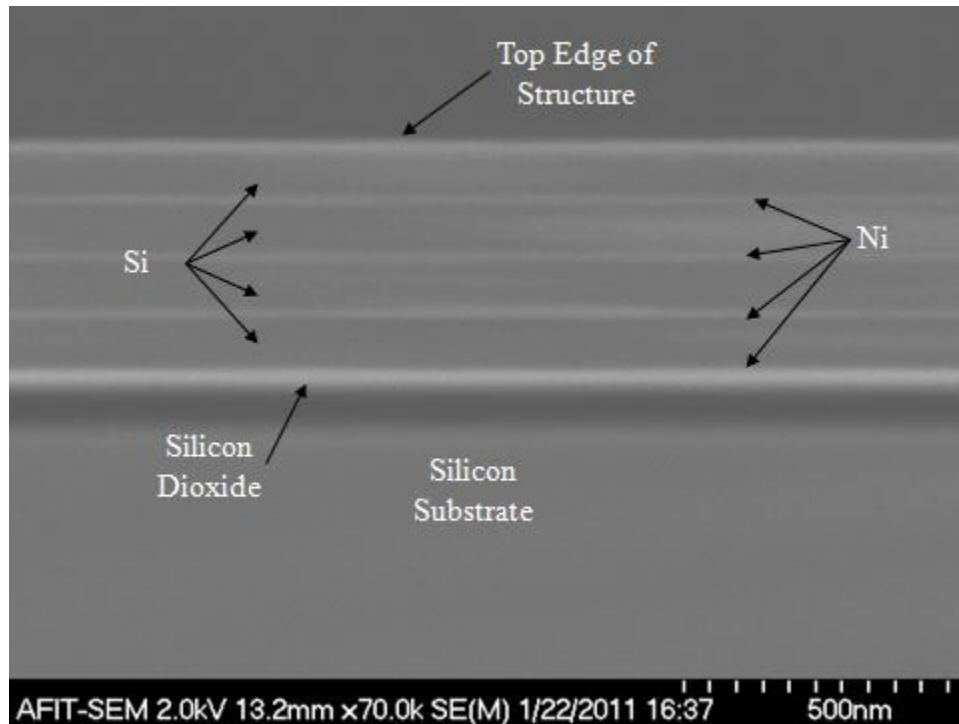
Figure 73 Micrograph of the fabricated Ni-Si structure. Note the thin layer of silicon dioxide on the from the silicon substrate at the bottom of the structure.

Testing and Analysis.

The first analysis that could be done was to compute the reflection and transmission of the fabricated structure as a layered material or a homogeneous material. This modeling will use the thicknesses observed thicknesses of 11nm and 89nm for the Ni and Si. If the calculations are redone for the new layer thickness and period, it is found that the point at which the effective permittivity becomes zero has shifted to a shorter

wavelength of 3.16μm, and can be seen in new plots of the effective permittivity and index in Figure 74 and Figure 75.
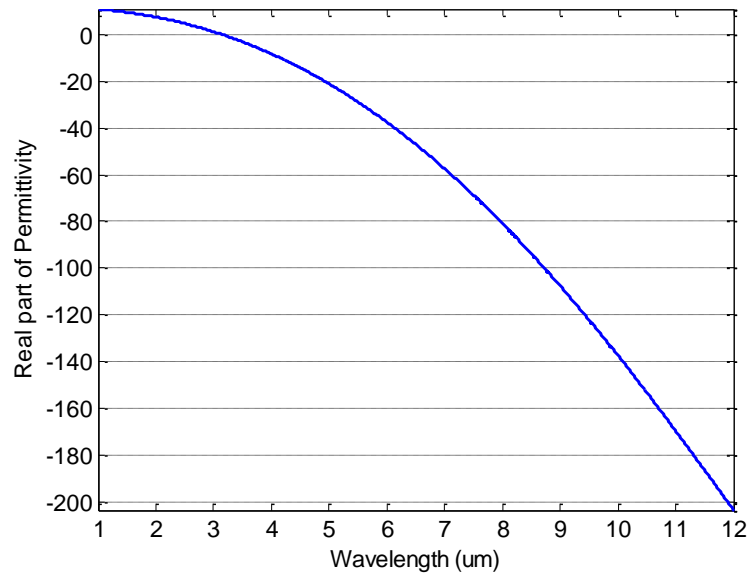
Figure 74 Revised plot of the real part of the effective permittivity with 89nm thick Si layers, showing the point where the effective permittivity becomes zero shifted to 3.16μm.
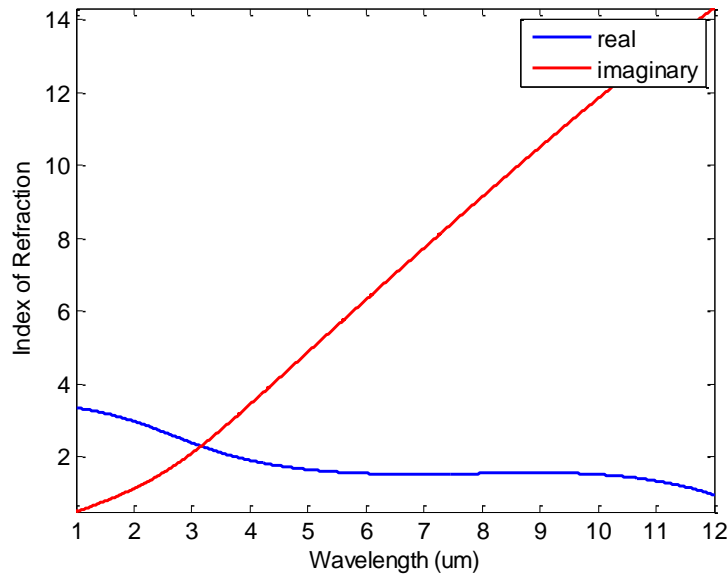
Figure 75 Plot of effective index based on recalculated effective permittivity with 89nm thick Si layers.

The results of this modeling can be seen in Figure 76 through Figure 79 for both the layered and homogeneous cases, using the angles of 61.3° for the reflection and 0° for transmission, as those were the angles at which the FTIR data was taken. This modeling also included a thin 2nm silicon dioxide layer on top of the silicon substrate, as was seen in Figure 73. This thin oxide layer was also out on top of the silicon layer in the structure, The results of the layered model can be seen in Figure 76 and Figure 77 and the homogeneous can be seen in Figure 78 and Figure 79.
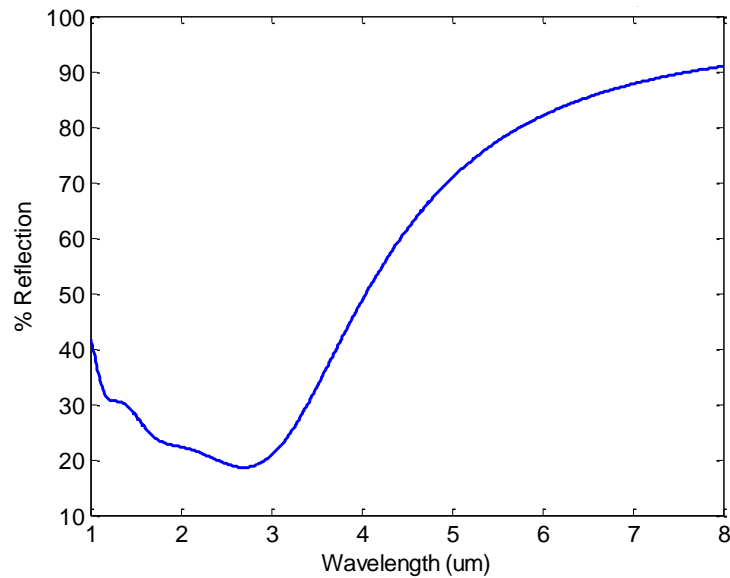
Figure 76 Reflection from Ni-Si structure modeled as layers at an incident angle of 61.3°.
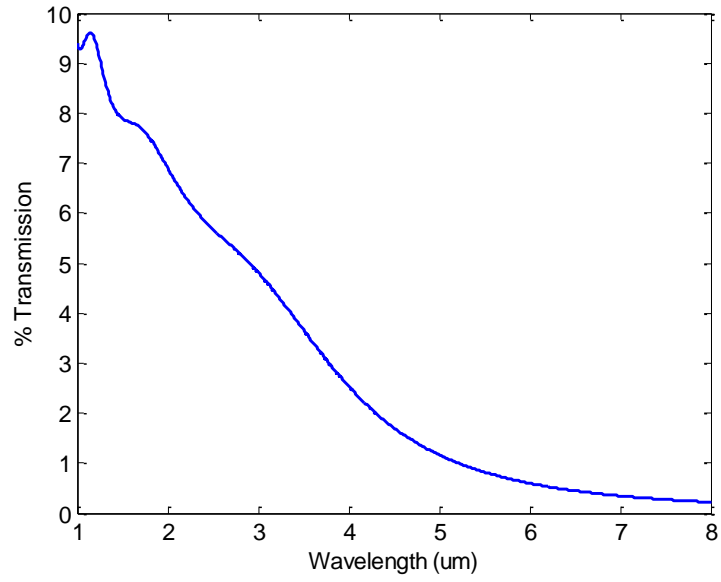
Figure 77 Transmission from Ni-Si structure modeled as layered media at an incident angle of 0˚.
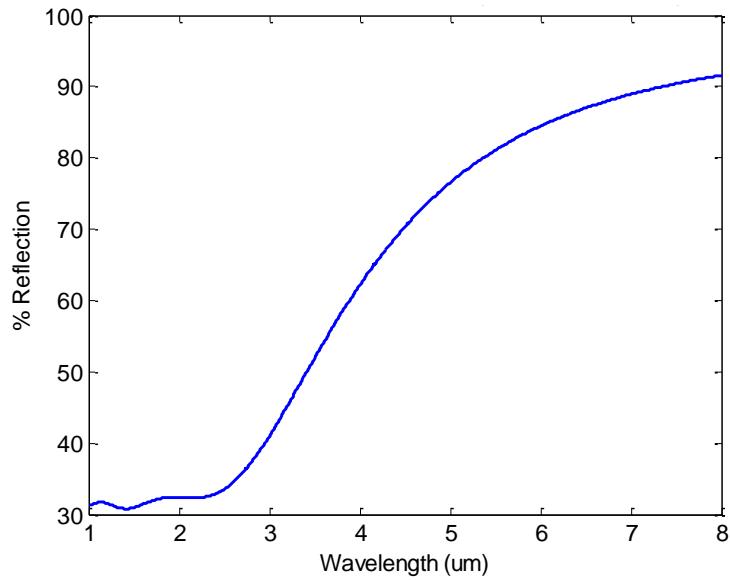

Figure 78 Plot of reflection from Ni-Si structure modeled as homogenous at 61.3˚.
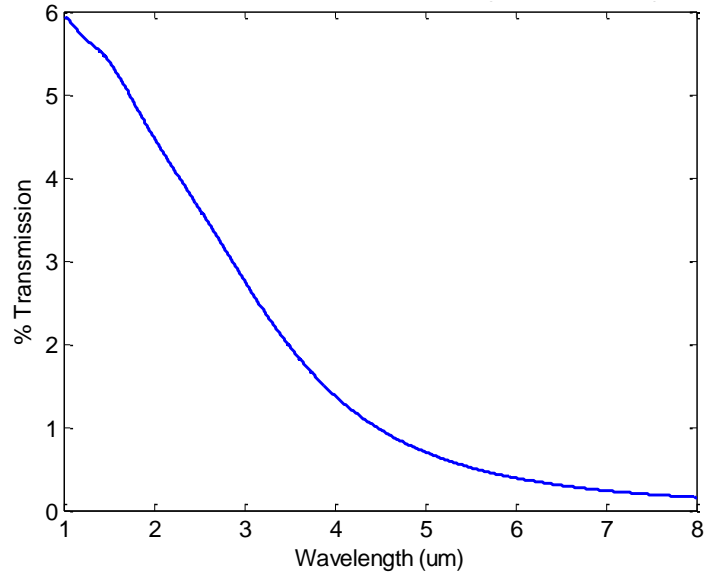
Figure 79 Plot of transmission from Ni-Si structure modeled as homogeneous at 0˚.

The fabricated layers were then tested using the FTIR, and reflection and transmission data collected at 61.3˚ and 0˚ angle of incidence, respectively. The reflection and transmission data is plotted below in Figure 80 and Figure 81.
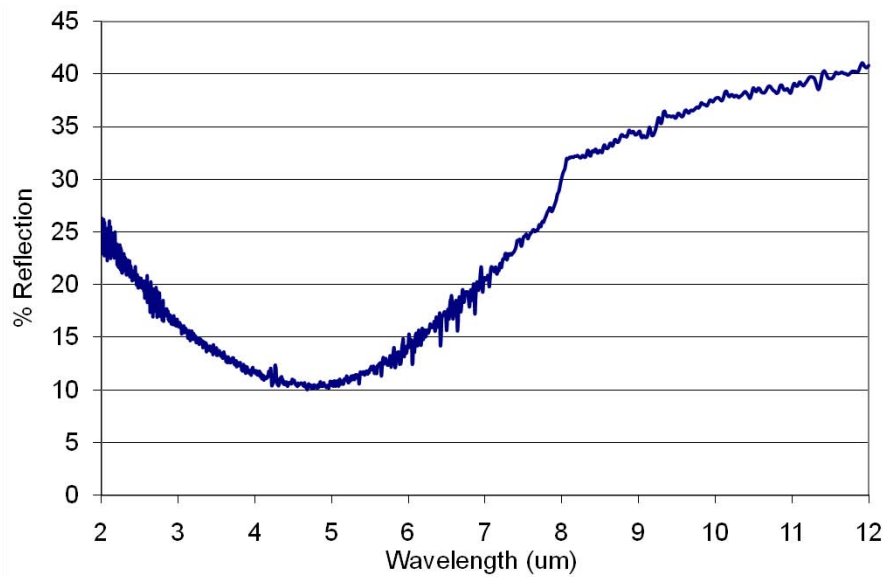
Figure 80 Plot of FTIR data for reflection from the Ni-Si structure. The noise towards 2um is a result of the data being collected at the edge of the instrument's range.
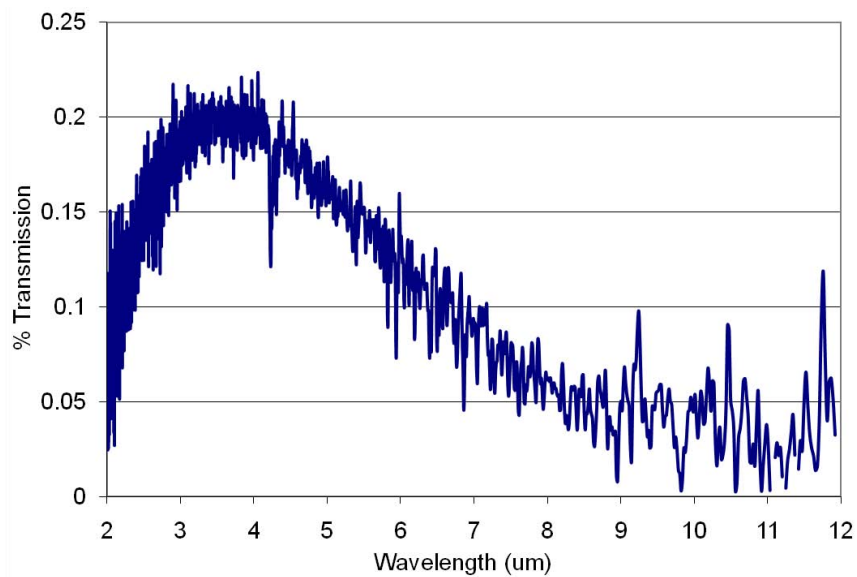
Figure 81 Plot of FTIR data collected on the transmission of the Ni-Si structure. Note that these numbers are very small and constitute essentially no transmission.

Results.

To compare the collected data plots of all the modeled and measured reflection and transmission data can be seen in Figure 82 and Figure 83. Comparing these results, a few things can be seen. The first thing is the similarity between the calculated reflection and transmission of the layered and homogeneous media, which is showing that at these layer thicknesses and wavelengths, the approximation of an effective medium is valid to use for design and analysis. When the calculated results are then compared to the experimental results, it can be seen that they do not line up. This is most likely due to differences in the material properties used in the modeling between those used in the fabricated structure. Looking only at the experimental data, it can be seen that there is a dip in the reflection going to a minimum near 4.75μm, not very far from the original

94

designed wavelength of 4.45µm. This drop in reflection is indicative the structure behaving as a homogeneous medium with a varying index of refraction, and becoming an antireflection coating, though the increase in transmission that should also be seen is not. This is likely due to the thickness of the structure, and the loss of all the layers causing essentially all the light to be absorbed. Though this structure may be acting as a homogeneous antireflection coating, it is not known if it has an ENZ point, or at what wavelength is occurs. Further work would need to be done to find the properties of the materials used in this structure, and then compare the homogeneous model to the measured data to determine if the structure is indeed acting as a homogeneous media with an ENZ point.
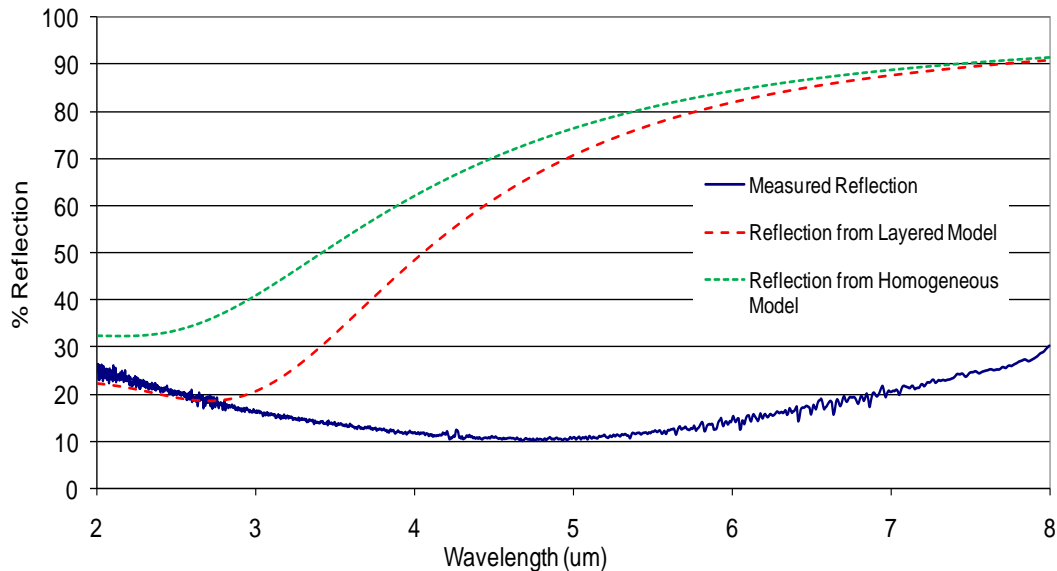
Figure 82 Plot comparing the modeled and measured reflection from the Ni-Si structure.
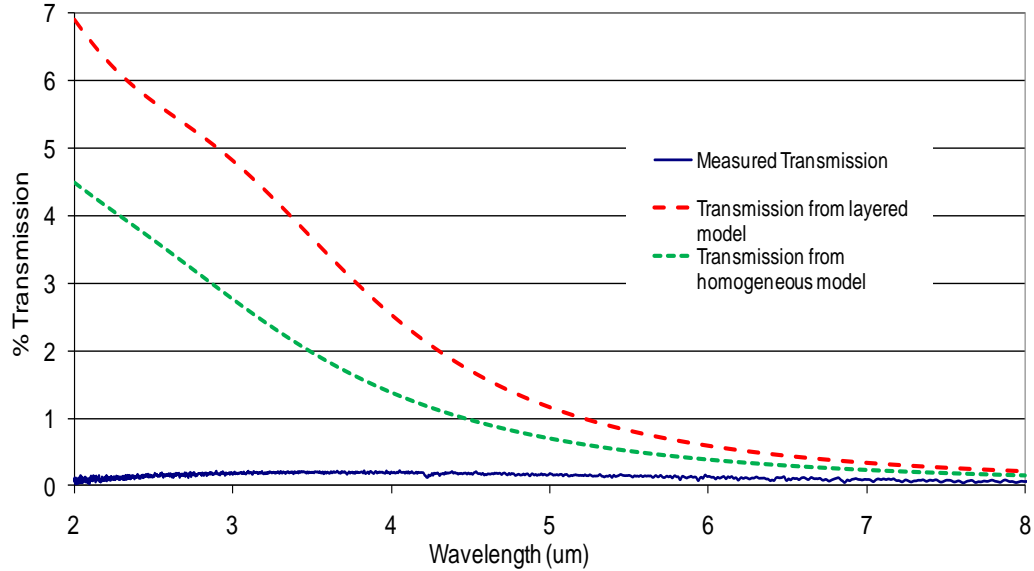
Figure 83 Plot comparing the modeled and measured transmission from the Ni-Si structure.

4.2 3D Metamaterials

The design and fabrication of the 3D metamaterial is discussed, starting from the initial design, and proceeding through the layer fabrication, lithography and etching. FDTD simulation was also done on this design to predict its optical behavior.

4.2.1 Gold-Hafnia

Structure design.

The first step in the process of developing this structure was to design it, though the design consists of a few intertwined factors that affect each other. The first consideration, and decision to be made, was the choice of materials to use. Gold was chosen as it has low losses in the infrared, does not tarnish and degrade like silver, and is easily etched [5]. Hafnium oxide, HfO_2 or hafnia, was chosen as the dielectric, as this material is known for its high relative permittivity. This could help the magnetic

96

resonator to function better by helping to guide the electric field between the gold layers of the magnetic resonator [5]. This material is also chosen because it is not a material that has been seen in literature for use in metamaterials, and its use here would be novel. Using these two materials, a MATLAB code written to find the width of the magnetic strips was run to determine what the possible widths to be used were. Using this program, it was determined that the largest possible width was 1.196µm, and of the possible widths, 1.12µm provided the best results. Of these results, a few different combinations of material thicknesses were listed, and the combination of Au thickness of t=78nm and HfO_2 thickness of d=93nm was chosen, as the other combinations included one with metal thicker than the dielectric, which is a configuration that has not been seen in any published work, and the other combination which had a thicker HfO_2 layer, which was a concern since the method of etching hafnia was not well known and was thought to be difficult; it was later found that a buffered hydrofluoric acid solution would work. Once the magnetic strip width was calculated, the rest of the design was laid out. A period of $2w$=2.24µm was used in both directions, and the width for the electric strips set at 1µm, the smallest feature size of the Heidelberg direct write laser system, which would be used to create the mask for the photolithography process.

Layer deposition.

After the calculations were done for the mask and the associated layer thicknesses were complete, the layers were then deposited following a characterization of both the gold and hafnia. In the hafnia depositions, it was found that the deposition monitor was not accurate in monitoring the deposition, giving a reading of 50nm for depositions that

were measured to be 60nm. This is possibly due to an inaccurate z-ratio, which is stated

to not be known in the deposition monitor manual. As a result of this, it was then decided

to make the hafnia deposition based only on time, using the rate of 7nm/second, which

was computed for the power of 250W. The characterization runs for the gold also tested

the use of hafnia as the adhesion layer for the gold. It was found that a 10nm layer of

hafnia, deposited at 250W, was able to create an adhesion layer. This was good because

using a layer like titanium would have added more loss to the design of the structure, as

metals have higher losses than dielectrics. The best gold deposition was found to be at

390V, with the deposition time determined by the deposition monitor. The parameters

used for the deposition of the hafnia and gold layers can be seen Table 7. A SEM

micrograph of the fabricated layers can be seen in Figure 84.

Table 7 Deposition parameters for Au- HfO$_2$ deposition

	Deposition Thickness	Pre-sputter Voltage/Power	Pre-sputter Time	Deposition Voltage/Power	Approximate Deposition Time
Au	78nm	390V	1 minute	390V	9 minutes
HfO$_2$	10nm	250W	1 minute	250W	1:03 minutes
	93nm	250W	1 minute	250W	13:02 minutes
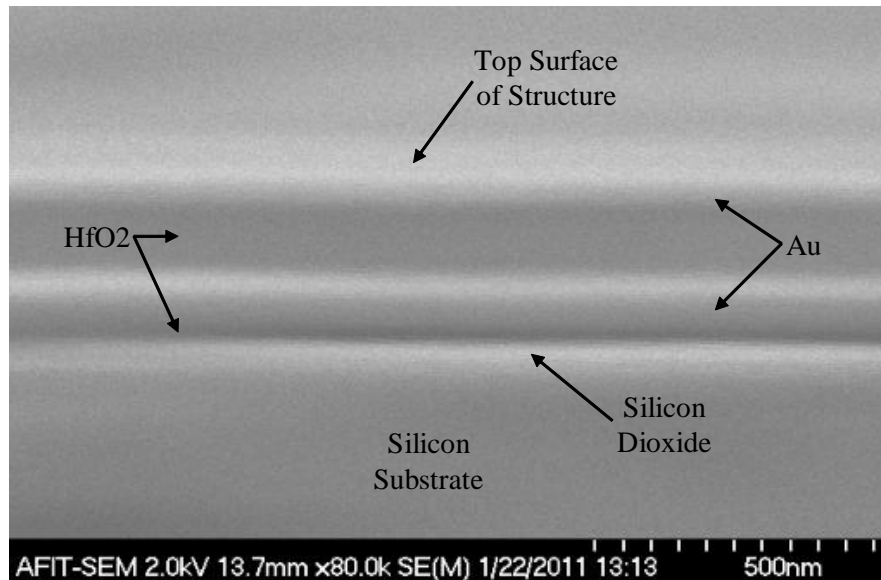
Figure 84 Micrograph of Au- HfO$_2$-Au layers. It appears that the top Au layer is thinner than the bottom Au layer, and only about 60nm.

Mask fabrication and lithography.

The first step in the lithography process was to create the design in L-Edit, the design software used to create the layout for a mask. Initially, a fishnet pattern with an area of 100mm^2 was to be made, as this would provide a large area to allow for easy testing of the structure using the FTIR or ellipsometry. It was attempted to create this pattern for an area that large, however, the sheer number of features created by making such a large area of a tiny objects would overload L-Edit and cause it to crash. As a solution to this, a smaller area of 5.01mm^2, and dimensions of 2.239mm x 2.239mm could be created in L-Edit without problems. To create a larger pattern, without creating a lager file in L-Edit, this pattern could be offset from the first place in the mask blank it was written within the Heidelberg direct write laser system software. By offsetting the center of the pattern three times, in the x, y, and in both the x and y, the length of the pattern, four copies of the pattern were written close enough together to create a larger

99

patterned area with dimensions of 4.478mm x 4.478 mm and an area of 20.05 mm^2. Using this mask, the process of patterning photoresist on the stack could now begin. The first step was to spin on photoresist at 4000 RPM for 30 seconds and then soft bake it for 75 seconds on a 110˚C hotplate. The photoresist was then exposed using the Suss MJB 3 mask aligner and the mask that was created for a variety of times, varying from the suggested time of 15 seconds for 1818. Samples were then developed using a 5:1 solution of DI water and 351 developer and DI water, rinsing the sample for 30 seconds with each on a 500 RPM spinner. It was found that the suggested exposure of 15 seconds was too long for the fine features, and produced dots instead of lines as can be seen in Figure 85.
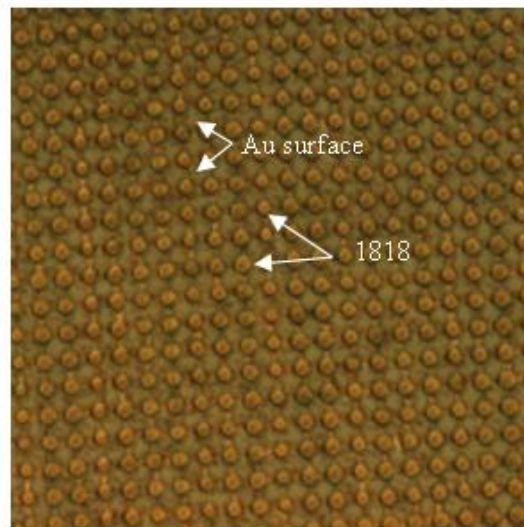
Figure 85 Micrograph of photoresist dots resulting from overexposure after photoresist development. This micrograph was taken with a light microscope at 100x magnification.

A much shorter exposure of 3 seconds was found to produce the fishnet pattern as can be seen in Figure 86, with the intended structure visible. Following development, the photoresist was then post baked for 2 minutes on a hot plate at 110˚C for two minutes to

stabilize and further solidify the photoresist. It was then attempted to etch the gold using this patterned 1818 as a mask. The gold etchant used was TFA, a potassium iodide/iodine solution, with an etch rate of approximately 30Å/s (3nm/s), giving an etch time of approximately 31 seconds for 78nm of gold. After etching for 30 seconds, the sample was then removed from the etchant and rinsed in DI water for 30 seconds before being dried with nitrogen. The sample was then examined under the light microscope where long streaks were observed, indicating that there was an inconsistent etch of the gold, with large areas where the holes in the 1818 did not clear, and the etchant did not reach the gold. These results can be seen in Figure 87.
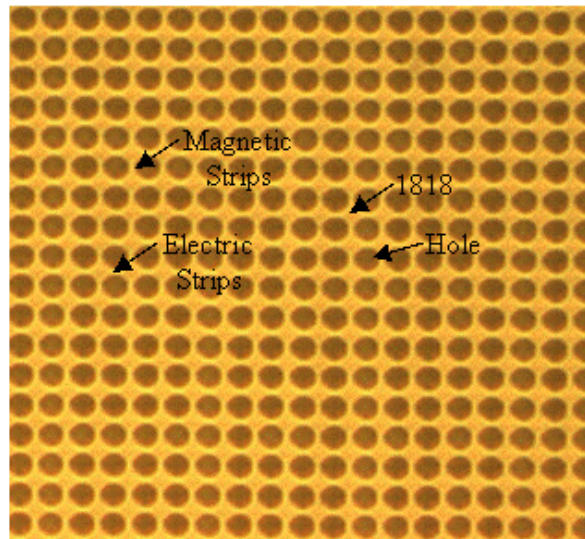
Figure 86 Micrograph of fishnet structure after 3 second exposure, showing the fishnet structure in photoresist.

To try and remedy this, the same procedure was done, only adding a plasma descum, a process to try and remove any residual exposed photoresist (scum) in the bottom of the holes with a plasma. The descum was done using an Anatech barrel asher

with an oxygen plasma. Samples were then descumed before being post baked and etched for 3 to 5 minutes at a RF power setting of 75W or 100W. Though this was attempted, the results of those processed with the descum were the same as those without the descum after the Au etch was performed and resembled those pictured in Figure 87.
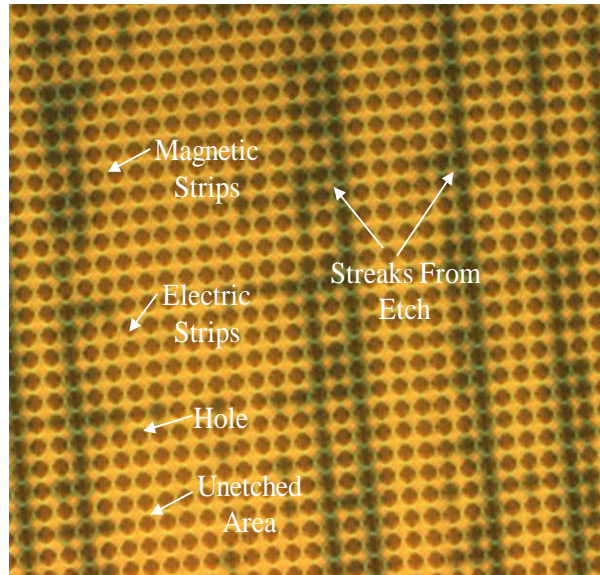
Figure 87 Micrograph of inconsistent gold etch. The dark streaks show areas where etching occurred, while the bright areas show where no etching occurred due to photoresist not clearing from the holes.

If a successful Au etch had been performed, the next step would have been the etching of the HfO_2 layer. This etch would have been done using buffered oxide etch (BOE), a buffered solution of hydrofluoric. This etchant was used based on the use of dilute hydrofluoric acid as HfO_2 etchant in [22]. A study of this etchant on HfO_2 was then done, and showed an etch rate of approximately 8Å/s (0.8nm/s), which would have meant an approximate etch time of 1 minute 54 seconds for 93nm of HfO_2, and been followed by a 30 second rinse in DI water, and then being dried with nitrogen. After this

etch, a final etch would be done of the Au at the bottom of the structure. This etch would have used the same process and times as the top layer. These last two etches were never carried out, as the lithography for this structure was never successfully completed, and the structure was never fully fabricated.

Testing and Analysis.

If it had been possible to create a testable a structure, the first test was to obtain the reflection and transmission from the layers using the FTIR. Since these results are not available, only simulated results were obtained.

The complexity of this structure did not allow the use of analytical means, and a simulation had to be used for analysis. The commercially available FDTD software Lumerical® was used to model the structure. This simulation involved the setup of one unit cell in the program, and the simulated reflection and transmission to be calculated from it. Though the software had a built in material library, the material properties for HfO_2 were not available and an index of 1.86 was used, with the materials library values used for Au based on data from [21]. A planewave source was used and monitors were placed above and below the structure to capture the transmission and reflection data by recording the power passing through the plane of the monitor and then normalizing it with respect to the power of the sourec. Periodic boundary conditions were used in the x and y interfaces of the generated mesh. This boundary condition is ideal for a structure like this that can be modeled as just one structure in an array of the same structure. Perfect electrical conductor boundary conditions used for the z interfaces, which make an interface from which no reflections would occur, as would be the case it this structure

were suspended in air. The meshed volume was made to be exactly the same size as the

unit cell in the x and y directions and the monitors were placed the same distance above

and below the structure. Screen shots showing the model geometry and setup can be seen

in Figure 88.
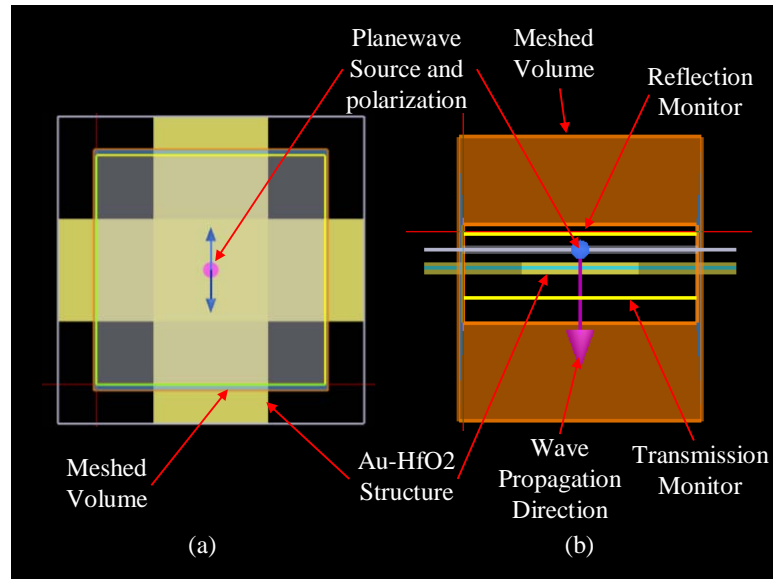
Figure 88 Screen shots showing the layout of the Lumerical simulation, with (a) showing a top view of the structure, and (b) a side view.

The simulation was run twice, one for each polarization of the planewave source

with respect to the orientation of the magnetic strips in the fishnet. The two polarizations

can be seen in Figure 89.
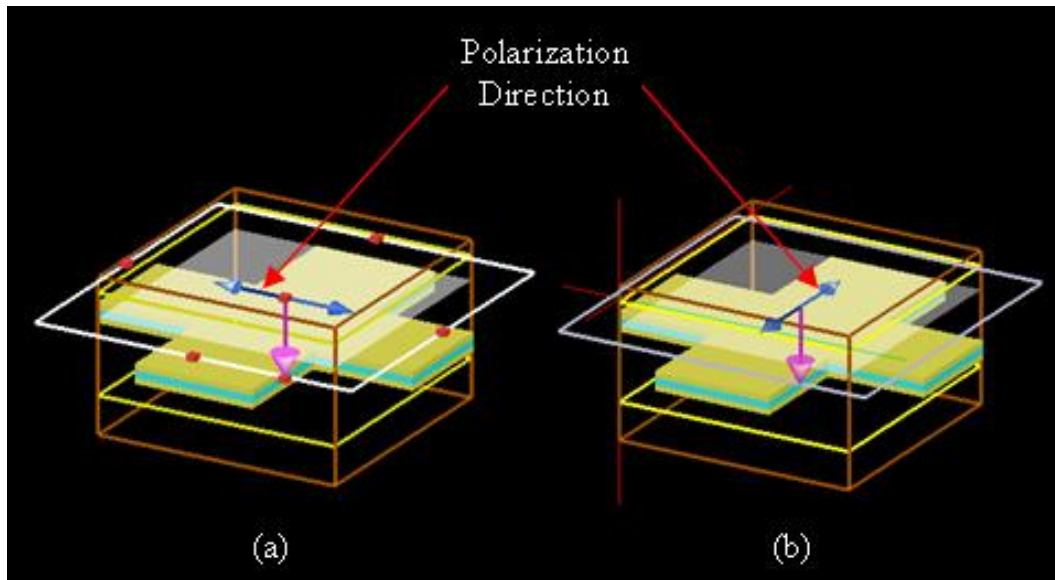
Figure 89 Screen shots of the different polarizations used for simulation, with (a) showing the light polarized to the electric strip and (b) showing the polarization to the magnetic strip.

The transmission and reflection of each polarization, as well as the average transmission and reflection and absorption, are seen in Figure 90, where the absorption is calculated by subtracting the transmission and reflection from one. The average values are plotted as they would be most like the data coming from the FTIR, which uses unpolarized light.
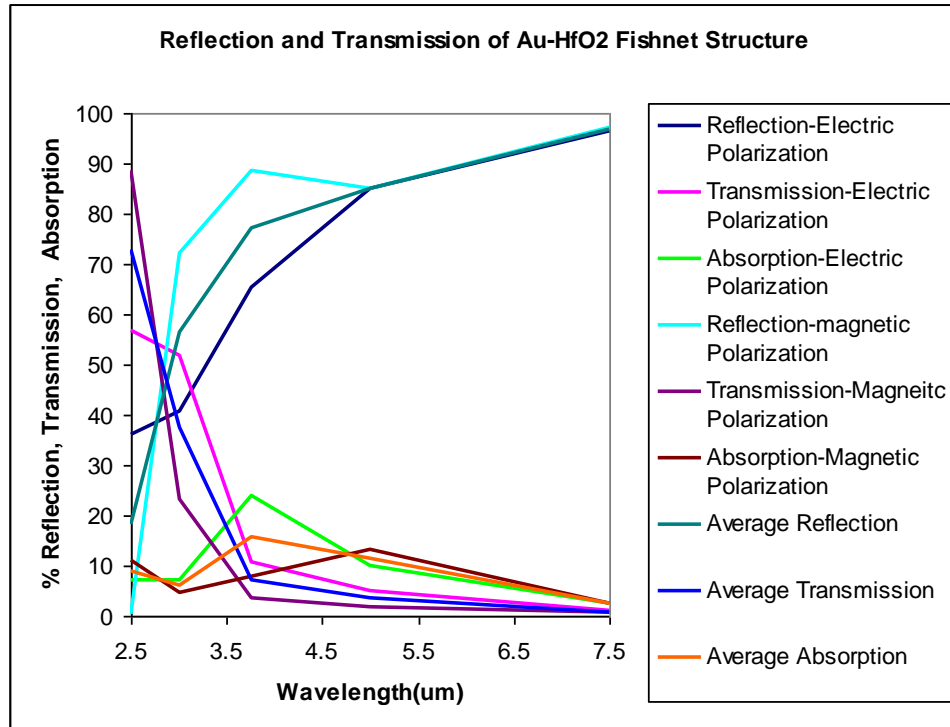
Figure 90 Plot of results from Lumerical simulation of the fishnet structure, showing the results of both polarizations and average values.

Results.

Examining the results that were produced, mainly the simulated data, it can be seen that there is a point to which the absorption for the electric polarization, and the average absorption increases at approximately 3.75μm. This rise in absorption is likely due to resonance in the structure, such as the resonance that occurs to form a negative permeability [5]. This is a promising result, but will require more research to determine if this absorption is due to a resonance that is producing a negative permeability, and negative index for this structure.

On the fabrication side, it was attempted to create this structure, and layers were deposited; however, a successful lithography and etching process was not developed.

The etching and fabrication of this structure is possible, but will require more effort to be achieved.

4.3 Summary

In order to fabricate a metamaterial, some of the fabrication techniques and methods first need to be studied and characterized. This study involves making deposits of material and analyzing the quality of the film, identifying how the layers of material needed for the epsilon near zero materials and negative index materials should be deposited. Layered epsilon near zero materials were fabricated, and test results compared with analytical results. It was then attempted to fabricate a 3D metamaterial with a negative index by etching a layered stack; however, more process development is needed to fabricate this structure. Simulation of this structure was done, with the results of it showing promise; however, more work still needs to be done to determine whether or not a negative index was produced in the simulation.

V. Conclusions and Recommendations

Investigations have been made into the fabrication and testing of layered and 3D metamaterials. Due to the ease of fabrication, many layered structures were fabricated and tested, while only one 3D material was attempted. When this investigation began, it was not clear what materials and methods would be successful, but now conclusions about what worked and what did not can be seen, and recommendations can be made.

5.1 Conclusions

This study has gone through the whole process of design, fabrication, and test for a few different optical metamaterials. The processes needed for fabrication were characterized, and then low permittivity ENZ materials were fabricated, using a process to determine the thickness of material based on the properties of the materials used. The fabricated structures were then able to be analyzed and tested to determine their optical characteristics. It was then determined that the Ag-Al$_2$O$_3$ and Au-SU-8 structures were behaving like a layered materials, while the Ti-Al$_2$O$_3$, Ti-MgF$_2$, and Ni-Si structures look to be acting like homogeneous media with a changing effective index, though low permittivity behavior could not be verified. The process of comparing the measured reflection and transmission to layered and homogeneous results could be used to determine the behavior of a structure, as was done for the Ag-Al$_2$O$_3$ structure, however, this process requires accurate material properties, which may not be found in literature.

A design for a 3D metamaterial was proposed and simulated; however, it was not fabricated and tested. Results from the simulation indicate that a negative index may be produced by this structure, however, more work would be needed to prove this.

5.2 Recommendations

There are many recommendations that can be made with the completion of this investigation. One of them would be to study the individual materials used to fabricate the metamaterial structures, and use the knowledge of each material to build up a single period stack, before making multiple periods. It was found from the ellipsometry that the Al_2O_3 used in the $Ag-Al_2O_3$ structure did not have the same optical properties found in published materials, and differences like this hamper one's ability to accurately design and predict the behavior of a structure. As such, in the same way studies were conducted to determine the thickness and surface properties of the deposited material, studies of the optical characteristics should also be done with each material. One of the most powerful tools for this is ellipsometry, which is able to determine whether a layer of material with certain optical properties is actually behaving like a layer of that material or if it has different properties. That being said, ellipsometry can and should be used to determine the properties of materials whose optical properties are unknown or not well known at certain wavelengths to be determined and used accurately. Only after the materials are characterized, should the work be done to determine layer thicknesses and make a structure. It is also of use to make single period structures first, characterize them, and then make multi-period stacks. This is useful, as it allows easier characterization, due to it being a simpler structure.

Other methods for the determination of the optical properties of the fabricated structure could also be used, and should be investigated, such as numerically solving for it from reflection and transmission values or using an extraction method. These methods

are useful in that they allow a direct extraction of the optical properties, and show exactly what the permittivity or index of a structure should be. Along with this, more thought should be given to the testing and analysis of the structure before it is made, with thought given to what can be measured and how those measurements can be related to effective or material properties.

Another suggestion would be to include more modeling and simulation, especially using the Lumerical® software package, which was not made available until late in this study. This is a powerful resource for modeling and predicting behavior of a metamaterial before it is fabricated, and the only effective way to model 3D metamaterials and can also deal with challenges to the modeling of the layered metamaterials due to total internal reflection. One following on in this work should become familiar with this software, as it would allow one to determine what materials and structures would be the best to fabricate.

Better methods to measure the reflection from these structures should be investigated, as total internal reflection resulting from a high angle of incidence led to difficulties in modeling and did not allow an accurate comparison of modeled and measured reflection. Improvements in this may be as simple as buying a new accessory for the FTIR, and should be investigated.

A final recommendation is that this research could be conducted in a more focused, team-based approach. When this research began, it was just thought that one should try to fabricate an optical metamaterial, but with no specifics as to what should be designed or what course of action to take. Future research should focus on only a couple of different material combinations and wavelengths, and go more in depth with the

characterization of the optical properties of the material, simulation and parameter extraction. Additionally, more of a team approach should be adopted, with the fabrication and optics people working side by side from the beginning. This way, the complex process of fabrication and testing can be fully understood, as each person has knowledge and experience that the other does not, and can share that to ensure that nothing is overlooked and the structure can be successfully designed, fabricated, and tested with meaningful results.

5.3 Contributions

Many contributions were made in the completion of this work. These contributions are listed in bullets below.

-A large amount of data on the index of refraction and permittivity of many materials that are available here at AFIT for fabrication was collected. This would be useful for future design and fabrication of optical materials and devices.

-A method was also developed to find the thicknesses of metal and dielectric layers to create a low permittivity metamaterial given the thickness of a period in the metamaterial.

-New low permittivity metamaterials were fabricated and shown to have these characteristics at 0.35μm and 2.6μm.

-A technique for characterizing low permittivity metamaterials by computing the reflection and transmission from the structure as a layered stack or as a homogeneous slab and comparing these numbers to the measured reflection and transmittance.

-A new 3D metamaterial using a unique dielectric of hafnium oxide was proposed, designed, and simulated.

Appendix A: MATERIAL PROPERTIES

The research conducted here depended heavily on the refractive index and permittivity of the metals and dielectrics used. Often, permittivity and refractive index values were found using the relationship of

$$\varepsilon = n^2, \varepsilon' + i\varepsilon'' = (n + ik)^2 \tag{22}$$

where either permittivity or refractive index values are known. The materials selected to be researched here were those materials that were available in the AFIT cleanroom and able to be deposited using the Discovery 18 sputtering system. Often times, accurate values or models could not be found, so the available values were used. The following details the equations and methods used to find the values used for this study.

B-1: Metals

The metals used in fabrication are described below; they are separated into two major groups, those that are described by a Drude model and those who had their model fit from experimental data.

Metals described by the Drude Model.

The metals of aluminum, copper, gold, silver and tungsten were modeled using Drude model which gives the complex permittivity as a function of wavelength. The Drude model is a commonly used model for the permittivity of metals and is based on the idea that the electrons behave like a gas in the metal [5]. This model has the form of

$$\varepsilon(\lambda) = 1 - \frac{\omega_p^2}{\left(\frac{hc}{\lambda}\right)^2 + i\left(\frac{hc}{\lambda}\right)\Gamma}$$

(23)

where ω_p is the plasma frequency in eV, Γ is the damping coefficient in eV, h is Planck's constant in eV, and c is the speed of light in micrometers. Table 8 displays the values used for these metals. Two sets of parameters were used for silver, which used the

Table 8 Drude parameters for selected metals

Metal	ω_p (eV)	Γ(eV)
Ag [23]	9.176	0.021
Ag [24]	8.9951	0.018
Al	14.764	0.0803
Au	8.2291	0.0268
Cu	7.9157	0.0345
W	6.005	0.0537

terms based off work done by Johnston and Christy and found in the PhotonicsDB tool on [23] for the 544nm Ag- Al$_2$O$_3$ stack, and numbers from [24] for all other calculations. This was done based on the ideal that the parameters in [23] were derived from visible light measurements, while the ones in [24] were derived from infrared measurements. Parameters for all other metals are from [24]. An interpolation of the data found in [20] was also done for 330nm-1.9μm, and was used in the modeling and analysis as well. It can be seen below.

$$n(\lambda)' = 4.4211\lambda^6 - 29.064\lambda^5 + 75.662\lambda^4 - 99.376\lambda^3 + 69.317\lambda^2 - 24.339\lambda + 3.4105$$ (24)
$$n(\lambda)'' = -3.52214\lambda^4 + 16.76\lambda^3 - 28.336\lambda^2 + 27.718\lambda - 5.541$$

Other Metals

The other metals used did not have models that accurately described them, so measurements of the index of these materials made at infrared frequencies were found, and a curve fit to the data. Each metal, the data that was found, and the fit equation are displayed below.

Nickel.

The model for Ni was based on numbers from Lynch et al and found in [24] for the range 1.5-12.4μm for n' and n''.

$$
\begin{aligned}
n(\lambda)' &= 0.0001\lambda^5 - 0.0062\lambda^4 + 0.1125\lambda^3 - 0.8515\lambda^2 + 2.8371\lambda + 0.6676 \\
n(\lambda)'' &= -6\times10^{-5}\lambda^4 - 0.008\lambda^3 + 0.2162\lambda^2 + 2.1\lambda + 3.1424
\end{aligned}
\tag{25}
$$

Iron.

The model for Fe was based on numbers from Weaver et al and found in [24] for the range 1-19μm for n' and n''.

$$
\begin{aligned}
n(\lambda)' &= 7\times10^{-5}\lambda^5 - 0.0035\lambda^4 + 0.0638\lambda^3 - 0.4762\lambda^2 + 1.9005\lambda + 0.7974 \\
n(\lambda)'' &= 0.0009\lambda^4 - 0.0404\lambda^3 + 0.5608\lambda^2 - 0.4658\lambda + 5.0077
\end{aligned}
\tag{26}
$$

Palladium.

The model for Pd was based on numbers from Weaver and Bendow and found in [24] for the range 1.55-12.4μm for n' and n''.

$$n(\lambda)'=-5\times10^{-5}\lambda^6+0.0024\lambda^5 - 0.0505\lambda^4 + 0.5417\lambda^3 - 3.0273\lambda^2 + 7.893\lambda - 3.4088$$
$$n(\lambda)''=-0.0103\lambda^3 + 0.2572\lambda^2 + 2.4465\lambda + 3.7496$$

(27)

Titanium.

The model for Ti was based on numbers from Kirillova and Charikov and found in [24] for the range 2.5-12μm for n' and n".

$$n(\lambda)'=-0.0068\lambda^3 + 0.1812\lambda^2 - 0.9281\lambda + 5.8689$$
$$n(\lambda)''=-0.0142\lambda^3 + 0.2736\lambda^2 + 0.2448\lambda + 2.8602$$

(28)

B-2: Dielectrics

The dielectrics considered in this study are described below, with either an equation or interpolation of available data. Sometimes data or models were only available for visible wavelengths, and had to be used as estimates for the properties of the material in the infrared. For this study, the dielectrics were considered to be lossless, except for certain cases, such as silicon in the visible.

Aluminium Oxide (alumina).

Two sources for data were used for this material, one for the 544nm Ag-Al_2O_3 stack and one for the Ti- Al_2O_3 IR stack. The model for the 544nm structure came from a regression of data found in [21]. The data was interpolated for a range of 300nm to 800nm and the following equation was produced.

$$n(\lambda) = -7\times10^{-10}\lambda^3 +1\times10^{-6}\lambda^2 - 0.0009\lambda +1.8739$$

(29)

The IR data came from a dispersion equation found in [25]. No data for amorphous or polycrystalline Al_2O_3 was found, so the dispersion equation for synthetic crystalline Al_2O_3, sapphire, was used, with a statement on the transmission of this material being from 0.17-6.5μm.

$$n(\lambda)^2 = 1 + \sum_{i=1}^{3} \frac{A_i \lambda^2}{\lambda^2 - \lambda_i^2} \tag{30}$$

where

$A_1=1.023798$ $\lambda_1^2=0.00377588$

$A_2=1.058264$ $\lambda_2^2=0.0122544$

$A_3=5.280792$ $\lambda_3^2=321.3616$

Barium Fluoride.

A dispersion equation for BaF_2 was found in [25], as well as a statement about this material being transparent from 0.15-15μm.

$$n(\lambda)^2 = 1 + \sum_{i=1}^{3} \frac{A_i}{\lambda^2 - \lambda_i^2} \tag{31}$$

where

$A_1=0.643356$ $\lambda_1=0.057789$

$A_2=0.506762$ $\lambda_2=0.10968$

$A_3=3.8261$ $\lambda_3=46.3864$

Calcium Fluoride.

A dispersion equation for CaF_2 was found in [25], as well as a statement about this material being transparent from 0.13-12μm.

$$n(\lambda)^2 = 1 + \sum_{i=1}^{3} \frac{A_i}{\lambda^2 - \lambda_i^2} \tag{32}$$

where

A₁=0.5675888   λ₁=0.050263605

A₂=0.4710914   λ₂=0.1003909

A₃=3.8484723   λ₃=34.64904

Hafnia Oxide (hafnia).

A Cauchy equation for HfO_2 was found in [26]. This equation was made from a fit of optical data, so it may not be very accurate in the infrared.

$$n(\lambda) = 1.86 + \frac{0.00716}{\lambda^2} \tag{33}$$

Magnesium Fluoride.

Dispersion equations for MgF_2 were found in [25], with the transmission window stated for 0.11-7.5μm. It was also found that the index of refraction is birefringent, with the index varying between an ordinary and extraordinary axis. Since the layer that will be deposited is likely to be polycrystalline, with no clear crystalline orientation, values for the index in both directions were averaged.

118

$$n(\lambda) = \frac{n_o(\lambda) + n_e(\lambda)}{2}$$

$$n_o(\lambda) = 1.36957 + \frac{0.0035821}{\lambda - 0.14925} \tag{34}$$

$$n_e(\lambda) = 1.381 + \frac{0.0037415}{\lambda - 0.14947}$$

Magnesium Oxide.

A dispersion equation for MgO was found in [27], with a statement about this material being transparent from 0.25-8.5μm found in [25].

$$n^2(\lambda) = 2.956362 - 0.01062378\lambda^2 - 0.0000204968\lambda^4 - \frac{0.02195770}{\lambda^2 - 0.01428322} \tag{35}$$

Polymethylglutarimide (PMGI or SF 11).

A Cauchy equation for PMGI was found in [28]. This equation was made from a fit of optical data, so it may not be very accurate in the infrared.

$$n(\lambda) = 1.524 + \frac{0.005176}{\lambda^2} + \frac{0.0002105}{\lambda^4} \tag{36}$$

Amorphous Silicon.

The model for amorphous Si was interpolated from data on amorphous Si published in [21]. This model interpolated data points from 2.473-16.73μm.

$$n(\lambda) = -3 \times 10^{-5}\lambda^4 + 0.001\lambda^3 - 0.0099\lambda^2 + 0.0139\lambda + 3.8777 \tag{37}$$

Crystalline Silicon.

The model for crystalline Si, which was used as the substrate for the fabricated

materials, was found in [25], with a statement for transparency present 1-10μm.

$$n(\lambda) = 3.41983 + 1.59906 \times 10^{-1} L - 1.23109 \times 10^{-1} L^2 + 1.26878 \times 10^{-6} \lambda^2 - 1.95104 \times 10^{-9} \lambda^4 \qquad (38)$$

Where L is a parameter defined by

$$L = \frac{1}{\lambda^2 - 0.028} \qquad (39)$$

For visible wavelengths, a regression of data found in [21] was done for the range

250-800nm. Two separate regressions were done, one for each part of the index.

$$n'(\lambda) = 1526.4\lambda^5 - 4885.4\lambda^4 + 6100.8\lambda^3 - 3696\lambda^2 + 1076.6\lambda - 114.91$$
$$n''(\lambda) = -26593\lambda^6 + 89496\lambda^5 - 122489\lambda^4 + 86937\lambda^3 - 33573\lambda^2 + 6637.6\lambda - 518.31 \qquad (40)$$

Silicon Dioxide.

The models for SiO_2 were interpolated from data on silicon dioxide glass published

in [21]. This models interpolated data points from .25-1μm in the visible and 3-8μm in

the IR.

$$n(\lambda) = 0.882\lambda^4 - 2.6084\lambda^3 + 2.8425\lambda^2 - 1.3745\lambda + 1.7088 \text{ (visible)}$$
$$n(\lambda) = -0.0053\lambda^5 + 0.1377\lambda^4 - 1.4127\lambda^3 + 7.1223\lambda^2 - 17.651\lambda + 18.618 \text{ (IR)} \qquad (41)$$

Silicon Carbide.

The model for SiC was found in [21], and was a model produced by Sptizer et al for

the 2-22μm wavelengths. This model includes a complex part of the index, but this was

ignored for the calculations done here as it is very small compared to the complex values found in metals.

$$n^2(\lambda)=\varepsilon_\infty\left(1+\frac{\omega_L^2-\omega_T^2}{\omega_T^2-\omega^2+i\Gamma\omega}\right)$$ (42)

Where wavelength is in cm^{-1}, and $\omega_L=969$, $\omega_T=793$, $\Gamma=4.76$, and $\varepsilon_\infty=6.7$

SU-8.

The model for SU-8 was found in [29] for SU-8 2000, which is simply a version of the SU-8 photoresist that has not been thinned with as much methanol as the SU-8 5 used in this study. The index of refraction was given in Cauchy coefficients. Though this data is for optical wavelengths and uncured SU-8, it was the only data available.

$$n(\lambda)=1.556+\frac{0.00796}{\lambda^2}+\frac{0.00014}{\lambda^4}$$ (43)

Titanium Dioxide.

The model for TiO$_2$ was interpolated from data on TiO$_2$ published in [21]. It was seen that this material had birefringence, and the average of the ordinary and extraordinary values was used to make an interpolation function. This model interpolated data points from 1.28-15.8μm.

$$n(\lambda)=-1\times10^{-6}\lambda^6+8\times10^{-5}\lambda^5-0.0023\lambda^4+0.0304\lambda^3-0.1921\lambda^2+0.5084\lambda+2.1931$$ (44)

Zinc Oxide.

The index of ZnO was modeled by a Sellmeir dispersion model found in [30], based on data collected from 0.250-1.2μm.

$$n^2(\lambda)=1+\frac{1.881\lambda^2}{\lambda^2-0.05382^2} \tag{45}$$

Zinc Sulfide.

A dispersion equation for ZnS was found in [25], as well as a statement about this material being transparent from 0.5-5μm and 8-10μm.

$$n^2(\lambda)=5.131+\frac{1.275\times10^7}{\lambda^2-0.732\times10^7} \tag{46}$$

Appendix B: LAYER SCHEDULES

After all the material properties were gathered, spreadsheets were then made using the data on the materials gathered in Appendix A. Calculations done here are for the permittivity weightings needed for the designed permittivity of the layered metamaterials, with the physical dimensions in nanometers, with the exception of SU-8, which was taken at the default thickness of 5μm or 5000nm), and the wavelengths of light in micrometers. The wavelengths of 3.39, 4.45, 5, 5.4, 6, 8, and 9μm were used due to the fact that these are wavelengths that would be the easiest for further testing to be done with. Some calculations were done for the wavelengths of 544 and 633nm. Material combinations that were actually fabricated are highlighted in yellow. The results are arranged by metal, with each paired with all the different dielectrics.

B-1: Silver, Ag

Wavelength (in um)	0.544	0.633	3.39	4.45	5	5.4	6	8	9
Al2O3 index	1.756	1.756	1.755	1.755	1.755	1.755	1.755	1.755	1.754
permittivity	3.083	3.082	3.081	3.081	3.081	3.081	3.080	3.079	3.078
Ag index	0.016+3.81i	0.021+4.478i	0.604+24.53i	1.039+32.19i	1.311+36.16i	1.528+39.04i	1.884+43.36i	3.338+57.70i	4.215+64.83i
permittivity	-14.5+0.12i	-20.05+0.19i	-6.0e2+2.9e1i	-1.0e3+6.6e1i	-1.30e3+9.4e1i	-1.522e3+1.193e2i	-1.877e3+1.634e2i	-3.318e3+3.852e2i	-4.18e3+5.46e2i

Ratio of dielectric to metal

	0.544	3.39	4.45	5	5.4	6	8	9
	4.721	195.230	335.924	423.982	494.063	609.371	1077.696	1359.685

metal thickness

period (nm)	0.544	3.39	4.45	5	5.4	6	8	9
75	13.109	0.382	0.223	0.176	0.151	0.123	0.070	0.055
100	17.479	0.510	0.297	0.235	0.202	0.164	0.093	0.073
150	29.718	0.764	0.445	0.353	0.303	0.246	0.139	0.110
200	34.957	1.019	0.594	0.471	0.404	0.328	0.185	0.147
300	52.436	1.529	0.890	0.706	0.606	0.492	0.278	0.220
400	69.914	2.038	1.187	0.941	0.808	0.655	0.371	0.294
500	87.393	2.548	1.484	1.177	1.010	0.819	0.464	0.367
600	104.871	3.058	1.781	1.412	1.212	0.983	0.556	0.441

Wavelength (in um)	0.544	0.633	3.39	4.45	5	5.4	6	8	9
BaF2 index	1.4759	1.4733	1.4596	1.4543	1.4510	1.4484	1.4440	1.4258	1.4144
permittivity	2.1784	2.1705	2.1303	2.1150	2.1055	2.0978	2.0852	2.0330	2.0006
Ag index	0.016+3.81i	0.021+4.478i	0.604+24.53i	1.039+32.19i	1.311+36.16i	1.528+39.04i	1.884+43.36i	3.338+57.70i	4.215+64.83i
permittivity	-14.5+0.12i	-20.05+0.19i	-6.0e2+2.9e1i	-1.0e3+6.6e1i	-1.30e3+9.4e1i	-1.522e3+1.193e2i	-1.877e3+1.634e2i	-3.318e3+3.852e2i	-4.18e3+5.46e2i

Ratio of dielectric to metal

0.544	3.39	4.45	5	5.4	6	8	9
6.681166	9.2419	282.4027	489.6465	620.3838	725.6999	900.1347	1632.2547

metal thickness

period (nm)	0.544	3.39	4.45	5	5.4	6	8	9
75	0.2646	0.1529	0.1207	0.1032	0.0832	0.0459	0.0358	0.2646
100	0.3529	0.2038	0.1609	0.1376	0.1110	0.0612	0.0478	0.3529
150	0.5293	0.3057	0.2414	0.2064	0.1665	0.0918	0.0717	0.5293
200	0.7057	0.4076	0.3219	0.2752	0.2219	0.1225	0.0956	0.7057
300	1.0586	0.6114	0.4828	0.4128	0.3329	0.1837	0.1433	1.0586
400	1.4114	0.8153	0.6437	0.5504	0.4439	0.2449	0.1911	1.4114
500	1.7643	1.0191	0.8047	0.6880	0.5549	0.3061	0.2389	1.7643
600	2.1171	1.2229	0.9656	0.8257	0.6658	0.3674	0.2867	2.1171

Wavelength (in um)	0.544	0.633	3.39	4.45	5	5.4	6	8	9
CaF2	index	1.4350	1.4329	1.4149	1.4052	1.3990	1.3939	1.3856	1.3498	1.3268
	permittivity	2.0592	2.0532	2.0020	1.9744	1.9571	1.9431	1.9199	1.8221	1.7603
Ag	index	0.016+3.81i	0.021+4.478i	0.604+24.53i	1.039+32.19i	1.311+36.16i	1.528+39.04i	1.884+43.36i	3.338+57.70i	4.215+64.83i
	permittivity	-14.5+0.12i	-20.05+0.19i	-6.0e2+2.9e1i	-1.0e3+6.6e1i	-1.30e3+9.4e1i	-1.522e3+1.193e2i	-1.877e3+1.634e2i	-3.318e3+3.852e2i	-4.18e3+5.46e2i

Ratio of dielectric to metal

	0.544	3.39	4.45	5	5.4	6	8	9
	7.067844	9.7702	300.4959	524.5006	667.4216	783.4940	977.6633	1821.1729

metal thickness

period (nm)	0.544	3.39	4.45	5	5.4	6	8	9
75	0.2488	0.1427	0.1122	0.0956	0.0766	0.0412	0.0315	0.2488
100	0.3317	0.1903	0.1496	0.1275	0.1022	0.0549	0.0420	0.3317
150	0.4975	0.2854	0.2244	0.1912	0.1533	0.0823	0.0631	0.4975
200	0.6634	0.3806	0.2992	0.2549	0.2044	0.1098	0.0841	0.6634
300	0.9950	0.5709	0.4488	0.3824	0.3065	0.1646	0.1261	0.9950
400	1.3267	0.7612	0.5984	0.5099	0.4087	0.2195	0.1682	1.3267
500	1.6584	0.9515	0.7480	0.6374	0.5109	0.2744	0.2102	1.6584
600	1.9901	1.1418	0.8976	0.7648	0.6131	0.3293	0.2523	1.9901

Wavelength (in um)	0.544	0.633	3.39	4.45	5	5.4	6	8	9
HfO2 index Cauchy	1.8842	1.8779	1.8606	1.8604	1.8603	1.8602	1.8602	1.8601	1.8601
permittivity	3.5502	3.5264	3.4619	3.4609	3.4607	3.4605	3.4603	3.4600	3.4599
Ag index	0.016+3.81i	0.021+4.478i	0.604+24.53i	1.039+32.19i	1.311+36.16i	1.528+39.04i	1.884+43.36i	3.338+57.70i	4.215+64.83i
permittivity	-14.5+0.12i	-20.05+0.19i	-6.0e2+2.9e1i	-1.0e3+6.6e1i	-1.30e3+9.4e1i	-1.522e3+1.193e2i	-1.877e3+1.634e2i	-3.318e3+3.852e2i	-4.18e3+5.46e2i

Ratio of dielectric to metal

0.544	3.39	4.45	5	5.4	6	8	9
4.099585	5.6884	173.7765	299.2246	377.4419	439.9347	542.4323	959.0418

metal thickness

period (nm)	0.544	3.39	4.45	5	5.4	6	8	9
75	0.4291	0.2498	0.1982	0.1701	0.1380	0.0781	0.0620	0.4291
100	0.5722	0.3331	0.2642	0.2268	0.1840	0.1042	0.0826	0.5722
150	0.8582	0.4996	0.3964	0.3402	0.2760	0.1562	0.1239	0.8582
200	1.1443	0.6662	0.5285	0.4536	0.3680	0.2083	0.1652	1.1443
300	1.7165	0.9993	0.7927	0.6804	0.5520	0.3125	0.2478	1.7165
400	2.2886	1.3323	1.0570	0.9072	0.7361	0.4166	0.3304	2.2886
500	2.8608	1.6654	1.3212	1.1340	0.9201	0.5208	0.4130	2.8608
600	3.4330	1.9985	1.5854	1.3607	1.1041	0.6250	0.4956	3.4330

Wavelength (in um)	0.544	0.633	3.39	4.45	5	5.4	6	8	9
MgF2 index	1.3753	1.3753	1.3753	1.3753	1.3753	1.3753	1.3753	1.3753	1.3753
permittivity	1.8914	1.8914	1.8914	1.8914	1.8914	1.8914	1.8914	1.8914	1.8914
Ag index	0.016+3.81i	0.021+4.478i	0.604+24.53i	1.039+32.19i	1.311+36.16i	1.528+39.04i	1.884+43.36i	3.338+57.70i	4.215+64.83i
permittivity	-14.5+0.12i	-20.05+0.19i	-6.0e2+2.9e1i	-1.0e3+6.6e1i	-1.30e3+9.4e1i	-1.522e3+1.193e2i	-1.877e3+1.634e2i	-3.318e3+3.852e2i	-4.18e3+5.46e2i

Ratio of dielectric to metal

0.544	3.39	4.45	5	5.4	6	8	9
7.6949	10.6056	318.0697	547.5283	690.5963	804.9026	992.3819	1754.4064

metal thickness

period (nm)	0.544	3.39	4.45	5	5.4	6	8	9
75	0.2351	0.1367	0.1084	0.0931	0.0755	0.0427	0.0339	0.2351
100	0.3134	0.1823	0.1446	0.1241	0.1007	0.0570	0.0452	0.3134
150	0.4701	0.2735	0.2169	0.1861	0.1510	0.0855	0.0678	0.4701
200	0.6268	0.3646	0.2892	0.2482	0.2013	0.1139	0.0903	0.6268
300	0.9402	0.5469	0.4338	0.3723	0.3020	0.1709	0.1355	0.9402
400	1.2536	0.7292	0.5784	0.4963	0.4027	0.2279	0.1807	1.2536
500	1.5671	0.9115	0.7230	0.6204	0.5033	0.2848	0.2259	1.5671
600	1.8805	1.0938	0.8676	0.7445	0.6040	0.3418	0.2710	1.8805

Wavelength (in um)	0.544	0.633	3.39	4.45	5	5.4	6	8	9
MgO index	1.6957	1.7016	1.6822	1.6543	1.6362	1.6212	1.5958	1.4806	1.4004
permittivity	2.8753	2.8953	2.8297	2.7368	2.6771	2.6284	2.5467	2.1921	1.9611
Ag index	0.016+3.81i	0.021+4.478i	0.604+24.53i	1.039+32.19i	1.311+36.16i	1.528+39.04i	1.884+43.36i	3.338+57.70i	4.215+64.83i
permittivity	-14.5+0.12i	-20.05+0.19i	-6.0e2+2.9e1i	-1.0e3+6.6e1i	-1.30e3+9.4e1i	-1.522e3+1.193e2i	-1.877e3+1.634e2i	-3.318e3+3.852e2i	-4.18e3+5.46e2i

Ratio of dielectric to metal

0.544	3.39	4.45	5	5.4	6	8	9
5.0619	6.9284	212.6056	378.3930	487.9200	579.2137	737.0230	1513.7249

metal thickness

period (nm)	0.544	3.39	4.45	5	5.4	6	8	9
75	0.3511	0.1977	0.1534	0.1293	0.1016	0.0495	0.0351	0.3511
100	0.4682	0.2636	0.2045	0.1724	0.1355	0.0660	0.0468	0.4682
150	0.7022	0.3954	0.3068	0.2585	0.2032	0.0990	0.0703	0.7022
200	0.9363	0.5272	0.4091	0.3447	0.2710	0.1320	0.0937	0.9363
300	1.4045	0.7907	0.6136	0.5171	0.4065	0.1981	0.1405	1.4045
400	1.8726	1.0543	0.8181	0.6894	0.5420	0.2641	0.1873	1.8726
500	2.3408	1.3179	1.0227	0.8618	0.6775	0.3301	0.2342	2.3408
600	2.8089	1.5815	1.2272	1.0341	0.8130	0.3961	0.2810	2.8089

Wavelength (in um)	0.544	0.633	3.39	4.45	5	5.4	6	8	9
SF 11 index	1.5439	1.5382	1.5245	1.5243	1.5242	1.5242	1.5241	1.5241	1.5241
permittivity	2.3836	2.3661	2.3240	2.3234	2.3232	2.3231	2.3230	2.3228	2.3228
Ag index	0.016+3.81i	0.021+4.478i	0.604+24.53i	1.039+32.19i	1.311+36.16i	1.528+39.04i	1.884+43.36i	3.338+57.70i	4.215+64.83i
permittivity	-14.5+0.12i	-20.05+0.19i	-6.0e2+2.9e1i	-1.0e3+6.6e1i	-1.30e3+9.4e1i	-1.522e3+1.193e2i	-1.877e3+1.634e2i	-3.318e3+3.852e2i	-4.18e3+5.46e2i

Ratio of dielectric to metal

	0.544	3.39	4.45	5	5.4	6	8	9
	6.1060	8.4777	258.8692	445.7310	562.2398	655.3262	808.0018	1428.5636

metal thickness

period (nm)	0.544	3.39	4.45	5	5.4	6	8	9
75	0.2886	0.1679	0.1332	0.1143	0.0927	0.0525	0.0416	0.2886
100	0.3848	0.2238	0.1775	0.1524	0.1236	0.0700	0.0555	0.3848
150	0.5772	0.3358	0.2663	0.2285	0.1854	0.1049	0.0832	0.5772
200	0.7696	0.4477	0.3551	0.3047	0.2472	0.1399	0.1109	0.7696
300	1.1544	0.6715	0.5326	0.4571	0.3708	0.2099	0.1664	1.1544
400	1.5392	0.8954	0.7102	0.6095	0.4944	0.2798	0.2219	1.5392
500	1.9240	1.1192	0.8877	0.7618	0.6180	0.3498	0.2773	1.9240
600	2.3089	1.3431	1.0653	0.9142	0.7417	0.4197	0.3328	2.3089

Wavelength (in um)		0.544	0.633	3.39	4.45	5	5.4	6	8	9
amorphous	index	3.8825	3.8828	3.8460	3.8199	3.8060	3.7960	3.7818	3.7444	3.7331
Si	permittivity	15.0737	15.0760	14.7921	14.5914	14.4853	14.4099	14.3022	14.0207	13.9358
Ag	index	0.016+3.81i	0.021+4.478i	0.604+24.53i	1.039+32.19i	1.311+36.16i	1.528+39.04i	1.884+43.36i	3.338+57.70i	4.215+64.83i
	permittivity	-14.5+0.12i	-20.05+0.19i	-6.0e2+2.9e1i	-1.0e3+6.6e1i	-1.30e3+9.4e1i	-1.522e3+1.193e2i	-1.877e3+1.634e2i	-3.318e3+3.852e2i	-4.18e3+5.46e2i

Ratio of dielectric to metal

0.544	3.39	4.45	5	5.4	6	8	9
0.9655	1.3306	40.6705	70.9734	90.1745	105.6500	131.2389	236.6718

metal thickness

period (nm)	0.544	3.39	4.45	5	5.4	6	8	9
75	1.7998	1.0421	0.8226	0.7032	0.5672	0.3156	0.2489	1.7998
100	2.3998	1.3894	1.0968	0.9376	0.7562	0.4207	0.3319	2.3998
150	3.5997	2.0841	1.6452	1.4065	1.1343	0.6311	0.4978	3.5997
200	4.7996	2.7788	2.1936	1.8753	1.5124	0.8415	0.6637	4.7996
300	7.1993	4.1682	3.2904	2.8129	2.2686	1.2622	0.9956	7.1993
400	9.5991	5.5576	4.3872	3.7506	3.0248	1.6830	1.3275	9.5991
500	11.9989	6.9470	5.4840	4.6882	3.7810	2.1037	1.6594	11.9989
600	14.3987	8.3364	6.5808	5.6259	4.5372	2.5245	1.9912	14.3987

Wavelength (in um)	0.544	0.633	3.39	4.45	5	5.4	6	8	9
SiC index	2.5872	2.5868	2.5382	2.4960	2.5868	2.4409	2.3944	2.1153	1.8083
permittivity	6.6938	6.6917	6.4426	6.2300	6.0837	5.9581	5.7331	4.4747	3.2700
Ag index	0.016+3.81i	0.021+4.478i	0.604+24.53i	1.039+32.19i	1.311+36.16i	1.528+39.04i	1.884+43.36i	3.338+57.70i	4.215+64.83i
permittivity	-14.5+0.12i	-20.05+0.19i	-6.0e2+2.9e1i	-1.0e3+6.6e1i	-1.30e3+9.4e1i	-1.522e3+1.193e2i	-1.877e3+1.634e2i	-3.318e3+3.852e2i	-4.18e3+5.46e2i

Ratio of dielectric to metal

	0.544	3.39	4.45	5	5.4	6	8	9
	2.1743	2.9977	93.3781	166.2271	214.7058	255.5182	327.3950	741.5715

metal thickness

period (nm)	0.544	3.39	4.45	5	5.4	6	8	9
75	0.7947	0.4485	0.3477	0.2924	0.2284	0.1010	0.0586	0.7947
100	1.0596	0.5980	0.4636	0.3898	0.3045	0.1347	0.0781	1.0596
150	1.5894	0.8970	0.6954	0.5848	0.4568	0.2020	0.1171	1.5894
200	2.1191	1.1960	0.9272	0.7797	0.6090	0.2693	0.1561	2.1191
300	3.1787	1.7940	1.3908	1.1695	0.9135	0.4040	0.2342	3.1787
400	4.2383	2.3920	1.8544	1.5593	1.2180	0.5387	0.3123	4.2383
500	5.2978	2.9899	2.3180	1.9492	1.5226	0.6733	0.3904	5.2978
600	6.3574	3.5879	2.7816	2.3390	1.8271	0.8080	0.4684	6.3574

Wavelength (in um)	0.544	0.633	3.39	4.45	5	5.4	6	8	9
TiO2 index	2.4175	2.4453	2.6269	2.5757	2.5607	2.5602	2.5822	2.9935	3.5353
permittivity	5.8444	5.9795	6.9003	6.6345	6.5573	6.5544	6.6679	8.9609	12.4981
Ag index	0.016+3.81i	0.021+4.478i	0.604+24.53i	1.039+32.19i	1.311+36.16i	1.528+39.04i	1.884+43.36i	3.338+57.70i	4.215+64.83i
permittivity	-14.5+0.12i	-20.05+0.19i	-6.0e2+2.9e1i	-1.0e3+6.6e1i	-1.30e3+9.4e1i	-1.522e3+1.193e2i	-1.877e3+1.634e2i	-3.318e3+3.852e2i	-4.18e3+5.46e2i

Ratio of dielectric to metal

	0.544	3.39	4.45	5	5.4	6	8	9
	2.4903	3.3547	87.1840	156.0935	199.1975	232.2719	281.4961	370.3069

metal thickness

period (nm)	0.544	3.39	4.45	5	5.4	6	8	9
75	0.8505	0.4774	0.3746	0.3215	0.2655	0.2020	0.2233	0.8505
100	1.1340	0.6366	0.4995	0.4287	0.3540	0.2693	0.2977	1.1340
150	1.7010	0.9548	0.7493	0.6430	0.5310	0.4040	0.4466	1.7010
200	2.2680	1.2731	0.9990	0.8574	0.7080	0.5386	0.5955	2.2680
300	3.4020	1.9097	1.4985	1.2861	1.0620	0.8080	0.8932	3.4020
400	4.5360	2.5463	1.9980	1.7147	1.4159	1.0773	1.1909	4.5360
500	5.6700	3.1828	2.4975	2.1434	1.7699	1.3466	1.4887	5.6700
600	6.8040	3.8194	2.9970	2.5721	2.1239	1.6159	1.7864	6.8040

Wavelength (in um)	0.544	0.633	3.39	4.45	5	5.4	6	8	9
ZnO index	1.7028	1.7014	1.6975	1.6974	1.6974	1.6974	1.6974	1.6974	1.6974
permittivity	2.8996	2.8947	2.8815	2.8813	2.8812	2.8812	2.8812	2.8811	2.8811
Ag index	0.016+3.81i	0.021+4.478i	0.604+24.53i	1.039+32.19i	1.311+36.16i	1.528+39.04i	1.884+43.36i	3.338+57.70i	4.215+64.83i
permittivity	-14.5+0.12i	-20.05+0.19i	-6.0e2+2.9e1i	-1.0e3+6.6e1i	-1.30e3+9.4e1i	-1.522e3+1.193e2i	-1.877e3+1.634e2i	-3.318e3+3.852e2i	-4.18e3+5.46e2i

Ratio of dielectric to metal

0.544	3.39	4.45	5	5.4	6	8	9
5.0194	6.9298	208.7820	359.4242	453.3499	528.3934	651.4757	1151.7535

metal thickness

period (nm)	0.544	3.39	4.45	5	5.4	6	8	9
75	0.3575	0.2081	0.1651	0.1417	0.1149	0.0651	0.0516	0.3575
100	0.4767	0.2775	0.2201	0.1889	0.1533	0.0867	0.0688	0.4767
150	0.7150	0.4162	0.3301	0.2833	0.2299	0.1301	0.1032	0.7150
200	0.9534	0.5549	0.4402	0.3778	0.3065	0.1735	0.1376	0.9534
300	1.4301	0.8324	0.6603	0.5667	0.4598	0.2602	0.2064	1.4301
400	1.9067	1.1098	0.8804	0.7556	0.6130	0.3470	0.2752	1.9067
500	2.3834	1.3873	1.1005	0.9445	0.7663	0.4337	0.3440	2.3834
600	2.8601	1.6647	1.3206	1.1334	0.9196	0.5205	0.4128	2.8601

Wavelength (in um)	0.544	0.633	3.39	4.45	5	5.4	6	8	9
ZnS index	1.8410	1.8410	1.8410	1.8410	1.8410	1.8410	1.8410	1.8410	1.8410
permittivity	3.3892	3.3892	3.3892	3.3892	3.3892	3.3892	3.3892	3.3892	3.3892
Ag index	0.016+3.81i	0.021+4.478i	0.604+24.53i	1.039+32.19i	1.311+36.16i	1.528+39.04i	1.884+43.36i	3.338+57.70i	4.215+64.83i
permittivity	-14.5+0.12i	-20.05+0.19i	-6.0e2+2.9e1i	-1.0e3+6.6e1i	-1.30e3+9.4e1i	-1.522e3+1.193e2i	-1.877e3+1.634e2i	-3.318e3+3.852e2i	-4.18e3+5.46e2i

Ratio of dielectric to metal								
	0.544	3.39	4.45	5	5.4	6	8	9
	4.2943	5.9187	177.5053	305.5596	385.4017	449.1929	553.8199	979.0860

				metal thickness				
period (nm)	0.544	3.39	4.45	5	5.4	6	8	9
75	0.4202	0.2447	0.1941	0.1666	0.1352	0.0765	0.0607	0.4202
100	0.5602	0.3262	0.2588	0.2221	0.1802	0.1020	0.0809	0.5602
150	0.8403	0.4893	0.3882	0.3332	0.2704	0.1530	0.1214	0.8403
200	1.1204	0.6524	0.5176	0.4443	0.3605	0.2041	0.1618	1.1204
300	1.6806	0.9786	0.7764	0.6664	0.5407	0.3061	0.2427	1.6806
400	2.2408	1.3048	1.0352	0.8885	0.7210	0.4081	0.3237	2.2408
500	2.8010	1.6310	1.2940	1.1106	0.9012	0.5102	0.4046	2.8010
600	3.3612	1.9572	1.5528	1.3328	1.0814	0.6122	0.4855	3.3612

B-2: Gold, Au

Wavelength (in um)	0.544	0.633	3.39	4.45	5	5.4	6	8	9
Al2O3 Index	1.756	1.756	1.755	1.755	1.755	1.755	1.755	1.755	1.754
permittivity	3.083	3.082	3.081	3.081	3.081	3.081	3.080	3.079	3.078
Au Index	0.024+3.814i	0.032+4.478i	0.897+24.508i	1.542+32.136i	1.944+36.079i	2.264+38.93i	2.790+43.217i	4.920 +57.35i	6.197+64.342i
permittivity	-14.55+0.182i	-20.05+0.28i	-5.99e2+4.39e1i	-1.03e3+9.913e1i	-1.29e3+1.40e2i	-1.51e3+1.7e2i	-1.86e3 +2.41e2i	-3.265e3+5.64e2i	-4.10e3+7.97e2i

Ratio of dielectric to metal

0.544	3.39	4.45	5	5.4	6	8	9
4.7210	194.6461	334.3008	420.9959	490.4926	603.8519	1060.4815	1332.3937

metal thickness

period (nm)	0.544	3.39	4.45	5	5.4	6	8	9
75	0.3833	0.2237	0.1777	0.1526	0.1240	0.0707	0.0562	0.3833
100	0.5111	0.2982	0.2370	0.2035	0.1653	0.0942	0.0750	0.5111
150	0.7667	0.4474	0.3555	0.3052	0.2480	0.1413	0.1125	0.7667
200	1.0223	0.5965	0.4739	0.4069	0.3307	0.1884	0.1500	1.0223
300	1.5334	0.8947	0.7109	0.6104	0.4960	0.2826	0.2250	1.5334
400	2.0445	1.1930	0.9479	0.8138	0.6613	0.3768	0.3000	2.0445
500	2.5556	1.4912	1.1848	1.0173	0.8266	0.4710	0.3750	2.5556
600	3.0668	1.7894	1.4218	1.2208	0.9920	0.5652	0.4500	3.0668

Wavelength (in um)	0.544	0.633	3.39	4.45	5	5.4	6	8	9
BaF2 Index	1.4759	1.4733	1.4596	1.4543	1.4510	1.4484	1.4440	1.4258	1.4144
permittivity	2.1784	2.1705	2.1303	2.1150	2.1055	2.0978	2.0852	2.0330	2.0006
Au Index	0.024+3.814i	0.032+4.478i	0.897+24.508i	1.542+32.136i	1.944+36.079i	2.264+38.93i	2.790+43.217i	4.920 +57.35i	6.197+64.342i
permittivity	-14.55+0.182i	-20.05+0.28i	-5.99e2+4.39e1i	-1.03e3+9.913e1i	-1.29e3+1.40e2i	-1.51e3+1.7e2i	-1.86e3 +2.41e2i	-3.265e3+5.64e2i	-4.10e3+7.97e2i

Ratio of dielectric to metal

	0.544	3.39	4.45	5	5.4	6	8	9
	6.6806	281.5765	487.1406	616.4417	720.3611	891.9822	1606.2826	2050.1828

metal thickness

period (nm)	0.544	3.39	4.45	5	5.4	6	8	9
75	0.2654	0.1536	0.1215	0.1040	0.0840	0.0467	0.0366	0.2654
100	0.3539	0.2049	0.1620	0.1386	0.1120	0.0622	0.0488	0.3539
150	0.5308	0.3073	0.2429	0.2079	0.1680	0.0933	0.0731	0.5308
200	0.7078	0.4097	0.3239	0.2773	0.2240	0.1244	0.0975	0.7078
300	1.0617	0.6146	0.4859	0.4159	0.3360	0.1867	0.1463	1.0617
400	1.4155	0.8194	0.6478	0.5545	0.4479	0.2489	0.1950	1.4155
500	1.7694	1.0243	0.8098	0.6931	0.5599	0.3111	0.2438	1.7694
600	2.1233	1.2292	0.9718	0.8318	0.6719	0.3733	0.2925	2.1233

Wavelength (in um)	0.544	0.633	3.39	4.45	5	5.4	6	8	9
CaF2 Index	1.4350	1.4329	1.4149	1.4052	1.3990	1.3939	1.3856	1.3498	1.3268
permittivity	2.0592	2.0532	2.0020	1.9744	1.9571	1.9431	1.9199	1.8221	1.7603
Au Index	0.024+3.814i	0.032+4.478i	0.897+24.508i	1.542+32.136i	1.944+36.079i	2.264+38.93i	2.790+43.217i	4.920 +57.35i	6.197+64.342i
permittivity	-14.55+0.182i	-20.05+0.28i	-5.99e2+4.39e1i	-1.03e3+9.913e1i	-1.29e3+1.40e2i	-1.51e3+1.7e2i	-1.86e3 +2.41e2i	-3.265e3+5.64e2i	-4.10e3+7.97e2i

Ratio of dielectric to metal

	0.544	3.39	4.45	5	5.4	6	8	9	
	7.0673	299.6168	521.8163	663.1806	777.7300	968.8086	1792.1948	2329.9753	

metal thickness

period (nm)	0.544	3.39	4.45	5	5.4	6	8	9	
75	0.2495	0.1435	0.1129	0.0963	0.0773	0.0418	0.2495	0.1435	
100	0.3326	0.1913	0.1506	0.1284	0.1031	0.0558	0.3326	0.1913	
150	0.4990	0.2869	0.2258	0.1926	0.1547	0.0836	0.4990	0.2869	
200	0.6653	0.3825	0.3011	0.2568	0.2062	0.1115	0.6653	0.3825	
300	0.9979	0.5738	0.4517	0.3852	0.3093	0.1673	0.9979	0.5738	
400	1.3306	0.7651	0.6022	0.5137	0.4125	0.2231	1.3306	0.7651	
500	1.6632	0.9564	0.7528	0.6421	0.5156	0.2788	1.6632	0.9564	
600	1.9959	1.1476	0.9034	0.7705	0.6187	0.3346	1.9959	1.1476	

	Wavelength (in um)	0.544	0.633	3.39	4.45	5	5.4	6	8	9
HfO2	index Cauchy	1.8842	1.8779	1.8606	1.8604	1.8603	1.8602	1.8602	1.8601	1.8601
	permittivity	3.5502	3.5264	3.4619	3.4609	3.4607	3.4605	3.4603	3.4600	3.4599
Au	Index	0.024+3.814i	0.032+4.478i	0.897+24.508i	1.542+32.136i	1.944+36.079i	2.264+38.93i	2.790+43.217i	4.920 +57.35i	6.197+64.342i
	permittivity	-14.55+0.182i	-20.05+0.28i	-5.99e2+4.39e1i	-1.03e3+9.913e1i	-1.29e3+1.40e2i	-1.51e3+1.7e2i	-1.86e3 +2.41e2i	-3.265e3+5.64e2i	-4.10e3+7.97e2i

Ratio of dielectric to metal							
0.544	3.39	4.45	5	5.4	6	8	9
4.099246993	5.6878	173.2681	297.6932	375.0435	436.6982	537.5194	943.7817

	metal thickness						
period (nm)	0.544	3.39	4.45	5	5.4	6	8	9
75	0.4304	0.2511	0.1994	0.1714	0.1393	0.0794	0.0632	0.4304
100	0.5738	0.3348	0.2659	0.2285	0.1857	0.1058	0.0843	0.5738
150	0.8607	0.5022	0.3989	0.3427	0.2785	0.1588	0.1264	0.8607
200	1.1477	0.6696	0.5319	0.4569	0.3714	0.2117	0.1686	1.1477
300	1.7215	1.0044	0.7978	0.6854	0.5571	0.3175	0.2529	1.7215
400	2.2953	1.3392	1.0637	0.9139	0.7428	0.4234	0.3371	2.2953
500	2.8691	1.6740	1.3296	1.1423	0.9285	0.5292	0.4214	2.8691
600	3.4430	2.0087	1.5956	1.3708	1.1142	0.6351	0.5057	3.4430

Wavelength (in um)		0.544	0.633	3.39	4.45	5	5.4	6	8	9
MgF2	Index	1.3753	1.3753	1.3753	1.3753	1.3753	1.3753	1.3753	1.3753	1.3753
	permittivity	1.8914	1.8914	1.8914	1.8914	1.8914	1.8914	1.8914	1.8914	1.8914
Au	Index	0.024+3.814i	0.032+4.478i	0.897+24.508i	1.542+32.136i	1.944+36.079i	2.264+38.93i	2.790+43.217i	4.920 +57.35i	6.197+64.342i
	permittivity	-14.55+0.182i	-20.05+0.28i	-5.99e2+4.39e1i	-1.03e3+9.913e1i	-1.29e3+1.40e2i	-1.51e3+1.7e2i	-1.86e3 +2.41e2i	-3.265e3+5.64e2i	-4.10e3+7.97e2i

Ratio of dielectric to metal

	0.544	3.39	4.45	5	5.4	6	8	9
	7.6949	10.6056	318.0697	547.5283	690.5963	804.9026	992.3819	1754.4064

metal thickness

period (nm)	0.544	3.39	4.45	5	5.4	6	8	9
75	0.2357	0.1374	0.1091	0.0938	0.0762	0.0434	0.0346	0.2357
100	0.3143	0.1832	0.1455	0.1250	0.1016	0.0579	0.0461	0.3143
150	0.4715	0.2749	0.2183	0.1875	0.1524	0.0868	0.0691	0.4715
200	0.6287	0.3665	0.2910	0.2500	0.2032	0.1158	0.0922	0.6287
300	0.9430	0.5497	0.4365	0.3750	0.3048	0.1737	0.1383	0.9430
400	1.2573	0.7330	0.5821	0.5000	0.4063	0.2315	0.1844	1.2573
500	1.5716	0.9162	0.7276	0.6250	0.5079	0.2894	0.2305	1.5716
600	1.8860	1.0995	0.8731	0.7500	0.6095	0.3473	0.2766	1.8860

Wavelength (in um)	0.544	0.633	3.39	4.45	5	5.4	6	8	9
MgO index	1.6957	1.7016	1.6822	1.6543	1.6362	1.6212	1.5958	1.4806	1.4004
permittivity	2.8753	2.8953	2.8297	2.7368	2.6771	2.6284	2.5467	2.1921	1.9611
Au index	0.024+3.814i	0.032+4.478i	0.897+24.508i	1.542+32.136i	1.944+36.079i	2.264+38.93i	2.790+43.217i	4.920 +57.35i	6.197+64.342i
permittivity	-14.55+0.182i	-20.05+0.28i	-5.99e2+4.39e1i	-1.03e3+9.913e1i	-1.29e3+1.40e2i	-1.51e3+1.7e2i	-1.86e3 +2.41e2i	-3.265e3+5.64e2i	-4.10e3+7.97e2i

Ratio of dielectric to metal

	0.544	3.39	4.45	5	5.4	6	8	9
	5.0615	6.9276	211.9836	376.4564	484.8196	574.9526	5.0615	6.9276

metal thickness

period (nm)	0.544	3.39	4.45	5	5.4	6	8	9
75	0.3521	0.1987	0.1544	0.1302	0.3521	0.1987	0.1544	0.1302
100	0.4695	0.2649	0.2058	0.1736	0.4695	0.2649	0.2058	0.1736
150	0.7043	0.3974	0.3088	0.2604	0.7043	0.3974	0.3088	0.2604
200	0.9390	0.5299	0.4117	0.3473	0.9390	0.5299	0.4117	0.3473
300	1.4086	0.7948	0.6175	0.5209	1.4086	0.7948	0.6175	0.5209
400	1.8781	1.0597	0.8234	0.6945	1.8781	1.0597	0.8234	0.6945
500	2.3476	1.3247	1.0292	0.8681	2.3476	1.3247	1.0292	0.8681
600	2.8171	1.5896	1.2350	1.0418	2.8171	1.5896	1.2350	1.0418

Wavelength (in um)	0.544	0.633	3.39	4.45	5	5.4	6	8	9
SF 11 index	1.5439	1.5382	1.5245	1.5243	1.5242	1.5242	1.5241	1.5241	1.5241
permittivity	2.3836	2.3661	2.3240	2.3234	2.3232	2.3231	2.3230	2.3228	2.3228
Au index	0.024+3.814i	0.032+4.478i	0.897+24.508i	1.542+32.136i	1.944+36.079i	2.264+38.93i	2.790+43.217i	4.920 +57.35i	6.197+64.342i
permittivity	-14.55+0.182i	-20.05+0.28i	-5.99e2+4.39e1i	-1.03e3+9.913e1i	-1.29e3+1.40e2i	-1.51e3+1.7e2i	-1.86e3 +2.41e2i	-3.265e3+5.64e2i	-4.10e3+7.97e2i

Ratio of dielectric to metal

	0.544	3.39	4.45	5	5.4	6	8	9
	6.1055	8.4768	258.1118	443.4498	558.6671	650.5051	800.6837	1405.8327

metal thickness

period (nm)	0.544	3.39	4.45	5	5.4	6	8	9
75	0.2895	0.1687	0.1340	0.1151	0.0936	0.0533	0.0425	0.2895
100	0.3859	0.2250	0.1787	0.1535	0.1247	0.0711	0.0566	0.3859
150	0.5789	0.3375	0.2680	0.2302	0.1871	0.1066	0.0849	0.5789
200	0.7719	0.4500	0.3574	0.3070	0.2495	0.1422	0.1132	0.7719
300	1.1578	0.6750	0.5360	0.4605	0.3742	0.2132	0.1698	1.1578
400	1.5437	0.9000	0.7147	0.6140	0.4989	0.2843	0.2264	1.5437
500	1.9297	1.1250	0.8934	0.7675	0.6237	0.3554	0.2830	1.9297
600	2.3156	1.3500	1.0721	0.9209	0.7484	0.4265	0.3396	2.3156

Wavelength (in um)		0.544	0.633	3.39	4.45	5	5.4	6	8	9
amorphous Si	index	3.8825	3.8828	3.8460	3.8199	3.8060	3.7960	3.7818	3.7444	3.7331
	permittivity	15.0737	15.0760	14.7921	14.5914	14.4853	14.4099	14.3022	14.0207	13.9358
Au	index	0.024+3.814i	0.032+4.478i	0.897+24.508i	1.542+32.136i	1.944+36.079i	2.264+38.93i	2.790+43.217i	4.920 +57.35i	6.197+64.342i
	permittivity	-14.55+0.182i	-20.05+0.28i	-5.99e2+4.39e1i	-1.03e3+9.91e1i	-1.29e3+1.40e2i	-1.51e3+1.7e2i	-1.86e3 +2.41e2i	-3.26e3+5.64e2i	-4.10e3+7.97e2i

Ratio of dielectric to metal

0.544	3.39	4.45	5	5.4	6	8	9
0.9655	1.3304	40.5515	70.6102	89.6015	104.8727	130.0503	232.9059

metal thickness

period (nm)	0.544	3.39	4.45	5	5.4	6	8	9
75	1.8050	1.0473	0.8278	0.7084	0.5723	0.3206	0.2540	1.8050
100	2.4067	1.3964	1.1037	0.9445	0.7631	0.4275	0.3386	2.4067
150	3.6100	2.0947	1.6556	1.4168	1.1446	0.6413	0.5079	3.6100
200	4.8133	2.7929	2.2075	1.8891	1.5261	0.8550	0.6772	4.8133
300	7.2200	4.1893	3.3112	2.8336	2.2892	1.2826	1.0159	7.2200
400	9.6266	5.5858	4.4149	3.7781	3.0523	1.7101	1.3545	9.6266
500	12.0333	6.9822	5.5187	4.7227	3.8153	2.1376	1.6931	12.0333
600	14.4399	8.3787	6.6224	5.6672	4.5784	2.5651	2.0317	14.4399

Wavelength (in um)	0.544	0.633	3.39	4.45	5	5.4	6	8	9
SiC index	2.5872	2.5868	2.5382	2.4960	2.5868	2.4409	2.3944	2.1153	1.8083
permittivity	6.6938	6.6917	6.4426	6.2300	6.0837	5.9581	5.7331	4.4747	3.2700
Au index	0.024+3.814i	0.032+4.478i	0.897+24.508i	1.542+32.136i	1.944+36.079i	2.264+38.93i	2.790+43.217i	4.920 +57.35i	6.197+64.342i
permittivity	-14.55+0.182i	-20.05+0.28i	-5.99e2+4.39e1i	-1.03e3+9.91e1i	-1.29e3+1.40e2i	-1.51e3+1.7e2i	-1.86e3 +2.41e2i	-3.26e3+5.64e2i	-4.10e3+7.97e2i

Ratio of dielectric to metal								
	0.544	3.39	4.45	5	5.4	6	8	9
	2.1741	93.1049	165.3764	213.3415	253.6384	324.4298	729.7718	1254.2663

			metal thickness					
period (nm)	0.544	3.39	4.45	5	5.4	6	8	9
75	0.7970	0.4508	0.3499	0.2945	0.2305	0.1026	0.0597	0.7970
100	1.0626	0.6010	0.4665	0.3927	0.3073	0.1368	0.0797	1.0626
150	1.5940	0.9016	0.6998	0.5891	0.4609	0.2053	0.1195	1.5940
200	2.1253	1.2021	0.9331	0.7854	0.6146	0.2737	0.1593	2.1253
300	3.1879	1.8031	1.3996	1.1781	0.9219	0.4105	0.2390	3.1879
400	4.2506	2.4042	1.8662	1.5709	1.2291	0.5474	0.3187	4.2506
500	5.3132	3.0052	2.3327	1.9636	1.5364	0.6842	0.3983	5.3132
600	6.3759	3.6063	2.7993	2.3563	1.8437	0.8210	0.4780	6.3759

	0.544	0.633	3.39	4.45	5	5.4	6	8	9
Wavelength (in um)	0.544	0.633	3.39	4.45	5	5.4	6	8	9
SU-8 index	1.5770	1.5770	1.5770	1.5770	1.5770	1.5770	1.5770	1.5770	1.5770
permittivity	2.4869	2.4869	2.4869	2.4869	2.4869	2.4869	2.4869	2.4869	2.4869
Au index	0.024+3.814i	0.032+4.478i	0.897+24.508i	1.542+32.136i	1.944+36.079i	2.264+38.93i	2.790+43.217i	4.920 +57.35i	6.197+64.342i
permittivity	-14.55+0.182i	-20.05+0.28i	-5.99e2+4.39e1i	-1.03e3+9.91e1i	-1.29e3+1.40e2i	-1.51e3+1.7e2i	-1.86e3 +2.41e2i	-3.26e3+5.64e2i	-4.10e3+7.97e2i
Ratio of dielectric to metal									
	0.544	3.39	4.45	5	5.4	6	8	9	
	5.8518	8.0651	241.1971	414.2861	521.8886	607.6571	747.9104	1313.0652	
				metal thickness					
period (nm)	0.544	3.39	4.45	5	5.4	6	8	9	
75	0.3097	0.1806	0.1434	0.1232	0.1001	0.0571	0.0454	75	
100	0.4129	0.2408	0.1912	0.1643	0.1335	0.0761	0.0606	100	
150	0.6193	0.3612	0.2869	0.2464	0.2003	0.1141	0.0909	150	
200	0.8258	0.4816	0.3825	0.3286	0.2671	0.1522	0.1212	200	
300	1.2387	0.7224	0.5737	0.4929	0.4006	0.2283	0.1818	300	
400	1.6515	0.9632	0.7650	0.6572	0.5341	0.3044	0.2424	400	
5000	20.6443	12.0399	9.5623	8.2148	6.6764	3.8050	3.0299	5000	

Wavelength (in um)	0.544	0.633	3.39	4.45	5	5.4	6	8	9
TiO2 index	2.4175	2.4453	2.6269	2.5757	2.5607	2.5602	2.5822	2.9935	3.5353
permittivity	5.8444	5.9795	6.9003	6.6345	6.5573	6.5544	6.6679	8.9609	12.4981
Au index	0.024+3.814i	0.032+4.478i	0.897+24.508i	1.542+32.136i	1.944+36.079i	2.264+38.93i	2.790+43.217i	4.920 +57.35i	6.197+64.342i
permittivity	-14.55+0.182i	-20.05+0.28i	-5.99e2+4.39e1i	-1.03e3+9.91e1i	-1.29e3+1.40e2i	-1.51e3+1.7e2i	-1.86e3 +2.41e2i	-3.26e3+5.64e2i	-4.10e3+7.97e2i

Ratio of dielectric to metal

	0.544	3.39	4.45	5	5.4	6	8	9
	2.4901	86.9290	155.2947	197.9317	230.5631	278.9466	364.4146	328.1707

metal thickness

period (nm)	0.544	3.39	4.45	5	5.4	6	8	9
75	0.8530	0.4799	0.3770	0.3239	0.2679	0.2052	0.2278	0.8530
100	1.1373	0.6398	0.5027	0.4318	0.3572	0.2737	0.3038	1.1373
150	1.7059	0.9597	0.7540	0.6478	0.5358	0.4105	0.4557	1.7059
200	2.2746	1.2796	1.0054	0.8637	0.7144	0.5473	0.6076	2.2746
300	3.4118	1.9195	1.5081	1.2955	1.0716	0.8210	0.9114	3.4118
400	4.5491	2.5593	2.0107	1.7274	1.4288	1.0946	1.2152	4.5491
500	5.6864	3.1991	2.5134	2.1592	1.7861	1.3683	1.5190	5.6864
600	6.8237	3.8389	3.0161	2.5911	2.1433	1.6420	1.8228	6.8237

Wavelength (in um)	0.544	0.633	3.39	4.45	5	5.4	6	8	9
ZnO	index	1.7028	1.7014	1.6975	1.6974	1.6974	1.6974	1.6974	1.6974	1.6974
	permittivity	2.8996	2.8947	2.8815	2.8813	2.8812	2.8812	2.8812	2.8811	2.8811
Au	index	0.024+3.814i	0.032+4.478i	0.897+24.508i	1.542+32.136i	1.944+36.079i	2.264+38.93i	2.790+43.217i	4.920 +57.35i	6.197+64.342i
	permittivity	-14.55+0.182i	-20.05+0.28i	-5.99e2+4.39e1i	-1.03e3+9.91e1i	-1.29e3+1.40e2i	-1.51e3+1.7e2i	-1.86e3 +2.41e2i	-3.26e3+5.64e2i	-4.10e3+7.97e2i

Ratio of dielectric to metal

0.544	3.39	4.45	5	5.4	6	8	9
5.0190	6.9290	208.1712	357.5847	450.4692	524.5061	645.5752	1133.4271

metal thickness

period (nm)	3.39	4.45	5	5.4	6	8	9
75	0.3586	0.2092	0.1661	0.1427	0.1160	0.0661	0.0526
100	0.4781	0.2789	0.2215	0.1903	0.1547	0.0882	0.0702
150	0.7171	0.4183	0.3322	0.2854	0.2320	0.1322	0.1053
200	0.9562	0.5577	0.4430	0.3806	0.3093	0.1763	0.1404
300	1.4342	0.8366	0.6645	0.5709	0.4640	0.2645	0.2106
400	1.9123	1.1155	0.8860	0.7612	0.6186	0.3526	0.2808
500	2.3904	1.3944	1.1075	0.9515	0.7733	0.4408	0.3510
600	2.8685	1.6732	1.3290	1.1418	0.9280	0.5289	0.4212

Wavelength (in um)	0.544	0.633	3.39	4.45	5	5.4	6	8	9
ZnS index	1.8410	1.8410	1.8410	1.8410	1.8410	1.8410	1.8410	1.8410	1.8410
permittivity	3.3892	3.3892	3.3892	3.3892	3.3892	3.3892	3.3892	3.3892	3.3892
Au index	0.024+3.814i	0.032+4.478i	0.897+24.508i	1.542+32.136i	1.944+36.079i	2.264+38.93i	2.790+43.217i	4.920 +57.35i	6.197+64.342i
permittivity	-14.55+0.182i	-20.05+0.28i	-5.99e2+4.39e1i	-1.03e3+9.91e1i	-1.29e3+1.40e2i	-1.51e3+1.7e2i	-1.86e3 +2.41e2i	-3.26e3+5.64e2i	-4.10e3+7.97e2i

Ratio of dielectric to metal

0.544	3.39	4.45	5	5.4	6	8	9
4.2940	5.9180	176.9860	303.9958	382.9528	445.8883	548.8040	963.5070

metal thickness

period (nm)	3.39	4.45	5	5.4	6	8	9
75	0.4214	0.2459	0.1953	0.1678	0.1364	0.0778	0.0619
100	0.5618	0.3279	0.2604	0.2238	0.1819	0.1037	0.0826
150	0.8428	0.4918	0.3907	0.3357	0.2728	0.1555	0.1238
200	1.1237	0.6557	0.5209	0.4475	0.3638	0.2074	0.1651
300	1.6855	0.9836	0.7813	0.6713	0.5456	0.3110	0.2477
400	2.2474	1.3115	1.0418	0.8951	0.7275	0.4147	0.3303
500	2.8092	1.6394	1.3022	1.1188	0.9094	0.5184	0.4128
600	3.3711	1.9672	1.5627	1.3426	1.0913	0.6221	0.4954

B-3: Copper, Cu

Wavelength (in um)	0.544	0.633	3.39	4.45	5	5.4	6	8	9
Al2O3 index	1.756	1.756	1.755	1.755	1.755	1.755	1.755	1.755	1.754
permittivity	3.083	3.082	3.081	3.081	3.081	3.081	3.080	3.079	3.078
Cu index	0.027+3.323i	0.036+3.912i	1.015+21.53i	1.741+28.21i	2.192+31.66i	2.551+34.15i	3.14+37.88i	5.509+50.11i	6.918+56.12i
permittivity	-11.04+0.18i	-15.30+0.287i	-4.62e2+4.371e+1i	-7.92e2+9.823e1i	-9.97e2+1.38e2i	-1.16e3+1.74e2i	-1.42e3+2.37e2i	-2.48e3+5.52e2i	-3.10e3+7.76e2i

Ratio of dielectric to metal									
	0.544	0.633	3.39	4.45	5	5.4	6	8	9
	3.582	4.965	150.142	257.347	323.722	376.488	462.531	805.933	1007.759

				metal thickness				
period (nm)	3.39	4.45	5	5.4	6	8	9	period (nm)
75	0.496	0.290	0.231	0.199	0.162	0.093	0.074	75
100	0.662	0.387	0.308	0.265	0.216	0.124	0.099	100
150	0.992	0.581	0.462	0.397	0.324	0.186	0.149	150
200	1.323	0.774	0.616	0.530	0.431	0.248	0.198	200
300	1.985	1.161	0.924	0.795	0.647	0.372	0.297	300
400	2.647	1.548	1.232	1.060	0.863	0.496	0.397	400
500	3.308	1.935	1.540	1.325	1.079	0.620	0.496	500
600	3.970	2.322	1.848	1.589	1.294	0.744	0.595	600

Wavelength (in um)	0.544	0.633	3.39	4.45	5	5.4	6	8	9
BaF2 index	1.4759	1.4733	1.4596	1.4543	1.4510	1.4484	1.4440	1.4258	1.4144
permittivity	2.1784	2.1705	2.1303	2.1150	2.1055	2.0978	2.0852	2.0330	2.0006
Cu index	0.027+3.323i	0.036+3.912i	1.015+21.53i	1.741+28.21i	2.192+31.66i	2.551+34.15i	3.14+37.88i	5.509+50.11i	6.918+56.12i
permittivity	-11.04+0.18i	-15.30+0.287i	-4.62e2+4.371e+1i	-7.92e2+9.823e1i	-9.97e2+1.38e2i	-1.16e3+1.74e2i	-1.42e3+2.37e2i	-2.48e3+5.52e2i	-3.10e3+7.76e2i

Ratio of dielectric to metal

0.544	0.633	3.39	4.45	5	5.4	6	8	9
5.069	7.051	217.182	374.894	473.680	552.855	683.230	1220.539	1550.471

metal thickness

period (nm)	3.39	4.45	5	5.4	6	8	9
75	0.344	0.200	0.158	0.135	0.110	0.061	0.048
100	0.458	0.266	0.211	0.181	0.146	0.082	0.064
150	0.688	0.399	0.316	0.271	0.219	0.123	0.097
200	0.917	0.532	0.421	0.361	0.292	0.164	0.129
300	1.375	0.798	0.632	0.542	0.438	0.246	0.193
400	1.833	1.064	0.843	0.722	0.585	0.327	0.258
500	2.292	1.330	1.053	0.903	0.731	0.409	0.322
600	2.750	1.596	1.264	1.083	0.877	0.491	0.387

Wavelength (in um)	0.544	0.633	3.39	4.45	5	5.4	6	8	9
CaF2 index	1.4350	1.4329	1.4149	1.4052	1.3990	1.3939	1.3856	1.3498	1.3268
permittivity	2.0592	2.0532	2.0020	1.9744	1.9571	1.9431	1.9199	1.8221	1.7603
Cu index	0.027+3.323i	0.036+3.912i	1.015+21.53i	1.741+28.21i	2.192+31.66i	2.551+34.15i	3.14+37.88i	5.509+50.11i	6.918+56.12i
permittivity	-11.04+0.18i	-15.30+0.287i	-4.62e2+4.371e+1i	-7.92e2+9.823e1i	-9.97e2+1.38e2i	-1.16e3+1.74e2i	-1.42e3+2.37e2i	-2.48e3+5.52e2i	-3.10e3+7.76e2i

Ratio of dielectric to metal

0.544	0.633	3.39	4.45	5	5.4	6	8	9
5.363	7.454	231.096	401.580	509.595	596.884	742.076	1361.805	1762.067

metal thickness

period (nm)	3.39	4.45	5	5.4	6	8	9
75	0.323	0.186	0.147	0.125	0.101	0.055	0.043
100	0.431	0.248	0.196	0.167	0.135	0.073	0.057
150	0.646	0.373	0.294	0.251	0.202	0.110	0.085
200	0.862	0.497	0.392	0.335	0.269	0.147	0.113
300	1.293	0.745	0.588	0.502	0.404	0.220	0.170
400	1.723	0.994	0.783	0.669	0.538	0.294	0.227
500	2.154	1.242	0.979	0.836	0.673	0.367	0.284
600	2.585	1.490	1.175	1.004	0.807	0.440	0.340

redo

	Wavelength (in um)	0.544	0.633	3.39	4.45	5	5.4	6	8	9
HfO2	index Cauchy	1.8842	1.8779	1.8606	1.8604	1.8603	1.8602	1.8602	1.8601	1.8601
	permittivity	3.5502	3.5264	3.4619	3.4609	3.4607	3.4605	3.4603	3.4600	3.4599
Cu	index	0.027+3.323i	0.036+3.912i	1.015+21.53i	1.741+28.21i	2.192+31.66i	2.551+34.15i	3.14+37.88i	5.509+50.11i	6.918+56.12i
	permittivity	-11.04+0.18i	-15.30+0.287i	-4.62e2+4.371e+1i	-7.92e2+9.823e1i	-9.97e2+1.38e2i	-1.16e3+1.74e2i	-1.42e3+2.37e2i	-2.48e3+5.52e2i	-3.10e3+7.76e2i

Ratio of dielectric to metal									
0.544	0.633	3.39	4.45	5	5.4	6	8	9	
3.111	4.340	133.643	229.099	288.187	335.153	411.723	717.135	896.492	

				metal thickness					
period (nm)	3.39	4.45	5	5.4	6	8	9		
75	0.557	0.326	0.259	0.223	0.182	0.104	0.084		
100	0.743	0.435	0.346	0.297	0.242	0.139	0.111		
150	1.114	0.652	0.519	0.446	0.363	0.209	0.167		
200	1.485	0.869	0.692	0.595	0.485	0.278	0.223		
300	2.228	1.304	1.037	0.892	0.727	0.418	0.334		
400	2.971	1.738	1.383	1.190	0.969	0.557	0.446		
500	3.714	2.173	1.729	1.487	1.211	0.696	0.557		
600	4.456	2.608	2.075	1.785	1.454	0.835	0.669		

Wavelength (in um)	0.544	0.633	3.39	4.45	5	5.4	6	8	9
MgF2 index	1.3753	1.3753	1.3753	1.3753	1.3753	1.3753	1.3753	1.3753	1.3753
permittivity	1.8914	1.8914	1.8914	1.8914	1.8914	1.8914	1.8914	1.8914	1.8914
Cu index	0.027+3.323i	0.036+3.912i	1.015+21.53i	1.741+28.21i	2.192+31.66i	2.551+34.15i	3.14+37.88i	5.509+50.11i	6.918+56.12i
permittivity	-11.04+0.18i	-15.30+0.287i	-4.62e2+4.371e+1i	-7.92e2+9.823e1i	-9.97e2+1.38e2i	-1.16e3+1.74e2i	-1.42e3+2.37e2i	-2.48e3+5.52e2i	-3.10e3+7.76e2i

Ratio of dielectric to metal

0.544	0.633	3.39	4.45	5	5.4	6	8	9
3.841	5.286	163.504	289.714	372.540	441.259	559.423	1131.907	1581.675

metal thickness

period (nm)	3.39	4.45	5	5.4	6	8	9
75	0.456	0.258	0.201	0.170	0.134	0.066	0.047
100	0.608	0.344	0.268	0.226	0.178	0.088	0.063
150	0.912	0.516	0.402	0.339	0.268	0.132	0.095
200	1.216	0.688	0.535	0.452	0.357	0.177	0.126
300	1.824	1.032	0.803	0.678	0.535	0.265	0.190
400	2.432	1.376	1.071	0.904	0.714	0.353	0.253
500	3.039	1.720	1.339	1.131	0.892	0.441	0.316
600	3.647	2.064	1.606	1.357	1.071	0.530	0.379

Wavelength (in um)	0.544	0.633	3.39	4.45	5	5.4	6	8	9
MgO index	1.6957	1.7016	1.6822	1.6543	1.6362	1.6212	1.5958	1.4806	1.4004
permittivity	2.8753	2.8953	2.8297	2.7368	2.6771	2.6284	2.5467	2.1921	1.9611
Cu index	0.027+3.323i	0.036+3.912i	1.015+21.53i	1.741+28.21i	2.192+31.66i	2.551+34.15i	3.14+37.88i	5.509+50.11i	6.918+56.12i
permittivity	-11.04+0.18i	-15.30+0.287i	-4.62e2+4.371e+1i	-7.92e2+9.823e1i	-9.97e2+1.38e2i	-1.16e3+1.74e2i	-1.42e3+2.37e2i	-2.48e3+5.52e2i	-3.10e3+7.76e2i

Ratio of dielectric to metal

0.544	0.633	3.39	4.45	5	5.4	6	8	9
3.841	5.286	163.504	289.714	372.540	441.259	559.423	1131.907	1581.675

metal thickness

period (nm)	3.39	4.45	5	5.4	6	8	9
75	0.456	0.258	0.201	0.170	0.134	0.066	0.047
100	0.608	0.344	0.268	0.226	0.178	0.088	0.063
150	0.912	0.516	0.402	0.339	0.268	0.132	0.095
200	1.216	0.688	0.535	0.452	0.357	0.177	0.126
300	1.824	1.032	0.803	0.678	0.535	0.265	0.190
400	2.432	1.376	1.071	0.904	0.714	0.353	0.253
500	3.039	1.720	1.339	1.131	0.892	0.441	0.316
600	3.647	2.064	1.606	1.357	1.071	0.530	0.379

Wavelength (in um)	0.544	0.633	3.39	4.45	5	5.4	6	8	9
SF 11 index	1.5439	1.5382	1.5245	1.5243	1.5242	1.5242	1.5241	1.5241	1.5241
permittivity	2.3836	2.3661	2.3240	2.3234	2.3232	2.3231	2.3230	2.3228	2.3228
Cu index	0.027+3.323i	0.036+3.912i	1.015+21.53i	1.741+28.21i	2.192+31.66i	2.551+34.15i	3.14+37.88i	5.509+50.11i	6.918+56.12i
Cu permittivity	-11.04+0.18i	-15.30+0.287i	-4.62e2+4.371e+1i	-7.92e2+9.823e1i	-9.97e2+1.38e2i	-1.16e3+1.74e2i	-1.42e3+2.37e2i	-2.48e3+5.52e2i	-3.10e3+7.76e2i

Ratio of dielectric to metal

	0.544	0.633	3.39	4.45	5	5.4	6	8
	4.633	6.468	199.083	341.271	429.286	499.243	613.298	1068.226

metal thickness

period (nm)	3.39	4.45	5	5.4	6	8
75	0.375	0.219	0.174	0.150	0.122	0.070
100	0.500	0.292	0.232	0.200	0.163	0.094
150	0.750	0.438	0.349	0.300	0.244	0.140
200	1.000	0.584	0.465	0.400	0.326	0.187
300	1.499	0.876	0.697	0.600	0.488	0.281
400	1.999	1.169	0.930	0.800	0.651	0.374
500	2.499	1.461	1.162	1.000	0.814	0.468
600	2.999	1.753	1.394	1.199	0.977	0.561

Wavelength (in um)		0.544	0.633	3.39	4.45	5	5.4	6	8	9
amorphous	index	3.8825	3.8828	3.8460	3.8199	3.8060	3.7960	3.7818	3.7444	3.7331
Si	permittivity	15.0737	15.0760	14.7921	14.5914	14.4853	14.4099	14.3022	14.0207	13.9358
Cu	index	0.027+3.323i	0.036+3.912i	1.015+21.53i	1.741+28.21i	2.192+31.66i	2.551+34.15i	3.14+37.88i	5.509+50.11i	6.918+56.12i
	permittivity	-11.04+0.18i	-15.30+0.287i	-4.62e2+4.371e+1i	-7.92e2+9.823e1i	-9.97e2+1.38e2i	-1.16e3+1.74e2i	-1.42e3+2.37e2i	-2.48e3+5.52e2i	-3.10e3+7.76e2i

Ratio of dielectric to metal

0.544	0.633	3.39	4.45	5	5.4	6	8	9
0.733	1.015	31.278	54.340	68.851	80.487	99.614	176.974	222.578

metal thickness

period (nm)	3.39	4.45	5	5.4	6	8	9
75	2.324	1.355	1.074	0.920	0.745	0.421	0.335
100	3.098	1.807	1.432	1.227	0.994	0.562	0.447
150	4.647	2.711	2.147	1.841	1.491	0.843	0.671
200	6.196	3.614	2.863	2.454	1.988	1.124	0.895
350	10.843	6.325	5.011	4.295	3.479	1.967	1.565
400	12.393	7.228	5.726	4.909	3.976	2.248	1.789
500	15.491	9.035	7.158	6.136	4.969	2.809	2.236
600	18.589	10.842	8.590	7.363	5.963	3.371	2.684

Wavelength (in um)		0.544	0.633	3.39	4.45	5	5.4	6	8	9
SiC	index	2.5872	2.5868	2.5382	2.4960	2.5868	2.4409	2.3944	2.1153	1.8083
	permittivity	6.6938	6.6917	6.4426	6.2300	6.0837	5.9581	5.7331	4.4747	3.2700
Cu	index	0.027+3.323i	0.036+3.912i	1.015+21.53i	1.741+28.21i	2.192+31.66i	2.551+34.15i	3.14+37.88i	5.509+50.11i	6.918+56.12i
	permittivity	-11.04+0.18i	-15.30+0.287i	-4.62e2+4.371e+1i	-7.92e2+9.823e1i	-9.97e2+1.38e2i	-1.16e3+1.74e2i	-1.42e3+2.37e2i	-2.48e3+5.52e2i	-3.10e3+7.76e2i
	Ratio of dielectric to metal									
			3.39	4.45	5	5.4	6	8	9	
			3.39	4.45	5	5.4	6	8	9	
			71.812	127.271	163.934	194.660	248.503	554.519	948.551	
		period (nm)			metal thickness					
		75	3.39	4.45	5	5.4	6	8	9	
		100	1.030	0.585	0.455	0.383	0.301	0.135	0.079	
		150	1.373	0.780	0.606	0.511	0.401	0.180	0.105	
		200	2.060	1.169	0.909	0.767	0.601	0.270	0.158	
		300	2.747	1.559	1.213	1.022	0.802	0.360	0.211	
		400	4.120	2.339	1.819	1.533	1.202	0.540	0.316	
		500	5.494	3.118	2.425	2.044	1.603	0.720	0.421	
		600	6.867	3.898	3.032	2.555	2.004	0.900	0.527	

Wavelength (in um)	0.544	0.633	3.39	4.45	5	5.4	6	8	9
TiO2 index	2.4175	2.4453	2.6269	2.5757	2.5607	2.5602	2.5822	2.9935	3.5353
permittivity	5.8444	5.9795	6.9003	6.6345	6.5573	6.5544	6.6679	8.9609	12.4981
Cu index	0.027+3.323i	0.036+3.912i	1.015+21.53i	1.741+28.21i	2.192+31.66i	2.551+34.15i	3.14+37.88i	5.509+50.11i	6.918+56.12i
permittivity	-11.04+0.18i	-15.30+0.287i	-4.62e2+4.371e+1i	-7.92e2+9.823e1i	-9.97e2+1.38e2i	-1.16e3+1.74e2i	-1.42e3+2.37e2i	-2.48e3+5.52e2i	-3.10e3+7.76e2i

Ratio of dielectric to metal

	0.544	0.633	3.39	4.45	5	5.4	6	8
	1.890	2.560	67.049	119.512	152.093	176.950	213.664	276.902

metal thickness

period (nm)	3.39	4.45	5	5.4	6	8
75	1.102	0.622	0.490	0.421	0.349	0.270
100	1.470	0.830	0.653	0.562	0.466	0.360
150	2.204	1.245	0.980	0.843	0.699	0.540
200	2.939	1.660	1.306	1.124	0.932	0.720
300	4.409	2.489	1.960	1.686	1.398	1.080
400	5.878	3.319	2.613	2.248	1.863	1.439
500	7.348	4.149	3.266	2.810	2.329	1.799
600	8.817	4.979	3.919	3.372	2.795	2.159

Wavelength (in um)	0.544	0.633	3.39	4.45	5	5.4	6	8	9
ZnO index	1.7028	1.7014	1.6975	1.6974	1.6974	1.6974	1.6974	1.6974	1.6974
permittivity	2.8996	2.8947	2.8815	2.8813	2.8812	2.8812	2.8812	2.8811	2.8811
Cu index	0.027+3.323i	0.036+3.912i	1.015+21.53i	1.741+28.21i	2.192+31.66i	2.551+34.15i	3.14+37.88i	5.509+50.11i	6.918+56.12i
permittivity	-11.04+0.18i	-15.30+0.287i	-4.62e2+4.371e+1i	-7.92e2+9.823e1i	-9.97e2+1.38e2i	-1.16e3+1.74e2i	-1.42e3+2.37e2i	-2.48e3+5.52e2i	-3.10e3+7.76e2i

Ratio of dielectric to metal

0.544	0.633	3.39	4.45	5	5.4	6	8
3.809	5.287	160.564	275.191	346.145	402.542	494.490	861.238

metal thickness

period (nm)	3.39	4.45	5	5.4	6	8
75	0.464	0.272	0.216	0.186	0.151	0.087
100	0.619	0.362	0.288	0.248	0.202	0.116
150	0.928	0.543	0.432	0.372	0.303	0.174
200	1.238	0.724	0.576	0.496	0.404	0.232
300	1.857	1.086	0.864	0.743	0.605	0.348
400	2.476	1.448	1.152	0.991	0.807	0.464
500	3.095	1.810	1.440	1.239	1.009	0.580
600	3.714	2.172	1.728	1.487	1.211	0.696

Wavelength (in um)	0.544	0.633	3.39	4.45	5	5.4	6	8	9
ZnS	index	1.8410	1.8410	1.8410	1.8410	1.8410	1.8410	1.8410	1.8410	1.8410
	permittivity	3.3892	3.3892	3.3892	3.3892	3.3892	3.3892	3.3892	3.3892	3.3892
Cu	index	0.027+3.323i	0.036+3.912i	1.015+21.53i	1.741+28.21i	2.192+31.66i	2.551+34.15i	3.14+37.88i	5.509+50.11i	6.918+56.12i
	permittivity	-11.04+0.18i	-15.30+0.287i	-4.62e2+4.371e+1i	-7.92e2+9.823e1i	-9.97e2+1.38e2i	-1.16e3+1.74e2i	-1.42e3+2.37e2i	-2.48e3+5.52e2i	-3.10e3+7.76e2i

Ratio of dielectric to metal

	0.544	0.633	3.39	4.45	5	5.4	6	8
	3.258	4.516	136.510	233.950	294.265	342.206	420.366	732.124

metal thickness

period (nm)	3.39	4.45	5	5.4	6	8
75	0.545	0.319	0.254	0.219	0.178	0.102
100	0.727	0.426	0.339	0.291	0.237	0.136
150	1.091	0.638	0.508	0.437	0.356	0.205
200	1.454	0.851	0.677	0.583	0.475	0.273
300	2.182	1.277	1.016	0.874	0.712	0.409
400	2.909	1.702	1.355	1.165	0.949	0.546
500	3.636	2.128	1.693	1.457	1.187	0.682
600	4.363	2.554	2.032	1.748	1.424	0.818

B-4: Aluminum, Al

		0.544	0.633	3.39	4.45	5	5.4	6	8	9
Wavelength (in um)		0.544	0.633	3.39	4.45	5	5.4	6	8	9
Al2O3	index	1.756	1.756	1.755	1.755	1.755	1.755	1.755	1.755	1.754
	permittivity	3.083	3.082	3.081	3.081	3.081	3.081	3.080	3.079	3.078
Al	index	0.115+6.39i	0.155+7.461i	4.298+39.62i	7.255+51.39i	9.046+57.31i	10.44+61.54i	12.69+67.74i	21.22+87.15i	25.95+96.10i
	permittivity	-40.85+1.47i	-55.64+2.32i	-1.55e3+3.40e2i	-2.58e3+7.45e2i	-3.20e3+1.03e3i	-3.6787e3+1.28e3i	-4.42e3+1.72e3i	-7.14e3+3.7e3i	-8.56e3+4.98e3i

Ratio of dielectric to metal

0.544	0.633	3.39	4.45	5	5.4	6	8	9
13.253	18.052	503.523	840.069	1039.831	1194.160	1437.784	2320.944	2782.107

metal thickness

period (nm)	3.39	4.45	5	5.4	6	8	9
75	0.149	0.089	0.072	0.063	0.052	0.032	0.027
100	0.198	0.119	0.096	0.084	0.070	0.043	0.036
150	0.297	0.178	0.144	0.126	0.104	0.065	0.054
200	0.396	0.238	0.192	0.167	0.139	0.086	0.072
300	0.595	0.357	0.288	0.251	0.209	0.129	0.108
400	0.793	0.476	0.384	0.335	0.278	0.172	0.144
500	0.991	0.594	0.480	0.418	0.348	0.215	0.180
600	1.189	0.713	0.576	0.502	0.417	0.258	0.216

		0.544	0.633	3.39	4.45	5	5.4	6	8	9
Wavelength (in um)		0.544	0.633	3.39	4.45	5	5.4	6	8	9
BaF2	index	1.4759	1.4733	1.4596	1.4543	1.4510	1.4484	1.4440	1.4258	1.4144
	permittivity	2.1784	2.1705	2.1303	2.1150	2.1055	2.0978	2.0852	2.0330	2.0006
Al	index	0.115+6.39i	0.155+7.461i	4.298+39.62i	7.255+51.39i	9.046+57.31i	10.44+61.54i	12.69+67.74i	21.22+87.15i	25.95+96.10i
	permittivity	-40.85+1.47i	-55.64+2.32i	-1.55e3+3.40e2i	-2.58e3+7.45e2i	-3.20e3+1.03e3i	-3.6787e3+1.28e3i	-4.42e3+1.72e3i	-7.14e3+3.7e3i	-8.56e3+4.98e3i

Ratio of dielectric to metal									
0.544	0.633	3.39	4.45	5	5.4	6	8	9
18.754	25.637	728.351	1223.785	1521.512	1753.568	2123.829	3514.933	4280.366

	metal thickness						
period (nm)	3.39	4.45	5	5.4	6	8	9
75	0.103	0.061	0.049	0.043	0.035	0.021	0.018
100	0.137	0.082	0.066	0.057	0.047	0.028	0.023
150	0.206	0.122	0.099	0.085	0.071	0.043	0.035
200	0.274	0.163	0.131	0.114	0.094	0.057	0.047
300	0.411	0.245	0.197	0.171	0.141	0.085	0.070
400	0.548	0.327	0.263	0.228	0.188	0.114	0.093
500	0.686	0.408	0.328	0.285	0.235	0.142	0.117
600	0.823	0.490	0.394	0.342	0.282	0.171	0.140

Wavelength (in um)	0.544	0.633	3.39	4.45	5	5.4	6	8	9
CaF2 index	1.4350	1.4329	1.4149	1.4052	1.3990	1.3939	1.3856	1.3498	1.3268
permittivity	2.0592	2.0532	2.0020	1.9744	1.9571	1.9431	1.9199	1.8221	1.7603
Al index	0.115+6.39i	0.155+7.461i	4.298+39.62i	7.255+51.39i	9.046+57.31i	10.44+61.54i	12.69+67.74i	21.22+87.15i	25.95+96.10i
permittivity	-40.85+1.47i	-55.64+2.32i	-1.55e3+3.40e2i	-2.58e3+7.45e2i	-3.20e3+1.03e3i	-3.6787e3+1.28e3i	-4.42e3+1.72e3i	-7.14e3+3.7e3i	-8.56e3+4.98e3i

Ratio of dielectric to metal								
0.544	0.633	3.39	4.45	5	5.4	6	8	9
19.839	27.102	775.016	1310.897	1636.874	1893.221	2306.754	3921.754	4864.516

period (nm)	metal thickness						
	3.39	4.45	5	5.4	6	8	9
75	0.097	0.057	0.046	0.040	0.032	0.019	0.015
100	0.129	0.076	0.061	0.053	0.043	0.025	0.021
150	0.193	0.114	0.092	0.079	0.065	0.038	0.031
200	0.258	0.152	0.122	0.106	0.087	0.051	0.041
300	0.387	0.229	0.183	0.158	0.130	0.076	0.062
400	0.515	0.305	0.244	0.211	0.173	0.102	0.082
500	0.644	0.381	0.305	0.264	0.217	0.127	0.103
600	0.773	0.457	0.366	0.317	0.260	0.153	0.123

Wavelength (in um)	0.544	0.633	3.39	4.45	5	5.4	6	8	9
HfO2 index Cauchy	1.8842	1.8779	1.8606	1.8604	1.8603	1.8602	1.8602	1.8601	1.8601
permittivity	3.5502	3.5264	3.4619	3.4609	3.4607	3.4605	3.4603	3.4600	3.4599
Al index	0.115+6.39i	0.155+7.461i	4.298+39.62i	7.255+51.39i	9.046+57.31i	10.44+61.54i	12.69+67.74i	21.22+87.15i	25.95+96.10i
permittivity	-40.85+1.47i	-55.64+2.32i	-1.55e3+3.40e2i	-2.58e3+7.45e2i	-3.20e3+1.03e3i	-3.6787e3+1.28e3i	-4.42e3+1.72e3i	-7.14e3+3.7e3i	-8.56e3+4.98e3i

Ratio of dielectric to metal

0.544	0.633	3.39	4.45	5	5.4	6	8	9
11.507	15.779	448.191	747.859	925.689	1063.050	1279.845	2065.222	2474.935

metal thickness

period (nm)	3.39	4.45	5	5.4	6	8	9
75	0.167	0.100	0.081	0.070	0.059	0.036	0.030
100	0.223	0.134	0.108	0.094	0.078	0.048	0.040
150	0.334	0.200	0.162	0.141	0.117	0.073	0.061
200	0.445	0.267	0.216	0.188	0.156	0.097	0.081
300	0.668	0.401	0.324	0.282	0.234	0.145	0.121
400	0.890	0.534	0.432	0.376	0.312	0.194	0.162
500	1.113	0.668	0.540	0.470	0.390	0.242	0.202
600	1.336	0.801	0.647	0.564	0.468	0.290	0.242
600	1.336	0.801	0.647	0.564	0.468	0.290	0.242

		0.544	0.633	3.39	4.45	5	5.4	6	8	9
Wavelength (in um)		0.544	0.633	3.39	4.45	5	5.4	6	8	9
MgF2	index	1.3753	1.3753	1.3753	1.3753	1.3753	1.3753	1.3753	1.3753	1.3753
	permittivity	1.8914	1.8914	1.8914	1.8914	1.8914	1.8914	1.8914	1.8914	1.8914
Al	index	0.115+6.39i	0.155+7.461i	4.298+39.62i	7.255+51.39i	9.046+57.31i	10.44+61.54i	12.69+67.74i	21.22+87.15i	25.95+96.10i
	permittivity	-40.85+1.47i	-55.64+2.32i	-1.55e3+3.40e2i	-2.58e3+7.45e2i	-3.20e3+1.03e3i	-3.6787e3+1.28e3i	-4.42e3+1.72e3i	-7.14e3+3.7e3i	-8.56e3+4.98e3i

Ratio of dielectric to metal									
0.544	0.633	3.39	4.45	5	5.4	6	8	9
21.600	29.419	820.341	1368.451	1693.711	1944.952	2341.482	3777.977	4527.366

metal thickness

period (nm)	3.39	4.45	5	5.4	6	8	9
75	0.091	0.055	0.044	0.039	0.032	0.020	0.017
100	0.122	0.073	0.059	0.051	0.043	0.026	0.022
150	0.183	0.110	0.089	0.077	0.064	0.040	0.033
200	0.244	0.146	0.118	0.103	0.085	0.053	0.044
300	0.365	0.219	0.177	0.154	0.128	0.079	0.066
400	0.487	0.292	0.236	0.206	0.171	0.106	0.088
500	0.609	0.365	0.295	0.257	0.213	0.132	0.110
600	0.731	0.438	0.354	0.308	0.256	0.159	0.132

Wavelength (in um)	0.544	0.633	3.39	4.45	5	5.4	6	8	9
MgO index	1.6957	1.7016	1.6822	1.6543	1.6362	1.6212	1.5958	1.4806	1.4004
permittivity	2.8753	2.8953	2.8297	2.7368	2.6771	2.6284	2.5467	2.1921	1.9611
Al index	0.115+6.39i	0.155+7.461i	4.298+39.62i	7.255+51.39i	9.046+57.31i	10.44+61.54i	12.69+67.74i	21.22+87.15i	25.95+96.10i
permittivity	-40.85+1.47i	-55.64+2.32i	-1.55e3+3.40e2i	-2.58e3+7.45e2i	-3.20e3+1.03e3i	-3.6787e3+1.28e3i	-4.42e3+1.72e3i	-7.14e3+3.7e3i	-8.56e3+4.98e3i

Ratio of dielectric to metal									
0.544	0.633	3.39	4.45	5	5.4	6	8	9	
14.209	19.219	548.336	945.727	1196.640	1399.602	1738.974	3259.688	4366.511	

				metal thickness					
period (nm)	3.39	4.45	5	5.4	6	8	9		
75	0.137	0.079	0.063	0.054	0.043	0.023	0.017		
100	0.182	0.106	0.083	0.071	0.057	0.031	0.023		
150	0.273	0.158	0.125	0.107	0.086	0.046	0.034		
200	0.364	0.211	0.167	0.143	0.115	0.061	0.046		
300	0.546	0.317	0.250	0.214	0.172	0.092	0.069		
400	0.728	0.423	0.334	0.286	0.230	0.123	0.092		
500	0.910	0.528	0.417	0.357	0.287	0.153	0.114		
600	1.092	0.634	0.501	0.428	0.345	0.184	0.137		

Wavelength (in um)	0.544	0.633	3.39	4.45	5	5.4	6	8	9
SF 11 index	1.5439	1.5382	1.5245	1.5243	1.5242	1.5242	1.5241	1.5241	1.5241
permittivity	2.3836	2.3661	2.3240	2.3234	2.3232	2.3231	2.3230	2.3228	2.3228
Al index	0.115+6.39i	0.155+7.461i	4.298+39.62i	7.255+51.39i	9.046+57.31i	10.44+61.54i	12.69+67.74i	21.22+87.15i	25.95+96.10i
permittivity	-40.85+1.47i	-55.64+2.32i	-1.55e3+3.40e2i	-2.58e3+7.45e2i	-3.20e3+1.03e3i	-3.6787e3+1.28e3i	-4.42e3+1.72e3i	-7.14e3+3.7e3i	-8.56e3+4.98e3i

Ratio of dielectric to metal

0.544	0.633	3.39	4.45	5	5.4	6	8	9
17.139	23.517	667.655	1114.026	1378.912	1583.518	1906.445	3076.300	3686.588

metal thickness

period (nm)	3.39	4.45	5	5.4	6	8	9
75	0.112	0.067	0.054	0.047	0.039	0.024	0.020
100	0.150	0.090	0.072	0.063	0.052	0.032	0.027
150	0.224	0.135	0.109	0.095	0.079	0.049	0.041
200	0.299	0.179	0.145	0.126	0.105	0.065	0.054
300	0.449	0.269	0.217	0.189	0.157	0.097	0.081
400	0.598	0.359	0.290	0.252	0.210	0.130	0.108
500	0.748	0.448	0.362	0.316	0.262	0.162	0.136
2000	2.991	1.794	1.449	1.262	1.049	0.650	0.542

Wavelength (in um)		0.544	0.633	3.39	4.45	5	5.4	6	8	9
amorphous	index	3.8825	3.8828	3.8460	3.8199	3.8060	3.7960	3.7818	3.7444	3.7331
Si	permittivity	15.0737	15.0760	14.7921	14.5914	14.4853	14.4099	14.3022	14.0207	13.9358
Al	index	0.115+6.39i	0.155+7.461i	4.298+39.62i	7.255+51.39i	9.046+57.31i	10.44+61.54i	12.69+67.74i	21.22+87.15i	25.95+96.10i
	permittivity	-40.85+1.47i	-55.64+2.32i	-1.55e3+3.40e2i	-2.58e3+7.45e2i	-3.20e3+1.03e3i	-3.6787e3+1.28e3i	-4.42e3+1.72e3i	-7.14e3+3.7e3i	-8.56e3+4.98e3i

Ratio of dielectric to metal

0.544	0.633	3.39	4.45	5	5.4	6	8	9
2.710	3.691	104.894	177.385	221.156	255.291	309.652	509.654	614.467

metal thickness

period (nm)	3.39	4.45	5	5.4	6	8	9
75	0.708	0.420	0.338	0.293	0.241	0.147	0.122
100	0.944	0.561	0.450	0.390	0.322	0.196	0.162
150	1.417	0.841	0.675	0.585	0.483	0.294	0.244
200	1.889	1.121	0.900	0.780	0.644	0.392	0.325
300	2.833	1.682	1.350	1.171	0.966	0.587	0.487
400	3.777	2.242	1.801	1.561	1.288	0.783	0.650
500	4.722	2.803	2.251	1.951	1.610	0.979	0.812
600	5.666	3.364	2.701	2.341	1.931	1.175	0.975

Wavelength (in um)	0.544	0.633	3.39	4.45	5	5.4	6	8	9
SiC index	2.5872	2.5868	2.5382	2.4960	2.5868	2.4409	2.3944	2.1153	1.8083
permittivity	6.6938	6.6917	6.4426	6.2300	6.0837	5.9581	5.7331	4.4747	3.2700
Al index	0.115+6.39i	0.155+7.461i	4.298+39.62i	7.255+51.39i	9.046+57.31i	10.44+61.54i	12.69+67.74i	21.22+87.15i	25.95+96.10i
permittivity	-40.85+1.47i	-55.64+2.32i	-1.55e3+3.40e2i	-2.58e3+7.45e2i	-3.20e3+1.03e3i	-3.6787e3+1.28e3i	-4.42e3+1.72e3i	-7.14e3+3.7e3i	-8.56e3+4.98e3i

Ratio of dielectric to metal							
	3.39	4.45	5	5.4	6	8	9
	240.834	415.455	526.573	617.430	772.474	1596.916	2618.654

metal thickness

period (nm)	3.39	4.45	5	5.4	6	8	9
75	0.310	0.180	0.142	0.121	0.097	0.047	0.029
100	0.414	0.240	0.190	0.162	0.129	0.063	0.038
150	0.620	0.360	0.284	0.243	0.194	0.094	0.057
200	0.827	0.480	0.379	0.323	0.259	0.125	0.076
300	1.241	0.720	0.569	0.485	0.388	0.188	0.115
400	1.654	0.960	0.758	0.647	0.517	0.250	0.153
500	2.068	1.201	0.948	0.808	0.646	0.313	0.191
600	2.481	1.441	1.137	0.970	0.776	0.375	0.229
600	2.481	1.441	1.137	0.970	0.776	0.375	0.229

Wavelength (in um)	0.544	0.633	3.39	4.45	5	5.4	6	8	9
TiO2 index	2.4175	2.4453	2.6269	2.5757	2.5607	2.5602	2.5822	2.9935	3.5353
permittivity	5.8444	5.9795	6.9003	6.6345	6.5573	6.5544	6.6679	8.9609	12.4981
Al index	0.115+6.39i	0.155+7.461i	4.298+39.62i	7.255+51.39i	9.046+57.31i	10.44+61.54i	12.69+67.74i	21.22+87.15i	25.95+96.10i
permittivity	-40.85+1.47i	-55.64+2.32i	-1.55e3+3.40e2i	-2.58e3+7.45e2i	-3.20e3+1.03e3i	-3.6787e3+1.28e3i	-4.42e3+1.72e3i	-7.14e3+3.7e3i	-8.56e3+4.98e3i

Ratio of dielectric to metal

0.544	0.633	3.39	4.45	5	5.4	6	8	9
6.990	9.306	224.858	390.128	488.539	561.258	664.178	797.427	685.154

metal thickness

period (nm)	3.39	4.45	5	5.4	6	8	9
75	0.332	0.192	0.153	0.133	0.113	0.094	0.109
100	0.443	0.256	0.204	0.178	0.150	0.125	0.146
150	0.664	0.384	0.306	0.267	0.226	0.188	0.219
200	0.886	0.511	0.409	0.356	0.301	0.250	0.291
300	1.328	0.767	0.613	0.534	0.451	0.376	0.437
400	1.771	1.023	0.817	0.711	0.601	0.501	0.583
500	2.214	1.278	1.021	0.889	0.752	0.626	0.729
600	2.657	1.534	1.226	1.067	0.902	0.751	0.874

Wavelength (in um)	0.544	0.633	3.39	4.45	5	5.4	6	8	9
ZnO index	1.7028	1.7014	1.6975	1.6974	1.6974	1.6974	1.6974	1.6974	1.6974
permittivity	2.8996	2.8947	2.8815	2.8813	2.8812	2.8812	2.8812	2.8811	2.8811
Al index	0.115+6.39i	0.155+7.461i	4.298+39.62i	7.255+51.39i	9.046+57.31i	10.44+61.54i	12.69+67.74i	21.22+87.15i	25.95+96.10i
permittivity	-40.85+1.47i	-55.64+2.32i	-1.55e3+3.40e2i	-2.58e3+7.45e2i	-3.20e3+1.03e3i	-3.6787e3+1.28e3i	-4.42e3+1.72e3i	-7.14e3+3.7e3i	-8.56e3+4.98e3i

Ratio of dielectric to metal

	0.544	0.633	3.39	4.45	5	5.4	6	8	9
	14.089	19.223	538.474	898.318	1111.856	1276.800	1537.129	2480.211	2972.197

metal thickness

period (nm)	3.39	4.45	5	5.4	6	8	9
75	0.139	0.083	0.067	0.059	0.049	0.030	0.025
100	0.185	0.111	0.090	0.078	0.065	0.040	0.034
150	0.278	0.167	0.135	0.117	0.098	0.060	0.050
200	0.371	0.222	0.180	0.157	0.130	0.081	0.067
300	0.556	0.334	0.270	0.235	0.195	0.121	0.101
400	0.741	0.445	0.359	0.313	0.260	0.161	0.135
500	0.927	0.556	0.449	0.391	0.325	0.202	0.168
600	1.112	0.667	0.539	0.470	0.390	0.242	0.202

	Wavelength (in um)	0.544	0.633	3.39	4.45	5	5.4	6	8	9
ZnS	index	1.8410	1.8410	1.8410	1.8410	1.8410	1.8410	1.8410	1.8410	1.8410
	permittivity	3.3892	3.3892	3.3892	3.3892	3.3892	3.3892	3.3892	3.3892	3.3892
Al	index	0.115+6.39i	0.155+7.461i	4.298+39.62i	7.255+51.39i	9.046+57.31i	10.44+61.54i	12.69+67.74i	21.22+87.15i	25.95+96.10i
	permittivity	-40.85+1.47i	-55.64+2.32i	-1.55e3+3.40e2i	-2.58e3+7.45e2i	-3.20e3+1.03e3i	-3.6787e3+1.28e3i	-4.42e3+1.72e3i	-7.14e3+3.7e3i	-8.56e3+4.98e3i

Ratio of dielectric to metal

0.544	0.633	3.39	4.45	5	5.4	6	8	9
12.054	16.418	457.808	763.692	945.211	1085.422	1306.714	2108.385	2526.601

metal thickness

period (nm)	3.39	4.45	5	5.4	6	8	9
75	0.163	0.098	0.079	0.069	0.057	0.036	0.030
100	0.218	0.131	0.106	0.092	0.076	0.047	0.040
150	0.327	0.196	0.159	0.138	0.115	0.071	0.059
200	0.436	0.262	0.211	0.184	0.153	0.095	0.079
300	0.654	0.392	0.317	0.276	0.229	0.142	0.119
400	0.872	0.523	0.423	0.368	0.306	0.190	0.158
500	1.090	0.654	0.528	0.460	0.382	0.237	0.198
600	1.308	0.785	0.634	0.552	0.459	0.284	0.237

B-4: Iron, Fe

Wavelength (in um)	0.544	0.633	3.39	4.45	5	5.4	6	8	9
Al2O3 Index	1.756	1.756	1.755	1.755	1.755	1.755	1.755	1.755	1.754
permittivity	3.083	3.082	3.081	3.081	3.081	3.081	3.080	3.079	3.078
Fe index	1.70+4.91i	1.82+4.92i	3.82+8.42i	4.19+10.83i	4.40+12.21i	4.56+13.24i	4.84+14.84i	6.14+20.17i	7.01+22.69i
permittivity	-21.25+16.71i	-20.98+17.98i	-56.25+64.35i	-99.74+90.92i	-129.74+107.48i	-154.69+120.98i	-196.78+143.85i	-369.19+248.06i	-465.9+318.15i

Ratio of dielectric to metal

0.544	0.633	3.39	4.45	5	5.4	6	8	9
6.895	6.796	18.257	32.373	42.114	50.215	63.888	119.916	151.356

metal thickness

period (nm)	3.39	4.45	5	5.4	6	8	9
75	3.895	2.247	1.740	1.464	1.156	0.620	0.492
100	5.193	2.996	2.319	1.953	1.541	0.827	0.656
150	7.789	4.495	3.479	2.929	2.312	1.241	0.985
200	10.386	5.993	4.639	3.905	3.082	1.654	1.313
300	15.579	8.989	6.958	5.858	4.623	2.481	1.969
400	20.771	11.986	9.278	7.810	6.164	3.308	2.625
500	25.964	14.982	11.597	9.763	7.706	4.135	3.282
600	31.157	17.979	13.917	11.715	9.247	4.962	3.938

Wavelength (in um)		0.544	0.633	3.39	4.45	5	5.4	6	8	9
BaF2	Index	1.4759	1.4733	1.4596	1.4543	1.4510	1.4484	1.4440	1.4258	1.4144
	permittivity	2.1784	2.1705	2.1303	2.1150	2.1055	2.0978	2.0852	2.0330	2.0006
Fe	index	1.70+4.91i	1.82+4.92i	3.82+8.42i	4.19+10.83i	4.40+12.21i	4.56+13.24i	4.84+14.84i	6.14+20.17i	7.01+22.69i
	permittivity	-21.25+16.71i	-20.98+17.98i	-56.25+64.35i	-99.74+90.92i	-129.74+107.48i	-154.69+120.98i	-196.78+143.85i	-369.19+248.06i	-465.9+318.15i

Ratio of dielectric to metal

0.544	0.633	3.39	4.45	5	5.4	6	8	9
9.757	9.651	26.409	47.160	61.622	73.739	94.372	181.606	232.866

metal thickness

period (nm)	3.39	4.45	5	5.4	6	8	9
75	2.736	1.557	1.198	1.003	0.786	0.411	0.321
100	3.648	2.076	1.597	1.338	1.049	0.548	0.428
150	5.473	3.115	2.395	2.007	1.573	0.821	0.641
200	7.297	4.153	3.194	2.676	2.097	1.095	0.855
300	10.945	6.229	4.791	4.014	3.146	1.643	1.283
400	14.594	8.306	6.388	5.352	4.194	2.191	1.710
500	18.242	10.382	7.984	6.690	5.243	2.738	2.138
600	21.890	12.459	9.581	8.028	6.291	3.286	2.566

Wavelength (in um)	0.544	0.633	3.39	4.45	5	5.4	6	8	9
CaF2 Index	1.4350	1.4329	1.4149	1.4052	1.3990	1.3939	1.3856	1.3498	1.3268
permittivity	2.0592	2.0532	2.0020	1.9744	1.9571	1.9431	1.9199	1.8221	1.7603
Fe index	1.70+4.91i	1.82+4.92i	3.82+8.42i	4.19+10.83i	4.40+12.21i	4.56+13.24i	4.84+14.84i	6.14+20.17i	7.01+22.69i
permittivity	-21.25+16.71i	-20.98+17.98i	-56.25+64.35i	-99.74+90.92i	-129.74+107.48i	-154.69+120.98i	-196.78+143.85i	-369.19+248.06i	-465.9+318.15i

Ratio of dielectric to metal

0.544	0.633	3.39	4.45	5	5.4	6	8	9
10.322	10.203	28.101	50.517	66.294	79.611	102.501	202.625	264.646

metal thickness

period (nm)	3.39	4.45	5	5.4	6	8	9
75	2.577	1.456	1.115	0.930	0.725	0.368	0.282
100	3.436	1.941	1.486	1.241	0.966	0.491	0.376
150	5.154	2.912	2.229	1.861	1.449	0.737	0.565
200	6.873	3.882	2.972	2.481	1.932	0.982	0.753
300	10.309	5.823	4.458	3.722	2.899	1.473	1.129
400	13.745	7.764	5.944	4.962	3.865	1.964	1.506
500	17.181	9.706	7.430	6.203	4.831	2.455	1.882
600	20.618	11.647	8.916	7.443	5.797	2.947	2.259

Wavelength (in um)	0.544	0.633	3.39	4.45	5	5.4	6	8	9
HfO2 index Cauchy	1.8842	1.8779	1.8606	1.8604	1.8603	1.8602	1.8602	1.8601	1.8601
permittivity	3.5502	3.5264	3.4619	3.4609	3.4607	3.4605	3.4603	3.4600	3.4599
Fe index	1.70+4.91i	1.82+4.92i	3.82+8.42i	4.19+10.83i	4.40+12.21i	4.56+13.24i	4.84+14.84i	6.14+20.17i	7.01+22.69i
permittivity	-21.25+16.71i	-20.98+17.98i	-56.25+64.35i	-99.74+90.92i	-129.74+107.48i	-154.69+120.98i	-196.78+143.85i	-369.19+248.06i	-465.9+318.15i

Ratio of dielectric to metal

0.544	0.633	3.39	4.45	5	5.4	6	8	9
5.987	5.940	16.251	28.820	37.491	44.702	56.870	106.704	134.645

metal thickness

period (nm)	3.39	4.45	5	5.4	6	8	9
75	4.348	2.515	1.949	1.641	1.296	0.696	0.553
100	5.797	3.354	2.598	2.188	1.728	0.928	0.737
150	8.695	5.030	3.897	3.282	2.592	1.393	1.106
200	11.594	6.707	5.196	4.376	3.456	1.857	1.474
300	17.390	10.061	7.794	6.564	5.184	2.785	2.212
400	23.187	13.414	10.392	8.752	6.912	3.714	2.949
500	28.984	16.768	12.990	10.940	8.640	4.642	3.686
600	34.781	20.121	15.588	13.129	10.368	5.571	4.423

Wavelength (in um)	0.544	0.633	3.39	4.45	5	5.4	6	8	9
MgF2 Index	1.3753	1.3753	1.3753	1.3753	1.3753	1.3753	1.3753	1.3753	1.3753
permittivity	1.8914	1.8914	1.8914	1.8914	1.8914	1.8914	1.8914	1.8914	1.8914
Fe index	1.70+4.91i	1.82+4.92i	3.82+8.42i	4.19+10.83i	4.40+12.21i	4.56+13.24i	4.84+14.84i	6.14+20.17i	7.01+22.69i
permittivity	-21.25+16.71i	-20.98+17.98i	-56.25+64.35i	-99.74+90.92i	-129.74+107.48i	-154.69+120.98i	-196.78+143.85i	-369.19+248.06i	-465.9+318.15i

Ratio of dielectric to metal

0.544	0.633	3.39	4.45	5	5.4	6	8	9
11.238	11.075	29.745	52.735	68.596	81.787	104.044	195.197	246.304

metal thickness

period (nm)	3.39	4.45	5	5.4	6	8	9
75	2.439	1.396	1.078	0.906	0.714	0.382	0.303
100	3.253	1.861	1.437	1.208	0.952	0.510	0.404
150	4.879	2.791	2.155	1.812	1.428	0.765	0.607
200	6.505	3.722	2.874	2.416	1.904	1.019	0.809
300	9.758	5.583	4.311	3.624	2.856	1.529	1.213
400	13.010	7.444	5.747	4.832	3.808	2.039	1.617
500	16.263	9.305	7.184	6.040	4.760	2.548	2.022
600	19.515	11.166	8.621	7.248	5.712	3.058	2.426

		0.544	0.633	3.39	4.45	5	5.4	6	8	9
Wavelength (in um)		0.544	0.633	3.39	4.45	5	5.4	6	8	9
MgO	index	1.6957	1.7016	1.6822	1.6543	1.6362	1.6212	1.5958	1.4806	1.4004
	permittivity	2.8753	2.8953	2.8297	2.7368	2.6771	2.6284	2.5467	2.1921	1.9611
Fe	index	1.70+4.91i	1.82+4.92i	3.82+8.42i	4.19+10.83i	4.40+12.21i	4.56+13.24i	4.84+14.84i	6.14+20.17i	7.01+22.69i
	permittivity	-21.25+16.71i	-20.98+17.98i	-56.25+64.35i	-99.74+90.92i	-129.74+107.48i	-154.69+120.98i	-196.78+143.85i	-369.19+248.06i	-465.9+318.15i

Ratio of dielectric to metal								
0.544	0.633	3.39	4.45	5	5.4	6	8	9
7.392	7.235	19.882	36.445	48.465	58.854	77.271	168.418	237.553

	metal thickness						
period (nm)	3.39	4.45	5	5.4	6	8	9
75	3.592	2.003	1.516	1.253	0.958	0.443	0.314
100	4.789	2.671	2.022	1.671	1.278	0.590	0.419
150	7.183	4.006	3.032	2.506	1.916	0.885	0.629
200	9.578	5.341	4.043	3.341	2.555	1.181	0.838
300	14.366	8.012	6.065	5.012	3.833	1.771	1.258
400	19.155	10.682	8.087	6.683	5.110	2.361	1.677
500	23.944	13.353	10.108	8.354	6.388	2.951	2.096
600	28.733	16.024	12.130	10.024	7.666	3.542	2.515

Wavelength (in um)	0.544	0.633	3.39	4.45	5	5.4	6	8	9
SF 11 index	1.5439	1.5382	1.5245	1.5243	1.5242	1.5242	1.5241	1.5241	1.5241
permittivity	2.3836	2.3661	2.3240	2.3234	2.3232	2.3231	2.3230	2.3228	2.3228
Fe index	1.70+4.91i	1.82+4.92i	3.82+8.42i	4.19+10.83i	4.40+12.21i	4.56+13.24i	4.84+14.84i	6.14+20.17i	7.01+22.69i
permittivity	-21.25+16.71i	-20.98+17.98i	-56.25+64.35i	-99.74+90.92i	-129.74+107.48i	-154.69+120.98i	-196.78+143.85i	-369.19+248.06i	-465.9+318.15i

Ratio of dielectric to metal

0.544	0.633	3.39	4.45	5	5.4	6	8	9
8.917	8.853	24.209	42.930	55.847	66.588	84.713	158.943	200.563

metal thickness

period (nm)	3.39	4.45	5	5.4	6	8	9
75	2.975	1.707	1.319	1.110	0.875	0.469	0.372
100	3.967	2.276	1.759	1.480	1.167	0.625	0.496
150	5.950	3.415	2.639	2.219	1.750	0.938	0.744
200	7.934	4.553	3.518	2.959	2.333	1.250	0.992
300	11.901	6.829	5.277	4.439	3.500	1.876	1.488
400	15.868	9.105	7.036	5.918	4.667	2.501	1.984
500	19.835	11.382	8.796	7.398	5.833	3.126	2.481
600	23.801	13.658	10.555	8.877	7.000	3.751	2.977

Wavelength (in um)		0.544	0.633	3.39	4.45	5	5.4	6	8	9
amorphous	index	3.8825	3.8828	3.8460	3.8199	3.8060	3.7960	3.7818	3.7444	3.7331
Si	permittivity	15.0737	15.0760	14.7921	14.5914	14.4853	14.4099	14.3022	14.0207	13.9358
Fe	index	1.70+4.91i	1.82+4.92i	3.82+8.42i	4.19+10.83i	4.40+12.21i	4.56+13.24i	4.84+14.84i	6.14+20.17i	7.01+22.69i
	permittivity	-21.25+16.71i	-20.98+17.98i	-56.25+64.35i	-99.74+90.92i	-129.74+107.48i	-154.69+120.98i	-196.78+143.85i	-369.19+248.06i	-465.9+318.15i
	Ratio of dielectric to metal									
		1.410	1.390	3.803	6.836	8.957	10.735	13.759	26.332	33.429
				metal thickness						
	period (nm)	3.39	4.45	5			5.4	6	8	9
	75	15.614	9.572	7.532	6.391	5.082	2.744	2.178		
	100	20.819	12.762	10.043	8.521	6.775	3.659	2.905		
	150	31.228	19.143	15.065	12.782	10.163	5.488	4.357		
	200	41.637	25.524	20.087	17.043	13.551	7.317	5.809		
	300	62.456	38.286	30.130	25.564	20.326	10.976	8.714		
	400	83.275	51.048	40.173	34.086	27.101	14.635	11.618		
	500	104.094	63.810	50.216	42.607	33.877	18.293	14.523		
	600	124.912	76.572	60.260	51.128	40.652	21.952	17.427		

Wavelength (in um)	0.544	0.633	3.39	4.45	5	5.4	6	8	9
SiC index	2.5872	2.5868	2.5382	2.4960	2.5868	2.4409	2.3944	2.1153	1.8083
permittivity	6.6938	6.6917	6.4426	6.2300	6.0837	5.9581	5.7331	4.4747	3.2700
Fe index	1.70+4.91i	1.82+4.92i	3.82+8.42i	4.19+10.83i	4.40+12.21i	4.56+13.24i	4.84+14.84i	6.14+20.17i	7.01+22.69i
permittivity	-21.25+16.71i	-20.98+17.98i	-56.25+64.35i	-99.74+90.92i	-129.74+107.48i	-154.69+120.98i	-196.78+143.85i	-369.19+248.06i	-465.9+318.15i

Ratio of dielectric to metal

	3.39	4.45	5	5.4	6	8	9	
		8.732	16.010	21.326	25.963	34.325	82.508	142.464

metal thickness

period (nm)	3.39	4.45	5	5.4	6	8	9
75	7.706	4.409	3.359	2.782	2.123	0.898	0.523
100	10.275	5.879	4.479	3.709	2.831	1.197	0.697
150	15.412	8.818	6.718	5.563	4.246	1.796	1.046
200	20.550	11.758	8.958	7.417	5.662	2.395	1.394
300	30.825	17.637	13.437	11.126	8.493	3.592	2.091
400	41.100	23.516	17.916	14.835	11.323	4.790	2.788
500	51.375	29.394	22.395	18.544	14.154	5.987	3.485
600	61.650	35.273	26.874	22.252	16.985	7.185	4.182
600	61.650	35.273	26.874	22.252	16.985	7.185	4.182

Wavelength (in um)	0.544	0.633	3.39	4.45	5	5.4	6	8	9
TiO2 index	2.4175	2.4453	2.6269	2.5757	2.5607	2.5602	2.5822	2.9935	3.5353
permittivity	5.8444	5.9795	6.9003	6.6345	6.5573	6.5544	6.6679	8.9609	12.4981
Fe index	1.70+4.91i	1.82+4.92i	3.82+8.42i	4.19+10.83i	4.40+12.21i	4.56+13.24i	4.84+14.84i	6.14+20.17i	7.01+22.69i
permittivity	-21.25+16.71i	-20.98+17.98i	-56.25+64.35i	-99.74+90.92i	-129.74+107.48i	-154.69+120.98i	-196.78+143.85i	-369.19+248.06i	-465.9+318.15i
Ratio of dielectric to metal									
0.544	0.633	3.39	4.45	5	5.4	6	8	9	
3.637	3.503	8.153	15.034	19.786	23.601	29.513	41.201	37.275	
			metal thickness						
period (nm)	3.39	4.45	5	5.4	6	8	9		
75	8.194	4.678	3.608	3.049	2.458	1.777	1.960		
100	10.925	6.237	4.811	4.065	3.277	2.370	2.613		
150	16.388	9.355	7.216	6.097	4.916	3.554	3.919		
200	21.850	12.474	9.622	8.130	6.555	4.739	5.225		
300	32.776	18.710	14.433	12.194	9.832	7.109	7.838		
400	43.701	24.947	19.244	16.259	13.109	9.479	10.451		
500	54.626	31.184	24.055	20.324	16.387	11.848	13.063		
600	65.551	37.421	28.866	24.389	19.664	14.218	15.676		

Wavelength (in um)	0.544	0.633	3.39	4.45	5	5.4	6	8	9
ZnO index	1.7028	1.7014	1.6975	1.6974	1.6974	1.6974	1.6974	1.6974	1.6974
permittivity	2.8996	2.8947	2.8815	2.8813	2.8812	2.8812	2.8812	2.8811	2.8811
Fe index	1.70+4.91i	1.82+4.92i	3.82+8.42i	4.19+10.83i	4.40+12.21i	4.56+13.24i	4.84+14.84i	6.14+20.17i	7.01+22.69i
permittivity	-21.25+16.71i	-20.98+17.98i	-56.25+64.35i	-99.74+90.92i	-129.74+107.48i	-154.69+120.98i	-196.78+143.85i	-369.19+248.06i	-465.9+318.15i

Ratio of dielectric to metal									
0.544	0.633	3.39	4.45	5	5.4	6	8	9	
7.330	7.237	19.525	34.618	45.031	53.690	68.302	128.145	161.698	

			metal thickness					
period (nm)	3.39	4.45	5	5.4	6	8	9	
75	3.654	2.106	1.629	1.371	1.082	0.581	0.461	
100	4.872	2.808	2.172	1.828	1.443	0.774	0.615	
150	7.308	4.211	3.259	2.743	2.164	1.161	0.922	
200	9.744	5.615	4.345	3.657	2.886	1.549	1.229	
300	14.617	8.423	6.517	5.485	4.329	2.323	1.844	
400	19.489	11.230	8.690	7.314	5.772	3.097	2.459	
500	24.361	14.038	10.862	9.142	7.215	3.872	3.073	
600	29.233	16.846	13.035	10.971	8.658	4.646	3.688	

Wavelength (in um)	0.544	0.633	3.39	4.45	5	5.4	6	8	9
ZnS	index	1.8410	1.8410	1.8410	1.8410	1.8410	1.8410	1.8410	1.8410	1.8410
	permittivity	3.3892	3.3892	3.3892	3.3892	3.3892	3.3892	3.3892	3.3892	3.3892
Fe	index	1.70+4.91i	1.82+4.92i	3.82+8.42i	4.19+10.83i	4.40+12.21i	4.56+13.24i	4.84+14.84i	6.14+20.17i	7.01+22.69i
	permittivity	-21.25+16.71i	-20.98+17.98i	-56.25+64.35i	-99.74+90.92i	-129.74+107.48i	-154.69+120.98i	-196.78+143.85i	-369.19+248.06i	-465.9+318.15i

Ratio of dielectric to metal

0.544	0.633	3.39	4.45	5	5.4	6	8	9
6.271	6.181	16.600	29.430	38.281	45.643	58.064	108.934	137.456

metal thickness

period (nm)	3.39	4.45	5	5.4	6	8	9
75	4.261	2.465	1.909	1.608	1.270	0.682	0.542
100	5.682	3.286	2.546	2.144	1.693	0.910	0.722
150	8.523	4.929	3.819	3.216	2.540	1.364	1.083
200	11.364	6.573	5.091	4.288	3.386	1.819	1.445
300	17.046	9.859	7.637	6.432	5.079	2.729	2.167
400	22.728	13.145	10.183	8.576	6.772	3.639	2.889
500	28.410	16.431	12.729	10.720	8.465	4.548	3.611
600	34.091	19.718	15.274	12.864	10.159	5.458	4.334

B-5: Nickel, Ni

Wavelength (in um)	0.544	0.633	3.39	4.45	5	5.4	6	8	9
Al2O3 Index	1.756	1.756	1.755	1.755	1.755	1.755	1.755	1.755	1.754
permittivity	3.083	3.082	3.081	3.081	3.081	3.081	3.080	3.079	3.078
Ni index	1.97+4.34i	2.15+4.55i	4.11+12.43i	4.08+16.04i	4.06+18.01i	4.06+19.47i	4.07+21.71i	4.35+29.43i	4.46+33.32i
permittivity	-14.99+17.18i	-16.13+19.59i	-137.53+102.11i	-240.57+131.13i	-307.82+146.44i	-362.83+158.15i	-455.11+177.17i	-847.64+256.10i	-1090.8+297.9i

Ratio of dielectric to metal									
0.544	0.633	3.39	4.45	5	5.4	6	8	9	
4.864	5.235	44.633	78.083	99.918	117.781	147.754	275.316	354.410	

		metal thickness							
period (nm)	3.39	4.45	5	5.4	6	8	9	
75	1.644	0.948	0.743	0.631	0.504	0.271	0.211	
100	2.191	1.264	0.991	0.842	0.672	0.362	0.281	
150	3.287	1.897	1.486	1.263	1.008	0.543	0.422	
200	4.383	2.529	1.982	1.684	1.344	0.724	0.563	
300	6.574	3.793	2.973	2.526	2.017	1.086	0.844	
400	8.766	5.058	3.964	3.368	2.689	1.448	1.125	
500	10.957	6.322	4.955	4.209	3.361	1.810	1.407	
600	13.148	7.587	5.945	5.051	4.033	2.171	1.688	

Wavelength (in um)	0.544	0.633	3.39	4.45	5	5.4	6	8	9
BaF2 Index	1.4759	1.4733	1.4596	1.4543	1.4510	1.4484	1.4440	1.4258	1.4144
permittivity	2.1784	2.1705	2.1303	2.1150	2.1055	2.0978	2.0852	2.0330	2.0006
Ni index	1.97+4.34i	2.15+4.55i	4.11+12.43i	4.08+16.04i	4.06+18.01i	4.06+19.47i	4.07+21.71i	4.35+29.43i	4.46+33.32i
permittivity	-14.99+17.18i	-16.13+19.59i	-137.53+102.11i	-240.57+131.13i	-307.82+146.44i	-362.83+158.15i	-455.11+177.17i	-847.64+256.10i	-1090.8+297.9i

Ratio of dielectric to metal

0.544	0.633	3.39	4.45	5	5.4	6	8	9
6.883	7.435	64.562	113.749	146.204	172.955	218.256	416.950	545.271

metal thickness

period (nm)	3.39	4.45	5	5.4	6	8	9
75	1.144	0.654	0.509	0.431	0.342	0.179	0.137
100	1.525	0.871	0.679	0.575	0.456	0.239	0.183
150	2.288	1.307	1.019	0.862	0.684	0.359	0.275
200	3.051	1.743	1.359	1.150	0.912	0.479	0.366
300	4.576	2.614	2.038	1.725	1.368	0.718	0.549
400	6.101	3.486	2.717	2.299	1.824	0.957	0.732
500	7.626	4.357	3.397	2.874	2.280	1.196	0.915
600	9.152	5.229	4.076	3.449	2.737	1.436	1.098

Wavelength (in um)	0.544	0.633	3.39	4.45	5	5.4	6	8	9
CaF2 Index	1.4350	1.4329	1.4149	1.4052	1.3990	1.3939	1.3856	1.3498	1.3268
permittivity	2.0592	2.0532	2.0020	1.9744	1.9571	1.9431	1.9199	1.8221	1.7603
Ni index	1.97+4.34i	2.15+4.55i	4.11+12.43i	4.08+16.04i	4.06+18.01i	4.06+19.47i	4.07+21.71i	4.35+29.43i	4.46+33.32i
permittivity	-14.99+17.18i	-16.13+19.59i	-137.53+102.11i	-240.57+131.13i	-307.82+146.44i	-362.83+158.15i	-455.11+177.17i	-847.64+256.10i	-1090.8+297.9i

Ratio of dielectric to metal

0.544	0.633	3.39	4.45	5	5.4	6	8	9
7.281	7.860	68.698	121.846	157.289	186.729	237.054	465.208	619.686

metal thickness

period (nm)	3.39	4.45	5	5.4	6	8	9
75	1.076	0.611	0.474	0.400	0.315	0.161	0.121
100	1.435	0.814	0.632	0.533	0.420	0.214	0.161
150	2.152	1.221	0.948	0.799	0.630	0.322	0.242
200	2.870	1.628	1.264	1.065	0.840	0.429	0.322
300	4.304	2.442	1.895	1.598	1.260	0.643	0.483
400	5.739	3.256	2.527	2.131	1.680	0.858	0.644
500	7.174	4.070	3.159	2.663	2.100	1.072	0.806
600	8.609	4.884	3.791	3.196	2.520	1.287	0.967

Wavelength (in um)	0.544	0.633	3.39	4.45	5	5.4	6	8	9
HfO2 index Cauchy	1.8842	1.8779	1.8606	1.8604	1.8603	1.8602	1.8602	1.8601	1.8601
permittivity	3.5502	3.5264	3.4619	3.4609	3.4607	3.4605	3.4603	3.4600	3.4599
Ni index	1.97+4.34i	2.15+4.55i	4.11+12.43i	4.08+16.04i	4.06+18.01i	4.06+19.47i	4.07+21.71i	4.35+29.43i	4.46+33.32i
permittivity	-14.99+17.18i	-16.13+19.59i	-137.53+102.11i	-240.57+131.13i	-307.82+146.44i	-362.83+158.15i	-455.11+177.17i	-847.64+256.10i	-1090.8+297.9i

Ratio of dielectric to metal

0.544	0.633	3.39	4.45	5	5.4	6	8	9
4.223	4.576	39.728	69.512	88.950	104.849	131.524	244.982	315.279

metal thickness

period (nm)	3.39	4.45	5	5.4	6	8	9
75	1.841	1.064	0.834	0.709	0.566	0.305	0.237
100	2.455	1.418	1.112	0.945	0.755	0.407	0.316
150	3.683	2.127	1.668	1.417	1.132	0.610	0.474
200	4.911	2.836	2.223	1.889	1.509	0.813	0.632
300	7.366	4.255	3.335	2.834	2.264	1.220	0.949
400	9.821	5.673	4.447	3.779	3.018	1.626	1.265
500	12.277	7.091	5.559	4.724	3.773	2.033	1.581
600	14.732	8.509	6.670	5.668	4.527	2.439	1.897

Wavelength (in um)		0.544	0.633	3.39	4.45	5	5.4	6	8	9
MgF2	Index	1.3753	1.3753	1.3753	1.3753	1.3753	1.3753	1.3753	1.3753	1.3753
	permittivity	1.8914	1.8914	1.8914	1.8914	1.8914	1.8914	1.8914	1.8914	1.8914
Ni	index	1.97+4.34i	2.15+4.55i	4.11+12.43i	4.08+16.04i	4.06+18.01i	4.06+19.47i	4.07+21.71i	4.35+29.43i	4.46+33.32i
	permittivity	-14.99+17.18i	-16.13+19.59i	-137.53+102.11i	-240.57+131.13i	-307.82+146.44i	-362.83+158.15i	-455.11+177.17i	-847.64+256.10i	-1090.8+297.9i

Ratio of dielectric to metal

0.544	0.633	3.39	4.45	5	5.4	6	8	9
7.927	8.532	72.716	127.195	162.750	191.832	240.623	448.153	576.736

metal thickness

period (nm)	3.39	4.45	5	5.4	6	8	9
75	1.017	0.585	0.458	0.389	0.310	0.167	0.130
100	1.357	0.780	0.611	0.519	0.414	0.223	0.173
150	2.035	1.170	0.916	0.778	0.621	0.334	0.260
200	2.713	1.560	1.221	1.037	0.828	0.445	0.346
300	4.070	2.340	1.832	1.556	1.242	0.668	0.519
400	5.426	3.120	2.443	2.074	1.655	0.891	0.692
500	6.783	3.900	3.053	2.593	2.069	1.113	0.865
600	8.139	4.680	3.664	3.112	2.483	1.336	1.039

Wavelength (in um)	0.544	0.633	3.39	4.45	5	5.4	6	8	9
MgO	index	1.6957	1.7016	1.6822	1.6543	1.6362	1.6212	1.5958	1.4806	1.4004
	permittivity	2.8753	2.8953	2.8297	2.7368	2.6771	2.6284	2.5467	2.1921	1.9611
Ni	index	1.97+4.34i	2.15+4.55i	4.11+12.43i	4.08+16.04i	4.06+18.01i	4.06+19.47i	4.07+21.71i	4.35+29.43i	4.46+33.32i
	permittivity	-14.99+17.18i	-16.13+19.59i	-137.53+102.11i	-240.57+131.13i	-307.82+146.44i	-362.83+158.15i	-455.11+177.17i	-847.64+256.10i	-1090.8+297.9i

Ratio of dielectric to metal

0.544	0.633	3.39	4.45	5	5.4	6	8	9
5.215	5.574	48.605	87.904	114.986	138.043	178.706	386.672	556.245

period (nm)	3.39	4.45	5	5.4	6	8	9
			metal thickness				
75	1.512	0.844	0.647	0.539	0.417	0.193	0.135
100	2.016	1.125	0.862	0.719	0.556	0.258	0.179
150	3.024	1.687	1.293	1.079	0.835	0.387	0.269
200	4.032	2.250	1.724	1.438	1.113	0.516	0.359
300	6.048	3.374	2.587	2.158	1.669	0.774	0.538
400	8.064	4.499	3.449	2.877	2.226	1.032	0.718
500	10.080	5.624	4.311	3.596	2.782	1.290	0.897
600	12.096	6.749	5.173	4.315	3.339	1.548	1.077

Wavelength (in um)	0.544	0.633	3.39	4.45	5	5.4	6	8	9
SF 11 index	1.5439	1.5382	1.5245	1.5243	1.5242	1.5242	1.5241	1.5241	1.5241
permittivity	2.3836	2.3661	2.3240	2.3234	2.3232	2.3231	2.3230	2.3228	2.3228
Ni index	1.97+4.34i	2.15+4.55i	4.11+12.43i	4.08+16.04i	4.06+18.01i	4.06+19.47i	4.07+21.71i	4.35+29.43i	4.46+33.32i
permittivity	-14.99+17.18i	-16.13+19.59i	-137.53+102.11i	-240.57+131.13i	-307.82+146.44i	-362.83+158.15i	-455.11+177.17i	-847.64+256.10i	-1090.8+297.9i

Ratio of dielectric to metal

0.544	0.633	3.39	4.45	5	5.4	6	8	9
6.290	6.820	59.181	103.547	132.501	156.183	195.916	364.918	469.631

metal thickness

period (nm)	3.39	4.45	5	5.4	6	8	9
75	1.246	0.717	0.562	0.477	0.381	0.205	0.159
100	1.662	0.957	0.749	0.636	0.508	0.273	0.212
150	2.492	1.435	1.124	0.954	0.762	0.410	0.319
200	3.323	1.913	1.498	1.272	1.016	0.547	0.425
300	4.985	2.870	2.247	1.909	1.523	0.820	0.637
400	6.647	3.826	2.996	2.545	2.031	1.093	0.850
500	8.308	4.783	3.745	3.181	2.539	1.366	1.062
600	9.970	5.739	4.494	3.817	3.047	1.640	1.275

Wavelength (in um)	0.544	0.633	3.39	4.45	5	5.4	6	8	9
amorphous index	3.8825	3.8828	3.8460	3.8199	3.8060	3.7960	3.7818	3.7444	3.7331
Si permittivity	15.0737	15.0760	14.7921	14.5914	14.4853	14.4099	14.3022	14.0207	13.9358
Ni index	1.97+4.34i	2.15+4.55i	4.11+12.43i	4.08+16.04i	4.06+18.01i	4.06+19.47i	4.07+21.71i	4.35+29.43i	4.46+33.32i
permittivity	-14.99+17.18i	-16.13+19.59i	-137.53+102.11i	-240.57+131.13i	-307.82+146.44i	-362.83+158.15i	-455.11+177.17i	-847.64+256.10i	-1090.8+297.9i

Ratio of dielectric to metal

0.544	0.633	3.39	4.45	5	5.4	6	8	9
0.995	1.070	9.298	16.488	21.251	25.179	31.822	60.456	78.276

metal thickness

period (nm)	3.39	4.45	5	5.4	6	8	9
75	7.283	4.289	3.371	2.865	2.285	1.220	0.946
100	9.711	5.718	4.494	3.820	3.047	1.627	1.261
150	14.566	8.577	6.741	5.730	4.570	2.441	1.892
200	19.421	11.437	8.988	7.640	6.094	3.254	2.523
300	29.132	17.155	13.482	11.459	9.140	4.882	3.784
400	38.843	22.873	17.977	15.279	12.187	6.509	5.046
500	48.554	28.592	22.471	19.099	15.234	8.136	6.307
600	58.264	34.310	26.965	22.919	18.281	9.763	7.568

Wavelength (in um)	0.544	0.633	3.39	4.45	5	5.4	6	8	9
SiC index	2.5872	2.5868	2.5382	2.4960	2.5868	2.4409	2.3944	2.1153	1.8083
permittivity	6.6938	6.6917	6.4426	6.2300	6.0837	5.9581	5.7331	4.4747	3.2700
Ni index	1.97+4.34i	2.15+4.55i	4.11+12.43i	4.08+16.04i	4.06+18.01i	4.06+19.47i	4.07+21.71i	4.35+29.43i	4.46+33.32i
permittivity	-14.99+17.18i	-16.13+19.59i	-137.53+102.11i	-240.57+131.13i	-307.82+146.44i	-362.83+158.15i	-455.11+177.17i	-847.64+256.10i	-1090.8+297.9i

Ratio of dielectric to metal

3.39	4.45	5	5.4	6	8	9
21.348	38.616	50.599	60.897	79.384	189.430	333.588

metal thickness

period (nm)	3.39	4.45	5	5.4	6	8	9
75	3.356	1.893	1.454	1.212	0.933	0.394	0.224
100	4.475	2.524	1.938	1.616	1.244	0.525	0.299
150	6.712	3.786	2.907	2.423	1.866	0.788	0.448
200	8.949	5.048	3.876	3.231	2.488	1.050	0.598
300	13.424	7.573	5.814	4.847	3.732	1.575	0.897
400	17.899	10.097	7.752	6.462	4.976	2.101	1.196
500	22.374	12.621	9.690	8.078	6.220	2.626	1.494
600	26.848	15.145	11.628	9.693	7.464	3.151	1.793
600	26.848	15.145	11.628	9.693	7.464	3.151	1.793

Wavelength (in um)	0.544	0.633	3.39	4.45	5	5.4	6	8	9
SU-8 index	1.5770	1.5770	1.5770	1.5770	1.5770	1.5770	1.5770	1.5770	1.5770
permittivity	2.4869	2.4869	2.4869	2.4869	2.4869	2.4869	2.4869	2.4869	2.4869
Ni index	1.97+4.34i	2.15+4.55i	4.11+12.43i	4.08+16.04i	4.06+18.01i	4.06+19.47i	4.07+21.71i	4.35+29.43i	4.46+33.32i
permittivity	-14.99+17.18i	-16.13+19.59i	-137.53+102.11i	-240.57+131.13i	-307.82+146.44i	-362.83+158.15i	-455.11+177.17i	-847.64+256.10i	-1090.8+297.9i

Ratio of dielectric to metal

0.544	0.633	3.39	4.45	5	5.4	6	8	9
6.029	6.489	55.303	96.737	123.778	145.896	183.003	340.838	438.631

metal thickness

period (nm)	3.39	4.45	5	5.4	6	8	9
75	1.332	0.767	0.601	0.511	0.408	0.219	0.171
100	1.776	1.023	0.801	0.681	0.543	0.293	0.227
150	2.664	1.535	1.202	1.021	0.815	0.439	0.341
200	3.552	2.046	1.603	1.362	1.087	0.585	0.455
300	5.328	3.069	2.404	2.042	1.630	0.878	0.682
400	7.104	4.093	3.206	2.723	2.174	1.170	0.910
5000	88.805	51.158	40.071	34.038	27.173	14.627	11.373
600	10.657	6.139	4.809	4.085	3.261	1.755	1.365

Wavelength (in um)	0.544	0.633	3.39	4.45	5	5.4	6	8	9
TiO2 index	2.4175	2.4453	2.6269	2.5757	2.5607	2.5602	2.5822	2.9935	3.5353
permittivity	5.8444	5.9795	6.9003	6.6345	6.5573	6.5544	6.6679	8.9609	12.4981
Ni index	1.97+4.34i	2.15+4.55i	4.11+12.43i	4.08+16.04i	4.06+18.01i	4.06+19.47i	4.07+21.71i	4.35+29.43i	4.46+33.32i
permittivity	-14.99+17.18i	-16.13+19.59i	-137.53+102.11i	-240.57+131.13i	-307.82+146.44i	-362.83+158.15i	-455.11+177.17i	-847.64+256.10i	-1090.8+297.9i

Ratio of dielectric to metal									
0.544	0.633	3.39	4.45	5	5.4	6	8	9	
2.566	2.699	19.932	36.262	46.944	55.357	68.254	94.593	87.281	

	metal thickness						
period (nm)	3.39	4.45	5	5.4	6	8	9
75	3.583	2.013	1.564	1.331	1.083	0.785	0.850
100	4.777	2.684	2.086	1.774	1.444	1.046	1.133
150	7.166	4.026	3.129	2.662	2.166	1.569	1.699
200	9.555	5.367	4.172	3.549	2.888	2.092	2.265
300	14.332	8.051	6.257	5.323	4.332	3.138	3.398
400	19.110	10.735	8.343	7.098	5.776	4.184	4.531
500	23.887	13.419	10.429	8.872	7.220	5.231	5.664
600	28.665	16.102	12.515	10.646	8.664	6.277	6.796

Wavelength (in um)	0.544	0.633	3.39	4.45	5	5.4	6	8	9
ZnO index	1.7028	1.7014	1.6975	1.6974	1.6974	1.6974	1.6974	1.6974	1.6974
permittivity	2.8996	2.8947	2.8815	2.8813	2.8812	2.8812	2.8812	2.8811	2.8811
Ni index	1.97+4.34i	2.15+4.55i	4.11+12.43i	4.08+16.04i	4.06+18.01i	4.06+19.47i	4.07+21.71i	4.35+29.43i	4.46+33.32i
permittivity	-14.99+17.18i	-16.13+19.59i	-137.53+102.11i	-240.57+131.13i	-307.82+146.44i	-362.83+158.15i	-455.11+177.17i	-847.64+256.10i	-1090.8+297.9i

Ratio of dielectric to metal

0.544	0.633	3.39	4.45	5	5.4	6	8	9
5.171	5.575	47.731	83.497	106.839	125.931	157.963	294.209	378.625

metal thickness

period (nm)	3.39	4.45	5	5.4	6	8	9
75	1.539	0.888	0.695	0.591	0.472	0.254	0.198
100	2.052	1.183	0.927	0.788	0.629	0.339	0.263
150	3.078	1.775	1.391	1.182	0.944	0.508	0.395
200	4.104	2.367	1.855	1.576	1.258	0.677	0.527
300	6.156	3.550	2.782	2.363	1.887	1.016	0.790
400	8.208	4.734	3.709	3.151	2.516	1.355	1.054
500	10.260	5.917	4.637	3.939	3.145	1.694	1.317
600	12.313	7.101	5.564	4.727	3.774	2.032	1.581

		0.544	0.633	3.39	4.45	5	5.4	6	8	9
Wavelength (in um)		0.544	0.633	3.39	4.45	5	5.4	6	8	9
ZnS	index	1.8410	1.8410	1.8410	1.8410	1.8410	1.8410	1.8410	1.8410	1.8410
	permittivity	3.3892	3.3892	3.3892	3.3892	3.3892	3.3892	3.3892	3.3892	3.3892
Ni	index	1.97+4.34i	2.15+4.55i	4.11+12.43i	4.08+16.04i	4.06+18.01i	4.06+19.47i	4.07+21.71i	4.35+29.43i	4.46+33.32i
	permittivity	-14.99+17.18i	-16.13+19.59i	-137.53+102.11i	-240.57+131.13i	-307.82+146.44i	-362.83+158.15i	-455.11+177.17i	-847.64+256.10i	-1090.8+297.9i

Ratio of dielectric to metal

0.544	0.633	3.39	4.45	5	5.4	6	8	9
4.424	4.762	40.580	70.984	90.826	107.056	134.285	250.102	321.861

	metal thickness						
period (nm)	3.39	4.45	5	5.4	6	8	9
75	1.804	1.042	0.817	0.694	0.554	0.299	0.232
100	2.405	1.389	1.089	0.925	0.739	0.398	0.310
150	3.607	2.084	1.634	1.388	1.109	0.597	0.465
200	4.810	2.778	2.178	1.851	1.478	0.796	0.619
300	7.215	4.168	3.267	2.776	2.218	1.195	0.929
400	9.620	5.557	4.356	3.702	2.957	1.593	1.239
500	12.025	6.946	5.445	4.627	3.696	1.991	1.549
600	14.430	8.335	6.534	5.553	4.435	2.389	1.858

B-6: Palladium, Pd

Wavelength (in um)	0.544	0.633	3.39	4.45	5	5.4	6	8	9
Al2O3	Index	1.756	1.756	1.755	1.755	1.755	1.755	1.755	1.755	1.754
	permittivity	3.083	3.082	3.081	3.081	3.081	3.081	3.080	3.079	3.078
Pd	index	7.20E-2+5.15i	0.50+5.39i	3.99+14.60i	3.49+18.82i	3.24+21.12i	3.07+22.83i	2.85+25.46i	2.02+34.50i	1.13+39.09i
	permittivity	-26.56+0.74i	-28.89+5.44i	-197.16+116.52i	-342.02+131.71i	-435.73+136.99i	-512.15+140.47i	-640.2+145.4i	-1186.7+139.8i	-1526.9+88.4i

Ratio of dielectric to metal								
0.544	0.633	3.39	4.45	5	5.4	6	8	9
8.619	9.373	63.983	111.010	141.436	166.252	207.846	385.460	496.099

		metal thickness					
period (nm)	3.39	4.45	5	5.4	6	8	9
75	1.154	0.670	0.527	0.448	0.359	0.194	0.151
100	1.539	0.893	0.702	0.598	0.479	0.259	0.201
150	2.308	1.339	1.053	0.897	0.718	0.388	0.302
200	3.078	1.786	1.404	1.196	0.958	0.518	0.402
300	4.617	2.678	2.106	1.794	1.436	0.776	0.604
400	6.155	3.571	2.808	2.392	1.915	1.035	0.805
500	7.694	4.464	3.510	2.990	2.394	1.294	1.006
600	9.233	5.357	4.212	3.587	2.873	1.553	1.207

Wavelength (in um)	0.544	0.633	3.39	4.45	5	5.4	6	8	9
BaF2 Index	1.4759	1.4733	1.4596	1.4543	1.4510	1.4484	1.4440	1.4258	1.4144
permittivity	2.1784	2.1705	2.1303	2.1150	2.1055	2.0978	2.0852	2.0330	2.0006
Pd index	7.20E-2+5.15i	0.50+5.39i	3.99+14.60i	3.49+18.82i	3.24+21.12i	3.07+22.83i	2.85+25.46i	2.02+34.50i	1.13+39.09i
permittivity	-26.56+0.74i	-28.89+5.44i	-197.16+116.52i	-342.02+131.71i	-435.73+136.99i	-512.15+140.47i	-640.2+145.4i	-1186.7+139.8i	-1526.9+88.4i

Ratio of dielectric to metal

0.544	0.633	3.39	4.45	5	5.4	6	8	9
12.196	13.311	92.552	161.716	206.954	244.133	307.020	583.757	763.265

metal thickness

period (nm)	3.39	4.45	5	5.4	6	8	9
75	0.802	0.461	0.361	0.306	0.243	0.128	0.098
100	1.069	0.615	0.481	0.408	0.325	0.171	0.131
150	1.603	0.922	0.721	0.612	0.487	0.257	0.196
200	2.138	1.229	0.962	0.816	0.649	0.342	0.262
300	3.207	1.844	1.443	1.224	0.974	0.513	0.393
400	4.276	2.458	1.924	1.632	1.299	0.684	0.523
500	5.345	3.073	2.404	2.040	1.623	0.855	0.654
600	6.414	3.687	2.885	2.448	1.948	1.026	0.785

		0.544	0.633	3.39	4.45	5	5.4	6	8	9
Wavelength (in um)		0.544	0.633	3.39	4.45	5	5.4	6	8	9
CaF2	Index	1.4350	1.4329	1.4149	1.4052	1.3990	1.3939	1.3856	1.3498	1.3268
	permittivity	2.0592	2.0532	2.0020	1.9744	1.9571	1.9431	1.9199	1.8221	1.7603
Pd	index	7.20E-2+5.15i	0.50+5.39i	3.99+14.60i	3.49+18.82i	3.24+21.12i	3.07+22.83i	2.85+25.46i	2.02+34.50i	1.13+39.09i
	permittivity	-26.56+0.74i	-28.89+5.44i	-197.16+116.52i	-342.02+131.71i	-435.73+136.99i	-512.15+140.47i	-640.2+145.4i	-1186.7+139.8i	-1526.9+88.4i

Ratio of dielectric to metal

0.544	0.633	3.39	4.45	5	5.4	6	8	9
7.484	8.193	56.952	98.825	125.911	147.999	185.014	342.990	441.325

metal thickness

period (nm)	3.39	4.45	5	5.4	6	8	9
75	1.294	0.751	0.591	0.503	0.403	0.218	0.170
100	1.726	1.002	0.788	0.671	0.538	0.291	0.226
150	2.588	1.503	1.182	1.007	0.806	0.436	0.339
200	3.451	2.004	1.576	1.342	1.075	0.581	0.452
300	5.177	3.005	2.364	2.013	1.613	0.872	0.678
400	6.902	4.007	3.152	2.685	2.150	1.163	0.904
500	8.628	5.009	3.940	3.356	2.688	1.454	1.130
600	10.353	6.011	4.728	4.027	3.226	1.744	1.356

		Wavelength (in um)								
Wavelength (in um)		0.544	0.633	3.39	4.45	5	5.4	6	8	9
HfO2	index Cauchy	1.8842	1.8779	1.8606	1.8604	1.8603	1.8602	1.8602	1.8601	1.8601
	permittivity	3.5502	3.5264	3.4619	3.4609	3.4607	3.4605	3.4603	3.4600	3.4599
Pd	index	7.20E-2+5.15i	0.50+5.39i	3.99+14.60i	3.49+18.82i	3.24+21.12i	3.07+22.83i	2.85+25.46i	2.02+34.50i	1.13+39.09i
	permittivity	-26.56+0.74i	-28.89+5.44i	-197.16+116.52i	-342.02+131.71i	-435.73+136.99i	-512.15+140.47i	-640.2+145.4i	-1186.7+139.8i	-1526.9+88.4i

Ratio of dielectric to metal

0.544	3.39	4.45	5	5.4	6	8	9
4.099246993	5.6878	173.2681	297.6932	375.0435	436.6982	537.5194	943.7817

metal thickness

period (nm)	0.544	3.39	4.45	5	5.4	6	8	9
75	0.4304	0.2511	0.1994	0.1714	0.1393	0.0794	0.0632	0.4304
100	0.5738	0.3348	0.2659	0.2285	0.1857	0.1058	0.0843	0.5738
150	0.8607	0.5022	0.3989	0.3427	0.2785	0.1588	0.1264	0.8607
200	1.1477	0.6696	0.5319	0.4569	0.3714	0.2117	0.1686	1.1477
300	1.7215	1.0044	0.7978	0.6854	0.5571	0.3175	0.2529	1.7215
400	2.2953	1.3392	1.0637	0.9139	0.7428	0.4234	0.3371	2.2953
500	2.8691	1.6740	1.3296	1.1423	0.9285	0.5292	0.4214	2.8691
600	3.4430	2.0087	1.5956	1.3708	1.1142	0.6351	0.5057	3.4430

	Wavelength (in um)	0.544	0.633	3.39	4.45	5	5.4	6	8	9
MgF2	Index	1.3753	1.3753	1.3753	1.3753	1.3753	1.3753	1.3753	1.3753	1.3753
	permittivity	1.8914	1.8914	1.8914	1.8914	1.8914	1.8914	1.8914	1.8914	1.8914
Pd	index	7.20E-2+5.15i	0.50+5.39i	3.99+14.60i	3.49+18.82i	3.24+21.12i	3.07+22.83i	2.85+25.46i	2.02+34.50i	1.13+39.09i
	permittivity	-26.56+0.74i	-28.89+5.44i	-197.16+116.52i	-342.02+131.71i	-435.73+136.99i	-512.15+140.47i	-640.2+145.4i	-1186.7+139.8i	-1526.9+88.4i

Ratio of dielectric to metal

0.544	0.633	3.39	4.45	5	5.4	6	8	9
14.047	15.275	104.242	180.833	230.376	270.778	338.484	627.443	807.309

metal thickness

period (nm)	3.39	4.45	5	5.4	6	8	9
75	0.713	0.412	0.324	0.276	0.221	0.119	0.093
100	0.950	0.550	0.432	0.368	0.295	0.159	0.124
150	1.425	0.825	0.648	0.552	0.442	0.239	0.186
200	1.900	1.100	0.864	0.736	0.589	0.318	0.247
300	2.851	1.650	1.297	1.104	0.884	0.477	0.371
400	3.801	2.200	1.729	1.472	1.178	0.636	0.495
500	4.751	2.750	2.161	1.840	1.473	0.796	0.619
600	5.701	3.300	2.593	2.208	1.767	0.955	0.742

Wavelength (in um)		0.544	0.633	3.39	4.45	5	5.4	6	8	9
MgO	index	1.6957	1.7016	1.6822	1.6543	1.6362	1.6212	1.5958	1.4806	1.4004
	permittivity	2.8753	2.8953	2.8297	2.7368	2.6771	2.6284	2.5467	2.1921	1.9611
Pd	index	7.20E-2+5.15i	0.50+5.39i	3.99+14.60i	3.49+18.82i	3.24+21.12i	3.07+22.83i	2.85+25.46i	2.02+34.50i	1.13+39.09i
	permittivity	-26.56+0.74i	-28.89+5.44i	-197.16+116.52i	-342.02+131.71i	-435.73+136.99i	-512.15+140.47i	-640.2+145.4i	-1186.7+139.8i	-1526.9+88.4i

Ratio of dielectric to metal

0.544	0.633	3.39	4.45	5	5.4	6	8	9
9.240	9.979	69.678	124.972	162.765	194.854	251.386	541.366	778.626

metal thickness

period (nm)	3.39	4.45	5	5.4	6	8	9
75	1.061	0.595	0.458	0.383	0.297	0.138	0.096
100	1.415	0.794	0.611	0.511	0.396	0.184	0.128
150	2.122	1.191	0.916	0.766	0.594	0.277	0.192
200	2.830	1.588	1.221	1.021	0.792	0.369	0.257
300	4.245	2.381	1.832	1.532	1.189	0.553	0.385
400	5.659	3.175	2.443	2.042	1.585	0.738	0.513
500	7.074	3.969	3.053	2.553	1.981	0.922	0.641
600	8.489	4.763	3.664	3.064	2.377	1.106	0.770

	Wavelength (in um)	0.544	0.633	3.39	4.45	5	5.4	6	8	9
SF 11	index	1.5439	1.5382	1.5245	1.5243	1.5242	1.5242	1.5241	1.5241	1.5241
	permittivity	2.3836	2.3661	2.3240	2.3234	2.3232	2.3231	2.3230	2.3228	2.3228
Pd	index	7.20E-2+5.15i	0.50+5.39i	3.99+14.60i	3.49+18.82i	3.24+21.12i	3.07+22.83i	2.85+25.46i	2.02+34.50i	1.13+39.09i
	permittivity	-26.56+0.74i	-28.89+5.44i	-197.16+116.52i	-342.02+131.71i	-435.73+136.99i	-512.15+140.47i	-640.2+145.4i	-1186.7+139.8i	-1526.9+88.4i

Ratio of dielectric to metal

0.544	0.633	3.39	4.45	5	5.4	6	8	9
11.146	12.210	84.840	147.212	187.558	220.459	275.595	510.909	657.384

metal thickness

period (nm)	3.39	4.45	5	5.4	6	8	9
75	0.874	0.506	0.398	0.339	0.271	0.147	0.114
100	1.165	0.675	0.530	0.452	0.362	0.195	0.152
150	1.747	1.012	0.796	0.677	0.542	0.293	0.228
200	2.330	1.349	1.061	0.903	0.723	0.391	0.304
300	3.495	2.024	1.591	1.355	1.085	0.586	0.456
400	4.660	2.699	2.121	1.806	1.446	0.781	0.608
500	5.825	3.374	2.652	2.258	1.808	0.977	0.759
1010	11.766	6.815	5.356	4.561	3.652	1.973	1.534

		0.544	0.633	3.39	4.45	5	5.4	6	8	9
Wavelength (in um)		0.544	0.633	3.39	4.45	5	5.4	6	8	9
amorphous	index	3.8825	3.8828	3.8460	3.8199	3.8060	3.7960	3.7818	3.7444	3.7331
Si	permittivity	15.0737	15.0760	14.7921	14.5914	14.4853	14.4099	14.3022	14.0207	13.9358
Pd	index	7.20E-2+5.15i	0.50+5.39i	3.99+14.60i	3.49+18.82i	3.24+21.12i	3.07+22.83i	2.85+25.46i	2.02+34.50i	1.13+39.09i
	permittivity	-26.56+0.74i	-28.89+5.44i	-197.16+116.52i	-342.02+131.71i	-435.73+136.99i	-512.15+140.47i	-640.2+145.4i	-1186.7+139.8i	-1526.9+88.4i

Ratio of dielectric to metal

0.544	0.633	3.39	4.45	5	5.4	6	8	9
1.763	1.916	13.329	23.440	30.081	35.542	44.763	84.643	109.570

metal thickness

period (nm)	3.39	4.45	5	5.4	6	8	9
75	5.234	3.069	2.413	2.052	1.639	0.876	0.678
100	6.979	4.092	3.217	2.737	2.185	1.168	0.904
150	10.468	6.137	4.826	4.105	3.278	1.751	1.357
200	13.958	8.183	6.435	5.473	4.370	2.335	1.809
300	20.937	12.275	9.652	8.210	6.555	3.503	2.713
400	27.915	16.366	12.869	10.946	8.741	4.671	3.618
500	34.894	20.458	16.087	13.683	10.926	5.838	4.522
600	41.873	24.549	19.304	16.420	13.111	7.006	5.426

		0.544	0.633	3.39	4.45	5	5.4	6	8	9
Wavelength (in um)		0.544	0.633	3.39	4.45	5	5.4	6	8	9
SiC	index	2.5872	2.5868	2.5382	2.4960	2.5868	2.4409	2.3944	2.1153	1.8083
	permittivity	6.6938	6.6917	6.4426	6.2300	6.0837	5.9581	5.7331	4.4747	3.2700
Pd	index	7.20E-2+5.15i	0.50+5.39i	3.99+14.60i	3.49+18.82i	3.24+21.12i	3.07+22.83i	2.85+25.46i	2.02+34.50i	1.13+39.09i
	permittivity	-26.56+0.74i	-28.89+5.44i	-197.16+116.52i	-342.02+131.71i	-435.73+136.99i	-512.15+140.47i	-640.2+145.4i	-1186.7+139.8i	-1526.9+88.4i
Ratio of dielectric to metal										
			3.39	4.45	5	5.4	6	8	9	
			30.603	54.900	71.624	85.959	111.669	265.214	466.952	
					metal thickness					
	period (nm)		3.39	4.45	5	5.4	6	8	9	
	75		2.373	1.342	1.033	0.862	0.666	0.282	0.160	
	100		3.164	1.789	1.377	1.150	0.888	0.376	0.214	
	150		4.746	2.683	2.065	1.725	1.331	0.563	0.321	
	200		6.329	3.578	2.754	2.300	1.775	0.751	0.427	
	300		9.493	5.367	4.131	3.450	2.663	1.127	0.641	
	400		12.657	7.156	5.508	4.600	3.550	1.503	0.855	
	500		15.821	8.945	6.885	5.750	4.438	1.878	1.068	
	600		18.986	10.733	8.262	6.900	5.325	2.254	1.282	
	600		18.986	10.733	8.262	6.900	5.325	2.254	1.282	

Wavelength (in um)	0.544	0.633	3.39	4.45	5	5.4	6	8	9
TiO2 index	2.4175	2.4453	2.6269	2.5757	2.5607	2.5602	2.5822	2.9935	3.5353
permittivity	5.8444	5.9795	6.9003	6.6345	6.5573	6.5544	6.6679	8.9609	12.4981
Pd index	7.20E-2+5.15i	0.50+5.39i	3.99+14.60i	3.49+18.82i	3.24+21.12i	3.07+22.83i	2.85+25.46i	2.02+34.50i	1.13+39.09i
permittivity	-26.56+0.74i	-28.89+5.44i	-197.16+116.52i	-342.02+131.71i	-435.73+136.99i	-512.15+140.47i	-640.2+145.4i	-1186.7+139.8i	-1526.9+88.4i

Ratio of dielectric to metal

0.544	0.633	3.39	4.45	5	5.4	6	8	9
4.546	4.832	28.573	51.553	66.450	78.139	96.013	132.436	122.175

metal thickness

period (nm)	3.39	4.45	5	5.4	6	8	9
75	2.536	1.427	1.112	0.948	0.773	0.562	0.609
100	3.381	1.903	1.483	1.264	1.031	0.749	0.812
150	5.072	2.854	2.224	1.895	1.546	1.124	1.218
200	6.763	3.806	2.965	2.527	2.062	1.499	1.624
300	10.144	5.709	4.448	3.791	3.092	2.248	2.436
400	13.526	7.611	5.930	5.054	4.123	2.998	3.247
500	16.907	9.514	7.413	6.318	5.154	3.747	4.059
600	20.289	11.417	8.895	7.582	6.185	4.497	4.871

Wavelength (in um)		0.544	0.633	3.39	4.45	5	5.4	6	8	9
ZnO	index	1.7028	1.7014	1.6975	1.6974	1.6974	1.6974	1.6974	1.6974	1.6974
	permittivity	2.8996	2.8947	2.8815	2.8813	2.8812	2.8812	2.8812	2.8811	2.8811
Pd	index	7.20E-2+5.15i	0.50+5.39i	3.99+14.60i	3.49+18.82i	3.24+21.12i	3.07+22.83i	2.85+25.46i	2.02+34.50i	1.13+39.09i
	permittivity	-26.56+0.74i	-28.89+5.44i	-197.16+116.52i	-342.02+131.71i	-435.73+136.99i	-512.15+140.47i	-640.2+145.4i	-1186.7+139.8i	-1526.9+88.4i

Ratio of dielectric to metal

0.544	0.633	3.39	4.45	5	5.4	6	8	9
9.163	9.981	68.425	118.707	151.233	177.757	222.207	411.911	529.995

metal thickness

period (nm)	3.39	4.45	5	5.4	6	8	9
75	1.080	0.627	0.493	0.420	0.336	0.182	0.141
100	1.440	0.835	0.657	0.559	0.448	0.242	0.188
150	2.161	1.253	0.985	0.839	0.672	0.363	0.282
200	2.881	1.671	1.314	1.119	0.896	0.484	0.377
300	4.321	2.506	1.971	1.678	1.344	0.727	0.565
400	5.762	3.341	2.628	2.238	1.792	0.969	0.753
500	7.202	4.177	3.284	2.797	2.240	1.211	0.942
600	8.642	5.012	3.941	3.357	2.688	1.453	1.130

Wavelength (in um)	0.544	0.633	3.39	4.45	5	5.4	6	8	9
ZnS index	1.8410	1.8410	1.8410	1.8410	1.8410	1.8410	1.8410	1.8410	1.8410
permittivity	3.3892	3.3892	3.3892	3.3892	3.3892	3.3892	3.3892	3.3892	3.3892
Pd index	7.20E-2+5.15i	0.50+5.39i	3.99+14.60i	3.49+18.82i	3.24+21.12i	3.07+22.83i	2.85+25.46i	2.02+34.50i	1.13+39.09i
permittivity	-26.56+0.74i	-28.89+5.44i	-197.16+116.52i	-342.02+131.71i	-435.73+136.99i	-512.15+140.47i	-640.2+145.4i	-1186.7+139.8i	-1526.9+88.4i

Ratio of dielectric to metal

0.544	0.633	3.39	4.45	5	5.4	6	8	9
7.839	8.525	58.174	100.917	128.566	151.113	188.898	350.159	450.538

metal thickness

period (nm)	3.39	4.45	5	5.4	6	8	9
75	1.267	0.736	0.579	0.493	0.395	0.214	0.166
100	1.690	0.981	0.772	0.657	0.527	0.285	0.221
150	2.535	1.472	1.158	0.986	0.790	0.427	0.332
200	3.380	1.962	1.544	1.315	1.053	0.570	0.443
300	5.070	2.944	2.315	1.972	1.580	0.854	0.664
400	6.760	3.925	3.087	2.630	2.106	1.139	0.886
500	8.450	4.906	3.859	3.287	2.633	1.424	1.107
600	10.140	5.887	4.631	3.944	3.160	1.709	1.329

B-6: Titanium, Ti

Wavelength (in um)		0.544	0.633	3.39	4.45	5	5.4	6	8	9
Al2O3	Index	1.756	1.756	1.755	1.755	1.755	1.755	1.755	1.755	1.754
	permittivity	3.083	3.082	3.081	3.081	3.081	3.081	3.080	3.079	3.078
Ti	index	5.41+3.07i	5.35+3.12i	4.54+6.28i	4.72+8.11i	4.90+9.14i	5.07+9.92i	5.35+11.11i	6.55+15.05i	7.23+16.87i
	permittivity	19.90+33.27i	18.90+33.41i	-18.83+57.03i	-43.52+76.74i	-59.61+89.81i	-72.78+100.6i	-94.79+118.9i	-183.73+197.5i	-232.34+244.1i

Ratio of dielectric to metal							
	3.39	4.45	5	5.4	6	8	9
	6.114	14.125	19.351	23.627	30.774	59.678	75.488

metal thickness							
period (nm)	3.39	4.45	5	5.4	6	8	9
75	10.543	4.959	3.685	3.045	2.360	1.236	0.981
100	14.057	6.612	4.914	4.061	3.147	1.648	1.307
150	21.086	9.917	7.371	6.091	4.721	2.472	1.961
200	28.114	13.223	9.828	8.121	6.294	3.296	2.615
300	42.171	19.835	14.742	12.182	9.442	4.944	3.922
400	56.228	26.446	19.655	16.242	12.589	6.592	5.230
500	70.285	33.058	24.569	20.303	15.736	8.240	6.537
600	84.342	39.669	29.483	24.363	18.883	9.888	7.844

Wavelength (in um)		0.544	0.633	3.39	4.45	5	5.4	6	8	9
BaF2	Index	1.4759	1.4733	1.4596	1.4543	1.4510	1.4484	1.4440	1.4258	1.4144
	permittivity	2.1784	2.1705	2.1303	2.1150	2.1055	2.0978	2.0852	2.0330	2.0006
Ti	index	5.41+3.07i	5.35+3.12i	4.54+6.28i	4.72+8.11i	4.90+9.14i	5.07+9.92i	5.35+11.11i	6.55+15.05i	7.23+16.87i
	permittivity	19.90+33.27i	18.90+33.41i	-18.83+57.03i	-43.52+76.74i	-59.61+89.81i	-72.78+100.6i	-94.79+118.9i	-183.73+197.5i	-232.34+244.1i

Ratio of dielectric to metal

	3.39	4.45	5	5.4	6	8	9
	8.844	20.577	28.315	34.695	45.458	90.379	116.140

metal thickness

period (nm)	3.39	4.45	5	5.4	6	8	9
75	7.619	3.476	2.558	2.101	1.614	0.821	0.640
100	10.159	4.635	3.411	2.801	2.152	1.094	0.854
150	15.238	6.952	5.117	4.202	3.229	1.642	1.281
200	20.317	9.269	6.823	5.603	4.305	2.189	1.707
300	30.476	13.904	10.234	8.404	6.457	3.283	2.561
400	40.635	18.538	13.645	11.206	8.610	4.377	3.415
500	50.794	23.173	17.056	14.007	10.762	5.472	4.268
600	60.952	27.807	20.468	16.809	12.915	6.566	5.122

	Wavelength (in um)	0.544	0.633	3.39	4.45	5	5.4	6	8	9
CaF2	Index	1.4350	1.4329	1.4149	1.4052	1.3990	1.3939	1.3856	1.3498	1.3268
	permittivity	2.0592	2.0532	2.0020	1.9744	1.9571	1.9431	1.9199	1.8221	1.7603
Ti	index	5.41+3.07i	5.35+3.12i	4.54+6.28i	4.72+8.11i	4.90+9.14i	5.07+9.92i	5.35+11.11i	6.55+15.05i	7.23+16.87i
	permittivity	19.90+33.27i	18.90+33.41i	-18.83+57.03i	-43.52+76.74i	-59.61+89.81i	-72.78+100.6i	-94.79+118.9i	-183.73+197.5i	-232.34+244.1i

	Ratio of dielectric to metal								
		3.39	4.45	5	5.4	6	8	9
		9.410	22.042	30.461	37.458	49.373	100.840	131.990

				metal thickness				
	period (nm)	3.39	4.45	5	5.4	6	8	9
	75	7.204	3.255	2.384	1.950	1.489	0.736	0.564
	100	9.606	4.340	3.179	2.600	1.985	0.982	0.752
	150	14.409	6.510	4.768	3.900	2.978	1.473	1.128
	200	19.212	8.680	6.357	5.200	3.970	1.964	1.504
	300	28.817	13.020	9.536	7.801	5.956	2.946	2.256
	400	38.423	17.360	12.714	10.401	7.941	3.928	3.008
	500	48.029	21.700	15.893	13.001	9.926	4.910	3.760
	600	57.635	26.040	19.071	15.601	11.911	5.892	4.512

Wavelength (in um)	0.544	0.633	3.39	4.45	5	5.4	6	8	9
HfO2 index Cauchy	1.8842	1.8779	1.8606	1.8604	1.8603	1.8602	1.8602	1.8601	1.8601
permittivity	3.5502	3.5264	3.4619	3.4609	3.4607	3.4605	3.4603	3.4600	3.4599
Ti index	5.41+3.07i	5.35+3.12i	4.54+6.28i	4.72+8.11i	4.90+9.14i	5.07+9.92i	5.35+11.11i	6.55+15.05i	7.23+16.87i
permittivity	19.90+33.27i	18.90+33.41i	-18.83+57.03i	-43.52+76.74i	-59.61+89.81i	-72.78+100.6i	-94.79+118.9i	-183.73+197.5i	-232.34+244.1i

Ratio of dielectric to metal

	3.39	4.45	5	5.4	6	8	9
	5.442	12.575	17.227	21.033	27.393	53.103	67.153

metal thickness

period (nm)	3.39	4.45	5	5.4	6	8	9
75	11.642	5.525	4.115	3.404	2.641	1.386	1.100
100	15.523	7.367	5.486	4.539	3.522	1.848	1.467
150	23.285	11.050	8.230	6.808	5.283	2.772	2.201
200	31.046	14.733	10.973	9.077	7.044	3.697	2.935
300	46.569	22.100	16.459	13.616	10.566	5.545	4.402
400	62.092	29.467	21.946	18.155	14.088	7.393	5.869
500	77.615	36.833	27.432	22.693	17.610	9.242	7.336
600	93.139	44.200	32.919	27.232	21.132	11.090	8.804

Wavelength (in um)		0.544	0.633	3.39	4.45	5	5.4	6	8	9
MgF2	Index	1.3753	1.3753	1.3753	1.3753	1.3753	1.3753	1.3753	1.3753	1.3753
	permittivity	1.8914	1.8914	1.8914	1.8914	1.8914	1.8914	1.8914	1.8914	1.8914
Ti	index	5.41+3.07i	5.35+3.12i	4.54+6.28i	4.72+8.11i	4.90+9.14i	5.07+9.92i	5.35+11.11i	6.55+15.05i	7.23+16.87i
	permittivity	19.90+33.27i	18.90+33.41i	-18.83+57.03i	-43.52+76.74i	-59.61+89.81i	-72.78+100.6i	-94.79+118.9i	-183.73+197.5i	-232.34+244.1i

Ratio of dielectric to metal							
3.39	4.45	5	5.4	6	8	9	
9.961	23.009	31.519	38.482	50.116	97.143	122.842	

metal thickness

period (nm)	3.39	4.45	5	5.4	6	8	9
75	6.843	3.124	2.306	1.900	1.467	0.764	0.606
100	9.123	4.165	3.075	2.533	1.956	1.019	0.807
150	13.685	6.248	4.613	3.799	2.934	1.528	1.211
200	18.247	8.330	6.150	5.066	3.913	2.038	1.615
300	27.370	**12.495**	9.225	7.598	5.869	3.057	2.422
400	36.494	16.660	12.300	10.131	7.825	4.076	3.230
500	45.617	20.825	15.376	12.664	9.782	5.095	4.037
600	54.741	24.990	18.451	15.197	11.738	6.114	4.845

Wavelength (in um)	0.544	0.633	3.39	4.45	5	5.4	6	8	9
MgO index	1.6957	1.7016	1.6822	1.6543	1.6362	1.6212	1.5958	1.4806	1.4004
permittivity	2.8753	2.8953	2.8297	2.7368	2.6771	2.6284	2.5467	2.1921	1.9611
Ti index	5.41+3.07i	5.35+3.12i	4.54+6.28i	4.72+8.11i	4.90+9.14i	5.07+9.92i	5.35+11.11i	6.55+15.05i	7.23+16.87i
permittivity	19.90+33.27i	18.90+33.41i	-18.83+57.03i	-43.52+76.74i	-59.61+89.81i	-72.78+100.6i	-94.79+118.9i	-183.73+197.5i	-232.34+244.1i

Ratio of dielectric to metal

	3.39	4.45	5	5.4	6	8	9
	6.658	15.902	22.269	27.692	37.220	83.816	118.478

metal thickness

period (nm)	3.39	4.45	5	5.4	6	8	9
75	9.794	4.437	3.223	2.614	1.962	0.884	0.628
100	13.058	5.917	4.298	3.485	2.616	1.179	0.837
150	19.587	8.875	6.446	5.228	3.925	1.769	1.255
200	26.116	11.833	8.595	6.971	5.233	2.358	1.674
300	39.175	17.750	12.893	10.456	7.849	3.537	2.511
400	52.233	23.666	17.190	13.941	10.466	4.716	3.348
500	65.291	29.583	21.488	17.427	13.082	5.895	4.185
600	78.349	35.499	25.786	20.912	15.698	7.074	5.022

Wavelength (in um)	0.544	0.633	3.39	4.45	5	5.4	6	8	9
SF 11	index	1.5439	1.5382	1.5245	1.5243	1.5242	1.5242	1.5241	1.5241	1.5241
	permittivity	2.3836	2.3661	2.3240	2.3234	2.3232	2.3231	2.3230	2.3228	2.3228
Ti	index	5.41+3.07i	5.35+3.12i	4.54+6.28i	4.72+8.11i	4.90+9.14i	5.07+9.92i	5.35+11.11i	6.55+15.05i	7.23+16.87i
	permittivity	19.90+33.27i	18.90+33.41i	-18.83+57.03i	-43.52+76.74i	-59.61+89.81i	-72.78+100.6i	-94.79+118.9i	-183.73+197.5i	-232.34+244.1i

Ratio of dielectric to metal

	3.39	4.45	5	5.4	6	8	9
	8.107	18.731	25.661	31.331	40.805	79.101	100.029

metal thickness

period (nm)	3.39	4.45	5	5.4	6	8	9
75	8.236	3.801	2.813	2.320	1.794	0.936	0.742
100	10.981	5.068	3.751	3.093	2.392	1.248	0.990
150	16.471	7.602	5.626	4.640	3.588	1.873	1.485
200	21.962	10.136	7.502	6.186	4.784	2.497	1.980
300	32.942	15.204	11.252	9.279	7.176	3.745	2.969
400	43.923	20.272	15.003	12.372	9.568	4.994	3.959
500	54.904	25.340	18.754	15.465	11.960	6.242	4.949
1000	109.808	50.680	37.508	30.930	23.921	12.484	9.898

Wavelength (in um)		0.544	0.633	3.39	4.45	5	5.4	6	8	9
amorphous	index	3.8825	3.8828	3.8460	3.8199	3.8060	3.7960	3.7818	3.7444	3.7331
Si	permittivity	15.0737	15.0760	14.7921	14.5914	14.4853	14.4099	14.3022	14.0207	13.9358
Ti	index	5.41+3.07i	5.35+3.12i	4.54+6.28i	4.72+8.11i	4.90+9.14i	5.07+9.92i	5.35+11.11i	6.55+15.05i	7.23+16.87i
	permittivity	19.90+33.27i	18.90+33.41i	-18.83+57.03i	-43.52+76.74i	-59.61+89.81i	-72.78+100.6i	-94.79+118.9i	-183.73+197.5i	-232.34+244.1i

Ratio of dielectric to metal

3.39	4.45	5	5.4	6	8	9
1.274	2.983	4.116	5.051	6.628	13.105	16.673

metal thickness

period (nm)	3.39	4.45	5	5.4	6	8	9
75	32.987	18.832	14.661	12.395	9.833	5.317	4.244
100	43.982	25.109	19.548	16.526	13.110	7.090	5.659
150	65.973	37.664	29.322	24.789	19.665	10.635	8.488
200	87.965	50.218	39.096	33.052	26.220	14.180	11.317
300	131.947	75.328	58.644	49.578	39.330	21.269	16.976
400	175.929	100.437	78.192	66.104	52.440	28.359	22.634
500	219.911	125.546	97.740	82.630	65.551	35.449	28.293
600	263.894	150.655	117.288	99.156	78.661	42.539	33.951

Wavelength (in um)	0.544	0.633	3.39	4.45	5	5.4	6	8	9
SiC index	2.5872	2.5868	2.5382	2.4960	2.5868	2.4409	2.3944	2.1153	1.8083
permittivity	6.6938	6.6917	6.4426	6.2300	6.0837	5.9581	5.7331	4.4747	3.2700
Ti index	5.41+3.07i	5.35+3.12i	4.54+6.28i	4.72+8.11i	4.90+9.14i	5.07+9.92i	5.35+11.11i	6.55+15.05i	7.23+16.87i
permittivity	19.90+33.27i	18.90+33.41i	-18.83+57.03i	-43.52+76.74i	-59.61+89.81i	-72.78+100.6i	-94.79+118.9i	-183.73+197.5i	-232.34+244.1i

Ratio of dielectric to metal

	3.39	4.45	5	5.4	6	8	9
	2.924	6.986	9.799	12.216	16.534	41.061	71.053

metal thickness

period (nm)	3.39	4.45	5	5.4	6	8	9
75	19.112	9.392	6.945	5.675	4.277	1.783	1.041
100	25.483	12.523	9.260	7.566	5.703	2.377	1.388
150	38.224	18.784	13.890	11.350	8.555	3.566	2.082
200	50.965	25.045	18.520	15.133	11.407	4.755	2.776
300	76.448	37.568	27.780	22.699	17.110	7.132	4.164
400	101.930	50.090	37.040	30.266	22.813	9.510	5.551
500	127.413	62.613	46.299	37.832	28.516	11.887	6.939
600	152.896	75.136	55.559	45.399	34.220	14.265	8.327
600	152.896	75.136	55.559	45.399	34.220	14.265	8.327

Wavelength (in um)		0.544	0.633	3.39	4.45	5	5.4	6	8	9
TiO2	index	2.4175	2.4453	2.6269	2.5757	2.5607	2.5602	2.5822	2.9935	3.5353
	permittivity	5.8444	5.9795	6.9003	6.6345	6.5573	6.5544	6.6679	8.9609	12.4981
Ti	index	5.41+3.07i	5.35+3.12i	4.54+6.28i	4.72+8.11i	4.90+9.14i	5.07+9.92i	5.35+11.11i	6.55+15.05i	7.23+16.87i
	permittivity	19.90+33.27i	18.90+33.41i	-18.83+57.03i	-43.52+76.74i	-59.61+89.81i	-72.78+100.6i	-94.79+118.9i	-183.73+197.5i	-232.34+244.1i

Ratio of dielectric to metal

3.39	4.45	5	5.4	6	8	9
2.730	6.560	9.091	11.105	14.216	20.504	18.590

metal thickness

period (nm)	3.39	4.45	5	5.4	6	8	9
75	20.106	9.921	7.432	6.196	4.929	3.488	3.828
100	26.808	13.228	9.909	8.261	6.572	4.650	5.105
150	40.212	19.842	14.864	12.392	9.858	6.975	7.657
200	53.615	26.456	19.819	16.522	13.144	9.301	10.209
300	80.423	39.684	29.728	24.784	19.716	13.951	15.314
400	107.231	52.912	39.638	33.045	26.288	18.601	20.418
500	134.039	66.140	49.547	41.306	32.860	23.251	25.523
600	160.846	79.368	59.456	49.567	39.433	27.902	30.627

Wavelength (in um)	0.544	0.633	3.39	4.45	5	5.4	6	8	9
ZnO index	1.7028	1.7014	1.6975	1.6974	1.6974	1.6974	1.6974	1.6974	1.6974
permittivity	2.8996	2.8947	2.8815	2.8813	2.8812	2.8812	2.8812	2.8811	2.8811
Ti index	5.41+3.07i	5.35+3.12i	4.54+6.28i	4.72+8.11i	4.90+9.14i	5.07+9.92i	5.35+11.11i	6.55+15.05i	7.23+16.87i
permittivity	19.90+33.27i	18.90+33.41i	-18.83+57.03i	-43.52+76.74i	-59.61+89.81i	-72.78+100.6i	-94.79+118.9i	-183.73+197.5i	-232.34+244.1i

Ratio of dielectric to metal								
	3.39	4.45	5	5.4	6	8	9	
	6.538	15.105	20.691	25.262	32.900	63.774	80.646	

	metal thickness							
period (nm)	3.39	4.45	5	5.4	6	8	9	
75	9.949	4.657	3.458	2.856	2.212	1.158	0.919	
100	13.266	6.209	4.610	3.808	2.950	1.544	1.225	
150	19.899	9.314	6.915	5.712	4.425	2.316	1.837	
200	26.531	12.419	9.220	7.616	5.900	3.088	2.450	
300	39.797	18.628	13.831	11.423	8.850	4.632	3.674	
400	53.063	24.838	18.441	15.231	11.799	6.175	4.899	
500	66.328	31.047	23.051	19.039	14.749	7.719	6.124	
600	79.594	37.257	27.661	22.847	17.699	9.263	7.349	

Wavelength (in um)		0.544	0.633	3.39	4.45	5	5.4	6	8	9
ZnS	index	1.8410	1.8410	1.8410	1.8410	1.8410	1.8410	1.8410	1.8410	1.8410
	permittivity	3.3892	3.3892	3.3892	3.3892	3.3892	3.3892	3.3892	3.3892	3.3892
Ti	index	5.41+3.07i	5.35+3.12i	4.54+6.28i	4.72+8.11i	4.90+9.14i	5.07+9.92i	5.35+11.11i	6.55+15.05i	7.23+16.87i
	permittivity	19.90+33.27i	18.90+33.41i	-18.83+57.03i	-43.52+76.74i	-59.61+89.81i	-72.78+100.6i	-94.79+118.9i	-183.73+197.5i	-232.34+244.1i

Ratio of dielectric to metal

	3.39	4.45	5	5.4	6	8	9
	5.559	12.841	17.590	21.476	27.968	54.213	68.555

metal thickness

period (nm)	3.39	4.45	5	5.4	6	8	9
75	11.435	5.419	4.034	3.337	2.589	1.358	1.078
100	15.247	7.225	5.379	4.449	3.452	1.811	1.438
150	22.870	10.837	8.069	6.674	5.178	2.717	2.157
200	30.493	14.450	10.759	8.899	6.904	3.622	2.875
300	45.740	21.675	16.138	13.348	10.356	5.434	4.313
400	60.987	28.900	21.517	17.797	13.808	7.245	5.751
500	76.234	36.125	26.896	22.246	17.260	9.056	7.189
600	91.480	43.350	32.276	26.696	20.712	10.867	8.626

B-7: Tungsten, W

Wavelength (in um)	0.544	0.633	3.39	4.45	5	5.4	6	8	9
Al2O3 Index	1.756	1.756	1.755	1.755	1.755	1.755	1.755	1.755	1.754
permittivity	3.083	3.082	3.081	3.081	3.081	3.081	3.080	3.079	3.078
W index			1.19+16.24i	2.03+21.22i	2.54+23.77i	2.96+25.60i	3.62+28.32	6.24+ 37.10i	7.76+41.31i
permittivity			-262.53+38.67i	-446.29+86.15i	-558.44+121.07i	-646.71+151.38	-789.04+205.16i	-1337.7+463.54i	-1646.5+641.7i

Ratio of dielectric to metal

	3.39	4.45	5	5.4	6	8	9
	85.198	144.851	181.266	209.932	256.164	434.501	534.936

metal thickness

period (nm)	3.39	4.45	5	5.4	6	8	9
75	0.870	0.514	0.411	0.356	0.292	0.172	0.140
100	1.160	0.686	0.549	0.474	0.389	0.230	0.187
150	1.740	1.028	0.823	0.711	0.583	0.344	0.280
200	2.320	1.371	1.097	0.948	0.778	0.459	0.373
300	3.480	2.057	1.646	1.422	1.167	0.689	0.560
400	4.640	2.743	2.195	1.896	1.555	0.918	0.746
500	5.801	3.428	2.743	2.370	1.944	1.148	0.933
600	6.961	4.114	3.292	2.845	2.333	1.378	1.120

Wavelength (in um)	0.544	0.633	3.39	4.45	5	5.4	6	8	9
BaF2 Index	1.4759	1.4733	1.4596	1.4543	1.4510	1.4484	1.4440	1.4258	1.4144
permittivity	2.1784	2.1705	2.1303	2.1150	2.1055	2.0978	2.0852	2.0330	2.0006
W index			$1.19+16.24i$	$2.03+21.22i$	$2.54+23.77i$	$2.96+25.60i$	$3.62+28.32$	$6.24+37.10i$	$7.76+41.31i$
permittivity			$-262.53+38.67i$	$-446.29+86.15i$	$-558.44+121.07i$	$-646.71+151.38$	$-789.04+205.16i$	$-1337.7+463.54i$	$-1646.5+641.7i$

Ratio of dielectric to metal								
	3.39	4.45	5	5.4	6	8	9
	123.240	211.014	265.234	308.275	378.394	658.027	823.018

	metal thickness						
period (nm)	3.39	4.45	5	5.4	6	8	9
75	0.604	0.354	0.282	0.243	0.198	0.114	0.091
100	0.805	0.472	0.376	0.323	0.264	0.152	0.121
150	1.207	0.707	0.563	0.485	0.395	0.228	0.182
200	1.610	0.943	0.751	0.647	0.527	0.303	0.243
300	2.415	1.415	1.127	0.970	0.791	0.455	0.364
400	3.220	1.887	1.502	1.293	1.054	0.607	0.485
500	4.024	2.358	1.878	1.617	1.318	0.759	0.607
600	4.829	2.830	2.254	1.940	1.581	0.910	0.728

Wavelength (in um)	0.544	0.633	3.39	4.45	5	5.4	6	8	9
CaF2	Index	1.4350	1.4329	1.4149	1.4052	1.3990	1.3939	1.3856	1.3498	1.3268
	permittivity	2.0592	2.0532	2.0020	1.9744	1.9571	1.9431	1.9199	1.8221	1.7603
W	index			1.19+16.24i	2.03+21.22i	2.54+23.77i	2.96+25.60i	3.62+28.32	6.24+ 37.10i	7.76+41.31i
	permittivity			-262.53+38.67i	-446.29+86.15i	-558.44+121.07i	-646.71+151.38	-789.04+205.16i	-1337.7+463.54i	-1646.5+641.7i
	Ratio of dielectric to metal									
			3.39	4.45	5	5.4	6	8	9	
			131.136	226.035	285.344	332.826	410.985	734.187	935.336	
					metal thickness					
		period (nm)	3.39	4.45	5	5.4	6	8	9	
		75	0.568	0.330	0.262	0.225	0.182	0.102	0.080	
		100	0.757	0.440	0.349	0.300	0.243	0.136	0.107	
		150	1.135	0.661	0.524	0.449	0.364	0.204	0.160	
		200	1.514	0.881	0.698	0.599	0.485	0.272	0.214	
		300	2.270	1.321	1.048	0.899	0.728	0.408	0.320	
		400	3.027	1.762	1.397	1.198	0.971	0.544	0.427	
		500	3.784	2.202	1.746	1.498	1.214	0.680	0.534	
		600	4.541	2.643	2.095	1.797	1.456	0.816	0.641	

	Wavelength (in um)	0.544	0.633	3.39	4.45	5	5.4	6	8	9
HfO2	index Cauchy	1.8842	1.8779	1.8606	1.8604	1.8603	1.8602	1.8602	1.8601	1.8601
	permittivity	3.5502	3.5264	3.4619	3.4609	3.4607	3.4605	3.4603	3.4600	3.4599
W	index			1.19+16.24i	2.03+21.22i	2.54+23.77i	2.96+25.60i	3.62+28.32	6.24+ 37.10i	7.76+41.31i
	permittivity			-262.53+38.67i	-446.29+86.15i	-558.44+121.07i	-646.71+151.38	-789.04+205.16i	-1337.7+463.54i	-1646.5+641.7i
Ratio of dielectric to metal										
			3.39	4.45	5	5.4	6	8	9	
			75.836	128.952	161.368	186.883	228.025	386.628	475.874	
					metal thickness					
		period (nm)	3.39	4.45	5	5.4	6	8	9	
		75	0.976	0.577	0.462	0.399	0.327	0.193	0.157	
		100	1.301	0.770	0.616	0.532	0.437	0.258	0.210	
		150	1.952	1.154	0.924	0.798	0.655	0.387	0.315	
		200	2.603	1.539	1.232	1.064	0.873	0.516	0.419	
		300	3.904	2.309	1.848	1.597	1.310	0.774	0.629	
		400	5.206	3.078	2.464	2.129	1.747	1.032	0.839	
		500	6.507	3.848	3.079	2.661	2.183	1.290	1.048	
		600	7.809	4.617	3.695	3.193	2.620	1.548	1.258	
		600	7.809	4.617	3.695	3.193	2.620	1.548	1.258	

Wavelength (in um)		0.544	0.633	3.39	4.45	5	5.4	6	8	9
MgF2	Index	1.3753	1.3753	1.3753	1.3753	1.3753	1.3753	1.3753	1.3753	1.3753
	permittivity	1.8914	1.8914	1.8914	1.8914	1.8914	1.8914	1.8914	1.8914	1.8914
W	index			1.19+16.24i	2.03+21.22i	2.54+23.77i	2.96+25.60i	3.62+28.32	6.24+ 37.10i	7.76+41.31i
	permittivity			-262.53+38.67i	-446.29+86.15i	-558.44+121.07i	-646.71+151.38	-789.04+205.16i	-1337.7+463.54i	-1646.5+641.7i

Ratio of dielectric to metal

	3.39	4.45	5	5.4	6	8	9
	138.805	235.959	295.252	341.920	417.173	707.271	870.510

metal thickness

period (nm)	3.39	4.45	5	5.4	6	8	9
75	0.536	0.317	0.253	0.219	0.179	0.106	0.086
100	0.715	0.422	0.338	0.292	0.239	0.141	0.115
150	1.073	0.633	0.506	0.437	0.359	0.212	0.172
200	1.431	0.844	0.675	0.583	0.478	0.282	0.229
300	2.146	1.266	1.013	0.875	0.717	0.424	0.344
400	2.861	1.688	1.350	1.166	0.957	0.565	0.459
500	3.576	2.110	1.688	1.458	1.196	0.706	0.574
600	4.292	2.532	2.025	1.750	1.435	0.847	0.688

Wavelength (in um)	0.544	0.633	3.39	4.45	5	5.4	6	8	9
MgO index	1.6957	1.7016	1.6822	1.6543	1.6362	1.6212	1.5958	1.4806	1.4004
permittivity	2.8753	2.8953	2.8297	2.7368	2.6771	2.6284	2.5467	2.1921	1.9611
W index			1.19+16.24i	2.03+21.22i	2.54+23.77i	2.96+25.60i	3.62+28.32	6.24+ 37.10i	7.76+41.31i
permittivity			-262.53+38.67i	-446.29+86.15i	-558.44+121.07i	-646.71+151.38	-789.04+205.16i	-1337.7+463.54i	-1646.5+641.7i

Ratio of dielectric to metal

3.39	4.45	5	5.4	6	8	9
92.781	163.069	208.601	246.048	309.826	610.243	839.581

metal thickness

period (nm)	3.39	4.45	5	5.4	6	8	9
75	0.800	0.457	0.358	0.304	0.241	0.123	0.089
100	1.066	0.609	0.477	0.405	0.322	0.164	0.119
150	1.599	0.914	0.716	0.607	0.483	0.245	0.178
200	2.133	1.219	0.954	0.810	0.643	0.327	0.238
300	3.199	1.828	1.431	1.214	0.965	0.491	0.357
400	4.265	2.438	1.908	1.619	1.287	0.654	0.476
500	5.332	3.047	2.385	2.024	1.609	0.818	0.595
600	6.398	3.657	2.863	2.429	1.930	0.982	0.714

Wavelength (in um)		0.544	0.633	3.39	4.45	5	5.4	6	8	9
SF 11	index	1.5439	1.5382	1.5245	1.5243	1.5242	1.5242	1.5241	1.5241	1.5241
	permittivity	2.3836	2.3661	2.3240	2.3234	2.3232	2.3231	2.3230	2.3228	2.3228
W	index			1.19+16.24i	2.03+21.22i	2.54+23.77i	2.96+25.60i	3.62+28.32	6.24+ 37.10i	7.76+41.31i
	permittivity			-262.53+38.67i	-446.29+86.15i	-558.44+121.07i	-646.71+151.38	-789.04+205.16i	-1337.7+463.54i	-1646.5+641.7i

Ratio of dielectric to metal

	3.39	4.45	5	5.4	6	8	9
	112.970	192.089	240.375	278.381	339.664	575.911	708.848

metal thickness

period (nm)	3.39	4.45	5	5.4	6	8	9
75	0.658	0.388	0.311	0.268	0.220	0.130	0.106
100	0.877	0.518	0.414	0.358	0.294	0.173	0.141
150	1.316	0.777	0.621	0.537	0.440	0.260	0.211
200	1.755	1.036	0.829	0.716	0.587	0.347	0.282
300	2.632	1.554	1.243	1.074	0.881	0.520	0.423
400	3.510	2.072	1.657	1.432	1.174	0.693	0.564
500	4.387	2.589	2.071	1.790	1.468	0.867	0.704
600	5.265	3.107	2.486	2.148	1.761	1.040	0.845

Wavelength (in um)		0.544	0.633	3.39	4.45	5	5.4	6	8	9
amorphous	index	3.8825	3.8828	3.8460	3.8199	3.8060	3.7960	3.7818	3.7444	3.7331
Si	permittivity	15.0737	15.0760	14.7921	14.5914	14.4853	14.4099	14.3022	14.0207	13.9358
W	index			1.19+16.24i	2.03+21.22i	2.54+23.77i	2.96+25.60i	3.62+28.32	6.24+ 37.10i	7.76+41.31i
	permittivity			-262.53+38.67i	-446.29+86.15i	-558.44+121.07i	-646.71+151.38	-789.04+205.16i	-1337.7+463.54i	-1646.5+641.7i

Ratio of dielectric to metal

3.39	4.45	5	5.4	6	8	9
17.748	30.586	38.552	44.880	55.170	95.412	118.148

metal thickness

period (nm)	3.39	4.45	5	5.4	6	8	9
75	4.000	2.374	1.896	1.635	1.335	0.778	0.629
100	5.334	3.166	2.528	2.180	1.780	1.037	0.839
150	8.001	4.749	3.792	3.269	2.670	1.556	1.259
200	10.668	6.332	5.057	4.359	3.561	2.074	1.679
300	16.001	9.498	7.585	6.539	5.341	3.112	2.518
400	21.335	12.664	10.113	8.718	7.121	4.149	3.357
500	26.669	15.830	12.641	10.898	8.902	5.186	4.196
600	32.003	18.996	15.170	13.078	10.682	6.223	5.036

Wavelength (in um)	0.544	0.633	3.39	4.45	5	5.4	6	8	9
SiC index	2.5872	2.5868	2.5382	2.4960	2.5868	2.4409	2.3944	2.1153	1.8083
permittivity	6.6938	6.6917	6.4426	6.2300	6.0837	5.9581	5.7331	4.4747	3.2700
W index			1.19+16.24i	2.03+21.22i	2.54+23.77i	2.96+25.60i	3.62+28.32	6.24+ 37.10i	7.76+41.31i
permittivity			-262.53+38.67i	-446.29+86.15i	-558.44+121.07i	-646.71+151.38	-789.04+205.16i	-1337.7+463.54i	-1646.5+641.7i

Ratio of dielectric to metal

	3.39	4.45	5	5.4	6	8	9
	40.750	71.636	91.794	108.543	137.629	298.957	503.508

metal thickness

period (nm)	3.39	4.45	5	5.4	6	8	9
75	1.796	1.033	0.808	0.685	0.541	0.250	0.149
100	2.395	1.377	1.078	0.913	0.721	0.333	0.198
150	3.593	2.065	1.616	1.369	1.082	0.500	0.297
200	4.790	2.753	2.155	1.826	1.443	0.667	0.396
300	7.186	4.130	3.233	2.739	2.164	1.000	0.595
400	9.581	5.507	4.311	3.652	2.885	1.334	0.793
500	11.976	6.884	5.388	4.564	3.607	1.667	0.991
600	14.371	8.260	6.466	5.477	4.328	2.000	1.189

Wavelength (in um)		0.544	0.633	3.39	4.45	5	5.4	6	8	9
TiO2	index	2.4175	2.4453	2.6269	2.5757	2.5607	2.5602	2.5822	2.9935	3.5353
	permittivity	5.8444	5.9795	6.9003	6.6345	6.5573	6.5544	6.6679	8.9609	12.4981
W	index			1.19+16.24i	2.03+21.22i	2.54+23.77i	2.96+25.60i	3.62+28.32	6.24+ 37.10i	7.76+41.31i
	permittivity			-262.53+38.67i	-446.29+86.15i	-558.44+121.07i	-646.71+151.38	-789.04+205.16i	-1337.7+463.54i	-1646.5+641.7i

Ratio of dielectric to metal

	3.39	4.45	5	5.4	6	8	9
	38.047	67.269	85.163	98.668	118.334	149.285	131.740

metal thickness

period (nm)	3.39	4.45	5	5.4	6	8	9
75	1.921	1.099	0.870	0.752	0.628	0.499	0.565
100	2.561	1.465	1.161	1.003	0.838	0.665	0.753
150	3.842	2.197	1.741	1.505	1.257	0.998	1.130
200	5.122	2.930	2.321	2.007	1.676	1.331	1.507
300	7.683	4.394	3.482	3.010	2.514	1.996	2.260
400	10.244	5.859	4.642	4.013	3.352	2.662	3.013
500	12.805	7.324	5.803	5.017	4.190	3.327	3.767
600	15.366	8.789	6.964	6.020	5.028	3.992	4.520

	Wavelength (in um)	0.544	0.633	3.39	4.45	5	5.4	6	8	9
ZnO	index	1.7028	1.7014	1.6975	1.6974	1.6974	1.6974	1.6974	1.6974	1.6974
	permittivity	2.8996	2.8947	2.8815	2.8813	2.8812	2.8812	2.8812	2.8811	2.8811
W	index			1.19+16.24i	2.03+21.22i	2.54+23.77i	2.96+25.60i	3.62+28.32	6.24+ 37.10i	7.76+41.31i
	permittivity			-262.53+38.67i	-446.29+86.15i	-558.44+121.07i	-646.71+151.38	-789.04+205.16i	-1337.7+463.54i	-1646.5+641.7i

Ratio of dielectric to metal

3.39	4.45	5	5.4	6	8	9
91.112	154.895	193.821	224.460	273.864	464.318	571.486

metal thickness

period (nm)	3.39	4.45	5	5.4	6	8	9
75	0.814	0.481	0.385	0.333	0.273	0.161	0.131
100	1.086	0.641	0.513	0.444	0.364	0.215	0.175
150	1.628	0.962	0.770	0.665	0.546	0.322	0.262
200	2.171	1.283	1.027	0.887	0.728	0.430	0.349
300	3.257	1.924	1.540	1.331	1.091	0.645	0.524
400	4.343	2.566	2.053	1.774	1.455	0.860	0.699
500	5.428	3.207	2.566	2.218	1.819	1.075	0.873
600	6.514	3.849	3.080	2.661	2.183	1.289	1.048

Wavelength (in um)		0.544	0.633	3.39	4.45	5	5.4	6	8	9
ZnS	index	1.8410	1.8410	1.8410	1.8410	1.8410	1.8410	1.8410	1.8410	1.8410
	permittivity	3.3892	3.3892	3.3892	3.3892	3.3892	3.3892	3.3892	3.3892	3.3892
W	index			1.19+16.24i	2.03+21.22i	2.54+23.77i	2.96+25.60i	3.62+28.32	6.24+ 37.10i	7.76+41.31i
	permittivity			-262.53+38.67i	-446.29+86.15i	-558.44+121.07i	-646.71+151.38	-789.04+205.16i	-1337.7+463.54i	-1646.5+641.7i

Ratio of dielectric to metal									
			3.39	4.45	5	5.4	6	8	9
			77.463	131.682	164.771	190.816	232.812	394.708	485.808

				metal thickness					
		period (nm)	3.39	4.45	5	5.4	6	8	9
		75	0.956	0.565	0.452	0.391	0.321	0.190	0.154
		100	1.274	0.754	0.603	0.521	0.428	0.253	0.205
		150	1.912	1.131	0.905	0.782	0.642	0.379	0.308
		200	2.549	1.507	1.206	1.043	0.855	0.505	0.411
		300	3.823	2.261	1.810	1.564	1.283	0.758	0.616
		400	5.098	3.015	2.413	2.085	1.711	1.011	0.822
		500	6.372	3.768	3.016	2.607	2.138	1.264	1.027
		600	7.647	4.522	3.619	3.128	2.566	1.516	1.233

Appendix C: GENERAL DEPOSITION PROCEDURE

This section outlines the general procedure for the deposition of materials using the Denton Discovery 18 sputtering system. Within the individual sections, the parameters for the depositions are given in a table. Before a deposition was made, the substrates to be used were cleaved into quarters, in the case of 3 inch diameter, 375μm thick silicon wafers, and then cleaned by spinning then at 500 revolutions per minute on a photoresist spinner and spraying them with acetone, methanol, and DI water, and then drying with nitrogen. The samples were then placed on a 110˚C hotplate and baked two minutes to remove any residual water that may be on them. The samples were then loaded into the sputtering system, and the deposition monitor programmed with the information needed to give accurate results. After the samples are loaded and the chamber has pumped down to less than $1x10^{-6}$ Torr, a short, 1 minute 75W RF plasma clean of the samples is done to remove any remaining material on the substrate. If this could not be done, due to problems with the sputtering system, a 1 minute 75W plasma ash was done in a barrel asher before the samples were loaded. After this, a plasma was then lit on the DC cathode with the first material, a metal, to be used, and the voltage adjusted to the pre-sputter voltage, and the pre-sputter begun. After the pre-sputter is completed, the voltage is adjusted to the deposition level, and then the shutter is opened, the deposition monitor reset and timer begun. Once the desired thickness is reached on the deposition monitor, the shutter is then closed, stopping the deposition, and the voltage turned off, killing the plasma. Once the chamber pressure is again back to less than

1×10^{-6} Torr, the dielectric deposition process can then be started. The process for dielectrics is similar to that used for metals, except dielectrics must use RF and need to be ramped up to a deposition power from the initial power of 100W by 25W increments, stopping for 30 seconds at each increment. This is done to prevent the dielectric target, which is brittle, from cracking. Once up to the deposition power, a one minute pre-sputter is done, and then the deposition is begun by opening the shutter, zeroing the deposition monitor and starting a timer. Once the desired thickness is reached, the shutter is then closed, stopping the deposition, and the RF power is then ramped down to 100W, only at a slightly faster rate of 50W increments, stopping for 30 seconds at each increment. This process for depositing metal and dielectric layers can then be repeated as needed to produce stacks of layered material.

Appendix D: MATLAB CODE

D-1: Code for Ag- Al₂O₃ Structure

Code for effective permittivity and index plots

```matlab
%Jack Lombardi
%code for effective permittivity and index
%Ag-Al2O3, 150nm period, 4layer
%Ag for .33-1.9um
%Al2O3 for .17-6.5um

clear all

count=1;

for lambda=.33:.01:.8;
    wavelength(count,1)=lambda;

n1=1.8739+(-7e-10*lambda^3)+(1e-6*lambda^2)-.0009*lambda; %index of
Al2O3
d1=.120; %thickness of Al2O3
permitt1=n1^2;

n2=(4.4211*lambda^6 - 29.064*lambda^5 + 75.662*lambda^4 -...
    99.376*lambda^3 + 69.317*lambda^2 - 24.339*lambda + 3.4105)+...
    ((-3.5221*lambda^4 + 16.76*lambda^3 - 28.336*lambda^2 + ...
    27.718*lambda - 5.541)*1i); %index of Ag
permitt2=n2^2;
d2=.03; %thickness of Ag
period=d1+d2;

eff_permit(count,1)=((d1/period)*permitt1)+((d2/period)*real(permitt2))
;

eff_index(count,1)=(((d1/period)*permitt1)+(d2/period)*(permitt2))^.5;

count=count+1;
end

plot(wavelength,(eff_permit),'LineWidth',2)
xlabel('Wavelength (um)','Fontsize',12')
ylabel('Real part of Permittivity','Fontsize',12)
title('Revised Effective Permittivity of Ag-Al2O3
Structure','Fontsize',12)
axis tight

figure
plot(wavelength,real(eff_index),'LineWidth',2)
hold on
plot(wavelength,imag(eff_index),'r','LineWidth',2)
legend('real','imaginary','Fontsize',12)
```

```matlab
xlabel('Wavelength (um)','Fontsize',12)
ylabel('Index of Refraction','Fontsize',12)
title('Revised Effective Index of Ag-Al2O3 Structure','Fontsize',12)
axis tight
```

Code for reflection and transmission from Ag- Al_2O_3 as layered material

```matlab
%Jack Lombardi
%code for effective permittivity and index
%Ag-Al2O3, 150nm period, 4layer
%Ag for .33-1.9um
%Al2O3 for .17-6.5um

clear all

theata_i=(pi/180)*3; %% incident angle in radians

count=1;

for lambda=.33:.0005:.8;

    wavelength(count,1)=lambda;

k=(2*pi)/lambda;

% n1=1.8739+(-7e-10*lambda^3)+(1e-6*lambda^2)-.0009*lambda; %index of
Al2O3
n1=sqrt(1+((1.023798*lambda^2)/(lambda^2-(.00377588)))+...
    ((1.058264*lambda^2)/(lambda^2-(.0122544)))+ ...
    ((5.280792*lambda^2)/(lambda^2-(321.3616))));
d1=.120; %thickness of Al2O3
permitt1=n1^2;

n2=(4.4211*lambda^6 - 29.064*lambda^5 + 75.662*lambda^4 -...
    99.376*lambda^3 + 69.317*lambda^2 - 24.339*lambda + 3.4105)+...
    ((-3.5221*lambda^4 + 16.76*lambda^3 - 28.336*lambda^2 + ...
    27.718*lambda - 5.541)*1i); %index of Ag
permitt2=n2^2;
d2=.03; %thickness of Ag
period=d1+d2;



noxide=0.882*lambda^4 - 2.6084*lambda^3 + 2.8425*lambda^2 ...
    - 1.3745*lambda + 1.7088;
doxide=.002;

n3=(1526.4*lambda^5 - 4885.4*lambda^4 + 6100.8*lambda^3 ...
    - 3696*lambda^2 + 1076.6*lambda - 114.91)+((-26593*lambda^6 ...
    + 89496*lambda^5 - 122489*lambda^4 + 86937*lambda^3 ...
    - 33573*lambda^2 + 6637.6*lambda - 518.31)*1i); %index of Si

n0=n3; %index of substrate
ni=1; %index of superstrate
```

```matlab
%%% compute angle for each of the layers using Snells law

theata_1=asin(1*sin(theata_i)/n1);
theata_2=asin(n1*sin(theata_1)/real(n2));
theata_oxide=asin((n2)*sin(theata_2)/(noxide));
theata_3=asin((noxide)*sin(theata_oxide)/(n0));

angle_log(count,1:5)=...
    [lambda,theata_1*(180/pi), theata_2*(180/pi),
theata_oxide*(180/pi), theata_3*(180/pi)];
%code to log angles to use and check for total internal reflection




%%for TE first then TM
M1_TE=[cos(k*n1*d1*cos(theata_1)),...
    ((-1*1i/(n1*cos(theata_1)))*sin(k*n1*d1*cos(theata_1))); ...
    (-1i*n1*cos(theata_1)*sin(k*n1*d1*cos(theata_1))),...
    cos(k*n1*d1*cos(theata_1))];

M1_TM=[cos(k*n1*d1*cos(theata_1)),...
    (-1i*n1/cos(theata_1))*sin(k*n1*d1*cos(theata_1)); ...
    (-1i*cos(theata_1)/n1)*sin(k*n1*d1*cos(theata_1)),...
    cos(k*n1*d1*cos(theata_1))];

%n2
M2_TE=[cos(k*n2*d2*cos(theata_2)),...
    ((-1*1i/(n2*cos(theata_2)))*sin(k*n2*d2*cos(theata_2)));
    (-1i*n2*cos(theata_2)*sin(k*n2*d2*cos(theata_2))),...
    cos(k*n2*d2*cos(theata_2))];

M2_TM=[cos(k*n2*d2*cos(theata_2)),...
    (-1i*n2/cos(theata_2))*sin(k*n2*d2*cos(theata_2)); ...
    (-1i*cos(theata_2)/n2)*sin(k*n2*d2*cos(theata_2)),...
    cos(k*n2*d2*cos(theata_2))];

%noxide
Moxide_TE=[cos(k*noxide*doxide*cos(theata_oxide)),...
    ((-
1*1i/(noxide*cos(theata_oxide)))*sin(k*noxide*doxide*cos(theata_oxide))
);
    (-
1i*noxide*cos(theata_oxide)*sin(k*noxide*doxide*cos(theata_oxide))),...
    cos(k*noxide*doxide*cos(theata_oxide))];

Moxide_TM=[cos(k*noxide*doxide*cos(theata_oxide)),...
    (-
1i*noxide/cos(theata_oxide))*sin(k*noxide*doxide*cos(theata_oxide));
...
    (-
1i*cos(theata_oxide)/noxide)*sin(k*noxide*doxide*cos(theata_oxide)),...
    cos(k*noxide*doxide*cos(theata_oxide))];
```

```matlab
M_TE=M1_TE*M2_TE*M1_TE*M2_TE*M1_TE*M2_TE*M1_TE*M2_TE*Moxide_TE; %final
transfer matrix

M_TM=M1_TM*M2_TM*M1_TM*M2_TM*M1_TM*M2_TM*M1_TM*M2_TM*Moxide_TM; %final
transfer matrix

%compute final compex reflection and transmission

r_TE(count,1)=(((M_TE(1,1)+(n0*cos(theata_3)*M_TE(1,2)))*ni*cos(theata_
i))...
    -(M_TE(2,1)+(n0*cos(theata_3)*M_TE(2,2))))/ ...
    (((M_TE(1,1)+(n0*cos(theata_3)*M_TE(1,2)))*ni*cos(theata_i))...
    +(M_TE(2,1)+(n0*cos(theata_3)*M_TE(2,2))));

t_TE(count,1)=(2*ni*cos(theata_i))/...
    (((M_TE(1,1)+n0*cos(theata_3)*M_TE(1,2))*ni*cos(theata_i))...
    +(M_TE(2,1)+n0*cos(theata_3)*M_TE(2,2)));

R_TE(count,1)=(abs(r_TE(count,1))^2)*100;
T_TE(count,1)=((n0*cos(theata_3))/(ni*cos(theata_i)))...
    *(abs(t_TE(count,1))^2)*100;


r_TM(count,1)=(((M_TM(1,1)+(1/n0)*cos(theata_3)*M_TM(1,2))*(1/ni)*cos(t
heata_i))...
    -(M_TM(2,1)+(1/n0)*cos(theata_3)*M_TM(2,2)))/...

(((M_TM(1,1)+(1/n0)*cos(theata_3)*M_TM(1,2))*(1/ni)*cos(theata_i))...
    +(M_TM(2,1)+(1/n0)*cos(theata_3)*M_TM(2,2)));

t_TM(count,1)=(2*(1/ni)*cos(theata_i))/...

(((M_TM(1,1)+(1/n0)*cos(theata_3)*M_TM(1,2))*(1/ni)*cos(theata_i))...
    +(M_TM(2,1)+(1/n0)*cos(theata_3)*M_TM(2,2)));

R_TM(count,1)=(abs(r_TM(count,1))^2)*100;
T_TM(count,1)=(((1/n0)*cos(theata_3))/((1/ni)*cos(theata_i)))...
    *(abs(t_TM(count,1))^2)*100;

R(count,1)=(R_TE(count,1)+R_TM(count,1))/2;
T(count,1)=(T_TE(count,1)+T_TM(count,1))/2;

count=count+1;
end

axes('FontSize', 11.49)
plot(wavelength,R,'LineWidth',2)
xlabel('Wavelength (um)','Fontsize',12)
ylabel('% Reflection','Fontsize',12)
axis([.33 .8 0 100])
```

Code for Ag- Al_2O_3 structure as a homogeneous material

```matlab
%Jack Lombardi
%code for effective permittivity and index
%Ag-Al2O3, 150nm period, 4layer
%Ag for .33-1.9um
%Al2O3 for .17-6.5um

%for a homogeneous structure

clear all

theata_i=(pi/180)*3; %% incident angle in radians

count=1;

for lambda=.33:.0005:.8;
    wavelength(count,1)=lambda;

n1=1.8739+(-7e-10*lambda^3)+(1e-6*lambda^2)-.0009*lambda; %index of
Al2O3
d1=.120; %thickness of Al2O3
permitt1=n1^2;

n2=(4.4211*lambda^6 - 29.064*lambda^5 + 75.662*lambda^4 -...
    99.376*lambda^3 + 69.317*lambda^2 - 24.339*lambda + 3.4105)+...
    ((-3.5221*lambda^4 + 16.76*lambda^3 - 28.336*lambda^2 + ...
    27.718*lambda - 5.541)*1i); %index of Ag
permitt2=n2^2;
d2=.03; %thickness of Ag
period=d1+d2;

noxide=0.882*lambda^4 - 2.6084*lambda^3 + 2.8425*lambda^2 -
1.3745*lambda + 1.7088;
doxide=.002;

neff=(((d1/(d1+d2))*permitt1)+((d2/(d1+d2))*permitt2))^.5;

n3=(1526.4*lambda^5 - 4885.4*lambda^4 + 6100.8*lambda^3 ...
    - 3696*lambda^2 + 1076.6*lambda - 114.91)+((-26593*lambda^6 ...
    + 89496*lambda^5 - 122489*lambda^4 + 86937*lambda^3 ...
    - 33573*lambda^2 + 6637.6*lambda - 518.31)*1i); %index of Si

n0=n3; %index of substrate
ni=1; %index of superstrate
d=.15*4; %thickness of whole structure
%%% compute angle for each of the layers using Snells law

theata_1=asin(1*sin(theata_i)/real(neff));
theata_oxide=asin(real(neff)*sin(theata_1)/real(noxide));
theata_3=asin(real(noxide)*sin(theata_oxide)/real(n3));


angle_log(count,1:4)=...
```

```matlab
    [lambda,theata_1*(180/pi), theata_oxide*(180/pi),
theata_3*(180/pi)];
%code to log angles to use and check for total internal reflection

k=2*pi/lambda;

Meff_TE=[cos(k*neff*d*cos(theata_1)),...
    ((-1*1i/(neff*cos(theata_1)))*sin(k*neff*d*cos(theata_1))); ...
    (-1i*neff*cos(theata_1)*sin(k*neff*d*cos(theata_1))),...
    cos(k*neff*d*cos(theata_1))];

Meff_TM=[cos(k*neff*d*cos(theata_1)),...
    (-1i*neff/cos(theata_1))*sin(k*neff*d*cos(theata_1)); ...
    (-1i*cos(theata_1)/neff)*sin(k*neff*d*cos(theata_1)),...
    cos(k*neff*d*cos(theata_1))];

%noxide
Moxide_TE=[cos(k*noxide*doxide*cos(theata_oxide)),...
    ((-
1*1i/(noxide*cos(theata_oxide)))*sin(k*noxide*doxide*cos(theata_oxide))
);
    (-
1i*noxide*cos(theata_oxide)*sin(k*noxide*doxide*cos(theata_oxide))),...
    cos(k*noxide*doxide*cos(theata_oxide))];

Moxide_TM=[cos(k*noxide*doxide*cos(theata_oxide)),...
    (-
1i*noxide/cos(theata_oxide))*sin(k*noxide*doxide*cos(theata_oxide));
...
    (-
1i*cos(theata_oxide)/noxide)*sin(k*noxide*doxide*cos(theata_oxide)),...
    cos(k*noxide*doxide*cos(theata_oxide))];

M_TE=Meff_TE*Moxide_TE;
M_TM=Meff_TM*Moxide_TM;

r_TE(count,1)=(((M_TE(1,1)+(n0*cos(theata_3)*M_TE(1,2)))*ni*cos(theata_
i))...
    -(M_TE(2,1)+(n0*cos(theata_3)*M_TE(2,2))))/ ...
    (((M_TE(1,1)+(n0*cos(theata_3)*M_TE(1,2)))*ni*cos(theata_i))...
    +(M_TE(2,1)+(n0*cos(theata_3)*M_TE(2,2))));

t_TE(count,1)=(2*ni*cos(theata_i))/...
    (((M_TE(1,1)+n0*cos(theata_3)*M_TE(1,2))*ni*cos(theata_i))...
    +(M_TE(2,1)+n0*cos(theata_3)*M_TE(2,2)));

R_TE(count,1)=(abs(r_TE(count,1))^2)*100;
T_TE(count,1)=((n0*cos(theata_3))/(ni*cos(theata_i)))...
    *(abs(t_TE(count,1))^2)*100;


r_TM(count,1)=(((M_TM(1,1)+(1/n0)*cos(theata_3)*M_TM(1,2))*(1/ni)*cos(t
heata_i))...
```

```matlab
      -(M_TM(2,1)+(1/n0)*cos(theata_3)*M_TM(2,2)))/...

(((M_TM(1,1)+(1/n0)*cos(theata_3)*M_TM(1,2))*(1/ni)*cos(theata_i))...
    +(M_TM(2,1)+(1/n0)*cos(theata_3)*M_TM(2,2)));

t_TM(count,1)=(2*(1/ni)*cos(theata_i))/...

(((M_TM(1,1)+(1/n0)*cos(theata_3)*M_TM(1,2))*(1/ni)*cos(theata_i))...
    +(M_TM(2,1)+(1/n0)*cos(theata_3)*M_TM(2,2)));

R_TM(count,1)=(abs(r_TM(count,1))^2)*100;
T_TM(count,1)=(((1/n0)*cos(theata_3))/((1/ni)*cos(theata_i)))...
    *(abs(t_TM(count,1))^2)*100;

R(count,1)=(R_TE(count,1)+R_TM(count,1))/2;
T(count,1)=(T_TE(count,1)+T_TM(count,1))/2;

count=count+1;
end


plot(wavelength,R,'LineWidth',2)
xlabel('Wavelength (um)','Fontsize',12)
ylabel('% Reflection','Fontsize',12)
axis([.33 .8 0 100])
```

Code for the reflection and transmission of one period of the Ag- Al_2O_3 structure on glass as layers

```matlab
%Jack Lombardi
%reflection and transmission from one period on glass
%Ag-Al2O3, 150nm period, 1period
%Ag for .33-1.9um
%Al2O3 for .17-6.5um

clear all

theata_i=(pi/180)*0; %% incident angle in radians

count=1;

for lambda=.33:.0005:.8;

    wavelength(count,1)=lambda;

k=(2*pi)/lambda;

n1=1.8739+(-7e-10*lambda^3)+(1e-6*lambda^2)-.0009*lambda; %index of
Al2O3
d1=.120; %thickness of Al2O3
permitt1=n1^2;

n2=(4.4211*lambda^6 - 29.064*lambda^5 + 75.662*lambda^4 -...
```

```matlab
        99.376*lambda^3 + 69.317*lambda^2 - 24.339*lambda + 3.4105)+...
        ((-3.5221*lambda^4 + 16.76*lambda^3 - 28.336*lambda^2 + ...
        27.718*lambda - 5.541)*1i); %index of Ag
permitt2=n2^2;
d2=.03; %thickness of Ag
period=d1+d2;



n3=0.882*lambda^4 - 2.6084*lambda^3 + 2.8425*lambda^2 - 1.3745*lambda +
1.7088;
doxide=.002;


%%% compute angle for each of the layers using Snells law

theata_1=asin(1*sin(theata_i)/n1);
theata_2=asin(n1*sin(theata_1)/real(n2));
theata_3=asin(real(n2)*sin(theata_2)/real(n3));


angle_log(count,1:4)=...
    [lambda,theata_1*(180/pi), theata_2*(180/pi), theata_3*(180/pi)];
%code to log angles to use and check for total internal reflection


n0=n3; %index of substrate
ni=1; %index of superstrate

%%for TE first then TM
M1_TE=[cos(k*n1*d1*cos(theata_1)),...
    ((-1*1i/(n1*cos(theata_1)))*sin(k*n1*d1*cos(theata_1))); ...
    (-1i*n1*cos(theata_1)*sin(k*n1*d1*cos(theata_1))),...
    cos(k*n1*d1*cos(theata_1))];

M1_TM=[cos(k*n1*d1*cos(theata_1)),...
    (-1i*n1/cos(theata_1))*sin(k*n1*d1*cos(theata_1)); ...
    (-1i*cos(theata_1)/n1)*sin(k*n1*d1*cos(theata_1)),...
    cos(k*n1*d1*cos(theata_1))];

%n2
M2_TE=[cos(k*n2*d2*cos(theata_2)),...
    ((-1*1i/(n2*cos(theata_2)))*sin(k*n2*d2*cos(theata_2)));
    (-1i*n2*cos(theata_2)*sin(k*n2*d2*cos(theata_2))),...
    cos(k*n2*d2*cos(theata_2))];

M2_TM=[cos(k*n2*d2*cos(theata_2)),...
    (-1i*n2/cos(theata_2))*sin(k*n2*d2*cos(theata_2)); ...
    (-1i*cos(theata_2)/n2)*sin(k*n2*d2*cos(theata_2)),...
    cos(k*n2*d2*cos(theata_2))];


M_TE=M1_TE*M2_TE; %final transfer matrix

M_TM=M1_TM*M2_TM; %final transfer matrix
```

```matlab
%compute final compex reflection and transmission

r_TE(count,1)=(((M_TE(1,1)+(n0*cos(theata_3)*M_TE(1,2)))*ni*cos(theata_i))...
    -(M_TE(2,1)+(n0*cos(theata_3)*M_TE(2,2))))/ ...
    (((M_TE(1,1)+(n0*cos(theata_3)*M_TE(1,2)))*ni*cos(theata_i))...
    +(M_TE(2,1)+(n0*cos(theata_3)*M_TE(2,2))));

t_TE(count,1)=(2*ni*cos(theata_i))/...
    (((M_TE(1,1)+n0*cos(theata_3)*M_TE(1,2))*ni*cos(theata_i))...
    +(M_TE(2,1)+n0*cos(theata_3)*M_TE(2,2)));

R_TE(count,1)=(abs(r_TE(count,1))^2)*100;
T_TE(count,1)=((n0*cos(theata_3))/(ni*cos(theata_i)))...
    *(abs(t_TE(count,1))^2)*100;



r_TM(count,1)=(((M_TM(1,1)+(1/n0)*cos(theata_3)*M_TM(1,2))*(1/ni)*cos(theata_i))...
    -(M_TM(2,1)+(1/n0)*cos(theata_3)*M_TM(2,2)))/...

(((M_TM(1,1)+(1/n0)*cos(theata_3)*M_TM(1,2))*(1/ni)*cos(theata_i))...
    +(M_TM(2,1)+(1/n0)*cos(theata_3)*M_TM(2,2)));

t_TM(count,1)=(2*(1/ni)*cos(theata_i))/...

(((M_TM(1,1)+(1/n0)*cos(theata_3)*M_TM(1,2))*(1/ni)*cos(theata_i))...
    +(M_TM(2,1)+(1/n0)*cos(theata_3)*M_TM(2,2)));

R_TM(count,1)=(abs(r_TM(count,1))^2)*100;
T_TM(count,1)=(((1/n0)*cos(theata_3))/((1/ni)*cos(theata_i)))...
    *(abs(t_TM(count,1))^2)*100;

R(count,1)=(R_TE(count,1)+R_TM(count,1))/2;
T(count,1)=(T_TE(count,1)+T_TM(count,1))/2;

count=count+1;
end

plot(wavelength,R,'LineWidth',2)
xlabel('Wavelength (um)','Fontsize',12)
ylabel('% Reflection','Fontsize',12)
title('Reflection from Ag-Al2O3 structure on glass as layers at 3 degees','Fontsize',12)
axis([.33 .8 0 100])

figure
plot(wavelength,T,'LineWidth',2)
xlabel('Wavelength (um)','Fontsize',12)
ylabel('% Transmission','Fontsize',12)
title('Transmission from Ag-Al2O3 structure on glass as layers at 0 degees','Fontsize',12)
```

Code for the reflection and transmission of one period of the Ag-Al2O3 structure on glass as homogenous material

```matlab
%Jack Lombardi
%code for effective permittivity and index
%Ag-Al2O3, 150nm period, 4layer
%Ag for .33-1.9um
%Al2O3 for .17-6.5um

%for a homogeneous structure

clear all

theata_i=(pi/180)*0; %% incident angle in radians

count=1;

for lambda=.33:.0005:.8;
    wavelength(count,1)=lambda;

n1=1.8739+(-7e-10*lambda^3)+(1e-6*lambda^2)-.0009*lambda; %index of
Al2O3
d1=.120; %thickness of Al2O3
permitt1=n1^2;

n2=(4.4211*lambda^6 - 29.064*lambda^5 + 75.662*lambda^4 -...
    99.376*lambda^3 + 69.317*lambda^2 - 24.339*lambda + 3.4105)+...
    ((-3.5221*lambda^4 + 16.76*lambda^3 - 28.336*lambda^2 + ...
    27.718*lambda - 5.541)*1i); %index of Ag
permitt2=n2^2;
d2=.03; %thickness of Ag
period=d1+d2;



n3=0.882*lambda^4 - 2.6084*lambda^3 + 2.8425*lambda^2 - 1.3745*lambda +
1.7088;
%index of SiO2, glass

neff=(((d1/(d1+d2))*permitt1)+((d2/(d1+d2))*permitt2))^.5;

%%% compute angle for each of the layers using Snells law

theata_1=asin(1*sin(theata_i)/real(neff));
theata_3=asin(real(neff)*sin(theata_1)/real(n3));



angle_log(count,1:3)=...
    [lambda,theata_1*(180/pi), theata_3*(180/pi)];
%code to log angles to use and check for total internal reflection

n0=n3; %index of substrate
ni=1; %index of superstrate
d=.15*1; %thickness of whole structure
```

```
k=2*pi/lambda;

Meff_TE=[cos(k*neff*d*cos(theata_1)),...
    ((-1*1i/(neff*cos(theata_1)))*sin(k*neff*d*cos(theata_1))); ...
    (-1i*neff*cos(theata_1)*sin(k*neff*d*cos(theata_1))),...
    cos(k*neff*d*cos(theata_1))];

Meff_TM=[cos(k*neff*d*cos(theata_1)),...
    (-1i*neff/cos(theata_1))*sin(k*neff*d*cos(theata_1)); ...
    (-1i*cos(theata_1)/neff)*sin(k*neff*d*cos(theata_1)),...
    cos(k*neff*d*cos(theata_1))];

M_TE=Meff_TE;
M_TM=Meff_TM;

r_TE(count,1)=(((M_TE(1,1)+(n0*cos(theata_3)*M_TE(1,2)))*ni*cos(theata_
i))...
    -(M_TE(2,1)+(n0*cos(theata_3)*M_TE(2,2))))/ ...
    (((M_TE(1,1)+(n0*cos(theata_3)*M_TE(1,2)))*ni*cos(theata_i))...
    +(M_TE(2,1)+(n0*cos(theata_3)*M_TE(2,2))));

t_TE(count,1)=(2*ni*cos(theata_i))/...
    (((M_TE(1,1)+n0*cos(theata_3)*M_TE(1,2))*ni*cos(theata_i))...
    +(M_TE(2,1)+n0*cos(theata_3)*M_TE(2,2)));

R_TE(count,1)=(abs(r_TE(count,1))^2)*100;
T_TE(count,1)=((n0*cos(theata_3))/(ni*cos(theata_i)))...
    *(abs(t_TE(count,1))^2)*100;


r_TM(count,1)=(((M_TM(1,1)+(1/n0)*cos(theata_3)*M_TM(1,2))*(1/ni)*cos(t
heata_i))...
    -(M_TM(2,1)+(1/n0)*cos(theata_3)*M_TM(2,2)))/...

(((M_TM(1,1)+(1/n0)*cos(theata_3)*M_TM(1,2))*(1/ni)*cos(theata_i))...
    +(M_TM(2,1)+(1/n0)*cos(theata_3)*M_TM(2,2)));

t_TM(count,1)=(2*(1/ni)*cos(theata_i))/...

(((M_TM(1,1)+(1/n0)*cos(theata_3)*M_TM(1,2))*(1/ni)*cos(theata_i))...
    +(M_TM(2,1)+(1/n0)*cos(theata_3)*M_TM(2,2)));

R_TM(count,1)=(abs(r_TM(count,1))^2)*100;
T_TM(count,1)=(((1/n0)*cos(theata_3))/((1/ni)*cos(theata_i)))...
    *(abs(t_TM(count,1))^2)*100;

R(count,1)=(R_TE(count,1)+R_TM(count,1))/2;
T(count,1)=(T_TE(count,1)+T_TM(count,1))/2;

count=count+1;
end
```

```matlab
plot(wavelength,R,'LineWidth',2)
xlabel('Wavelength (um)','Fontsize',12)
ylabel('% Reflection','Fontsize',12)
title('Reflection from Ag-Al2O3 structure on glass as homogeneous
material at 20 degees','Fontsize',12)
axis([.33 .8 0 100])

figure
plot(wavelength,T,'LineWidth',2)
xlabel('Wavelength (um)','Fontsize',12)
ylabel('% Transmission','Fontsize',12)
title('Transmission from Ag-Al2O3 structure on glass as homogeneous
material at 0 degees','Fontsize',12)
axis tight
```

D-2: Code for Ti- Al$_2$O$_3$ Structure

Code for effective permittivity and index plots

```matlab
%Jack Lombardi
%code for effective permittivity and index
%Ti-Al2O3, 200nm period, 4layer
%Ti for 2.5-12um
%Al2O3 for .17-6.5um


clear all


count=1;


for lambda=2.5:.01:8;
    wavelength(count,1)=lambda;


n1=sqrt(1+((1.023798*lambda^2)/(lambda^2-(.00377588)))+...
    ((1.058264*lambda^2)/(lambda^2-(.0122544)))+ ...
    ((5.280792*lambda^2)/(lambda^2-(321.3616)))); %index of Al2O3
    d1=.140; %thickness of Al2O3
permitt1=n1^2;


n2=(-.0068*lambda^3+.1812*lambda^2-.9281*lambda+5.8689)+ ...
    ((-.0142*lambda^3+.2736*lambda^2+.2448*lambda+2.8602)*1i); %index
of Ti
d2=.01; %thickness of Ti
permitt2=(n2)^2;


period=d1+d2; %period of structure


eff_permit(count,1)=((d1/period)*permitt1)+((d2/period)*real(permitt2))
;


eff_index(count,1)=(((d1/period)*permitt1)+(d2/period)*(permitt2))^.5;
```

```matlab
count=count+1;
end

plot(wavelength,(eff_permit),'LineWidth',2)
xlabel('Wavelength (um)','Fontsize',12')
ylabel('Real part of Permittivity','Fontsize',12)
title('Effective Permittivity of Ti-Al2O3 Structure','Fontsize',12)
axis tight

figure
plot(wavelength,real(eff_index),'LineWidth',2)
hold on
plot(wavelength,imag(eff_index),'r','LineWidth',2)
legend('real','imaginary','Fontsize',12)
xlabel('Wavelength (um)','Fontsize',12)
ylabel('Index of Refraction','Fontsize',12)
title('Revised Effective Index of Ti-Al2O3 Structure','Fontsize',12)
axis tight
```

Code for Reflection and Transmission of Ti- Al_2O_3 as layers

```matlab
%Jack Lombardi
%code for effective permittivity and index
%Ti-Al2O3, 150nm period, 2layer
%Ti for 2.5-12um
%Al2O3 for .17-6.5um
%SiO2 for 1.6-8um

clear all

theata_i=(pi/180)*61.3; %% incident angle in radians

count=1;

for lambda=2.5:.01:8;

    wavelength(count,1)=lambda;

k=(2*pi)/lambda;

n1=sqrt(1+((1.023798*lambda^2)/(lambda^2-(.00377588)))+...
    ((1.058264*lambda^2)/(lambda^2-(.0122544)))+ ...
    ((5.280792*lambda^2)/(lambda^2-(321.3616)))); %index of Al2O3
    d1=.140; %thickness of Al2O3

n2=(-.0068*lambda^3+.1812*lambda^2-.9281*lambda+5.8689)+ ...
    ((-.0142*lambda^3+.2736*lambda^2+.2448*lambda+2.8602)*1i); %index
of Ti
d2=.01; %thickness of Ti

noxide=-0.0015*lambda^5 + 0.0312*lambda^4 - 0.2478*lambda^3 +
0.9223*lambda^2 - 1.6158*lambda + 2.502;
```

```matlab
doxide=.002;

L=1/(lambda^2-.028); %parameter for Si model
n3=3.41983+1.59906e-1*L-(1.23109e-1)*L^2+1.26878e-6*lambda^2 ...
    -1.95104e-9*lambda^4; %index of Si substrate

%%% compute angle for each of the layers using Snells law

theata_1=asin(1*sin(theata_i)/n1);
theata_2=asin(n1*sin(theata_1)/real(n2));
theata_oxide=asin(real(n2)*sin(theata_2)/real(noxide));
theata_3=asin(real(noxide)*sin(theata_oxide)/real(n3));

angle_log(count,1:5)=...
    [lambda,theata_1*(180/pi), theata_2*(180/pi), theata_oxide,
theata_3*(180/pi)];
%code to log angles to use and check for total internal reflection

n0=n3; %index of substrate
ni=1; %index of superstrate

%%for TE first then TM
M1_TE=[cos(k*n1*d1*cos(theata_1)),...
    ((-1*1i/(n1*cos(theata_1)))*sin(k*n1*d1*cos(theata_1))); ...
    (-1i*n1*cos(theata_1)*sin(k*n1*d1*cos(theata_1))),...
    cos(k*n1*d1*cos(theata_1))];

M1_TM=[cos(k*n1*d1*cos(theata_1)),...
    (-1i*n1/cos(theata_1))*sin(k*n1*d1*cos(theata_1)); ...
    (-1i*cos(theata_1)/n1)*sin(k*n1*d1*cos(theata_1)),...
    cos(k*n1*d1*cos(theata_1))];

%n2
M2_TE=[cos(k*n2*d2*cos(theata_2)),...
    ((-1*1i/(n2*cos(theata_2)))*sin(k*n2*d2*cos(theata_2)));
    (-1i*n2*cos(theata_2)*sin(k*n2*d2*cos(theata_2))),...
    cos(k*n2*d2*cos(theata_2))];

M2_TM=[cos(k*n2*d2*cos(theata_2)),...
    (-1i*n2/cos(theata_2))*sin(k*n2*d2*cos(theata_2)); ...
    (-1i*cos(theata_2)/n2)*sin(k*n2*d2*cos(theata_2)),...
    cos(k*n2*d2*cos(theata_2))];

%noxide
Moxide_TE=[cos(k*noxide*doxide*cos(theata_oxide)),...
    ((-
1*1i/(noxide*cos(theata_oxide)))*sin(k*noxide*doxide*cos(theata_oxide))
);
    (-
1i*noxide*cos(theata_oxide)*sin(k*noxide*doxide*cos(theata_oxide))),...
    cos(k*noxide*doxide*cos(theata_oxide))];

Moxide_TM=[cos(k*noxide*doxide*cos(theata_oxide)),...
```

```matlab
        (-
1i*noxide/cos(theata_oxide))*sin(k*noxide*doxide*cos(theata_oxide));
...
        (-
1i*cos(theata_oxide)/noxide)*sin(k*noxide*doxide*cos(theata_oxide)),...
        cos(k*noxide*doxide*cos(theata_oxide))];


M_TE=M1_TE*M2_TE*M1_TE*M2_TE*Moxide_TE; %final transfer matrix

M_TM=M1_TM*M2_TM*M1_TM*M2_TM*Moxide_TM; %final transfer matrix

%compute final compex reflection and transmission

r_TE(count,1)=(((M_TE(1,1)+(n0*cos(theata_3)*M_TE(1,2)))*ni*cos(theata_
i))...
    -(M_TE(2,1)+(n0*cos(theata_3)*M_TE(2,2))))/ ...
    (((M_TE(1,1)+(n0*cos(theata_3)*M_TE(1,2)))*ni*cos(theata_i))...
    +(M_TE(2,1)+(n0*cos(theata_3)*M_TE(2,2))));

t_TE(count,1)=(2*ni*cos(theata_i))/...
    (((M_TE(1,1)+n0*cos(theata_3)*M_TE(1,2))*ni*cos(theata_i))...
    +(M_TE(2,1)+n0*cos(theata_3)*M_TE(2,2)));

R_TE(count,1)=(abs(r_TE(count,1))^2)*100;
T_TE(count,1)=((n0*cos(theata_3))/(ni*cos(theata_i)))...
    *(abs(t_TE(count,1))^2)*100;


r_TM(count,1)=(((M_TM(1,1)+(1/n0)*cos(theata_3)*M_TM(1,2))*(1/ni)*cos(t
heata_i))...
    -(M_TM(2,1)+(1/n0)*cos(theata_3)*M_TM(2,2)))/...

(((M_TM(1,1)+(1/n0)*cos(theata_3)*M_TM(1,2))*(1/ni)*cos(theata_i))...
    +(M_TM(2,1)+(1/n0)*cos(theata_3)*M_TM(2,2)));

t_TM(count,1)=(2*(1/ni)*cos(theata_i))/...

(((M_TM(1,1)+(1/n0)*cos(theata_3)*M_TM(1,2))*(1/ni)*cos(theata_i))...
    +(M_TM(2,1)+(1/n0)*cos(theata_3)*M_TM(2,2)));

R_TM(count,1)=(abs(r_TM(count,1))^2)*100;
T_TM(count,1)=(((1/n0)*cos(theata_3))/((1/ni)*cos(theata_i)))...
    *(abs(t_TM(count,1))^2)*100;

R(count,1)=(R_TE(count,1)+R_TM(count,1))/2;
T(count,1)=(T_TE(count,1)+T_TM(count,1))/2;

count=count+1;
end

plot(wavelength,R,'LineWidth',2)
xlabel('Wavelength (um)','Fontsize',12)
ylabel('% Reflection','Fontsize',12)
```

```matlab
title('Reflection from Ti-Al2O3 structure as layers at 61.3
degees','Fontsize',12)
axis([2.5 8 0 70])

figure
plot(wavelength,T,'LineWidth',2)
xlabel('Wavelength (um)','Fontsize',12)
ylabel('% Transmission','Fontsize',12)
title('Transmission from Ti-Al2O3 structure as layers at 0
degees','Fontsize',12)
axis([2.5 8 0 50])
```

Code for Reflection and Transmission of Ti- Al_2O_3 as a homogeneous structure

```matlab
%Jack Lombardi
%code for effective permittivity and index
%Ti-Al2O3, 200nm period, 2layer
%Ti for 2.5-12um
%Al2O3 for .17-6.5um
%SiO2 for 1.6-8um



%%try and now apply for a homogeneous structure

clear all

theata_i=(pi/180)*61.3; %% incident angle in radians

count=1;

for lambda=1:.01:8;
   wavelength(count,1)=lambda;

n1=sqrt(1+((1.023798*lambda^2)/(lambda^2-(.00377588)))+...
    ((1.058264*lambda^2)/(lambda^2-(.0122544)))+ ...
    ((5.280792*lambda^2)/(lambda^2-(321.3616)))); %index of Al2O3
    d1=.140; %thickness of Al2O3
permitt1=n1^2;

n2=(-.0068*lambda^3+.1812*lambda^2-.9281*lambda+5.8689)+ ...
    ((-.0142*lambda^3+.2736*lambda^2+.2448*lambda+2.8602)*1i); %index
of Ti
d2=.01; %thickness of Ti
permitt2=(n2)^2;

period=d1+d2; %period of structure
noxide=-0.0015*lambda^5 + 0.0312*lambda^4 - 0.2478*lambda^3 +
0.9223*lambda^2 - 1.6158*lambda + 2.502;
doxide=.002;

L=1/(lambda^2-.028); %parameter for Si model
n3=3.41983+1.59906e-1*L-(1.23109e-1)*L^2+1.26878e-6*lambda^2 ...
    -1.95104e-9*lambda^4; %index of Si substrate
```

```matlab
neff=(((d1/(d1+d2))*permitt1)+((d2/(d1+d2))*permitt2))^.5;

%%% compute angle for each of the layers using Snells law

theata_1=asin(1*sin(theata_i)/real(neff));
theata_oxide=asin(real(neff)*sin(theata_1)/real(noxide));
theata_3=asin(real(noxide)*sin(theata_oxide)/real(n3));


angle_log(count,1:4)=...
    [lambda,theata_1*(180/pi), theata_oxide, theata_3*(180/pi)];
%code to log angles to use and check for total internal reflection

n0=n3; %index of substrate
ni=1; %index of superstrate
d=period*2; %thickness of whole structure

k=2*pi/lambda;

Meff_TE=[cos(k*neff*d*cos(theata_1)),...
    ((-1*1i/(neff*cos(theata_1)))*sin(k*neff*d*cos(theata_1))); ...
    (-1i*neff*cos(theata_1)*sin(k*neff*d*cos(theata_1))),...
    cos(k*neff*d*cos(theata_1))];

Meff_TM=[cos(k*neff*d*cos(theata_1)),...
    (-1i*neff/cos(theata_1))*sin(k*neff*d*cos(theata_1)); ...
    (-1i*cos(theata_1)/neff)*sin(k*neff*d*cos(theata_1)),...
    cos(k*neff*d*cos(theata_1))];

%noxide
Moxide_TE=[cos(k*noxide*doxide*cos(theata_oxide)),...
    ((-
1*1i/(noxide*cos(theata_oxide)))*sin(k*noxide*doxide*cos(theata_oxide))
);
    (-
1i*noxide*cos(theata_oxide)*sin(k*noxide*doxide*cos(theata_oxide))),...
    cos(k*noxide*doxide*cos(theata_oxide))];

Moxide_TM=[cos(k*noxide*doxide*cos(theata_oxide)),...
    (-
1i*noxide/cos(theata_oxide))*sin(k*noxide*doxide*cos(theata_oxide));
...
    (-
1i*cos(theata_oxide)/noxide)*sin(k*noxide*doxide*cos(theata_oxide)),...
    cos(k*noxide*doxide*cos(theata_oxide))];

M_TE=Meff_TE*Moxide_TE;
M_TM=Meff_TM*Moxide_TM;

r_TE(count,1)=(((M_TE(1,1)+(n0*cos(theata_3)*M_TE(1,2)))*ni*cos(theata_
i))...
    -(M_TE(2,1)+(n0*cos(theata_3)*M_TE(2,2))))/ ...
```

```matlab
        (((M_TE(1,1)+(n0*cos(theata_3)*M_TE(1,2)))*ni*cos(theata_i))...
        +(M_TE(2,1)+(n0*cos(theata_3)*M_TE(2,2)))));

    t_TE(count,1)=(2*ni*cos(theata_i))/...
        (((M_TE(1,1)+n0*cos(theata_3)*M_TE(1,2))*ni*cos(theata_i))...
        +(M_TE(2,1)+n0*cos(theata_3)*M_TE(2,2)));

    R_TE(count,1)=(abs(r_TE(count,1))^2)*100;
    T_TE(count,1)=((n0*cos(theata_3))/(ni*cos(theata_i)))...
        *(abs(t_TE(count,1))^2)*100;


    r_TM(count,1)=(((M_TM(1,1)+(1/n0)*cos(theata_3)*M_TM(1,2))*(1/ni)*cos(t
heata_i))...
        -(M_TM(2,1)+(1/n0)*cos(theata_3)*M_TM(2,2)))/...

    (((M_TM(1,1)+(1/n0)*cos(theata_3)*M_TM(1,2))*(1/ni)*cos(theata_i))...
        +(M_TM(2,1)+(1/n0)*cos(theata_3)*M_TM(2,2)));

    t_TM(count,1)=(2*(1/ni)*cos(theata_i))/...

    (((M_TM(1,1)+(1/n0)*cos(theata_3)*M_TM(1,2))*(1/ni)*cos(theata_i))...
        +(M_TM(2,1)+(1/n0)*cos(theata_3)*M_TM(2,2)));

    R_TM(count,1)=(abs(r_TM(count,1))^2)*100;
    T_TM(count,1)=(((1/n0)*cos(theata_3))/((1/ni)*cos(theata_i)))...
        *(abs(t_TM(count,1))^2)*100;

    R(count,1)=(R_TE(count,1)+R_TM(count,1))/2;
    T(count,1)=(T_TE(count,1)+T_TM(count,1))/2;

    count=count+1;
end


plot(wavelength,R,'LineWidth',2)
xlabel('Wavelength (um)','Fontsize',12)
ylabel('% Reflection','Fontsize',12)
title('Reflection from Ti-Al2O3 structure as homogeneous material at
61.3 degees','Fontsize',12)
axis([2.5 8 0 70])

figure
plot(wavelength,T,'LineWidth',2)
xlabel('Wavelength (um)','Fontsize',12)
ylabel('% Transmission','Fontsize',12)
title('Transmission from Ti-Al2O3 structure as homogeneous material at
0 degees','Fontsize',12)
axis([2.5 8 0 30])
```

D-3: Code for Ti-MgF2 Structure

Code for effective permittivity and index plots

```matlab
%Jack Lombardi
%code for effective permittivity and index
%Ti-MgF2, 300nm period, 4layer
%Ti for 2.5-12um
%MgF2 for .11-7.5

clear all

count=1;

for lambda=2.5:.01:7.5;
    wavelength(count,1)=lambda;

n1=(1.36957+(.0035821/(lambda-.14925)+1.381+(.0037415/(lambda-
.14947)))))/2;
d1=.288; %thickness MgF2
permitt1=n1^2;

n2=(-.0068*lambda^3+.1812*lambda^2-.9281*lambda+5.8689)+ ...
    ((-.0142*lambda^3+.2736*lambda^2+.2448*lambda+2.8602)*1i); %index
of Ti
permitt2=n2^2;
d2=.012; %thickness of Ti
period=d1+d2; %period of structure

eff_permit(count,1)=((d1/period)*permitt1)+((d2/period)*real(permitt2))
;

eff_index(count,1)=(((d1/period)*permitt1)+(d2/period)*(permitt2))^.5;

count=count+1;
end

plot(wavelength,(eff_permit),'LineWidth',2)
xlabel('Wavelength (um)','Fontsize',12')
ylabel('Real part of Permittivity','Fontsize',12)
title('Effective Permittivity of Ti-MgF2 Structure','Fontsize',12)
axis tight

figure
plot(wavelength,real(eff_index),'LineWidth',2)
hold on
plot(wavelength,imag(eff_index),'r','LineWidth',2)
legend('real','imaginary','Fontsize',12)
xlabel('Wavelength (um)','Fontsize',12)
ylabel('Index of Refraction','Fontsize',12)
title('Effective Index of Ti-MgF2 Structure','Fontsize',12)
```

```matlab
axis tight
```

Code for the reflection and transmission of the Ti-MgF2 structure as layers

```matlab
%Jack Lombardi
%code for effective permittivity and index
%Ti-MgF2, 300nm period, 4layer
%Ni for 2.5-12um
%MgF2 for .11-7.5
%SiO2 for 1.6-8um

clear all

theata_i=(pi/180)*61.3; %% incident angle in radians

count=1;

for lambda=2.5:.01:7.5;

    wavelength(count,1)=lambda;

k=(2*pi)/lambda;

n1=(1.36957+(.0035821/(lambda-.14925)+1.381+(.0037415/(lambda-
.14947)))))/2;
d1=.155; %thickness MgF2

n2=(-.0068*lambda^3+.1812*lambda^2-.9281*lambda+5.8689)+ ...
    ((-.0142*lambda^3+.2736*lambda^2+.2448*lambda+2.8602)*1i); %index
of Ti
permitt2=n2^2;
d2=.012; %thickness of T

noxide=-.00015*lambda^5+.0312*lambda^4-.2478*lambda^3+.9223*lambda^2
...
    -1.6158*lambda+2.502;
doxide=.002;

L=1/(lambda^2-.028); %parameter for Si model
n3=3.41983+1.59906e-1*L-(1.23109e-1)*L^2+1.26878e-6*lambda^2 ...
    -1.95104e-9*lambda^4; %index of Si substrate

%%% compute angle for each of the layers using Snells law

theata_1=asin(1*sin(theata_i)/n1);
theata_2=asin(n1*sin(theata_1)/real(n2));
theata_oxide=asin(real(n2)*sin(theata_2)/real(noxide));
theata_3=asin(real(noxide)*sin(theata_oxide)/real(n3));

angle_log(count,1:5)=...
    [lambda,theata_1*(180/pi), theata_2*(180/pi), theata_oxide,
theata_3*(180/pi)];
%code to log angles to use and check for total internal reflection
```

```matlab
n0=n3; %index of substrate
ni=1; %index of superstrate

%%for TE first then TM
M1_TE=[cos(k*n1*d1*cos(theata_1)),...
    ((-1*1i/(n1*cos(theata_1)))*sin(k*n1*d1*cos(theata_1))); ...
    (-1i*n1*cos(theata_1)*sin(k*n1*d1*cos(theata_1))),...
    cos(k*n1*d1*cos(theata_1))];

M1_TM=[cos(k*n1*d1*cos(theata_1)),...
    (-1i*n1/cos(theata_1))*sin(k*n1*d1*cos(theata_1)); ...
    (-1i*cos(theata_1)/n1)*sin(k*n1*d1*cos(theata_1)),...
    cos(k*n1*d1*cos(theata_1))];

%n2
M2_TE=[cos(k*n2*d2*cos(theata_2)),...
    ((-1*1i/(n2*cos(theata_2)))*sin(k*n2*d2*cos(theata_2)));
    (-1i*n2*cos(theata_2)*sin(k*n2*d2*cos(theata_2))),...
    cos(k*n2*d2*cos(theata_2))];

M2_TM=[cos(k*n2*d2*cos(theata_2)),...
    (-1i*n2/cos(theata_2))*sin(k*n2*d2*cos(theata_2)); ...
    (-1i*cos(theata_2)/n2)*sin(k*n2*d2*cos(theata_2)),...
    cos(k*n2*d2*cos(theata_2))];

%noxide
Moxide_TE=[cos(k*noxide*doxide*cos(theata_oxide)),...
    ((-
1*1i/(noxide*cos(theata_oxide)))*sin(k*noxide*doxide*cos(theata_oxide))
);
    (-
1i*noxide*cos(theata_oxide)*sin(k*noxide*doxide*cos(theata_oxide))),...
    cos(k*noxide*doxide*cos(theata_oxide))];

Moxide_TM=[cos(k*noxide*doxide*cos(theata_oxide)),...
    (-
1i*noxide/cos(theata_oxide))*sin(k*noxide*doxide*cos(theata_oxide));
...
    (-
1i*cos(theata_oxide)/noxide)*sin(k*noxide*doxide*cos(theata_oxide)),...
    cos(k*noxide*doxide*cos(theata_oxide))];

M_TE=M1_TE*M2_TE*M1_TE*M2_TE*M1_TE*M2_TE*M1_TE*M2_TE*Moxide_TE; %final
transfer matrix

M_TM=M1_TM*M2_TM*M1_TM*M2_TM*M1_TM*M2_TM*M1_TM*M2_TM*Moxide_TM; %final
transfer matrix

%compute final compex reflection and transmission

r_TE(count,1)=(((M_TE(1,1)+(n0*cos(theata_3)*M_TE(1,2)))*ni*cos(theata_
i))...
```

```matlab
        -(M_TE(2,1)+(n0*cos(theata_3)*M_TE(2,2))))/ ...
        (((M_TE(1,1)+(n0*cos(theata_3)*M_TE(1,2)))*ni*cos(theata_i))...
        +(M_TE(2,1)+(n0*cos(theata_3)*M_TE(2,2)))));

    t_TE(count,1)=(2*ni*cos(theata_i))/...
        (((M_TE(1,1)+n0*cos(theata_3)*M_TE(1,2))*ni*cos(theata_i))...
        +(M_TE(2,1)+n0*cos(theata_3)*M_TE(2,2)));

    R_TE(count,1)=(abs(r_TE(count,1))^2)*100;
    T_TE(count,1)=((n0*cos(theata_3))/(ni*cos(theata_i)))...
        *(abs(t_TE(count,1))^2)*100;


    r_TM(count,1)=(((M_TM(1,1)+(1/n0)*cos(theata_3)*M_TM(1,2))*(1/ni)*cos(t
heata_i))...
        -(M_TM(2,1)+(1/n0)*cos(theata_3)*M_TM(2,2)))/...

    (((M_TM(1,1)+(1/n0)*cos(theata_3)*M_TM(1,2))*(1/ni)*cos(theata_i))...
        +(M_TM(2,1)+(1/n0)*cos(theata_3)*M_TM(2,2)));

    t_TM(count,1)=(2*(1/ni)*cos(theata_i))/...

    (((M_TM(1,1)+(1/n0)*cos(theata_3)*M_TM(1,2))*(1/ni)*cos(theata_i))...
        +(M_TM(2,1)+(1/n0)*cos(theata_3)*M_TM(2,2)));

    R_TM(count,1)=(abs(r_TM(count,1))^2)*100;
    T_TM(count,1)=(((1/n0)*cos(theata_3))/((1/ni)*cos(theata_i)))...
        *(abs(t_TM(count,1))^2)*100;

    R(count,1)=(R_TE(count,1)+R_TM(count,1))/2;
    T(count,1)=(T_TE(count,1)+T_TM(count,1))/2;

    count=count+1;
end

plot(wavelength,R,'LineWidth',2)
xlabel('Wavelength (um)','Fontsize',12)
ylabel('% Reflection','Fontsize',12)
title('Reflection from Ti-MgF2 structure as layers at 61.3
degees','Fontsize',12)
axis tight

figure
plot(wavelength,T,'LineWidth',2)
xlabel('Wavelength (um)','Fontsize',12)
ylabel('% Transmission','Fontsize',12)
title('Transmission from Ti-MgF2 structure as layers at 0
degees','Fontsize',12)
axis tight
```

Code for the reflection and transmission of the Ti-MgF2 structure as a layered structure

```matlab
%Jack Lombardi
%code for effective permittivity and index
```

```matlab
%Ti-MgF2, 300nm period, 4layer
%Ni for 2.5-12um
%MgF2 for .11-7.5
%SiO2 for 1.6-8um

clear all

theata_i=(pi/180)*61.3; %% incident angle in radians

count=1;

for lambda=2.5:.01:7.5;

    wavelength(count,1)=lambda;

k=(2*pi)/lambda;

n1=(1.36957+(.0035821/(lambda-.14925)+1.381+(.0037415/(lambda-
.14947)))))/2;
d1=.155; %thickness MgF2

n2=(-.0068*lambda^3+.1812*lambda^2-.9281*lambda+5.8689)+ ...
    ((-.0142*lambda^3+.2736*lambda^2+.2448*lambda+2.8602)*1i); %index
of Ti
permitt2=n2^2;
d2=.012; %thickness of T

noxide=-0.0015*lambda^5 + 0.0312*lambda^4 - 0.2478*lambda^3 +
0.9223*lambda^2 - 1.6158*lambda + 2.502;
doxide=.002;

L=1/(lambda^2-.028); %parameter for Si model
n3=3.41983+1.59906e-1*L-(1.23109e-1)*L^2+1.26878e-6*lambda^2 ...
    -1.95104e-9*lambda^4; %index of Si substrate

%%% compute angle for each of the layers using Snells law

theata_1=asin(1*sin(theata_i)/n1);
theata_2=asin(n1*sin(theata_1)/real(n2));
theata_oxide=asin(real(n2)*sin(theata_2)/real(noxide));
theata_3=asin(real(noxide)*sin(theata_oxide)/real(n3));

angle_log(count,1:5)=...
    [lambda,theata_1*(180/pi), theata_2*(180/pi), theata_oxide,
theata_3*(180/pi)];
%code to log angles to use and check for total internal reflection

n0=n3; %index of substrate
ni=1; %index of superstrate

%%for TE first then TM
M1_TE=[cos(k*n1*d1*cos(theata_1)),...
```

```matlab
    ((-1*1i/(n1*cos(theata_1)))*sin(k*n1*d1*cos(theata_1)));  ...
    (-1i*n1*cos(theata_1)*sin(k*n1*d1*cos(theata_1))),...
    cos(k*n1*d1*cos(theata_1))];

M1_TM=[cos(k*n1*d1*cos(theata_1)),...
    (-1i*n1/cos(theata_1))*sin(k*n1*d1*cos(theata_1));  ...
    (-1i*cos(theata_1)/n1)*sin(k*n1*d1*cos(theata_1)),...
    cos(k*n1*d1*cos(theata_1))];

%n2
M2_TE=[cos(k*n2*d2*cos(theata_2)),...
    ((-1*1i/(n2*cos(theata_2)))*sin(k*n2*d2*cos(theata_2)));
    (-1i*n2*cos(theata_2)*sin(k*n2*d2*cos(theata_2))),...
    cos(k*n2*d2*cos(theata_2))];

M2_TM=[cos(k*n2*d2*cos(theata_2)),...
    (-1i*n2/cos(theata_2))*sin(k*n2*d2*cos(theata_2));  ...
    (-1i*cos(theata_2)/n2)*sin(k*n2*d2*cos(theata_2)),...
    cos(k*n2*d2*cos(theata_2))];

%noxide
Moxide_TE=[cos(k*noxide*doxide*cos(theata_oxide)),...
    ((-
1*1i/(noxide*cos(theata_oxide)))*sin(k*noxide*doxide*cos(theata_oxide))
);
    (-
1i*noxide*cos(theata_oxide)*sin(k*noxide*doxide*cos(theata_oxide))),...
    cos(k*noxide*doxide*cos(theata_oxide))];

Moxide_TM=[cos(k*noxide*doxide*cos(theata_oxide)),...
    (-
1i*noxide/cos(theata_oxide))*sin(k*noxide*doxide*cos(theata_oxide));
...
    (-
1i*cos(theata_oxide)/noxide)*sin(k*noxide*doxide*cos(theata_oxide)),...
    cos(k*noxide*doxide*cos(theata_oxide))];

M_TE=M1_TE*M2_TE*M1_TE*M2_TE*M1_TE*M2_TE*M1_TE*M2_TE*Moxide_TE; %final
transfer matrix

M_TM=M1_TM*M2_TM*M1_TM*M2_TM*M1_TM*M2_TM*M1_TM*M2_TM*Moxide_TM; %final
transfer matrix

%compute final compex reflection and transmission

r_TE(count,1)=(((M_TE(1,1)+(n0*cos(theata_3)*M_TE(1,2)))*ni*cos(theata_
i))...
    -(M_TE(2,1)+(n0*cos(theata_3)*M_TE(2,2))))/ ...
    (((M_TE(1,1)+(n0*cos(theata_3)*M_TE(1,2)))*ni*cos(theata_i))...
    +(M_TE(2,1)+(n0*cos(theata_3)*M_TE(2,2))));

t_TE(count,1)=(2*ni*cos(theata_i))/...
    (((M_TE(1,1)+n0*cos(theata_3)*M_TE(1,2))*ni*cos(theata_i))...
```

259

```matlab
        +(M_TE(2,1)+n0*cos(theata_3)*M_TE(2,2)));

R_TE(count,1)=(abs(r_TE(count,1))^2)*100;
T_TE(count,1)=((n0*cos(theata_3))/(ni*cos(theata_i)))...
    *(abs(t_TE(count,1))^2)*100;


r_TM(count,1)=(((M_TM(1,1)+(1/n0)*cos(theata_3)*M_TM(1,2))*(1/ni)*cos(t
heata_i))...
    -(M_TM(2,1)+(1/n0)*cos(theata_3)*M_TM(2,2)))/...

(((M_TM(1,1)+(1/n0)*cos(theata_3)*M_TM(1,2))*(1/ni)*cos(theata_i))...
    +(M_TM(2,1)+(1/n0)*cos(theata_3)*M_TM(2,2)));

t_TM(count,1)=(2*(1/ni)*cos(theata_i))/...

(((M_TM(1,1)+(1/n0)*cos(theata_3)*M_TM(1,2))*(1/ni)*cos(theata_i))...
    +(M_TM(2,1)+(1/n0)*cos(theata_3)*M_TM(2,2)));

R_TM(count,1)=(abs(r_TM(count,1))^2)*100;
T_TM(count,1)=(((1/n0)*cos(theata_3))/((1/ni)*cos(theata_i)))...
    *(abs(t_TM(count,1))^2)*100;

R(count,1)=(R_TE(count,1)+R_TM(count,1))/2;
T(count,1)=(T_TE(count,1)+T_TM(count,1))/2;

count=count+1;
end

plot(wavelength,R,'LineWidth',2)
xlabel('Wavelength (um)','Fontsize',12)
ylabel('% Reflection','Fontsize',12)
title('Reflection from Ti-MgF2 structure as layers at 61.3
degees','Fontsize',12)
axis tight

figure
plot(wavelength,T,'LineWidth',2)
xlabel('Wavelength (um)','Fontsize',12)
ylabel('% Transmission','Fontsize',12)
title('Transmission from Ti-MgF2 structure as layers at 0
degees','Fontsize',12)
axis tight
```

Code for the reflection and transmission of the Ti-MgF2 structure as a homogeneous structure

```matlab
%Jack Lombardi
%code for effective permittivity and index
%Ti-MgF2, 300nm period, 4layer
%Ni for 2.5-12um
%MgF2 for .11-7.5
%SiO2 for 1.6-8um
```

```matlab
%%try and now apply for a homogeneous structure

clear all

theata_i=(pi/180)*61.3; %% incident angle in radians

count=1;

for lambda=2.5:.01:7.5;
    wavelength(count,1)=lambda;

n1=(1.36957+(.0035821/(lambda-.14925)+1.381+(.0037415/(lambda-
.14947)))))/2;
d1=.155; %thickness MgF2
permitt1=n1^2;

n2=(-.0068*lambda^3+.1812*lambda^2-.9281*lambda+5.8689)+ ...
    ((-.0142*lambda^3+.2736*lambda^2+.2448*lambda+2.8602)*1i); %index
of Ti
permitt2=n2^2;
d2=.012; %thickness of Ti

noxide=-0.0015*lambda^5 + 0.0312*lambda^4 - 0.2478*lambda^3 +
0.9223*lambda^2 - 1.6158*lambda + 2.502;
doxide=.002;

L=1/(lambda^2-.028); %parameter for Si model
n3=3.41983+1.59906e-1*L-(1.23109e-1)*L^2+1.26878e-6*lambda^2 ...
    -1.95104e-9*lambda^4; %index of Si substrate

neff=(((d1/(d1+d2))*permitt1)+((d2/(d1+d2))*permitt2))^.5;

%%% compute angle for each of the layers using Snells law

theata_1=asin(1*sin(theata_i)/real(neff));
theata_oxide=asin(real(neff)*sin(theata_1)/real(noxide));
theata_3=asin(real(noxide)*sin(theata_oxide)/real(n3));


angle_log(count,1:4)=...
    [lambda,theata_1*(180/pi), theata_oxide, theata_3*(180/pi)];
%code to log angles to use and check for total internal reflection

n0=n3; %index of substrate
ni=1; %index of superstrate
d=(d1+d2)*4; %thickness of whole structure

k=2*pi/lambda;

Meff_TE=[cos(k*neff*d*cos(theata_1)),...
    ((-1*1i/(neff*cos(theata_1)))*sin(k*neff*d*cos(theata_1))); ...
```

```matlab
    (-1i*neff*cos(theata_1)*sin(k*neff*d*cos(theata_1))),...
    cos(k*neff*d*cos(theata_1))];

Meff_TM=[cos(k*neff*d*cos(theata_1)),...
    (-1i*neff/cos(theata_1))*sin(k*neff*d*cos(theata_1)); ...
    (-1i*cos(theata_1)/neff)*sin(k*neff*d*cos(theata_1)),...
    cos(k*neff*d*cos(theata_1))];

%noxide
Moxide_TE=[cos(k*noxide*doxide*cos(theata_oxide)),...
    ((-
1*1i/(noxide*cos(theata_oxide)))*sin(k*noxide*doxide*cos(theata_oxide))
);
    (-
1i*noxide*cos(theata_oxide)*sin(k*noxide*doxide*cos(theata_oxide))),...
    cos(k*noxide*doxide*cos(theata_oxide))];

Moxide_TM=[cos(k*noxide*doxide*cos(theata_oxide)),...
    (-
1i*noxide/cos(theata_oxide))*sin(k*noxide*doxide*cos(theata_oxide));
...
    (-
1i*cos(theata_oxide)/noxide)*sin(k*noxide*doxide*cos(theata_oxide)),...
    cos(k*noxide*doxide*cos(theata_oxide))];

M_TE=Meff_TE*Moxide_TE;
M_TM=Meff_TM*Moxide_TM;

r_TE(count,1)=(((M_TE(1,1)+(n0*cos(theata_3)*M_TE(1,2)))*ni*cos(theata_
i))...
    -(M_TE(2,1)+(n0*cos(theata_3)*M_TE(2,2))))/ ...
    (((M_TE(1,1)+(n0*cos(theata_3)*M_TE(1,2)))*ni*cos(theata_i))...
    +(M_TE(2,1)+(n0*cos(theata_3)*M_TE(2,2))));

t_TE(count,1)=(2*ni*cos(theata_i))/...
    (((M_TE(1,1)+n0*cos(theata_3)*M_TE(1,2))*ni*cos(theata_i))...
    +(M_TE(2,1)+n0*cos(theata_3)*M_TE(2,2)));

R_TE(count,1)=(abs(r_TE(count,1))^2)*100;
T_TE(count,1)=((n0*cos(theata_3))/(ni*cos(theata_i)))...
    *(abs(t_TE(count,1))^2)*100;


r_TM(count,1)=(((M_TM(1,1)+(1/n0)*cos(theata_3)*M_TM(1,2))*(1/ni)*cos(t
heata_i))...
    -(M_TM(2,1)+(1/n0)*cos(theata_3)*M_TM(2,2)))/...

(((M_TM(1,1)+(1/n0)*cos(theata_3)*M_TM(1,2))*(1/ni)*cos(theata_i))...
    +(M_TM(2,1)+(1/n0)*cos(theata_3)*M_TM(2,2)));

t_TM(count,1)=(2*(1/ni)*cos(theata_i))/...

(((M_TM(1,1)+(1/n0)*cos(theata_3)*M_TM(1,2))*(1/ni)*cos(theata_i))...
```

```matlab
    +(M_TM(2,1)+(1/n0)*cos(theata_3)*M_TM(2,2)));

R_TM(count,1)=(abs(r_TM(count,1))^2)*100;
T_TM(count,1)=(((1/n0)*cos(theata_3))/((1/ni)*cos(theata_i)))...
    *(abs(t_TM(count,1))^2)*100;


R(count,1)=(R_TE(count,1)+R_TM(count,1))/2;
T(count,1)=(T_TE(count,1)+T_TM(count,1))/2;

count=count+1;
end


plot(wavelength,R,'LineWidth',2)
xlabel('Wavelength (um)','Fontsize',12)
ylabel('% Reflection','Fontsize',12)
title('Reflection from Ti-MgF2 structure as homogeneous material at
61.3 degees','Fontsize',12)
axis tight

figure
plot(wavelength,T,'LineWidth',2)
xlabel('Wavelength (um)','Fontsize',12)
ylabel('% Transmission','Fontsize',12)
title('Transmission from Ti-MgF2 structure as homogeneous material at 0
degees','Fontsize',12)
axis tight
```

D-4: Code for Au-SU-8 Structure

Code for effective permittivity and index
```matlab
%Jack Lombardi
%code for effective permittivity and index
%Au-SU-8,5010nm period, 4layer

clear all

h=4.135667e-15; %Plank's const in eV
c=3e14; %speed of light in um
count=1;

for lambda=1:.01:8;
    wavelength(count,1)=lambda;

n1=1.556+(.00796/lambda^2)+(.00014/lambda^4); %index of SU-8
d1=5; %thickness of SU-8
permitt1=n1^2;
```

```
permitt2=(1-((8.9951^2)/((h*c/lambda)^2+1i*.0268*(h*c/lambda))));
%index of Au
n2=permitt2^(.5);
d2=.010; %thickness of Au

period=d1+d2;

eff_permit(count,1)=((d1/period)*permitt1)+((d2/period)*real(permitt2))
;

eff_index(count,1)=(((d1/period)*permitt1)+(d2/period)*(permitt2))^.5;

count=count+1;
end

plot(wavelength,(eff_permit),'LineWidth',2)
xlabel('Wavelength (um)','Fontsize',12')
ylabel('Real part of Permittivity','Fontsize',12)
title('Effective Permittivity of Au-SU-8 Structure','Fontsize',12)
axis tight

figure
plot(wavelength,real(eff_index),'LineWidth',2)
hold on
plot(wavelength,imag(eff_index),'r','LineWidth',2)
legend('real','imaginary','Fontsize',12)
xlabel('Wavelength (um)','Fontsize',12)
ylabel('Index of Refraction','Fontsize',12)
title('Effective Index of Au-SU-8 Structure','Fontsize',12)
axis tight
```

Code for reflection and transmission of the Au-Su-8 structure as layered material

```
%Jack Lombardi
%code for effective permittivity and index
%Au-SU-8,5010nm period, 4layer

clear all

h=4.135667e-15; %Plank's const in eV
c=3e14; %speed of light in um

theata_i=(pi/180)*63.1; %% incident angle in radians

count=1;

for lambda=1:.01:8;

    wavelength(count,1)=lambda;

k=(2*pi)/lambda;

n1=1.556+(.00796/lambda^2)+(.00014/lambda^4); %index of SU-8
```

```matlab
d1=4; %thickness of SU-8


permitt2=(1-((8.9951^2)/((h*c/lambda)^2+1i*.0268*(h*c/lambda))));
%index of Au
n2=permitt2^(.5);
d2=.010; %thickness of Au

n3=1; %no substrate

%%% compute angle for each of the layers using Snells law

theata_1=asin(1*sin(theata_i)/n1);
theata_2=asin(n1*sin(theata_1)/real(n2));
theata_3=asin(real(n2)*sin(theata_2)/real(n3));

angle_log(count,1:4)=...
    [lambda,theata_1*(180/pi), theata_2*(180/pi), theata_3*(180/pi)];
%code to log angles to use and check for total internal reflection

n0=n3; %index of substrate
ni=1; %index of superstrate

%%for TE first then TM
M1_TE=[cos(k*n1*d1*cos(theata_1)),...
    ((-1*1i/(n1*cos(theata_1)))*sin(k*n1*d1*cos(theata_1))); ...
    (-1i*n1*cos(theata_1)*sin(k*n1*d1*cos(theata_1))),...
    cos(k*n1*d1*cos(theata_1))];

M1_TM=[cos(k*n1*d1*cos(theata_1)),...
    (-1i*n1/cos(theata_1))*sin(k*n1*d1*cos(theata_1)); ...
    (-1i*cos(theata_1)/n1)*sin(k*n1*d1*cos(theata_1)),...
    cos(k*n1*d1*cos(theata_1))];

%n2
M2_TE=[cos(k*n2*d2*cos(theata_2)),...
    ((-1*1i/(n2*cos(theata_2)))*sin(k*n2*d2*cos(theata_2)));
    (-1i*n2*cos(theata_2)*sin(k*n2*d2*cos(theata_2))),...
    cos(k*n2*d2*cos(theata_2))];

M2_TM=[cos(k*n2*d2*cos(theata_2)),...
    (-1i*n2/cos(theata_2))*sin(k*n2*d2*cos(theata_2)); ...
    (-1i*cos(theata_2)/n2)*sin(k*n2*d2*cos(theata_2)),...
    cos(k*n2*d2*cos(theata_2))];


M_TE=M1_TE*M2_TE*M1_TE*M2_TE*M1_TE*M2_TE*M1_TE*M2_TE; %final transfer
matrix

M_TM=M1_TM*M2_TM*M1_TM*M2_TM*M1_TM*M2_TM*M1_TM*M2_TM; %final transfer
matrix
```

```matlab
%compute final compex reflection and transmission

r_TE(count,1)=(((M_TE(1,1)+(n0*cos(theata_3)*M_TE(1,2)))*ni*cos(theata_i))...
    -(M_TE(2,1)+(n0*cos(theata_3)*M_TE(2,2))))/ ...
    (((M_TE(1,1)+(n0*cos(theata_3)*M_TE(1,2)))*ni*cos(theata_i))...
    +(M_TE(2,1)+(n0*cos(theata_3)*M_TE(2,2))));

t_TE(count,1)=(2*ni*cos(theata_i))/...
    (((M_TE(1,1)+n0*cos(theata_3)*M_TE(1,2))*ni*cos(theata_i))...
    +(M_TE(2,1)+n0*cos(theata_3)*M_TE(2,2)));

R_TE(count,1)=(abs(r_TE(count,1))^2)*100;
T_TE(count,1)=((n0*cos(theata_3))/(ni*cos(theata_i)))...
    *(abs(t_TE(count,1))^2)*100;


r_TM(count,1)=(((M_TM(1,1)+(1/n0)*cos(theata_3)*M_TM(1,2))*(1/ni)*cos(theata_i))...
    -(M_TM(2,1)+(1/n0)*cos(theata_3)*M_TM(2,2)))/...

(((M_TM(1,1)+(1/n0)*cos(theata_3)*M_TM(1,2))*(1/ni)*cos(theata_i))...
    +(M_TM(2,1)+(1/n0)*cos(theata_3)*M_TM(2,2)));

t_TM(count,1)=(2*(1/ni)*cos(theata_i))/...

(((M_TM(1,1)+(1/n0)*cos(theata_3)*M_TM(1,2))*(1/ni)*cos(theata_i))...
    +(M_TM(2,1)+(1/n0)*cos(theata_3)*M_TM(2,2)));

R_TM(count,1)=(abs(r_TM(count,1))^2)*100;
T_TM(count,1)=(((1/n0)*cos(theata_3))/((1/ni)*cos(theata_i)))...
    *(abs(t_TM(count,1))^2)*100;

R(count,1)=(R_TE(count,1)+R_TM(count,1))/2;
T(count,1)=(T_TE(count,1)+T_TM(count,1))/2;

count=count+1;
end

plot(wavelength,R,'LineWidth',2)
xlabel('Wavelength (um)','Fontsize',12)
ylabel('% Reflection','Fontsize',12)
title('Reflection from Au-SU-8 structure as layers at 61.3
degees','Fontsize',12)
axis([1 8 0 100]);

figure
plot(wavelength,T,'LineWidth',2)
xlabel('Wavelength (um)','Fontsize',12)
ylabel('% Transmission','Fontsize',12)
title('Transmission from Au-SU-8 structure as layers at 0
degees','Fontsize',12)
axis tight
```

Code for reflection and transmission from Au-SU-8 structure treated as homogeneous material

```
%Jack Lombardi
%code for effective permittivity and index
%Au-SU-8,5010nm period, 4layer

clear all
%%try and now apply for a homogeneous structure

h=4.135667e-15; %Plank's const in eV
c=3e14; %speed of light in um

theata_i=(pi/180)*0; %% incident angle in radians

count=1;

for lambda=1:.01:8;
    wavelength(count,1)=lambda;

n1=1.556+(.00796/lambda^2)+(.00014/lambda^4); %index of SU-8
permitt1=n1^2;
d1=4; %thickness of SU-8


permitt2=(1-((8.9951^2)/((h*c/lambda)^2+1i*.0268*(h*c/lambda))));
%index of Au
n2=permitt2^(.5);
d2=.010; %thickness of Au

n3=1; %no substrate

neff=(((d1/(d1+d2))*permitt1)+((d2/(d1+d2))*permitt2))^.5;

%%% compute angle for each of the layers using Snells law

theata_1=asin(1*sin(theata_i)/real(neff));

theata_3=asin(real(neff)*sin(theata_1)/real(n3));


angle_log(count,1:3)=...
    [lambda,theata_1*(180/pi), theata_3*(180/pi)];
%code to log angles to use and check for total internal reflection

n0=n3; %index of substrate
ni=1; %index of superstrate
d=(d1+d2)*4; %thickness of whole structure
```

```
k=2*pi/lambda;

Meff_TE=[cos(k*neff*d*cos(theata_1)),...
    ((-1*1i/(neff*cos(theata_1)))*sin(k*neff*d*cos(theata_1))); ...
    (-1i*neff*cos(theata_1)*sin(k*neff*d*cos(theata_1))),...
    cos(k*neff*d*cos(theata_1))];

Meff_TM=[cos(k*neff*d*cos(theata_1)),...
    (-1i*neff/cos(theata_1))*sin(k*neff*d*cos(theata_1)); ...
    (-1i*cos(theata_1)/neff)*sin(k*neff*d*cos(theata_1)),...
    cos(k*neff*d*cos(theata_1))];


M_TE=Meff_TE;
M_TM=Meff_TM;

r_TE(count,1)=(((M_TE(1,1)+(n0*cos(theata_3)*M_TE(1,2)))*ni*cos(theata_
i))...
    -(M_TE(2,1)+(n0*cos(theata_3)*M_TE(2,2))))/ ...
    (((M_TE(1,1)+(n0*cos(theata_3)*M_TE(1,2)))*ni*cos(theata_i))...
    +(M_TE(2,1)+(n0*cos(theata_3)*M_TE(2,2))));

t_TE(count,1)=(2*ni*cos(theata_i))/...
    (((M_TE(1,1)+n0*cos(theata_3)*M_TE(1,2))*ni*cos(theata_i))...
    +(M_TE(2,1)+n0*cos(theata_3)*M_TE(2,2)));

R_TE(count,1)=(abs(r_TE(count,1))^2)*100;
T_TE(count,1)=((n0*cos(theata_3))/(ni*cos(theata_i)))...
    *(abs(t_TE(count,1))^2)*100;


r_TM(count,1)=(((M_TM(1,1)+(1/n0)*cos(theata_3)*M_TM(1,2))*(1/ni)*cos(t
heata_i))...
    -(M_TM(2,1)+(1/n0)*cos(theata_3)*M_TM(2,2)))/...

(((M_TM(1,1)+(1/n0)*cos(theata_3)*M_TM(1,2))*(1/ni)*cos(theata_i))...
    +(M_TM(2,1)+(1/n0)*cos(theata_3)*M_TM(2,2)));

t_TM(count,1)=(2*(1/ni)*cos(theata_i))/...

(((M_TM(1,1)+(1/n0)*cos(theata_3)*M_TM(1,2))*(1/ni)*cos(theata_i))...
    +(M_TM(2,1)+(1/n0)*cos(theata_3)*M_TM(2,2)));

R_TM(count,1)=(abs(r_TM(count,1))^2)*100;
T_TM(count,1)=(((1/n0)*cos(theata_3))/((1/ni)*cos(theata_i)))...
    *(abs(t_TM(count,1))^2)*100;


R(count,1)=(R_TE(count,1)+R_TM(count,1))/2;
T(count,1)=(T_TE(count,1)+T_TM(count,1))/2;

count=count+1;
```

```
end

plot(wavelength,R,'LineWidth',2)
xlabel('Wavelength (um)','Fontsize',12)
ylabel('% Reflection','Fontsize',12)
title('Reflection from Au-SU-8 structure as homogeneous material at
61.3 degees','Fontsize',12)
axis([1 8 0 100]);

figure
plot(wavelength,T,'LineWidth',2)
xlabel('Wavelength (um)','Fontsize',12)
ylabel('% Transmission','Fontsize',12)
title('Transmission from Au-SU-8 structure as homogeneous material at 0
degees','Fontsize',12)
axis tight
```

D-5: Code for Ni-Si Structure

Code for effective permittivity and index

```
%Jack Lombardi
%code for effective permittivity and index
%Ni-Si, 200nm period, 4layer
%Ni for 1.5-12.4um
%Si for 2.473-16.73

clear all

count=1;

for lambda=1:.1:12;
    wavelength(count,1)=lambda;

n1=-3e-5*lambda^4+.001*lambda^3-.0099*lambda^2 ...
    +.0139*lambda+3.8777; %index of Si
d1=.189; %thickness Si
permitt1=n1^2;

n2=(.0001*lambda^5-.0062*lambda^4+.1125*lambda^3 ...
    -.8515*lambda^2+2.8371*lambda+.6676)+(-6e-5*lambda^4-.008*lambda^3
...
    +.2162*lambda^2+2.1*lambda+3.1424)*1i; %index of Ni
permitt2=n2^2;
d2=.011; %thickness of Ni
period=.2; %period of structure

eff_permit(count,1)=((d1/period)*permitt1)+((d2/period)*real(permitt2))
;
```

```matlab
eff_index(count,1)=(((d1/period)*permitt1)+(d2/period)*(permitt2))^.5;

count=count+1;
end

plot(wavelength,(eff_permit),'LineWidth',2)
xlabel('Wavelength (um)')
ylabel('Real part of Permittivity')
title('Effective Permittivity of Ni-Si Structure')
axis tight

figure
plot(wavelength,real(eff_index),'LineWidth',2)
hold on
plot(wavelength,imag(eff_index),'r','LineWidth',2)
legend('real','imaginary')
xlabel('Wavelength (um)')
ylabel('Index of Refraction')
title('Effective Index of Ni-Si Structure')
axis tight
```

Code for reflection and transmission as layered structure

```matlab
%Jack Lombardi
%Ni-Si at 4.45um, 200nm period, 4layer, on Si substrate, include
surface
%oxide
%Ni-Si, 200nm period, 4layer
%Ni for 1.5-12.4um
%Si for 2.473-16.73um
%SiO2 for 1.6-8um

clear all

theata_i=(pi/180)*0; %% incident angle in radians

count=1;

for lambda=1:.01:12;

   wavelength(count,1)=lambda;

k=(2*pi)/lambda;

n1=-3e-5*lambda^4+.001*lambda^3-.0099*lambda^2 ...
    +.0139*lambda+3.8777; %index of Si
d1=.089; %thickness Si

n2=(.0001*lambda^5-.0062*lambda^4+.1125*lambda^3 ...
    -.8515*lambda^2+2.8371*lambda+.6676)+(-6e-5*lambda^4-.008*lambda^3
    ...+.2162*lambda^2+2.1*lambda+3.1424)*1i; %index of Ni
d2=.011; %thickness of Ni
```

```matlab
noxide=-.00015*lambda^5+.0312*lambda^4-.2478*lambda^3+...
    .9223*lambda^2-1.6158*lambda+2.502;
doxide=.002;

L=1/(lambda^2-.028); %parameter for Si model
n3=3.41983+1.59906e-1*L-(1.23109e-1)*L^2+1.26878e-6*lambda^2 ...
    -1.95104e-9*lambda^4; %index of Si substrate

%%% compute angle for each of the layers using Snells law

theata_1=asin(1*sin(theata_i)/n1);
theata_2=asin(n1*sin(theata_1)/real(n2));
theata_oxide=asin(real(n2)*sin(theata_2)/real(noxide));
theata_3=asin(real(noxide)*sin(theata_oxide)/real(n3));

angle_log(count,1:4)=...
    [lambda,theata_1*(180/pi), theata_2*(180/pi), theata_3*(180/pi)];



n0=n3; %index of substrate
ni=1; %index of superstrate

%%for TE first then TM
M1_TE=[cos(k*n1*d1*cos(theata_1)),...
    ((-1*1i/(n1*cos(theata_1)))*sin(k*n1*d1*cos(theata_1))); ...
    (-1i*n1*cos(theata_1)*sin(k*n1*d1*cos(theata_1))),...
    cos(k*n1*d1*cos(theata_1))];

M1_TM=[cos(k*n1*d1*cos(theata_1)),...
    (-1i*n1/cos(theata_1))*sin(k*n1*d1*cos(theata_1)); ...
    (-1i*cos(theata_1)/n1)*sin(k*n1*d1*cos(theata_1)),...
    cos(k*n1*d1*cos(theata_1))];

%n2
M2_TE=[cos(k*n2*d2*cos(theata_2)),...
    ((-1*1i/(n2*cos(theata_2)))*sin(k*n2*d2*cos(theata_2)));
    (-1i*n2*cos(theata_2)*sin(k*n2*d2*cos(theata_2))),...
    cos(k*n2*d2*cos(theata_2))];

M2_TM=[cos(k*n2*d2*cos(theata_2)),...
    (-1i*n2/cos(theata_2))*sin(k*n2*d2*cos(theata_2)); ...
    (-1i*cos(theata_2)/n2)*sin(k*n2*d2*cos(theata_2)),...
    cos(k*n2*d2*cos(theata_2))];

%noxide
Moxide_TE=[cos(k*noxide*doxide*cos(theata_oxide)),...
    ((-
1*1i/(noxide*cos(theata_oxide)))*sin(k*noxide*doxide*cos(theata_oxide))
);
    (-
1i*noxide*cos(theata_oxide)*sin(k*noxide*doxide*cos(theata_oxide))),...
    cos(k*noxide*doxide*cos(theata_oxide))];
```

```matlab
Moxide_TM=[cos(k*noxide*doxide*cos(theata_oxide)),...
    (-
1i*noxide/cos(theata_oxide))*sin(k*noxide*doxide*cos(theata_oxide));
...
    (-
1i*cos(theata_oxide)/noxide)*sin(k*noxide*doxide*cos(theata_oxide)),...
    cos(k*noxide*doxide*cos(theata_oxide))];

M_TE=M1_TE*M2_TE*M1_TE*M2_TE*M1_TE*M2_TE*M1_TE*M2_TE*Moxide_TE; %final
transfer matrix

M_TM=M1_TM*M2_TM*M1_TM*M2_TM*M1_TM*M2_TM*M1_TM*M2_TM*Moxide_TM; %final
transfer matrix

%compute final complex reflection and transmission

r_TE(count,1)=(((M_TE(1,1)+(n0*cos(theata_3)*M_TE(1,2)))*ni*cos(theata_
i))...
    -(M_TE(2,1)+(n0*cos(theata_3)*M_TE(2,2))))/ ...
    (((M_TE(1,1)+(n0*cos(theata_3)*M_TE(1,2)))*ni*cos(theata_i))...
    +(M_TE(2,1)+(n0*cos(theata_3)*M_TE(2,2))));

t_TE(count,1)=(2*ni*cos(theata_i))/...
    (((M_TE(1,1)+n0*cos(theata_3)*M_TE(1,2))*ni*cos(theata_i))...
    +(M_TE(2,1)+n0*cos(theata_3)*M_TE(2,2)));

R_TE(count,1)=(abs(r_TE(count,1))^2)*100;
T_TE(count,1)=((n0*cos(theata_3))/(ni*cos(theata_i)))...
    *(abs(t_TE(count,1))^2)*100;


r_TM(count,1)=(((M_TM(1,1)+(1/n0)*cos(theata_3)*M_TM(1,2))*(1/ni)*cos(t
heata_i))...
    -(M_TM(2,1)+(1/n0)*cos(theata_3)*M_TM(2,2)))/...

(((M_TM(1,1)+(1/n0)*cos(theata_3)*M_TM(1,2))*(1/ni)*cos(theata_i))...
    +(M_TM(2,1)+(1/n0)*cos(theata_3)*M_TM(2,2)));

t_TM(count,1)=(2*(1/ni)*cos(theata_i))/...

(((M_TM(1,1)+(1/n0)*cos(theata_3)*M_TM(1,2))*(1/ni)*cos(theata_i))...
    +(M_TM(2,1)+(1/n0)*cos(theata_3)*M_TM(2,2)));

R_TM(count,1)=(abs(r_TM(count,1))^2)*100;
T_TM(count,1)=(((1/n0)*cos(theata_3))/((1/ni)*cos(theata_i)))...
    *(abs(t_TM(count,1))^2)*100;

R(count,1)=(R_TE(count,1)+R_TM(count,1))/2;
T(count,1)=(T_TE(count,1)+T_TM(count,1))/2;

count=count+1;
end
```

272

```
plot(wavelength,R,'LineWidth',2)
xlabel('Wavelength (um)','Fontsize',12)
ylabel('% Refelction','Fontsize',12)
title('Reflection from Ni-Si structure as layers at 61.3
degees','Fontsize',12)
axis tight

figure
plot(wavelength,T,'LineWidth',2)
xlabel('Wavelength (um)','Fontsize',12)
ylabel('% Transmission','Fontsize',12)
title('Transmission from Ni-Si structure as layers at 0
degees','Fontsize',12)
axis tight
```

Code for reflection and transmission as homogeneous structure

```
%Jack Lombardi
%Ni-Si at 4.45um, 200nm period, 4layer, on Si substrate, include
surface
%oxide
%Ni-Si, 200nm period, 4layer
%Ni for 1.5-12.4um
%Si for 2.473-16.73um
%SiO2 for 1.6-8um

clear all
%%try and now apply for a homogeneous structure

clear all

theata_i=(pi/180)*63.1; %% incident angle in radians

count=1;

for lambda=1:.01:12;
   wavelength(count,1)=lambda;

n1=-3e-5*lambda^4+.001*lambda^3-.0099*lambda^2 ...
    +.0139*lambda+3.8777; %index of Si
d1=.089; %thickness Si
permitt1=n1^2;

n2=(.0001*lambda^5-.0062*lambda^4+.1125*lambda^3 ...
    -.8515*lambda^2+2.8371*lambda+.6676)+(-6e-5*lambda^4-.008*lambda^3
...
    +.2162*lambda^2+2.1*lambda+3.1424)*1i; %index of Ni
d2=.011; %thickness of Ni
permitt2=n2^2;
```

```matlab
noxide=-.00015*lambda^5+.0312*lambda^4-.2478*lambda^3+.9223*lambda^2
...
    -1.6158*lambda+2.502;
doxide=.002;


L=1/(lambda^2-.028); %parameter for Si model
n3=3.41983+1.59906e-1*L-(1.23109e-1)*L^2+1.26878e-6*lambda^2 ...
    -1.95104e-9*lambda^4; %index of Si substrate


neff=(((d1/(d1+d2))*permitt1)+((d2/(d1+d2))*permitt2))^.5;

%%% compute angle for each of the layers using Snells law

theata_1=asin(1*sin(theata_i)/real(neff));
theata_oxide=asin(real(neff)*sin(theata_1)/real(noxide));
theata_3=asin(real(noxide)*sin(theata_oxide)/real(n3));



angle_log(count,1:4)=...
    [lambda,theata_1*(180/pi), theata_oxide, theata_3*(180/pi)];
%code to log angles to use and check for total internal reflection

n0=n3; %index of substrate
ni=1; %index of superstrate
d=.1*4; %thickness of whole structure

k=2*pi/lambda;

Meff_TE=[cos(k*neff*d*cos(theata_1)),...
    ((-1*1i/(neff*cos(theata_1)))*sin(k*neff*d*cos(theata_1))); ...
    (-1i*neff*cos(theata_1)*sin(k*neff*d*cos(theata_1))),...
    cos(k*neff*d*cos(theata_1))];

Meff_TM=[cos(k*neff*d*cos(theata_1)),...
    (-1i*neff/cos(theata_1))*sin(k*neff*d*cos(theata_1)); ...
    (-1i*cos(theata_1)/neff)*sin(k*neff*d*cos(theata_1)),...
    cos(k*neff*d*cos(theata_1))];

%noxide
Moxide_TE=[cos(k*noxide*doxide*cos(theata_oxide)),...
    ((-
1*1i/(noxide*cos(theata_oxide)))*sin(k*noxide*doxide*cos(theata_oxide))
);
    (-
1i*noxide*cos(theata_oxide)*sin(k*noxide*doxide*cos(theata_oxide))),...
    cos(k*noxide*doxide*cos(theata_oxide))];

Moxide_TM=[cos(k*noxide*doxide*cos(theata_oxide)),...
    (-
1i*noxide/cos(theata_oxide))*sin(k*noxide*doxide*cos(theata_oxide));
...
    (-
1i*cos(theata_oxide)/noxide)*sin(k*noxide*doxide*cos(theata_oxide)),...
```

```matlab
        cos(k*noxide*doxide*cos(theata_oxide))];

M_TE=Meff_TE*Moxide_TE;
M_TM=Meff_TM*Moxide_TM;

r_TE(count,1)=(((M_TE(1,1)+(n0*cos(theata_3)*M_TE(1,2)))*ni*cos(theata_
i))...
    -(M_TE(2,1)+(n0*cos(theata_3)*M_TE(2,2))))/ ...
    (((M_TE(1,1)+(n0*cos(theata_3)*M_TE(1,2)))*ni*cos(theata_i))...
    +(M_TE(2,1)+(n0*cos(theata_3)*M_TE(2,2))));

t_TE(count,1)=(2*ni*cos(theata_i))/...
    (((M_TE(1,1)+n0*cos(theata_3)*M_TE(1,2))*ni*cos(theata_i))...
    +(M_TE(2,1)+n0*cos(theata_3)*M_TE(2,2)));

R_TE(count,1)=(abs(r_TE(count,1))^2)*100;
T_TE(count,1)=((n0*cos(theata_3))/(ni*cos(theata_i)))...
    *(abs(t_TE(count,1))^2)*100;


r_TM(count,1)=(((M_TM(1,1)+(1/n0)*cos(theata_3)*M_TM(1,2))*(1/ni)*cos(t
heata_i))...
    -(M_TM(2,1)+(1/n0)*cos(theata_3)*M_TM(2,2)))/...

(((M_TM(1,1)+(1/n0)*cos(theata_3)*M_TM(1,2))*(1/ni)*cos(theata_i))...
    +(M_TM(2,1)+(1/n0)*cos(theata_3)*M_TM(2,2)));

t_TM(count,1)=(2*(1/ni)*cos(theata_i))/...

(((M_TM(1,1)+(1/n0)*cos(theata_3)*M_TM(1,2))*(1/ni)*cos(theata_i))...
    +(M_TM(2,1)+(1/n0)*cos(theata_3)*M_TM(2,2)));

R_TM(count,1)=(abs(r_TM(count,1))^2)*100;
T_TM(count,1)=(((1/n0)*cos(theata_3))/((1/ni)*cos(theata_i)))...
    *(abs(t_TM(count,1))^2)*100;

R(count,1)=(R_TE(count,1)+R_TM(count,1))/2;
T(count,1)=(T_TE(count,1)+T_TM(count,1))/2;

count=count+1;
end


plot(wavelength,R,'LineWidth',2)
xlabel('Wavelength (um)','Fontsize',12)
ylabel('% Reflection','Fontsize',12)
title('Reflection from Ni-Si structure as homogeneous material at 61.3
degees','Fontsize',12)
axis tight

figure
plot(wavelength,T,'LineWidth',2)
xlabel('Wavelength (um)','Fontsize',12)
```

```matlab
ylabel('% Transmission','Fontsize',12)
title('Transmission from Ni-Si structure as homogeneous material at 0
degees','Fontsize',12)
axis tight
```

D-6: Code for Gold Hafnium Oxide Structure

```matlab
%Program for shooting for thickness for magnetic resonance

%define some initial parameters and guesses, all dim in um

nd=1.86036; %index of dielectric spacer HfO2
lambdam=4.45; %wavelength where magnetic resonance is desired
permittivity=-1.0303e+003; %real part of metal permittivity at ...
%mag res wavelength, epsilon prime
x=1; y=1;
display('Au-HfO2')
wcrossover=lambdam/(2*nd)
difference=zeros(492,492);


for w=1:.04:wcrossover


for d=.01:.001:.5;
    for t=.01:.001:.5;
%check if numbers are valid, not imag
if ((2*pi*nd/lambdam)^2)>((pi/w)^2)
    difference(x,y)=550;
else
    kappa=sqrt((pi/w)^2-(2*pi*nd/lambdam)^2);
    magvalue=1-(nd^2/(t*kappa))*(1+coth(d*kappa/2)); %it is desired
that this
    %value be equal to the permittivity of the metal, permittivity
above
    difference(x+1,y+1)=magvalue-permittivity; %vary w,d,t until
difference is minimized

    %section to be used when finding mins, puts arbitrary high values
in edge cells
    difference(1,y)=300;
    difference(x,1)=300;
    difference(1,492)=300;
    difference(492,1)=300;


end

x=x+1;
    end
    x=1;
    y=y+1;
end
```

```
w
[row,col] = find(abs(difference)<.02);
if row>0
    location=[row,col];
metal_thick=.01+(.001.*(row-2));
dielec_thick=.01+(.001.*(col-2));

dims=[metal_thick, dielec_thick]

vals=zeros(length(row),1);
for q=1:1:length(row)
    vals(q)=difference(row(q),col(q));
end
vals
end
x=1; y=1;
end
```

References

[1] S. A. Ramakrishna and T. M. Grzegorczyk, *Physics and Applications of Negative Refractive Index Materials.* Boca Raton, FL: Taylor & Francis Group, LLC, 2009.

[2] A. Sihvola. (2007, 3). Metamaterials in electromagnetics. *Metamaterials 1(1),* pp. 2-11.

[3] U. K. Chettiar, A. V. Kildishev, W. Cai, H. Yuan, V. P. Drachev and V. M. Shalaev. (2008, Optical metamagnetism and negative index metamaterials. Available: http://www.citebase.org/abstract?id=oai:arXiv.org:0806.2677.

[4] B. Wood. (2009, 6). Metamaterials and invisibility. *Comptes Rendus Physique 10(5),* pp. 379-390.

[5] W. Cai and V. M. Shalaev, *Optical Metamaterials: Fundamentals and Applications.* New York: Springer Science+Business Media, LLC, 2010.

[6] A. Boltasseva and V. M. Shalaev. (2008, 5). Fabrication of optical negative-index metamaterials: Recent advances and outlook. *Metamaterials 2(1),* pp. 1-17.

[7] U. K. Chettiar, A. V. Kildishev, H. Yuan, W. Cai, S. Xiao, V. P. Drachev and V. M. Shalaev. (2007, Dual-band negative index metamaterial: Double negative at 813 nm and single negative at 772 nm. *Opt. Lett. 32(12),* pp. 1671-1673. Available: http://ol.osa.org/abstract.cfm?URI=ol-32-12-1671.

[8] I. AJA international. What is sputtering? *2010(June/12),* Available: http://www.ajaint.com/whatis.htm.

[9] Anonymous "XTM/2 Deposition Monitor Manual," .

[10] R. A. J. Coutu, "Course Notes: EENG 636," .

[11] Anonymous (2008, Heidelberg uPG 101 fact sheet. Available: http://www.himt.de/factsheets/muepg101.pdf.

[12] Anonymous (2004, Varian cary 4000, 5000, 6000i spectrophotometers. Agilent Technologies. Available: http://www.chem.agilent.com/Library/brochures/1942.pdf.

[13] Anonymous "Linear Dyanmic Range of the Cary 4000, 5000, 6000i: Internal Diffuse Reflectance Accessories," 2010.

[14] Anonymous (2011, Introduction to FT-IR spectroscopy. [online]. *2011(Jan/13),* Available: http://www.newport.com/store/genContent.aspx/Introduction-to-FT-IR-Spectroscopy/405840/1033.

[15] L. Yan. (2007, Ellipsometry training.

[16] Anonymous (2010, FDTD solutions online help: Reference guide. *2011(Jan/13),* Available: http://www.lumerical.com/fdtd_online_help/fdtd_online_help_reference_guide.php.

[17] J. Karri and A. R. Mickelson. Silver dielectric stack with near-zero epsilon at a visible wavelength. Presented at Nanotechnology Materials and Devices Conference, 2009. NMDC '09. IEEE.

[18] M. Born and E. Wolf, *Principles of Optics.* Cambridge: University Press, 2005.

[19] Xingjie Ni , Zhengtong Liu , Fan Gu , Marcos Gabriel Pacheco , Joshua Borneman and Alexander V. Kildishev . (2009, Aug). PhotonicsSHA-2D: Modeling of single-period multilayer optical gratings and metamaterials. Available: https://nanohub.org/resources/6977.

[20] P. B. Johnson and R. W. Christy. (1972, Dec). Optical constants of the noble metals. *Phys.Rev.B 6(12),* pp. 4370-4379.

[21] E. D. Palik, Ed., *Handbook of Optical Constants of Solids.* San Diego, CA: Academic Press, 1985.

[22] J. S. Starzynski. Etch rates and etch selectivities of a nonvolatile hafnium oxide etchant. Available: http://www.electrochem.org/dl/ma/206/pdfs/0906.pdf.

[23] Xingjie Ni , Zhengtong Liu and Alexander V. Kildishev . (2008, Feb). PhotonicsDB: Optical constants. Available: https://nanohub.org/resources/3692.

[24] M. A. Ordal, L. L. Long, R. J. Bell, S. E. Bell, R. R. Bell, R. W. A. Jr. and C. A. Ward. (1983, Apr). Optical properties of the metals al, co, cu, au, fe, pb, ni, pd, pt, ag, ti, and W in the infrared and far infrared. *Appl. Opt. 22(7),* pp. 1099-1119. Available: http://ao.osa.org/abstract.cfm?URI=ao-22-7-1099.

[25] P. Klocek, *Handbook of Infrared Optical Materials.* New York: Marcel Dekker, 1991.

[26] J. M. Khoshman and M. E. Kordesch. (2006, 12/4). Optical properties of a-HfO2 thin films. *Surface and Coatings Technology 201(6),* pp. 3530-3535.

[27] W. Wolfe and G. Zissis, Eds., *The Infrared Handbook.* The Infrared Information Analysis Center, Environmental Research Institute of Michigan, 1989.

[28] Anonymous LOR and PMGI resists. [[Online]]. Available: http://www.microchem.com/products/pdf/PMGI-Resists-data-sheetV-rhcedit-102206.pdf.

[29] Anonymous SU-8 2000 permenent epoxy negative photoresist. [[Online]]. Available: http://www.microchem.com/products/pdf/SU-82000DataSheet2000_5thru2015Ver4.pdf.

[30] P. L. Washington, H. C. Ong, J. Y. Dai and R. P. H. Chang. (1998, Determination of the optical constants of zinc oxide thin films by spectroscopic ellipsometry. *Applied Physics Letters 72(25),* pp. 3261-3263.

Vita

       Jack P. Lombardi III is a native of central New York and a 2005 graduate of Fabius-Pompey High School in Fabius, NY. He attended Rensselaer Polytechnic Institute in Troy, NY, earning a B.S. in Electrical Engineering, and a commission into the Air Force through AFROTC. His follow on assignment is to the AFRL Sensors Directorate at Wright-Patterson AFB, Ohio.

REPORT DOCUMENTATION PAGE			*Form Approved* OMB No. 074-0188

The public reporting burden for this collection of information is estimated to average 1 hour per response, including the time for reviewing instructions, searching existing data sources, gathering and maintaining the data needed, and completing and reviewing the collection of information. Send comments regarding this burden estimate or any other aspect of the collection of information, including suggestions for reducing this burden to Department of Defense, Washington Headquarters Services, Directorate for Information Operations and Reports (0704-0188), 1215 Jefferson Davis Highway, Suite 1204, Arlington, VA 22202-4302. Respondents should be aware that notwithstanding any other provision of law, no person shall be subject to an penalty for failing to comply with a collection of information if it does not display a currently valid OMB control number.
PLEASE DO NOT RETURN YOUR FORM TO THE ABOVE ADDRESS.

1. REPORT DATE *(DD-MM-YYYY)* 24-03-2011	2. REPORT TYPE **Master's Thesis**	3. DATES COVERED *(From – To)* August 2009-March 2011

4. TITLE AND SUBTITLE **Optical Metamaterial Design, Fabrication, and Test**	5a. CONTRACT NUMBER
	5b. GRANT NUMBER
	5c. PROGRAM ELEMENT NUMBER
6. AUTHOR(S) **Lombardi, Jack P. III, 2d Lt, USAF**	5d. PROJECT NUMBER 11G187
	5e. TASK NUMBER
	5f. WORK UNIT NUMBER

7. PERFORMING ORGANIZATION NAMES(S) AND ADDRESS(S) Air Force Institute of Technology Graduate School of Engineering and Management (AFIT/EN) 2950 Hobson Way, Building 640 WPAFB OH 45433-8865	8. PERFORMING ORGANIZATION REPORT NUMBER AFIT/GE/ENG/11-25

9. SPONSORING/MONITORING AGENCY NAME(S) AND ADDRESS(ES) Air Force Research Laboratory Attn: Augustine Urbas, Metamaterials Technical Lead, AFMC AFRL/RXB Augustine.Urbas@wpafb.af.mil, (937) 785-9371 3005 Hobson Way, Building 654 WPAFB, OH 45433	10. SPONSOR/MONITOR'S ACRONYM(S)
	11. SPONSOR/MONITOR'S REPORT NUMBER(S)

12. DISTRIBUTION/AVAILABILITY STATEMENT
This material is declared a work of the U.S. Government and is not subject to copyright protection in the United States.

13. SUPPLEMENTARY NOTES

14. ABSTRACT
Metamaterials, materials that make use of naturally occurring materials and designed structures to create materials with special properties not found in nature, are a fascinating new area of research, combining the fields of physics, microfabrication, and material science. This work will focus on the development of metamaterials operating in the visible and infrared which will be constructed and tested for basic optical properties. Possible applications for these materials will not be investigated. The this work will go into the fabrication and test of layered metal-dielectric structures, called layered metamaterials, as these structures hold potential for applications in advanced optical systems. These structures are designed to have a low index of refraction, with a designed permittivity approaching zero due to the permittivity of the metal, which is negative, and dielectric, which is positive, effectively canceling each other out. The other effort of this investigation is the fabrication and test of a 3D or "fishnet" metamaterial, one that is a sandwich of metal and dielectric, with holes in those layers, creating interwoven strips of layered material. These interwoven layered strips combine elements with negative permittivity and permeability to create a negative refractive index. In this work, five different combinations of metal and dielectric are fabricated and tested, with one showing behavior indicative of a low permittivity at an infrared wavelength. The investigations into the 3D material did yield a possible for design using a novel material for the dielectric, but fabrication was not completed and only results from simulation were obtained, which suggest a negative index may occur.

15. SUBJECT TERMS

16. SECURITY CLASSIFICATION OF: Unclassified			17. LIMITATION OF ABSTRACT	18. NUMBER OF PAGES 299	19a. NAME OF RESPONSIBLE PERSON **Ronald A. Coutu, Jr.**
a. REPORT **U**	b. ABSTRACT **U**	c. THIS PAGE **U**	**UU**		19b. TELEPHONE NUMBER *(Include area code)* Ronald.Coutu@afit.edu (937) 255-3636x7230

Standard Form 298 (Rev. 8-98)
Prescribed by ANSI Std. Z39-18